

LONDON
SCHOOL of
HYGIENE
& TROPICAL
MEDICINE



Investigation of the role of GC α in activating cGMP signalling in *Plasmodium falciparum* and how cyclic nucleotide signalling modulates molecular motor function.

Stephanie Diane Nofal

Thesis submitted in accordance with the requirements
for the degree of Doctor of Philosophy

University of London

September 2019

**Department of Infection Biology
Faculty of Infectious and Tropical Diseases
London School of Hygiene & Tropical Medicine**

Primary supervisor: David Baker
Secondary supervisor: Mike Blackman
Tertiary supervisor: Christian Flueck

Funded by the BBSRC

Declaration

I, Stephanie Diane Nofal, confirm that the work presented in this thesis is my own. Where information has been derived from other sources, I confirm that this has been indicated in the thesis.

Abstract

Cyclic guanosine monophosphate (cGMP) is an important signalling molecule which regulates critical events across all stages of the malaria parasite lifecycle. To further our understanding of how cGMP signalling governs important events involved in blood stage egress and invasion as well as gametocyte development and gametogenesis, this study investigates two different members of this signalling cascade in *Plasmodium falciparum* parasites. Guanylyl Cyclase α (GC α) is a large, seemingly bifunctional enzyme, which consists of a type IV P-type ATPase domain, which is predicted to flip aminophospholipids between lipid bilayer leaflets; and a GC domain, which is thought to be responsible for generating cGMP. Using a combination of approaches including mutagenesis and conditional disruption of PfGC α , work presented in this thesis confirms that GC α is responsible for cGMP synthesis and that both ATPase and GC domains are required for asexual blood stage growth. Although the exact role of the ATPase domain remains unknown, chemical complementation of GC α -deficient parasites, which lack both ATPase and GC domains, with a cGMP analogue has revealed that the ultimate role of the ATPase is in modulating cGMP synthesis.

Activation of this cGMP signalling cascade culminates in the phosphorylation of numerous effector proteins, many of which form part of the glideosome. This includes the actomyosin motor protein, Myosin A (MyoA), which is phosphorylated at serine 19 (S19). Since the glideosome generates the force required for merozoites to invade host cells, these cGMP-dependent phosphorylation events may be involved in modulating motor activity. In the second part of this thesis, conditional disruption of MyoA has confirmed that the actomyosin motor is essential for red blood cell invasion, however it is dispensable during gametocyte development and gametogenesis. Complementation of the MyoA knockout line with mutant versions of the protein that either mimic or ablate phosphorylation of S19 revealed that phosphorylation of this residue is important but not essential for parasite viability. *In vitro* motility assays using material derived from parasites expressing either wild type or mutant MyoA demonstrate that non-phosphorylated MyoA displays slower motility, providing evidence that cGMP-dependent phosphorylation is involved in modulating the activity of the actomyosin motor.

Acknowledgements

Firstly I would like to thank my supervisor David Baker for his encouragement and support along the course of my project. Thank you also to Mike Blackman for his useful advice and helpful discussions. I would also like to express my sincere gratitude to Christian Flueck for his continued guidance, patience and help throughout my PhD. For their invaluable help with the motility assays, I would also like to thank Justin Molloy and Juha Vahokoski.

I've been very lucky to have been part of such an incredible research group, so thank you to all Baker and Blackman group members, both past and present, including Christian Flueck, Avnish Patel, Eloise Walker, Gisela Henriques, Kostas Koussis and Abigail Perrin. I would also like to thank other members of 318 and 380, particularly Melissa Hart, Julian Muwanguzi, Ryan Henrici and Franziska Mohring for their support, friendship and the coffee breaks in particular! To Andrew Osborne, I am eternally grateful for your mentorship, help and all the exciting discussions we have had over the years.

Over the course of my time at LSHTM, I have come to meet some very special people who have made my time here unforgettable. Thank you to Fernanda Costa, Inke Lubis, Ernest Diez Benavente, Lotus van den Hoogen, Gurdip Mann, Shiromani Jayawardhana and Archie Khan. Your friendship and support has helped me make it through this PhD in one piece. To James, this PhD brought us together and for that I am forever grateful.

To my mom, my dad, Daniela, Yamen, Salma, Leana, Granddad, Grandma and Omi thank you for your undying love and support, I couldn't have done this without each and everyone of you.

Contents

1	Introduction	13
1.1	Malaria as a global health problem	13
1.2	Malaria is caused by <i>Plasmodium parasites</i>	13
1.3	Life Cycle	14
1.4	Malaria control	19
1.4.1	Vector control strategies	19
1.4.2	Malaria Prevention	20
1.4.3	Diagnosis	23
1.4.4	Treatment	24
1.5	The molecular and cellular events that govern egress and invasion	25
1.5.1	Egress	26
1.5.2	Invasion	27
1.6	Signalling pathways coordinate key life cycle events	31
1.7	Cyclic nucleotide signalling	32
1.7.1	Adenylyl Cyclases	32
1.7.2	Guanylyl Cyclases	33
1.7.3	Phosphodiesterases	36
1.7.4	PKG	37
1.7.5	PKA	38
1.8	Calcium signalling	39
1.9	Signalling pathways as drug targets	41
1.10	Project aims and objectives	42
2	Methods	44
2.1	Parasite culture	44
2.1.1	Asexual stage culture	44
2.1.2	Gametocyte induction and culture	44
2.1.3	Inducing gametogenesis	44
2.1.4	Synchronisation	45
2.1.5	Preparation and purification of merozoites	45
2.1.6	Rapamycin treatment of parasites	45

2.1.7	Parasite transfection	45
2.1.8	Cloning parasites by limiting dilution	46
2.1.9	Drug cycling parasites	46
2.1.10	Preparing parasite samples for western blot and DNA extraction	46
2.2	Parasite Assays	46
2.2.1	SYBR Green growth inhibition assay	46
2.2.2	Fluorescence activated cell sorting (FACS) growth assays	47
2.2.3	Calcium release assays	47
2.2.4	Measurement of intracellular cAMP and cGMP levels	48
2.2.5	Egress timepoint assays	49
2.2.6	Extraction of proteins by their solubility profile	49
2.2.7	RNA extraction and reverse transcription quantitative PCR (RT-qPCR)	49
2.3	Microscopy	50
2.3.1	Imaging Giemsa-stained blood films	50
2.3.2	Live parasite imaging	50
2.3.3	Time-lapse video microscopy	51
2.3.4	<i>In vitro</i> motility assays	51
2.4	Immunochemistry	52
2.4.1	Immunofluorescence analysis (IFA)	52
2.4.2	Western blot analysis	53
2.5	Molecular biology techniques	54
2.5.1	Identifying Cas9 targeting sites	54
2.5.2	Primer design	54
2.5.3	Synthetic gene design	54
2.5.4	Polymerase chain reaction (PCR)	56
2.5.5	Restriction digests	56
2.5.6	Ligation-based cloning	56
2.5.7	Ligation-independent cloning	56
2.5.8	Transformation of chemocompetent bacteria	57
2.5.9	Plasmid DNA isolation	57
2.5.10	Sequencing of DNA	57
2.5.11	Parasite genomic DNA isolation	57

3	GCα is an essential "bifunctional" Guanylyl Cyclase expressed in the asexual blood stage	58
3.1	Results	58
3.1.1	GC α is expressed during the asexual blood stages of the life cycle	58
3.2	GC α is essential for asexual blood stage growth and is required for egress	63
3.2.1	GC α displays guanylyl cyclase activity and is responsible for cGMP production in asexual blood stages	70
3.2.2	Chemical complementation of GC α knockout parasites with PET-cGMP rescues the egress defect	73
3.2.3	The ATPase domain is essential for parasite survival	77
3.2.4	Functional analysis of the ATPase domain of GC α	80
3.3	Discussion	82
4	Inducible knockdown of Myosin A using the <i>glmS</i> ribozyme	84
4.1	Results	86
4.1.1	Generating conditional Myosin A knockdown parasite lines	86
4.2	Glucosamine displays toxicity when used at high concentrations	88
4.2.1	A partial knockdown of Myosin A results in a slight growth defect	89
4.3	Discussion	94
5	Myosin A is vital for blood stage merozoite invasion but is dispensable for gametocyte development and gametogenesis	95
5.1	Results	95
5.1.1	Generation of a <i>P. falciparum</i> Myosin A conditional knockout line	95
5.1.2	Myosin A is essential for parasite invasion but not egress	97
5.1.3	Deletion of Myosin A does not disrupt expression of other glideosome components or formation of the IMC	102
5.1.4	Genetic complementation of MyoA:mCherry:cKO parasites rescues the growth defect when the endogenous MyoA gene is deleted	104
5.1.5	Myosin A displays a striking stripy pattern in gametocytes	107
5.1.6	Myosin A is not required for gametocyte development or rounding up and emerging from RBCs during gametogenesis.	109
5.2	Discussion	111

6	PKG-dependent phosphorylation of Myosin A modulates motor activity and is important for efficient parasite growth	113
6.1	Results	114
6.1.1	Myosin A S19 is rapidly phosphorylated upon activation of PKG, achieving maximal levels of phosphorylation in merozoites	114
6.1.2	Introducing mutations into the endogenous Myosin A locus to mimic or ablate Myosin A S19 phosphorylation	117
6.1.3	Genetic complementation of MyoA:mCherry:cKO parasites with MyoA(S19A) or MyoA(S19D) leads to a significant growth defect in asexual blood stages	119
6.1.4	Phosphorylation of Myosin A modulates motor activity by increasing the motor speed	122
6.1.5	Motor activity is not altered when PKAc is knocked out	128
6.2	Discussion	129
7	Conclusions	132
7.1	GC α - a tale of two domains that cooperate to mediate asexual blood stage egress	133
7.2	Phosphorylation of Myosin A S19 puts the motor in "turbo" mode	135
7.3	Morphological changes observed during gametocyte development and gametogenesis do not require Myosin A	137
7.4	Final conclusions	138
8	Appendix	139
8.1	Failed approach used to generate <i>P. falciparum</i> lines which conditionally express MyoA harbouring mutations which ablate or mimic phosphorylation of MyoA S19.	141
9	References	146

Abbreviations

AC	adenylyl cyclase
ACT	artemisinin combination therapy
ADP	adenosine diphosphate
AMA	apicam membrane antigen
ARO	armadillo repeats only protein
ATP	adenosine triphosphate
BSA	bovine serine albumin
BSD	blasticidin S
BSDr	blasticidin S deaminase
C1	compound 1 or catalytic domain 1
C2	compound 2 or catalytic domain 2
cAMP	3',5'-cyclic adenosine monophosphate
Cas	CRISPR associated protein
CDC	cell division control
cDNA	complementary deoxyribonucleic acid
CDKP	calcium dependent protein kinase
cGMP	3',5'-cyclic guanosine monophosphate
CM	complete medium
CRISPR	clustered regularly interspaced short palindromic repeat
CSP	circumsporozoite protein
CyRPA	cysteine-rich protective antigen
DAG	diacylglycerol
DIC	differential interference contrast
DiCre	dimerizable Cre recombinase
DMSO	dimethyl sulphoxide
DNA	deoxyribonucleic acid
DOC2	double C2
DOZI	development of zygote inhibited
DPAP	dipeptidyl aminopeptidase
EBA	erythrocyte-binding antigen
EBL	erythrocyte-binding ligand

EC ₅₀	half maximal response
EDTA	ethylenediaminetetraacetic acid
ELC	essential light chain
ELISA	enzyme-linked immunosorbent assay
ER	endoplasmic reticulum
FACS	fluorescent activated cell sorting
FDA	food and drug administration
G6PD	glucose-6-phosphoate dehydrogenase
GAC	glideosome-associated connector
GAP	glideosome associate protein
GAPDH	glyceraldehyde 3-phosphate dehydrogenase
GC	guanylyl cyclase
gDNA	genomic deoxyribonucleic acid
GDV1	gametocyte development 1
GFP	green fluorescent protein
GlcN	glucosamine
GlcN6P	glucosamine-6-phosphate
GPA	glycophorin A
gRNA	guide ribonucleic acid
GTP	guanosine triphosphate
HA	haemagglutinin
hDHFR	human dihydrofolate reductase
hpi	hours post invasion
HRP	histidine-rich protein
ICAM-1	intracellular adhesion molecule 1
IFA	immunofluorescence assay
IMC	inner membrane complex
IP3	inositol 1,4,5-triphosphate
IPT	intermittent preventative treatment
IRS	indoor residual spraying
ITN	insecticide-treated bed nets
kb	kilo basepair
kDa	kilo daltons

MACS	magnetic cell separation
MDA	mass drug administration
ml	milliliter
mM	millimolar
mRNA	messenger ribonucleic acid
MSP	merozoite surface protein
MTIP	myosin tail interacting protein
MyoA	myosin A
nM	nanomolar
P4-ATPase	type IV P-type ATPase
PA	phosphatidic acid
Pb	<i>Plasmodium berghei</i>
PBS	phosphate-buffered saline
PBST	phosphate-buffered saline Tween-20
PCR	polymerase chain reaction
PDE	phosphodiesterase
Pf	<i>Plasmodium falciparum</i>
PfEMP1	Plasmodium falciparum erythrocyte membrane antigen 1
PfRipr	<i>Plasmodium falciparum</i> RH5-interacting protein
PhIL1	photosensitized 5[125I] idonaphthalene-1-azide labeled protein 1
PIP1	PhIL1 interacting protein
PIP2	inositol(4,5)-bisphosphate
PKA	cAMP-dependent protein kinase
PKAc	cAMP-dependent protein kinase catalytic domain
PKAr	cAMP-dependent protein kinase regulatory domain
PKG	cGMP-dependent protein kinase
PLC	phospholipase c
PMCA	plasma membrane Ca ²⁺
PMSF	phenylmethylsulfonyl fluoride
PPM	parasite plasma membrane
PS	phosphatidylserine
PTEX	<i>Plasmodium falciparum</i> translocon of exported proteins
PV	parasitophorous vacuole

PVM	parasitophorous vacuole membrane
RAP	rapamycin
RBC	red blood cell
RBCM	red blood cell membrane
RDT	rapid diagnostic test
RFP	red fluorescent protein
RH	reticulocyte-binding protein homologue
RNA	ribonucleic acid
ROM	rhomboid protease
RON	rhoptry neck protein
RT-qPCR	reverse transcription quantitative polymerase chain reaction
RyR	ryanodine receptor
S19	serine 19
S21	serine 21
SDS	sodium dodecyl sulphate
SERA	serine repeat antigen
SERCA	sarcoendoplasmic reticular Ca^{2+}
SIT	sterile insect technique
SMC	subpellicular membrane complex
SP	sulfadoxine/pyrimethamine
SUB	subtilising like serine protease
TACT	triple artemisinin combination therapy
TBV	transmission blocking vaccine
TSP	thrombospondin
U	units
UGO	unique guanylyl cyclase organiser
UTR	untranslated region
WGA	wheat germ agglutinin
XA	xanthurenic acid
yDHODH	yeast dihydroorotate dehydrogenase
μ l	microliter
μ M	micromolar
μ m	micrometer

1 Introduction

1.1 Malaria as a global health problem

Malaria, caused by protozoan parasites from the genus *Plasmodium*, is a mosquito-borne disease which remains a major health burden in many parts of the world including Sub-Saharan Africa, Southeast Asia and South America. In 2017 alone, malaria was responsible for an estimated 219 million cases and 435,000 deaths (WHO, 2018). Between 2000 and 2015, a steady decrease in malaria incidence and mortality rates was observed namely due to improved vector control, an essential component of malaria prevention (Bhatt et al., 2015); and the availability of artemisinin combination therapies (ACTs), the current first line treatment for malaria infections. However, progress against malaria has stalled in certain regions with some countries reporting increased cases (WHO, 2018). Furthermore, tremendous selection pressure on parasite and mosquito populations over the years has resulted in the emergence of resistance to antimalarials (Blasco et al., 2017) and insecticides (Hemingway et al., 2016; Kleinschmidt et al., 2018) respectively, thus threatening global initiatives to control, eliminate and eradicate malaria.

1.2 Malaria is caused by *Plasmodium* parasites

Plasmodium parasites are single-celled eukaryotes that belong to the Apicomplexa phylum (Levine, 1970); a diverse group of organisms, which also includes the parasites responsible for diseases such as babesiosis, cryptosporidiosis and toxoplasmosis. Apicomplexans are closely related to ciliates such as *Paramecium* and *Tetrahymena*, as well as dinoflagellates. Collectively they belong to the superphylum Alveolata which are highly divergent from model organisms such as yeast and mice.

Malaria is transmitted by the female mosquito of the genus *Anopheles*. Six species of *Plasmodium* are known to infect humans: *P. falciparum*, *P. vivax*, *P. malariae*, *P. ovale curtisi*, *P. ovale wallikeri* and *P. knowlesi*. Of these species, *P. falciparum* gives rise to the most severe disease manifestation and is responsible for the most fatalities. However *P. knowlesi* infections also have the potential to cause severe disease (Cox-Singh et al., 2008), owing to this species' ability to cause high parasitemia infections in a short period of time. While infections by the other species are rarely fatal, they cause considerable

morbidity.

These species have different but often overlapping geographical distributions, which are limited to areas where the environmental conditions allow for parasite replication in the *Anopheles* mosquito (Shapiro et al., 2017). *P. falciparum* predominates in Africa but is also found in South America and Asia. *P. vivax* is the most common species found in South America but also has a wide geographical spread similar to *P. malariae*. The remaining species occupy distinct niches with *P. ovale* subspecies limited to West Africa and the zoonotic *P. knowlesi*, which is transmitted from macaques, restricted to South-east Asia. As molecular diagnostic tools improve, it is becoming more apparent that some *P. ovale* and *P. malariae* infections have gone underdiagnosed in the past, while *P. knowlesi* infections have been misdiagnosed as *P. malariae* infections (Cox-Singh et al., 2008). Therefore there is a growing appreciation for non-falciparum malaria infections.

1.3 Life Cycle

The highly complex life cycle of *Plasmodium* species encompasses two hosts; the female *Anopheles* mosquito and a vertebrate host (Figure 1.1). When an infected mosquito takes a blood meal, it releases saliva containing haploid sporozoites into the host's skin (Sidjanski and Vanderberg, 1997). These motile forms utilise gliding motility (Montagna et al., 2012; Santos et al., 2017) to travel through the dermis and penetrate microvasculature including capillaries and lymphatic vessels (Vanderberg and Frevert, 2004; Amino et al., 2006; Hopp et al., 2015). The parasites then migrate to the liver where they invade hepatocytes (Frevert et al., 2005), initiating the asymptomatic pre-erythrocytic stage. The parasite, which resides within a parasitophorous vacuole (PV), then undergoes multiple rounds of non-synchronous nuclear replication termed schizogony. A plasma membrane (PM) forms around the nuclei giving rise to thousands of hepatic merozoites. *P. vivax* and *P. ovale*, are able to form dormant hypnozoites, which persist in the liver for long periods of time, eventually causing relapses several weeks, months or years later (Cogswell, 1992).

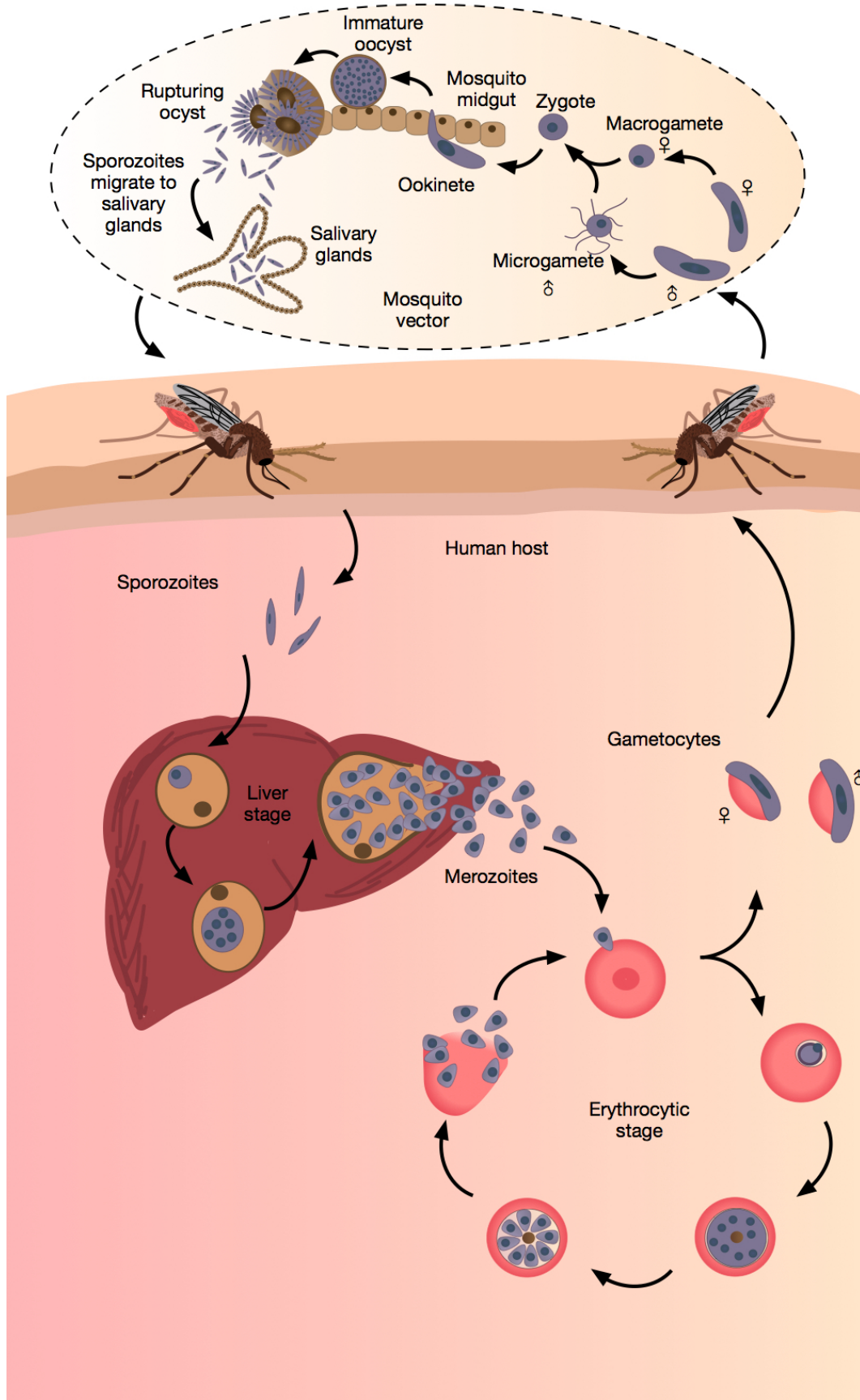


Figure 1.1. The *Plasmodium falciparum* life cycle.

The hepatic merozoites are released from the liver within host-derived vesicles called merosomes (Sturm et al., 2006), which protect the parasites from the host immune system. Once in the pulmonary capillaries, the merosomes rupture releasing the merozoites into the blood where they are able to rapidly invade erythrocytes, where they reside within a PV, and are termed ring-stage parasites due to their appearance in Giemsa-stained blood smears. The parasite then profoundly remodels the host cell by exporting proteins into the cytosol and onto the surface of the red blood cell (RBC), which allows the parasite to establish new permeability pathways for acquiring nutrients from the surroundings (Ginsburg et al., 1983). *P. falciparum* parasites are also able to avoid clearance by the spleen (Langreth and Peterson, 1985) by expressing adhesins such as members of the erythrocyte membrane protein 1 (PfEMP1) family on the surface of the RBC (Leech et al., 1984) that help the infected cell adhere to several endothelial receptors including CD36, thrombospondin (TSP) and intracellular adhesion molecule 1 (ICAM-1) (Pasloske and Howard, 1994; Baruch et al., 1996); and by exporting proteins which modify the erythrocyte cytoskeleton making the infected cell more rigid (Paulitschke and Nash, 1993; Dondorp et al., 2000).

The parasite then develops into a trophozoite which feeds on hemoglobin from the host cell (Goldberg et al., 1990), resulting in the liberation of free heme. Since free heme is toxic, it is detoxified and polymerised into crystalline hemozoin and stored in the food vacuole. Parasites eventually undergo further rounds of schizogony, producing a blood stage schizont containing between 16-32 nuclei (Janse et al., 1986). Budding of the plasma membrane and separation of the organelles results in the formation of merozoites. Around 48 hours post invasion for *P. falciparum* parasites, in a process termed egress, merozoites are released into the bloodstream where they rapidly reinvade RBCs, initiating the next asexual growth cycle. Successive cycles of egress and reinvasion result in the exponential proliferation of parasites. The molecular processes that govern egress and invasion will be discussed in further detail in section 1.5. It is during this asexual blood stage of the disease that the symptoms of malaria are observed; manifesting as flu-like symptoms, cyclical febrile episodes and fatigue (Bartoloni and Zammarchi, 2012). In more severe cases, complications can cause acute renal failure, cerebral malaria and severe anaemia and may eventually lead to death if left untreated (Idro et al., 2011).

In each cycle, a small proportion of parasites are able to exit asexual replication and commit to differentiation to the sexual stage of infection in a process termed gametocytogenesis, which results in the formation of male and female gametocytes. The sexually mature gametocyte is the only stage of the life cycle that can be transmitted to mosquitoes to establish an infection in the vector, however gametocytes represent a dead-end in the vertebrate host. Therefore there needs to be a balance between the production of asexual forms that sustain the infection, and the production of gametocytes which transmit the parasite to the mosquito where gamete formation and sexual reproduction occurs. Early work identified several factors that correlated with gametocyte formation in vitro including stress (Chaubey et al., 2014), nutrient availability (Brancucci et al., 2017) and high parasite burden (Bruce et al., 1990; Nacher et al., 2002). More recently, significant progress in understanding the genetic mechanisms underlying sexual commitment has been made. This process is regulated by the activation of AP2-G, a member of the ApiAP2 family of transcription factors, which triggers a transcriptional cascade that results in sexual commitment (Kafsack et al., 2014; Sinha et al., 2014). Expression of AP2-G is controlled by a protein called gametocyte development 1 (GDV1) (Eksi et al., 2012; Filarsky et al., 2018), however it is unknown how parasites regulate GDV1 expression to either induce or inhibit sexual commitment. Once an asexual parasite is sexually-committed, the parasite can either complete a replicative cycle to produce progeny that develop into gametocytes upon re-invasion, or can develop into a gametocyte within the same cycle (Bancells et al., 2019). The time required for gametocytes to complete development varies depending on the species; with *P. falciparum* gametocytes displaying the longest maturation period of 7-15 days (Hawking et al., 1971; Bousema and Drakeley, 2011). During this time, *P. falciparum* gametocytes undergo remarkable morphological changes categorised into distinct stages (I-V) shown in figure 1.2. Later stages adopt a crescent shape, unique to *P. falciparum*, which is driven by the assembly of the microtubular network and subpellicular membrane (Sinden, 1982; Dearnley et al., 2011; Parkyn Schneider et al., 2017), a membranous structure which is related to the inner membrane complex (IMC) in merozoites, ookinetes and sporozoites. This rigidity is thought to allow immature gametocytes (stages I-IV) to sequester in the bone marrow to avoid splenic clearance (Joice et al., 2014). Once mature, the microtubular network is disassembled (Dearnley et al., 2011), and stage V gametocytes are released from the bone marrow and are found circulating in the blood for up to 6 days (Bousema et al., 2010) where they can be taken up by a

mosquito during a blood meal.

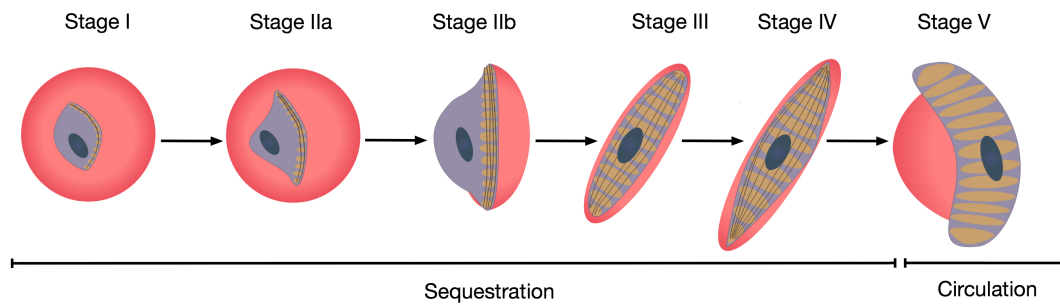


Figure 1.2. The stages of *Plasmodium falciparum* gametocyte development. The inner membrane complex (IMC), shown in orange, is deposited as 13 disk-like structures in gametocytes while the microtubule network, shown in brown, aligns on the IMC plates. As the gametocyte develops, the IMC plates extend laterally through the addition of membrane to the leading edges of the plates, eventually wrapping around the parasite. The microtubule network extends perpendicularly across the IMC plates, driving elongation of the gametocyte as it develops. In stage V gametocytes, the microtubule network is disassembled, while the IMC remains. Immature stage I-IV gametocytes are sequestered in the bone marrow, while mature stage V gametocytes are found circulating in the blood where they can be taken up by a feeding mosquito.

Once in the mosquito midgut, gametocytes are triggered to differentiate into gametes in response to environmental changes which include a drop in temperature coupled with either an increase in pH (Kawamoto et al., 1991; Billker et al., 1997) or exposure to xanthurenic acid (XA), a mosquito-derived molecule (Billker et al., 1998). Upon activation, both male and female gametocytes round up and emerge from the host RBC. The male gamete undergoes three rounds of DNA replication and mitosis (Janse et al., 1986) resulting in the formation of eight flagellated microgametes. Female gametogenesis on the other hand appears less dramatic, but involves the activation and translation of many transcripts which are transcriptionally repressed by the DDX6-type RNA helicase, development of zygote inhibited (DOZI) (Mair et al., 2007). In a process called exflagellation, the microgametes detach from the residual body and are able to fertilise female macrogametes to form a diploid zygote. The zygote then replicates its DNA to become tetraploid and develops into a motile ookinete which is able to traverse the midgut, eventually forming an oocyst which undergoes several rounds of replication. Uninuclear budding results in the formation of around 3,000 haploid sporozoites contained within the cyst (Janse et al., 1986; Rosenberg and Rungsiwongse, 1991). After 10-18 days, the oocyst ruptures, and motile sporozoites progress to the salivary glands where they mature and are able to be transmitted to the next vertebrate host when the female mosquito takes its next blood meal.

The ability to continuously culture *P. falciparum* (Trager and Jensen, 1976) and *P. knowlesi* (Moon et al., 2013; Lim et al., 2013) blood-stage parasites in human erythrocytes has greatly contributed to expanding our understanding of the biology of the parasite. Due to the difficulty of studying *P. falciparum* in the mosquito stages, much of our understanding of these stages comes from the use of mouse malaria models, including *P. berghei*, *P. yoelii* and *P. chabaudi*. Using animal models also allows for investigating the host-pathogen interactions such as immune responses and pathology during infection.

1.4 Malaria control

Several public health strategies are currently in place in order to prevent malaria transmission (WHO, 2018). These fall into four main categories which include vector control, malaria prevention, diagnosis and treatment. However, due to the highly adaptable nature of the parasites and the mosquito vectors, malaria control remains challenging. Ultimately, in order to effectively combat malaria, an integrated approach using a strategic combination of interventions will be required along with continued investment into the research and development of new tools.

1.4.1 Vector control strategies

Controlling mosquito populations is an integral part of malaria control, providing a highly effective method of disrupting transmission cycles and preventing malaria infection. Since mosquitos are vectors of other diseases such as zika, dengue, yellow fever and chikungunya; interventions that target mosquitos may also help protect against these diseases. The distribution of insecticide-treated bed nets (ITNs) and indoor residual spraying (IRS) have significantly contributed to reductions in malaria infections over the last 50 years (WHO, 2018). However, the expansion of mosquito populations resistant to pyrethroids (Hemingway et al., 2016; Kleinschmidt et al., 2018), the insecticide class used in ITNs, and other insecticides, presents a major obstacle to current vector control measures. Another issue is the behaviour of some *Anopheles* species, which tend to feed outdoors and/or bite during the day when people are not using ITNs (Steinhardt et al., 2017). Therefore new classes of insecticides are needed along with other interventions that target exophagic species that bite outdoors. It is becoming more apparent that tailored interventions, which are adapted to suit the behaviours of specific population groups, will

be required in order to make more effective use of current vector control measures (Nofal et al., 2019).

Another vector control measure is the treatment of humans with drugs that kill mosquitos when ingested during a blood meal. One example is Ivermectin, a well-tolerated and widely used broad-spectrum antihelminthic drug, which can also kill *Anopheles* mosquitos if a sufficient dose is ingested during a blood meal (Smit et al., 2018) and inhibit *P. falciparum* sporogony in surviving mosquitos (Kobylinski et al., 2012). A recent randomised clinical trial in Burkina Faso showed that mass drug administration (MDA) of Ivermectin resulted in a measurable reduction in malaria incidence (Foy et al., 2019).

Biocontrol strategies, which have proven effective at targeting mosquito populations, include the use of bacterial larvicides and the introduction of larvivorous fish which feed on mosquito larvae and pupae. A potential new biocontrol tool on the horizon is the use of *Wolbachia*, an endosymbiotic bacterium which can infect mosquitos, resulting in reduced *Plasmodium* oocyst density (Hughes et al., 2011; Shaw et al., 2016; Gomes and Barillas-Mury, 2018). The release of sterile irradiated male mosquitos known as the sterile insect technique (SIT), is another approach that can reduce mosquito numbers, however this method is laborious and will be difficult to implement globally (Lees et al., 2015). Recently, genetically modified *Anopheles* mosquitos harbouring a gene drive which results in the production of sterile females through inheritance bias, resulted in population collapse in a proof-of-principle lab-controlled experiment (Kyrou et al., 2018). Although this tool may be successful in eradicating certain *Anopheles* species, this may have broader ecological repercussions which must be considered before releasing mosquitos harbouring gene drives into the wild.

1.4.2 Malaria Prevention

Vaccines

Vaccines are arguably one of the most efficient and cost-effective ways of preventing or reducing the risk of contracting several infectious diseases including smallpox, polio, measles, shingles and rabies to name a few. The development of an efficacious malaria vaccine holds considerable promise in helping control malaria, yet despite decades of research a highly effective vaccine which provides long-lasting protection against the

parasite remains elusive (Draper et al., 2018). Although natural immunity to *Plasmodium* can be acquired in holoendemic areas through repeated exposure to the parasite, this does not confer complete protection but rather results in non-sterile immunity, where low level parasitemias persist in the absence of disease symptoms (Day and Marsh, 1991; Doolan et al., 2009). This partial immunity is short-lived, since in the absence of continued exposure to the parasite or during pregnancy, immunity is lost and formerly protected individuals become susceptible to the disease. These factors coupled with the complex life cycle and the antigenic diversity of the parasite (Anders and Smythe, 1989; Ferreira et al., 2004) have made developing an efficacious malaria vaccine challenging. Furthermore, several parasite antigens contain repetitive amino acid motifs, which may in-fact dampen immune responses (Davies et al., 2017). Current malaria vaccine efforts fall into three main categories which target different stages of the life cycle and include pre-erythrocytic vaccines, blood-stage vaccines, and transmission-blocking vaccines (TBVs).

Pre-erythrocytic vaccines, which generate an immune response targeting sporozoites, have been the most successful to date. Currently, the only licensed malaria vaccine candidate is RTS,S/AS01, a recombinant protein-based vaccine which directs an immune response against a subunit of the major circumsporozoite protein (PfCSP). Results from a Phase III clinical trial found that RTS,S/AS01 showed only moderate efficacy, reducing the incidence of clinical malaria by 39% after four doses (RTS, 2015). However, the partial immunity mediated by RTS,S/AS01 wanes over time and does not provide protection against *P. vivax*. Despite these shortcomings, the RTS,S/AS01 vaccine could provide an additional tool to use alongside other malaria control strategies, and may yield valuable insights upon which a next-generation vaccine can be designed. A pilot study is currently underway in three African countries to inform on the large scale implementation of RTS,S,AS01 (van den Berg et al., 2019). Currently, the only way to confer sterilising immunity is by immunising with developmentally attenuated whole sporozoites (Clyde et al., 1973; Hoffman et al., 2002). The PfSPZ vaccine, which consists of whole irradiated cryopreserved sporozoites, is currently undergoing Phase I clinical trials. Although highly efficacious in controlled human infections (Seder et al., 2013), results achieved in the field are considerably lower (Sissoko et al., 2017). It is possible that dose regimen optimisation may yield promising results (Ishizuka et al., 2016).

Blood-stage vaccines, which would target either infected RBCs or merozoites, would theoretically help reduce disease severity or parasite burden. Vaccines targeting infected RBCs include chemically attenuated whole-parasite blood-stage vaccines and subunits against VAR2CSA (Pehrson et al., 2017), an antigen expressed on surface of infected RBC that helps the parasite adhere to chondroitin sulfate A (CSA) and leads to sequestration in the placenta. Considerable effort has been invested into generating vaccines that block antigens found on the surface of merozoites from interacting with RBC receptors. Potential blood-stage antigens includes various merozoite surface proteins (MSPs), apical membrane antigen 1 (AMA1) and erythrocyte-binding antigen 175 (EBA175) to name a few. However, there are major obstacles to overcome with blood-stage vaccines, including antigenic diversity, the redundancy of invasion pathways and the short time that merozoites are exposed to the immune system. The identification of a non-redundant, highly conserved invasion ligand, reticulocyte-binding protein homologue 5 (Rh5) (Baum et al., 2009) which interacts with the basigin receptor on the surface of erythrocytes (Crosnier et al., 2012), has provided one of the most promising blood-stage vaccine candidates to date. Indeed, results from a Phase I study have shown promising results using an RH5-based vaccine which inhibited parasite growth in vitro and induced neutralising antimalarial antibodies in vaccinated individuals (Payne et al., 2017). Future Phase II testing will help determine the efficacy of this vaccine candidate.

Transmission-blocking vaccines (TBVs), which target the sexual stages of the life cycle, would not prevent infection or clinical manifestation of the disease in those vaccinated, but rather prevent parasite development within the mosquito, blocking onward transmission. Potential TBV antigens include Pfs25, found on the surface of zygotes and ookinetes; and Pfs230p and Pfs48/45, which are found on the surface of gametes (Kapulu et al., 2015). These antigens tend to be more conserved than blood-stage or pre-erythrocytic antigens, possibly due to limited immune pressure, therefore making attractive vaccine targets. Although TBVs have not progressed beyond Phase I trials, they could ultimately be very useful tools in low-transmission and elimination settings.

Chemoprophylaxis and preventative treatment

Antimalarial drugs such as atovaquone-proguanil, doxycycline and mefloquine can be taken to effectively prevent malaria infections. Although chemoprophylaxis is regularly

used by travellers visiting malaria endemic regions, it is rarely used to protect local populations; namely due to concerns regarding cost, sustainability, the potential emergence of wide-spread resistance and the loss of naturally acquired immunity (Greenwood, 2010). Instead, intermittent preventative treatment (IPT) is used on high risk populations in endemic regions including pregnant women, infants and children. This involves the administration of a curative dose of sulfadoxine/pyrimethamine (SP) (WHO, 2007), regardless of whether the individual is infected or not. However, the spread of resistance to SP, social factors that lead to poor adherence (Pell et al., 2011) and the high cost of IPT pose future concerns for its continued use (Parikh and Rosenthal, 2009).

1.4.3 Diagnosis

Malaria fatalities are preventable if detected and treated early. This relies on prompt and effective diagnostic techniques in often resource limited settings. The current gold standard for diagnosis involves identifying parasites by microscopy in thick or thin stained blood smears (Tangpukdee et al., 2009). However, this method requires considerable expertise, especially in successfully identifying malaria species. Alternatively, rapid diagnostic tests (RDTs), which can be used in rural settings and require minimal training, can also be used to rapidly and efficiently determine whether an individual has a malaria infection. RDTs react with malaria-specific antigens present in the blood, and can distinguish between *P. falciparum* and *P. vivax* infections. However, since some antigens used in RDTs, such as histidine-rich protein 2 (PfHRP2), are not essential for parasite survival, parasites possessing HRP2 deletions can result in false-negative RDTs (Beshir et al., 2017; Verma et al., 2018), potentially leading to the misdiagnosis of infections. RDTs also perform poorly on non-falciparum and non-vivax species (Tanizaki et al., 2014), therefore providing further limitations. Molecular diagnostic tools such as polymerase chain reaction (PCR) and loop-mediated isothermal amplification (LAMP) display high sensitivity, however these are not routinely used for diagnosis in the field. Similarly, serological tests including enzyme-linked immunosorbent assays (ELISAs) can be used as surveillance tools for identifying past infections and determining the transmission intensity of a certain region (Corran et al., 2007).

1.4.4 Treatment

Current drugs

Several drugs are available to treat malaria (WHO, 2018). Currently the first line treatment for malaria infections are ACTs, consisting of a potent fast-acting artemisinin derivative combined with a second less-potent slow acting partner drug. However, artemisinin resistant parasites, initially reported in Cambodia in 2008 (Noedl et al., 2008), are now widespread and have been reported in multiple countries in Southeast Asia including Vietnam, Laos and Thailand (Ashley et al., 2014). Although artemisinin resistance presents as a delay in parasite clearance rather than outright resistance, this facilitates the selection of partner drug resistance. As a result, not all parasites are cleared from the patient, leading to high treatment failures rates following treatment with ACTs.

The spread of drug resistance has been observed for several other drugs which were used prior to ACTs including chloroquine, SP, mefloquine, quinine and halofantrine (Ridley, 2002). With no alternative new therapies currently available for immediate use, the spread of artemisinin resistant parasites from Southeast Asia to Africa could lead to a public health disaster, reversing the progress made between 2000 and 2015. To delay this, existing drugs are currently being tested in triple artemisinin combination therapies (TACTs) in order to slow the evolution and spread of artemisinin resistance and prevent the concomitant development of partner drug resistance (Dini et al., 2018). This will be done using drugs that have opposing resistance mechanisms, such as artemether-lumefantrine and amodiaquine (Humphreys et al., 2007), to further suppress the emergence of drug resistance. Trials are currently underway in Cambodia and Vietnam to test the efficacy, safety and tolerability of TACTs (personal communication Tom Peto and Arjen Dondorp, Mahidol Oxford Research Unit).

Most antimalarials target the asexual blood stages of the infection, and are therefore unable to kill mature gametocytes and dormant *P. ovale* and *P. vivax* hypnozoites. Although primaquine can eliminate both gametocytes and hypnozoites; this drug can have life-threatening consequences if administered to individuals with glucose-6-phosphate dehydrogenase (G6PD) deficiency (Recht et al., 2018), an enzymopathy which is particularly prevalent among populations in malaria endemic regions (Howes et al., 2013). Therefore, even though primaquine is part of national treatment guidelines, it is not often

prescribed. Tafenoquine, which can also be used to treat *P. vivax* infections, has recently been approved by the United States food and drug administration (FDA). Although tafenoquine is also contraindicated in G6PD deficient individuals, it could be used as a single-dose treatment (Lacerda et al., 2019); unlike primaquine which has a much shorter half-life and requires a 14-day treatment course.

Approaches for developing new malaria chemotherapies

Due to the growing threat of the spread of artemisinin resistance and the lack of safe chemotherapies for clearing gametocyte and hypnozoite infections, there is an urgent need for the discovery of new antimalarial compounds to expand the arsenal of malaria chemotherapies available. This includes the development of drugs that can replace ACTs as the frontline treatment, prevent transmission by killing gametocytes and provide a radical cure to clear hypnozoites.

There are several approaches that can be used to identify and develop new drug candidates (Rosenthal, 2003; Flannery et al., 2003). Existing antimalarials can be improved upon by chemical modification of the compounds using medicinal chemistry-based approaches. This for example led to the development of chloroquine and mefloquine from quinine (Rosenthal, 2003) and could be used in the future to improve the potency, solubility and stability of potential drug candidates. Alternatively, phenotypic screens can also be conducted to test the effect of compounds developed for other diseases on parasite growth and survival (Hovlid and Winzeler, 2016). Since most of these drugs have already undergone clinical approval, it would therefore be inexpensive to repurpose them as antimalarials. Furthermore, this approach allows for the high throughput screening of compounds. Target-based drug discovery is another strategy that is increasingly being used for the development of antimalarial drugs (Flannery et al., 2003). This approach depends on broadening our understanding of the parasite's biology in order to identify and validate novel drug targets against which new drugs can be developed.

1.5 The molecular and cellular events that govern egress and invasion

Egress and invasion have been important areas of research due to the essential roles that they play during the blood-stages of the malaria life cycle. Since malaria pathology arises

due to successive rounds of parasite egress and invasion, understanding the mechanisms that underlie these processes will be important for developing new therapeutics, such as vaccines and novel drugs that target these stages.

1.5.1 Egress

Blood-stage egress is a rapid, tightly regulated process that results in the release of mature merozoites from infected erythrocytes. This is achieved by a co-ordinated series of proteolytic cleavage events, leading to the sequential rupture of the PVM, followed by the red blood cell membrane (RBCM) (Hale et al., 2017) as shown in figure 1.3.

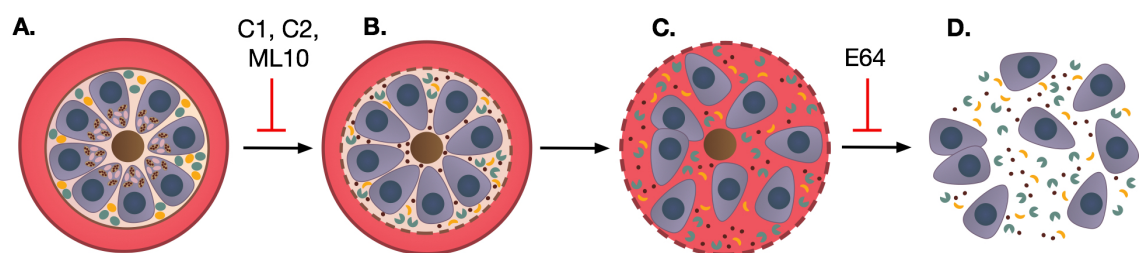


Figure 1.3. Schematic of the molecular events leading to merozoite egress from the erythrocyte. **A.** Exonemes (brown) storing SUB1 and micronemes (pink) are released by the merozoite. This can be blocked by adding PKG-specific inhibitors such as C1, C2 or ML10. **B.** SUB1 cleaves several substrates including SERA5 (yellow) and SERA6 (green) and the PVM becomes porated. **C.** The PVM ruptures and the RBCM becomes porated. **D.** The RBC ruptures, releasing merozoites into the supernatant. This can be inhibited by adding E64.

Just prior to egress, the contents of specialised apical organelles called micronemes and exonemes, are released onto the surface of the merozoite and into the PV, respectively. The discharge of these organelles is mediated by cyclic guanosine monophosphate (cGMP)-dependent protein kinase (PKG) (Collins et al., 2013b), which will be discussed in further detail in section 1.7.4. However the natural egress signal, which culminates in the activation of PKG remains unknown. Inhibition of PKG with selective adenosine triphosphate (ATP)-competitive inhibitors, including compound 1 (C1) (Gurnett et al., 2002), compound 2 (C2) (Donald et al., 2006) and ML10 (Baker et al., 2017b); can block egress by preventing microneme and exoneme discharge. Exonemes are responsible for the release of subtilisin like serine protease (SUB1) into the PV, while micronemes release several proteins including erythrocyte binding antigen 175 (EBA175) and apical membrane antigen 1 (AMA1), which play important downstream roles in invasion. Both AMA1 and SUB1 are proteolytically processed by plasmepsin X, a protease which plays an essential role in the maturation and or activation of both these proteins (Pino et al., 2017;

Nasamu et al., 2017). Once released into the PV, SUB1 processes several proteins including MSP1 (Koussis et al., 2009), as well as SERA5 and SERA6 (Yeoh et al., 2007; Ruecker et al., 2012), which are members of the serine repeat antigen (SERA) family of cysteine-like proteases. Although SUB1 release results in RBCM poration and the disruption of the PVM (Thomas et al., 2018), the mechanisms behind this remain unclear.

Once the PVM ruptures, the parasites are released into the RBC cytosol where merozoite surface-bound processed MSP1 is able to bind to and destabilise the erythrocyte spectrin cytoskeleton (Das et al., 2015). Cleavage of β -spectrin by the catalytically active SERA6 leads to further disruption of the cytoskeleton and results in disruption of the RBCM. The cysteine protease inhibitor E64, which is believed to inhibit SERA6, inhibits RBCM rupture once the PVM has ruptured (Hale et al., 2017). Proteases found in the erythrocyte, such as calpain-1, which is activated by elevated levels of calcium, are also involved in facilitating parasite egress (Chandramohanadas et al., 2009). Unlike SERA6; SERA5 does not display any proteolytic activity, due to the substitution of the catalytic cysteine for a serine residue (Stallmach et al., 2015). However, SERA5 plays an important role in regulating the kinetics of egress, since disruption of SERA5 results in the premature and inefficient egress of merozoites (Collins et al., 2017). Finally, once the RBCM ruptures, merozoites are released into the blood stream where they are able to invade erythrocytes to initiate another replicative growth cycle.

1.5.2 Invasion

Upon release into the blood stream, merozoites quickly identify and invade erythrocytes (Figure 1.4). The initial attachment of merozoites to RBCs is believed to be mediated by various MSPs however, the receptors that MSPs bind to remain elusive. The cysteine protease dipeptidyl aminopeptidase 3 (DPAP3) is also involved in mediating initial attachment to the RBC (Lehmann et al., 2018). Upon initial contact, the parasite induces weak deformations in the erythrocyte (Weiss et al., 2015) and utilise another subset of specialised apical organelles called rhoptries; resulting in the release of adhesins which are concentrated at the apical end on the surface of the merozoite. The maturation of rhoptry proteins, including rhoptry associated protein 1, is mediated by plasmepsin IX and is essential for invasion (Pino et al., 2017; Nasamu et al., 2017). Two classes of merozoite adhesins are involved in tight attachment to the erythrocyte including the reticulocyte

binding-like homologous proteins (RHs) which are rhoptry-derived; and the erythrocyte-binding antigens or ligands (EBAs or EBLs) which are micronemal proteins. These adhesins play an essential role during invasion by binding to receptors on the surface of the erythrocyte, however there is redundancy between invasion pathways (Lopaticki et al., 2011). One exception is RH5 (Baum et al., 2009), which binds to the basigin receptor on the surface of the erythrocyte (Crosnier et al., 2012) and is the only non-redundant ligand required for invasion. This interaction results in the formation of a pore between the parasite and erythrocyte (Weiss et al., 2015; Volz et al., 2016) and the release of the contents of the rhoptry bulb (Weiss et al., 2015). RH5 forms a complex with PfRH5-interacting protein (PfRipr) and cysteine-rich protective antigen (CyRPA) (Chen et al., 2011; Reddy et al., 2015). Although PfRipr and CyRPA do not bind to the erythrocyte, they play a role in establishing tight junction formation (Volz et al., 2016). Upon tight attachment, the parasite induces strong deformations in the RBC (Weiss et al., 2015) and is able to reorientate itself such that the apical end is facing the erythrocyte membrane. The rhoptry neck (RON) protein RON2, which is injected into the surface of the erythrocyte, forms a complex with RON4 and RON5 (Cao et al., 2009). RON2 binds to AMA1 on the surface of the parasite (Cao et al., 2009; Lamarque et al., 2011), marking the tight junction and committing the parasite to invasion (Srinivasan et al., 2011). Ligand-receptor interactions, such as EBA175 binding to glycophorin A (GPA) on the RBC surface, also mediate changes in the biophysical properties of the host cell, priming the erythrocyte for invasion (Koch et al., 2017).

The parasite then pushes its way into the RBC via substrate-dependent motility powered by the glideosome (Figure 1.5), which is localised between the parasite plasma membrane (PPM) and IMC. The glideosome consists of a class XIV actomyosin motor, Myosin A (MyoA) (Pinder et al., 1998), essential light chain (ELC) (Green et al., 2017; Bookwalter et al., 2017), Myosin A-tail interacting protein (MTIP) (Bergman, 2003); known as ELC1 in *Toxoplasma*, and the glideosome-associated proteins GAP40, GAP45 and GAP50 (Baum et al., 2005; Fréchal et al., 2010; Gaskins et al., 2004). MTIP and ELC bind to the tail region of MyoA (Green et al., 2006) and recruit it to GAP45, which tethers the PPM to the IMC (Rees-Channer et al., 2006). This complex then interacts with the integral IMC proteins GAP50 and GAP40 to form the assembled glideosome (Gaskins et al., 2004). Force generated by the motor translocates actin filaments tethered to extracellular receptors via the glideosome-associated connector (GAC) (Jacot et al., 2016) rearwards towards the

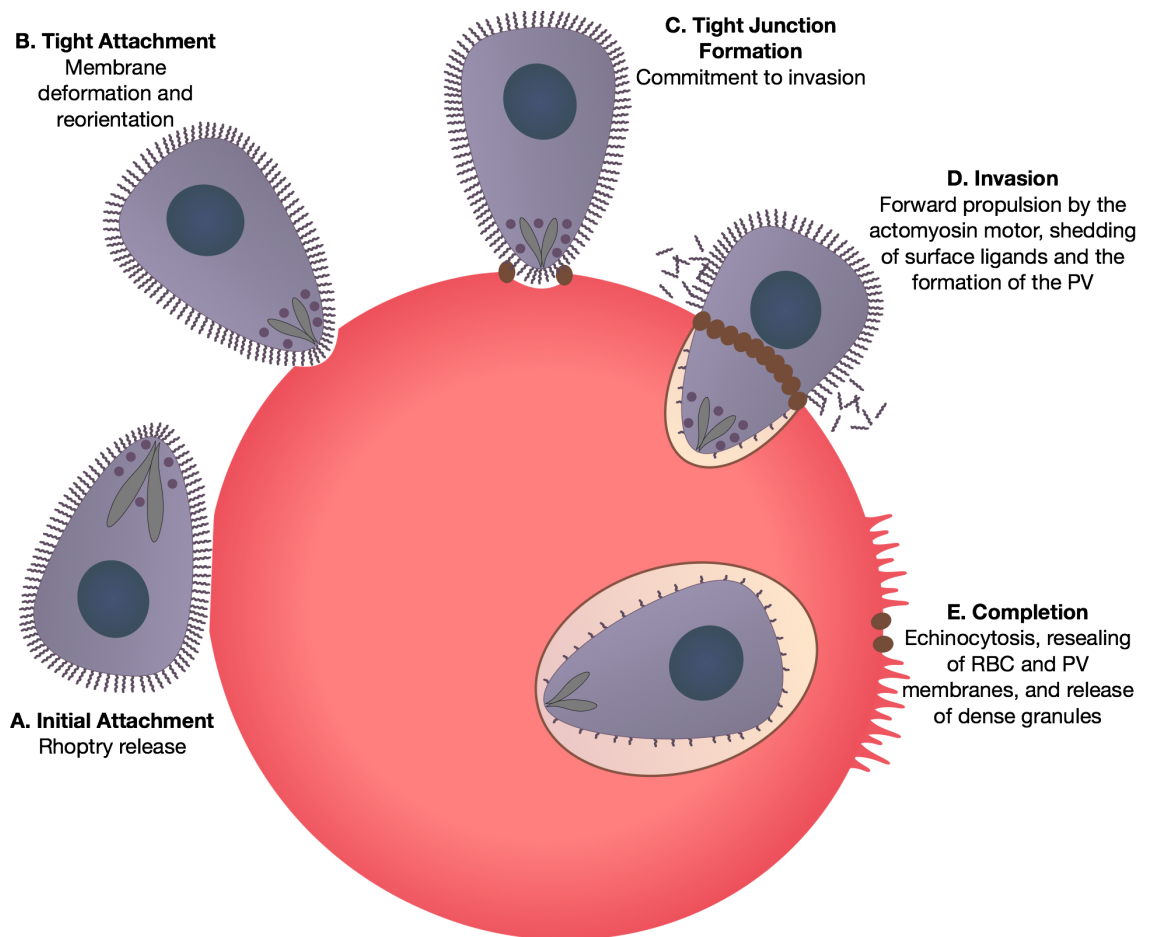


Figure 1.4. Schematic of merozoite invasion. **A.** The parasite forms initial attachment to the RBC which can occur in any orientation. This triggers the secretion of the rhoptries. **B.** The merozoite forms tight attachment via interactions between EBL and RH proteins and ligands on the surface of the RBC. The merozoite deforms the RBC as it reorientates itself. **C.** The tight junction forms, making a molecular seal between the parasite and the RBC. **D.** As the merozoite pushes itself into the RBC by force generated by the actomyosin motor, adhesins on its surface are shed by several proteases. **E.** The RBC reseals its membrane and undergoes echinocytosis once the parasite has fully invaded. The parasite secretes dense granules shortly after invasion is complete.

basal end of the parasite. This results in the forward propulsion of the parasite into the erythrocyte. Disruption of the actin cytoskeleton with compounds such as cytochalasin B, cytochalasin D or jasplakinolide prevents deformation of the RBC (Weiss et al., 2015) and parasite invasion (Miller et al., 1979; Mizuno et al., 2002) suggesting that the actomyosin motor is involved in this process. The role of the glideosome in invasion was definitively shown by the conditional deletion of MyoA (Robert-Paganin et al., 2019) and GAP45 (Perrin et al., 2018). Parasites lacking either of these glideosome components were able to egress, but remained attached to the erythrocyte and were unable to deform the cell or invade.

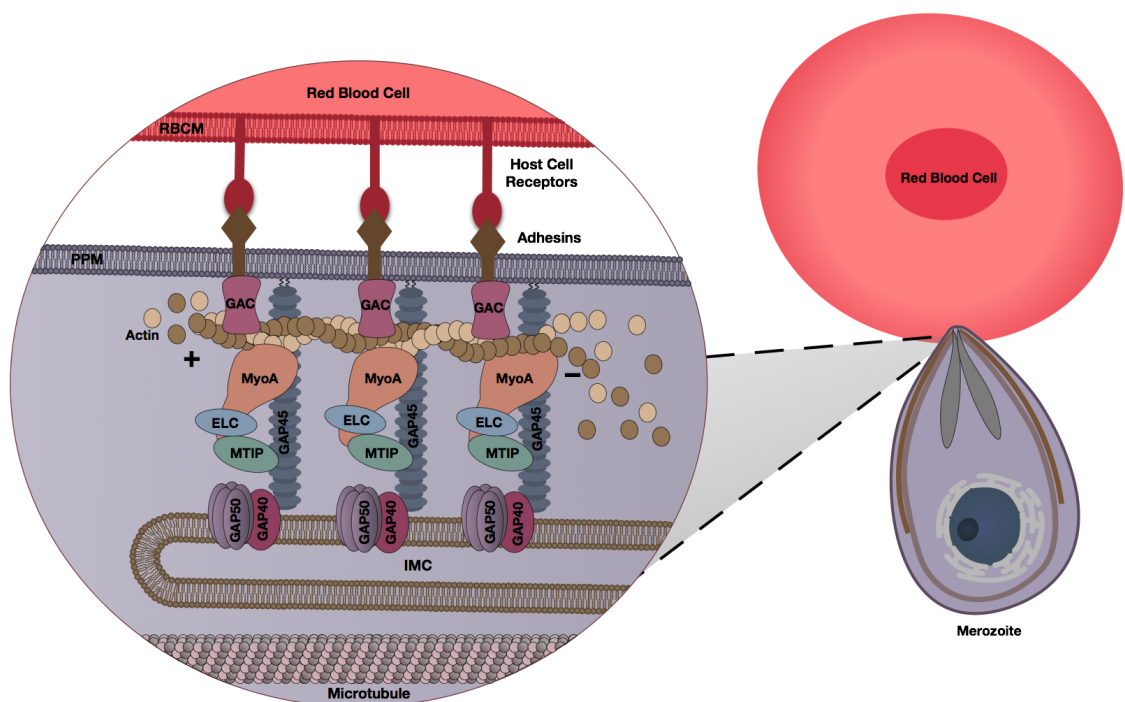


Figure 1.5. Schematic representation of the glideosome in *P. falciparum* merozoites.

Located at the parasite periphery, the glideosome is required for generating the force required for *Plasmodium* merozoite invasion of RBCs and also generates gliding motility seen in other Apicomplexans. It comprises MyoA, MTIP, ELC, GAP40, GAP45 and GAP50 which are anchored in the IMC. The glideosome generates force by propelling f-actin, which in turn is linked to adhesins on the surface of the parasite via GAC, to the posterior end of the parasite.

As the parasite pushes its way into the erythrocyte, it forms the PV and PVM which is made primarily from lipids stored in the rhoptry bulb, however it is possible that RBC-derived lipids also contribute to the PVM (Sherling and van Ooij, 2016). As the tight junction moves over the merozoite, rhomboid proteases (ROM1 and ROM4) cleave proteins on the surface of the merozoite such as EBA175 and AMA1 within their transmembrane

domains (O'Donnell et al., 2006; Olivieri et al., 2011), shedding them into the supernatant. SUB2, also acts as a sheddase, cleaving proteins such as AMA1 as it translocates from the apex to the basal end of the merozoite (Harris et al., 2005; Child et al., 2013). Once the parasite is fully within the erythrocyte, the RBC undergoes echinocytosis, which is characterised by small unevenly distributed projections giving it a spiky appearance, which is thought to trigger resealing of the RBCM (Gilson and Crabb, 2009). Once invasion is complete, the parasite secretes another set of specialised secretory organelles called dense granules. Dense granules contain several components of the *Plasmodium* translocon of exported proteins (PTEX) complex (Bullen et al., 2012), which is found in the PVM and is involved in exporting proteins from the PV into the erythrocyte (de Koning-ward et al., 2009; Elsworth et al., 2014; Beck et al., 2014).

1.6 Signalling pathways coordinate key life cycle events

Cell signalling pathways orchestrate fundamental processes required for cell survival by allowing cells to sense their surroundings and mediate internal responses. Usually, this requires a receptor found at the cell plasma membrane, which can bind extracellular signalling molecules or ligands. Once the receptor is activated, it is able to trigger a cascade of events that leads to a cellular response. 3',5'-cyclic adenosine monophosphate (cAMP), 3',5'-cyclic guanosine monophosphate (cGMP), calcium (Ca^{2+}), inositol 1,4,5-triphosphate (IP_3) and diacylglycerol (DAG), act as second messengers, amplifying the signal cascade by activating proteins or by opening ion channels. Phosphorylation is an important reversible post-translational modification, which plays a central role in signal transduction pathways, and is mediated by kinases and phosphatases, which phosphorylate and dephosphorylate proteins, respectively. Phosphorylation introduces a charged hydrophilic group to amino acid residues, potentially changing a protein's structure or producing binding sites to interact with other proteins. As a result, this can modulate the activity of a protein or modify its function. Cross-talk between different signalling pathways allows cells to integrate several signals to form complex signalling networks. Tight spatiotemporal coordination of key stages throughout the malaria life cycle is achieved through intracellular signal transduction pathways such as cyclic nucleotide, phosphoinositide and calcium signalling.

1.7 Cyclic nucleotide signalling

cGMP and cAMP signalling are known to regulate a wide range of processes including retinal phototransduction (Zhang and Cote, 2005), chemotaxis (Loomis, 2014), and smooth muscle relaxation (Eckly-Michel et al., 1997) to name a few. Adenylyl cyclases (ACs) catalyse the formation of cAMP from adenosine triphosphate (ATP), while guanylyl cyclases (GCs) catalyse the formation cGMP from guanosine triphosphate (GTP). Cyclic nucleotides are hydrolysed and inactivated by phosphodiesterases (PDEs), which can be dual- or mono-specific. The level of cyclic nucleotide in the cell is tightly regulated by the opposing activity of cyclases and PDEs. However, once the level of cyclic nucleotide reaches a critical threshold within the cell, cAMP and cGMP activate their respective kinases, cAMP-dependent protein kinase (PKA) and cGMP-dependent protein kinase (PKG). These serine/threonine kinases are then able to phosphorylate many downstream targets, initiating a cascade of events that culminate in a cellular response. *Plasmodium* parasites encode components of both cAMP and cGMP signalling pathways including two ACs, two GCs, four PDEs, one PKG and both the catalytic and regulatory subunits of PKA (Baker et al., 2017a).

1.7.1 Adenylyl Cyclases

Plasmodium parasites encode two ACs; AC α (PF3D7_1404600) and AC β (PF3D7_0802600), which are structurally divergent from mammalian ACs and from each other (Baker and Kelly, 2004). AC α contains 6 N-terminal transmembrane domains, which share homology with voltage-gated potassium (K⁺) channels; and a single C-terminal catalytic domain which contains all the canonical residues required for cAMP synthesis. In order to form a functional AC, it must homodimerize to form an active catalytic site. Although the cAMP activity of PfAC α has been confirmed by expression in *Dicyostelium* and *Xenopus* oocytes (Muhia et al., 2003), the activity of the putative voltage-gated potassium channel has not yet been demonstrated (Weber et al., 2004). Work on an AC found in *Paramecium*, which possesses similar domain architecture to AC α , has demonstrated that it acts as both a voltage-gated potassium channel and an adenylyl cyclase (Schultz et al., 1992). Therefore it is possible that the seemingly bifunctional nature of AC α -could couple changes in environmental ion concentrations to cAMP production (Baker and Kelly, 2004). AC α can form several splice variants with varying numbers of trans-

membrane domains (Muhia et al., 2003), however it remains unclear whether these splice variants are translated. It is maximally transcribed in stage V gametocytes, however transcripts can also be detected in ookinetes and sporozoites (López-Barragán et al., 2011; Zanghì et al., 2018). *AC α* -deficient *P. berghei* parasites show normal blood-stage growth and development in the mosquito, however sporozoites show reduced infectivity of cultured hepatocytes and mice due to the inability to secrete apical organelles (Ono et al., 2008).

AC β (PF3D7_0802600) is a soluble cyclase, with two pseudosymmetrical catalytic domains, and is an orthologue of bicarbonate-sensitive mammalian soluble ACs. High levels of mRNA can be detected in blood-stage schizonts (Salazar et al., 2012). Recent work has confirmed that *AC β* is the only AC capable of producing cAMP in blood-stage *P. falciparum* parasites and demonstrated that it is essential for merozoite invasion of erythrocytes, however *AC β* -null parasites also showed an egress delay (Patel et al., 2019). Pf*AC β* colocalises with armadillo repeats only protein (ARO) (Patel et al., 2019), indicating localisation to the rhoptries (Cabrera et al., 2012). In *Toxoplasma*, ARO mediates apical localisation of rhoptries (Mueller et al., 2013), however whether it performs a similar function in *Plasmodium* remains to be determined.

The only predicted cAMP effectors encoded by *Plasmodium* parasites are PKA and a protein called Epac that contains putative cAMP-binding domains. Although previous reports suggest that Epac is involved in the release of calcium and micronemes from merozoites and is required for invasion (Dawn et al., 2014), Epac can be knocked out and is not required for asexual growth in *P. falciparum* (Patel et al., 2019) and readily undergoes truncation in culture adapted isolates (Claessens et al., 2017). Therefore although Epac is not required for in vitro growth, it remains unclear whether it is essential for other stages of the life cycle.

1.7.2 Guanylyl Cyclases

Plasmodium falciparum encodes two guanylyl cyclases; *GC α* (PF3D7_1138400) and *GC β* (PF3D7_1360500), which are closely related to one another (Carucci et al., 2000). They are large integral membrane proteins which display a number of unusual characteristics. The GC domains consist of two catalytic domains (C1 and C2), each preceded by a

set of 6 transmembrane domains. Although the catalytic domains share structural homology to mammalian G-protein dependent adenylyl cyclases, the purine-binding residues are consistent with those found in GCs rather than ACs. The GC activity of GC β has been confirmed by recombinant expression of the catalytic domains in *E. coli* (Carucci et al., 2000), however neither AC nor GC activity have been demonstrated for GC α , but the presence of purine-binding residues that are characteristic of GCs strongly suggests that like GC β , GC α is a functional GC. Remarkably, the N-terminal portion of *Plasmodium* GCs contain a P-Type ATPase-like domain which contains a further 10 transmembrane domains. The functional role of the ATPase remains unknown, and although it resembles calcium transporting ATPases, key residues required for ion transport are absent (Baker and Kelly, 2004). Instead, it has been suggested that this domain may be involved in phospholipid transfer as the ATPase shares closest homology to aminophospholipid flippases (type IV ATPases) and therefore could be involved in regulating phosphatidylserine (PS) or phosphatidylethanolamine (PE) asymmetry across the membrane in which it is located; or it may also play a role in regulating the activity of the GC domain. In other organisms, type IV ATPases form complexes with cell division control 50 (CDC50) proteins, which are required for correct trafficking from the ER to the PM (Andersen et al., 2016). Therefore it is likely that *Plasmodium* GCs form an interaction with CDC50 proteins; three of which are encoded by the parasite. The bifunctional nature of *Plasmodium* GCs is conserved in alveolates, including other apicomplexans such as *Toxoplasma* and the ciliates *Paramecium* and *Tetrahymena* (Linder et al., 1999), which may signify a functional link between these two domains. The transcriptional profiles of GC α and GC β vary across the different stages of the *P. falciparum* lifecycle (López-Barragán et al., 2011; Zanghì et al., 2018). While GC α is maximally transcribed in late trophozoites and schizonts, with transcripts also detected in gametocytes and ookinetes; GC β transcripts are found at low levels during the asexual stages and predominate in stage V gametocytes and ookinetes.

GC β knockout lines have been generated in *P. falciparum*, *P. berghei* and *P. yoelii*, with no phenotype observed up to and including gametocytogenesis (Hirai et al., 2006; Taylor et al., 2008; Moon et al., 2009; Gao et al., 2018). However, in *P. berghei* and *P. yoelii*, ookinete motility and mosquito midgut invasion were impaired (Hirai et al., 2006; Moon et al., 2009; Gao et al., 2018). In *P. yoelii* GC β localises to a site posterior to the apical structure in the plasma membrane of mature ookinete where it creates local elevated

levels of cGMP, activating PKG and stimulating ookinete gliding (Gao et al., 2018). This study also revealed that the ATPase domain of GC β , which is a pseudo ATPase since it lacks several residues required for ATPase activity, is required for the correct localisation of the GC domain to stimulate ookinete motility. Interaction between GC β and CDC50.A is also required for cGMP production, since the latter acts as a chaperone which stabilises GC β (Gao et al., 2018).

Although recent whole genome screens in *P. falciparum* (Zhang et al., 2018) and *P. berghei* (Bushell et al., 2017) indicate that GC α is dispensable for asexual growth, repeated attempts to disrupt GC α in both these species have been unsuccessful, suggesting an essential function during the asexual blood stage (Taylor et al., 2008; Moon et al., 2009; Kenthirapalan et al., 2016). Using an antibody raised against the C2 domain of GC α , the protein was detected by immunoelectron microscopy in the parasitophorous vacuole (PV) or plasma membrane region of gametocytes, however it was not detected in schizonts (Carucci et al., 2000) despite being the only predicted GC expressed during the blood-stages. *P. falciparum* gametocyte membrane fractions display GC activity, which is further stimulated by the addition of XA (Muhia et al., 2001). Further work will be required to validate whether GC α is required for cGMP production in schizonts and to determine the functional role of the ATPase domain.

Recent work in *Toxoplasma gondii* has shed further light on the unique biology of apicomplexan GCs. *Toxoplasma* encodes a single GC, which shares greater homology to *Plasmodium* GC α , and localises to the PM at the basal and apical ends of the tachyzoites (Jia et al., 2017; Brown and Sibley, 2018; Yang et al., 2019; Günay-Esiyok et al., 2019). Conditional knockdown of TgGC revealed that it is responsible for cGMP production which is required for parasite egress, calcium release, microneme exocytosis, motility, host cell attachment and invasion. TgGC requires interaction with a CDC50 protein in addition to unique GC organiser (UGO), which act as chaperones for the ATPase and GC domains, respectively (Bisio et al., 2019). The ATPase domain is required for targeting TgGC to the apical end of the parasite (Brown and Sibley, 2018) and mutagenesis of key residues required for ATPase activity inhibit microneme release and lytic growth (Brown and Sibley, 2018; Bisio et al., 2019). GC-mediated phospholipid flipping activity could not be detected (Bisio et al., 2019), however TgGC seems to be involved in sensing extracellular pH

and K⁺ levels (Yang et al., 2019) as well as phosphatidic acid (PA) (Bisio et al., 2019), all of which are able to trigger Ca²⁺ release.

1.7.3 Phosphodiesterases

The *Plasmodium* genome encodes 4 PDEs (α , β , γ and δ), all of which contain up to six N-terminal transmembrane domains and a C-terminal catalytic domain which can be either dual specific or show selective cGMP hydrolytic activity. *Plasmodium* PDEs are expressed at specific stages of the life cycle, with PDE α (PF3D7_1209500) and PDE β (PF3D7_1321500) transcripts predominantly found in schizonts, PDE γ (PF3D7_1321600) in sporozoites and PDE δ (PF3D7_1470500) in gametocytes (López-Barragán et al., 2011; Zanghì et al., 2018). PDE inhibitors such as Zaprinast and BIPPO show activity against *Plasmodium* PDEs, and have been useful tools for studying cyclic nucleotide signalling in the parasite.

PDE β is the only PDE required for asexual growth. Conditional deletion of PfPDE β results in a premature rise in cAMP levels in schizonts, leading to hyper-activation of PKA which leads to dysregulated phosphorylation of several substrates and a severe invasion defect (Flueck et al., 2019). Although a small proportion of PDE β -null parasites were able to invade, they were unable to develop and died shortly post-invasion. PDE assays on affinity-purified PDE β showed that it can hydrolyse both cAMP and cGMP (Flueck et al., 2019), while PDE α is only capable of hydrolysing cGMP, and is not required for asexual growth (Wentzinger et al., 2008). Deletion of PDE γ in *P. yoelii* had a mild affect on asexual growth resulting in a 2-fold reduction in parasitemia, but did not affect gametocyte development or sporozoite formation. However PDE γ -deficient sporozoites exhibited elevated levels of cGMP and impaired substrate-dependent gliding motility which impaired their ability to infect salivary glands in mosquitos (Lakshmanan et al., 2015). Since cAMP levels were not measured in PDE γ -null parasites, it remains unclear whether it is a dual specific PDE. Both *P. falciparum* and *P. berghei* PDE δ knockouts have been generated, demonstrating that it is not required for asexual growth (Taylor et al., 2008; Moon et al., 2009). In *P. falciparum*, PDE δ -deficient gametocytes were able to develop normally, but displayed a significant increase in cGMP levels and impaired gametogenesis upon stimulation with XA (Taylor et al., 2008). These parasites were able to round up, but could not emerge from the erythrocyte and male gametes displayed reduced exflagellation. In con-

trast, *P. berghei* PDE δ -deficient parasites were able to undergo gametogenesis normally, however ookinete development was severely affected whereby ookinetes dedifferentiated into stumpy forms that did not display gliding motility (Moon et al., 2009).

1.7.4 PKG

Plasmodium species encode a single PKG (PF3D7_1436600), which is the only known cGMP effector protein in the parasite. Unlike mammalian PKGs, which possess two cGMP-binding domains and are able to form dimers, *Plasmodium* PKG is expressed as a monomer, consisting of an N-terminal regulatory domain and a C-terminal catalytic domain which contains four cGMP-binding domains (A, B, C and D) (Deng and Baker, 2002). However, only three of these domains display cGMP binding, since domain C is degenerate (Deng et al., 2003). At low concentrations of cGMP, PKG is inactive due to the docking of an autoinhibitory segment to the kinase domain (Bakkouri et al., 2019). When cGMP levels rise, cooperative binding of cGMP results in a series of conformational changes that leads to the release of the autoinhibitory segment to expose the active site, and the formation of a capping triad which stabilises the active form of the protein (Kim et al., 2015). Once activated, PKG can bind to and phosphorylate substrates.

PKG is maximally transcribed in schizonts, however transcripts can also be detected in gametocytes and ookinetes (López-Barragán et al., 2011; Zanghì et al., 2018). PKG is refractory to deletion in both *P. falciparum* and *P. berghei*, suggesting an essential role during the blood-stage of infection. However, highly specific reversible ATP-competitive inhibitors of PKG, including C1 (a pyrrole) (Gurnett et al., 2002) and C2 (an imidazopyridine) (Donald et al., 2006) mentioned previously, have been instrumental in elucidating the precise role of PKG throughout the life cycle. In apicomplexan PKGs, the gatekeeper residue of the ATP-binding site is a small threonine residue, which accommodates the binding of these inhibitors. However, mammalian PKGs possess a bulkier gatekeeper residue, preventing these inhibitors from accessing the gatekeeper pocket. Substitution of the gatekeeper residue with a bulkier glutamine residue (T618Q) renders transgenic parasites resistant to both inhibitors (McRobert et al., 2008; Brochet et al., 2014). The use of these inhibitors in conjunction with wild type and PKG(T618Q) transgenic parasites confirmed that PKG is the primary target of these inhibitors, however there is evidence that C2 can also target calcium-dependent protein kinase (CDPK4) (McRobert et al.,

2008; Fang et al., 2018), which also harbours a small gatekeeper residue adjacent to the ATP-binding site.

In schizonts, PfPKG is mainly cytosolic with a small subpopulation that also associates with the endoplasmic reticulum (ER) (Hopp et al., 2012). Treatment with C2 or the destabilisation of PKG blocks merozoite egress (Collins et al., 2013b; Ganter et al., 2017). These parasites are unable to undergo microneme and exoneme secretion, and are unable to disrupt the PV (Hale et al., 2017). C2 treatment also prevents the hydrolysis of IP3 and the release of calcium from internal stores (Brochet et al., 2014). Quantitative global phosphoproteomics of C2-treated WT and PKG(T618Q) parasites identified 69 proteins that are phosphorylated in a PKG-dependent manner (Alam et al., 2015). These proteins are involved in diverse cellular processes including egress, invasion, motor function, transcriptional regulation and proteolysis. Furthermore, several PKG-dependent phosphosites were identified in AC β , GC α and PDE β , possibly pointing towards a feedback loop between components of cAMP and cGMP signalling (Baker et al., 2017a). However, the exact role of these phosphorylation events in mediating egress and invasion remain unclear.

In gametocytes, XA-mediated rounding up and emergence from the host erythrocyte is PKG-dependent and also acts upstream of calcium release, which is essential for exflagellation (McRobert et al., 2008; Brochet et al., 2014). The inhibition of PKG also blocks ookinete and sporozoite motility, as well as hepatocyte invasion (Moon et al., 2009; Brochet et al., 2014; Govindasamy et al., 2016). Deletion of PKG in sporozoites, via a temperature sensitive recombinase, revealed its involvement in the release of merozoites from hepatocytes (Falae et al., 2010). The timing of PKG activation seems to be crucial, since premature activation of PKG in PDE δ knockout ookinetes resulted in dedifferentiation of the parasites. This phenotype could be reversed by the addition of C1 or by deletion of GC β in PDE δ -deficient parasites (Moon et al., 2009).

1.7.5 PKA

Plasmodium PKA consists of a regulatory domain (PKAr) containing two cAMP-binding sites and a catalytic domain (PKAc), which are encoded by two separate genes (PF3D7_1223100 and PF3D7_0934800, respectively). In its inactive form, PKAc is bound

by PKAr, forming a heterodimer. Binding of cAMP to PKAr results in the release of PKAc, which can then bind to and phosphorylate substrates.

PKAc and PKAr show similar expression profiles. They are maximally transcribed in schizonts and sporozoites, however transcripts can also be detected in trophozoites, gametocytes and ookinetes (López-Barragán et al., 2011; Zanghì et al., 2018). Conditional deletion of PKAc in *P. falciparum* revealed that similar to AC β , it is essential for merozoite invasion, and does not affect calcium release or any of the steps leading up to and including egress (Patel et al., 2019). Quantitative phosphoproteomics of both AC β and PKAc knockout lines identified several proteins which are phosphorylated in a cAMP-dependent manner, including the cytoplasmic tail of AMA1, which has been previously reported to be PKA-dependent and important for efficient invasion (Leykauf et al., 2010). Interestingly, Patel et al. also showed that AC β and PKAc-deficient parasites showed reduced shedding of AMA1. Conversely, elevated levels of cAMP in PDE β -deficient parasites, resulted in premature shedding of AMA1 (Flueck et al., 2019). Therefore it is likely that cAMP-mediated signalling plays a critical role in regulating the shedding of AMA1.

PKA may also play a role in regulating gametocytogenesis, since gametocyte producing lines show higher PKA activity than non-gametocyte producing lines (Read and Mikkelsen, 1991). While addition of cAMP has been reported to induce gametocytogenesis (Kaushal et al., 1980), attempts to reproduce these experiments have proved unsuccessful and resulted in an inhibition of gametogenesis and asexual growth (Inselburg and Banyal, 1984). Therefore it remains unclear whether PKA is involved in commitment to gametocytogenesis. A recent study conducted in *P. berghei* demonstrated that PKAc-deficient sporozoites are still able to glide and invade hepatocytes, eventually releasing merozoites. However, merozoites were unable to invade erythrocytes (Choudhary et al., 2019). Therefore it appears that PKA is not required for pre-erythrocytic stages.

1.8 Calcium signalling

Ca²⁺ is a ubiquitous signalling molecule that regulates a diverse range of cellular functions including cell motility, growth and differentiation (Bootman et al., 2015). Cells maintain low cytosolic calcium concentrations by actively pumping calcium ions outside of the cell via plasma membrane Ca²⁺ pumps (PMCA) and into intracellular stores such as

the endoplasmic reticulum (ER) via sarcoendoplasmic reticular Ca^{2+} ATPases (SERCA pumps). Specific signals can trigger the release of Ca^{2+} from the ER through ryanodine receptors (RyR), which are activated by elevated levels of Ca^{2+} ; and IP_3 receptors (IP_3R), which are activated upon binding of IP_3 , a second messenger which is produced by the hydrolysis of inositol(4,5)-bisphosphate (PIP_2) by phospholipase c (PLC). Once in the cytosol Ca^{2+} is able to bind to and activate various effector molecules, many of which possess common Ca^{2+} binding motifs including EF hand and C2 domains.

Compared to other eukaryotes, *Plasmodium* species possess a smaller repertoire of calcium-related genes, with a vast majority that remain poorly characterised (Moreno et al., 2011). At least two P-type ATPase Ca^{2+} pumps are encoded by the parasite, including ATP4, a non-SERCA subclass unique to apicomplexans; and ATP6, a canonical SERCA pump (Krishna et al., 2001). However, genes encoding canonical IP_3 or ryanodine receptors have not been identified, despite pharmacological evidence of IP_3 -mediated Ca^{2+} release (Passos and Garcia, 1998; Alves et al., 2011). *Plasmodium* parasites also encode around 30 proteins with putative Ca^{2+} binding domains including seven Ca^{2+} -dependent protein kinases (CDPKs) and three protein phosphatases.

CDPKs are serine/threonine kinases found in plants and alveolates, which consist of an N-terminal catalytic domain, an autoinhibitory domain, and a C-terminal calmodulin-like domain which contains several Ca^{2+} binding sites (Moreno et al., 2011). CDPKs display stage-specific expression patterns (López-Barragán et al., 2011; Zanghì et al., 2018). CDPK7 appears to be involved in early intraerythrocytic development from rings to trophozoites, with disruption of CDPK7 resulting in reduced growth (Kumar et al., 2014). CDPK1 is refractory to knockout, however work on TgCDPK3, its homologue in *Toxoplasma*, revealed that TgCDPK3 is involved in calcium-induced egress and also appears to modulate the activity of the actomyosin motor by phosphorylating Myosin A (Gaji et al., 2015). In blood-stages, conditional disruption of PfCDPK5 lead to a block in microneme release and egress (Dvorin et al., 2011; Absalon et al., 2018). This egress block appears to act downstream of PKG activity, since microneme release was unaffected. Mechanically released CDPK5-depleted parasites were however able to secrete micronemes and invade erythrocytes, while C2-treated parasites were unable to secrete micronemes or invade (Absalon et al., 2018). Another Ca^{2+} -binding protein, double C2 (DOC2), also ap-

appears to be required for microneme secretion in *P. falciparum* (Farrell et al., 2012). However, while DOC2-depleted parasites were still able to egress, they could not invade. It is likely that DOC2 facilitates microneme-plasma membrane fusion and acts downstream of CDPK5. The homologue of CDPK4 in *Toxoplasma* (TgCDPK1) is required for parasite motility, egress and invasion (Lourido et al., 2010), however disruption of CDPK4 in *P. falciparum* and *P. berghei* did not affect asexual growth (Dvorin et al., 2011; Billker et al., 2004). Instead, CDPK4 was required for cell cycle progression in male gametocytes upon XA mediated activation in *P. berghei* (Billker et al., 2004). Disruption of CDPK2 in *P. falciparum* revealed that it is required for exflagellation (Bansal et al., 2017). In *P. berghei* CDPK3 is required for ookinete motility and penetration of mosquito midgut wall to form oocysts (Ishino et al., 2006; Moon et al., 2009).

Calcium signalling is also involved in regulating several steps during invasion. Merozoites require Ca^{2+} release for microneme secretion and invasion. This can be triggered by exposing merozoites to low concentrations of K^+ , which mimic extracellular conditions in the blood plasma (Singh et al., 2010). Basal calcium levels are then restored once EBA175 interacts with its receptor on the surface of RBCs. Merozoite attachment to erythrocytes appears to require calcineurin, a Ca^{2+} -regulated phosphatase which stabilises the interaction between parasite adhesins and RBC receptors (Paul et al., 2015).

1.9 Signalling pathways as drug targets

Signalling pathways in the malaria parasite have garnered great research interest due to the critical roles that they play across all stages of the lifecycle. The use of chemical tools and reverse genetics approaches have greatly improved our understanding of how components of cGMP, cAMP and Ca^{2+} signalling, shown in figure 1.5, regulate egress and invasion. The essential nature of many of these signalling components, coupled with their divergent structure from their human orthologues, make them attractive drug targets. As such, components of signalling pathways have been the focus of several drug discovery programmes (Baker et al., 2017b; Penzo et al., 2019). Future work on these signalling pathways may pave the way for the discovery of novel drugs with distinct modes of action in the fight against antimalarial drug resistance.

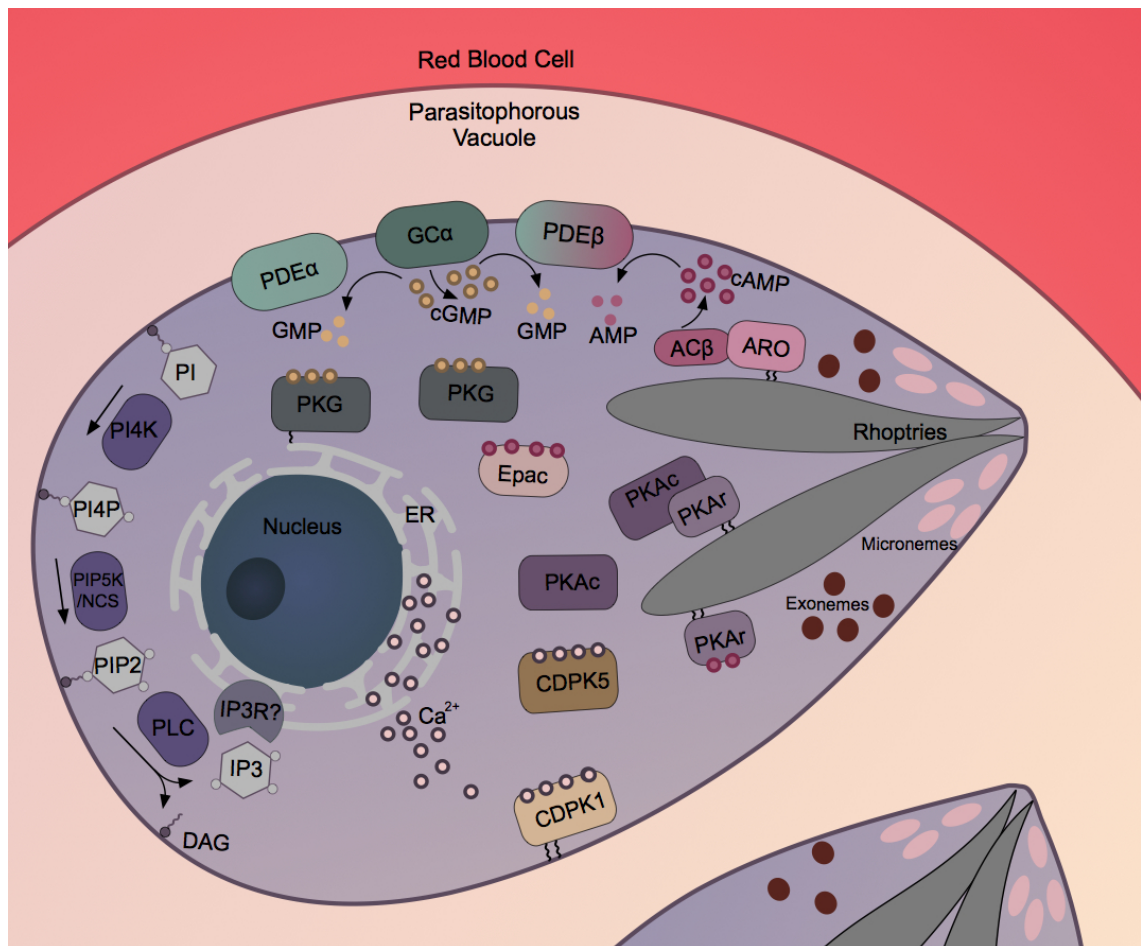


Figure 1. 6. Schematic representation of the components of cAMP, cGMP and Ca²⁺ signalling in *Plasmodium* merozoites.

1.10 Project aims and objectives

Although several of the key signalling components utilised by the parasite during egress and invasion have been identified, there remain gaps in our understanding of how both these processes are regulated. For example, the initial signal which triggers egress remains unknown. Work in *Toxoplasma* has revealed that this role may in part be fulfilled by TgGC which can sense changes in pH, K⁺ and PA levels (Yang et al., 2019; Bisio et al., 2019), leading to the activation of cGMP-signalling which triggers a cascade of events leading to parasite egress. Whether GC α performs a similar function in *Plasmodium* parasites remains unclear since it is refractory to deletion. Furthermore, although several proteins are phosphorylated as a result of cGMP, cAMP and Ca²⁺ signalling, the exact role of each of these phosphorylation events remains unclear. As mentioned previously, several proteins were identified in a phosphoproteome as being phosphorylated in a PKG-dependent manner (Alam et al., 2015). One protein that particularly stands out is MyoA, which was identified as being phosphorylated at a single site on serine 19

in a cGMP-dependent manner. Intriguingly, phosphorylation of the equivalent residue in *Toxoplasma* (serine 21) appears to be important for parasite motility and egress (Tang et al., 2014; Gaji et al., 2015). A recent study has shown that mutation of the S19 phosphosite in recombinant PfMyoA results in greatly reduced motor speed (Robert-Paganin et al., 2019), however it is unknown whether this phosphorylation of MyoA is required for blood-stage growth. This project therefore set out to functionally characterise GC α and to investigate the role of cGMP-dependent phosphorylation of MyoA at serine 19 in *P. falciparum* parasites.

2 Methods

2.1 Parasite culture

2.1.1 Asexual stage culture

P. falciparum asexual blood stages of various 3D7 background strains were cultured in human erythrocytes of various blood groups (National Blood Transfusion Service, London, United Kingdom) and complete medium (CM) consisting of RPMI-1640 medium (Life Technologies) supplemented with 0.5% AlbuMAX type II (Gibco), 50 μ M hypoxanthine and 2 mM L-glutamine. Parasite cultures were incubated at 37°C and gassed with 90% N₂, 5% CO₂ and 5% O₂ according to standard procedures (Trager and Jensen, 1976). Parasitemias were routinely monitored by light microscopy examination of thin blood films fixed with 100% methanol and stained with 10% Giemsa stain in 1x phosphate buffer (8 mM KH₂PO₄, 6 mM Na₂HPO₄, pH 7.0).

2.1.2 Gametocyte induction and culture

An adapted version of previously described techniques (Fivelman et al., 2007) was used to obtain synchronous gametocytes. Briefly, highly synchronous ring-stage parasites at 8-10% parasitemia, 4% hematocrit were stressed by retaining half the spent culture medium and replenishing the rest with fresh CM. The following day, the 'stressed' cultures were split to achieve a parasitemia of 2.5% at 4% hematocrit, once again retaining half the spent CM and replenishing the rest with fresh CM. Cultures were left shaking until the following day when all the schizonts had ruptured and reinvaded. A certain proportion of the reinvaded rings should then have committed to gametocytogenesis. From this point onwards, parasite culture medium was exchanged daily with pre-warmed CM supplemented with heparin at 20 units/ml to prevent asexual growth.

2.1.3 Inducing gametogenesis

Mature stage V gametocytes were resuspended in RPMI containing 100 μ M xanthurenic acid (XA) containing 0.5 μ g/ml α -Pfs25 and incubated at room temperature overnight.

2.1.4 Synchronisation

Tightly synchronous parasites were obtained by purifying segmented schizonts on a 70% Percoll (GE Healthcare) cushion and allowing them to invade fresh erythrocytes for 1-2 hours while shaking. This was followed by lysis of unruptured schizonts by treating with 5% D-sorbitol (Sigma) for 10 minutes (Lambros and Vanderberg, 1979) to obtain highly pure and synchronous ring stage cultures.

2.1.5 Preparation and purification of merozoites

Schizonts from tightly synchronised cultures were purified by magnetic cell separation (MACS) enrichment (Mata-Cantero et al., 2014) then allowed to rupture in pre-warmed RPMI for 1 hour while shaking. The culture was run through the MACS column (Miltenyi Biotech), retaining unruptured schizonts and hemozoin-associated cell debris on the magnet and allowing merozoites to elute in the flowthrough which was then centrifuged at 3,500 x g for 10 minutes. Merozoites samples were snap frozen in a dry ice/ethanol slurry.

2.1.6 Rapamycin treatment of parasites

The dimerisable Cre recombinase (DiCre), which is expressed as two separate inactive fragments each fused to a rapamycin-binding domain, can be activated in parasites by treatment with rapamycin. Synchronous ring stage parasites were split and treated for 2-4 hours at 37°C with either rapamycin at 50 or 100 nM, or the equivalent volume of DMSO which served as a solvent only control. Parasites were pelleted at 1500 x g and washed once in RPMI before culturing as standard. Typically 50 nM rapamycin was used for GC α -related experiments, while 100 nM was used for MyoA-related experiments.

2.1.7 Parasite transfection

Highly synchronous late stage schizonts were used for transfection as previously described for *P. falciparum* (Collins et al., 2013a) using the Amaxa™ 4D-Nucleofector system (Lonza). For each transfection 20-50 μ g DNA was precipitated by the addition of 0.1 volumes of 0.3 M sodium acetate (pH 5.2) and 2 volumes of 100% ethanol, followed by a 30 minute incubation at -20°C. DNA was pelleted by centrifuging at 12,000 x g for 10 minutes then washed twice with 70% ethanol. The DNA pellet was dried and resuspended in 10 μ L Tris-EDTA buffer (TE). 100 μ L of supplemented P3 primary cell solution was

added to the DNA and used to resuspend 25 μ L of schizonts ($\sim 1.25 \times 10^8$ cells) obtained from synchronous culture by Percoll enrichment before transferring to a Nucleocuvette. Parasites were electroporated using the FP158 setting then transferred back into culture and placed on the shaker overnight. Appropriate drug selection was applied 24 hours post transfection, unless otherwise stated.

2.1.8 Cloning parasites by limiting dilution

Clonal parasite lines were obtained by limiting dilution and assessing for single plaque formation as previously described (Thomas et al., 2016). The hematocrit and parasitemia of parasite cultures were determined by using a hemocytometer and counting Giemsa-stained slides. The cultures were diluted to give 0.3 parasites in 200 μ l of culture at 1% hematocrit per well in a 96-well plate. After 9 days, plaque formation was assessed using an EVOS FL Cell Imaging System. Wells containing single plaques were subsequently expanded and analysed for integration by PCR.

2.1.9 Drug cycling parasites

To promote the loss of episomes and improve the proportion of parasites that had integrated a drug selection cassette, parasites were cycled on/off drug up to four times. Each round involved culturing the parasites in the absence of drug for one week, followed by treating them with the appropriate drug for 5 days.

2.1.10 Preparing parasite samples for western blot and DNA extraction

Parasites were released from erythrocytes by lysing in at least 5 volumes of 0.15% saponin (Sigma) in PBS containing cComplete EDTA-free protease inhibitor (Roche) and 1 mM PMSF. The samples were pelleted at 12,000 x g for 1 minute then washed twice in 1x PBS also containing cComplete EDTA-free protease inhibitor (Roche) and 1 mM PMSF. The sample pellets were snap frozen in a dry ice/ethanol slurry and stored at -80°C .

2.2 Parasite Assays

2.2.1 SYBR Green growth inhibition assay

To determine the effect of various test compounds on parasite growth, their half maximal effective concentration (EC_{50}) values were determined by using the SYBR Green growth

inhibition assay adapted from (Smilkstein et al., 2004). Test compounds were set as a series of 2-fold serial dilutions in triplicate in a 96-well plate. Wells containing no drug or 10 nM chloroquine were also included in each plate and served as negative and positive controls, respectively. Ring stage parasites were added to achieve a starting parasitemia of 2% at 1% hematocrit and incubated at 37°C in a sealed gassed chamber. After 72 hours, the assay was terminated by freezing the plates at -20°C. After thawing the plates, the parasites were lysed in buffer containing 20 mM Tris, 5 mM EDTA, 0.008% saponin, 0.08% Triton X-100 and 1x SYBR Green I (Molecular Probes) at pH 7.5. After incubating at room temperature in the dark, SYBR Green fluorescence was measured using a Spectramax M3 plate reader (Molecular Devices) with excitation and emission wavelengths of 485 and 535 nm, respectively. Relative fluorescence units were plotted against the logarithm of drug concentrations in GraphPad Prism version 7. EC₅₀ values were determined by non-linear regression analysis.

2.2.2 Fluorescence activated cell sorting (FACS) growth assays

Parasites were fixed using high-quality methanol-free 4% formaldehyde (Thermo Scientific), 0.1% glutaraldehyde (Sigma) in 1x PBS and stored at 4°C until required. Cells were stained with 1x SYBR Green I (Molecular Probes) overnight. The fixative was aspirated and the cells washed in PBS. The samples were analysed using a BD LSR II flow cytometer (BD Biosciences), with 50,000 events collected for each sample. FlowJo 7 analysis software (FlowJo LLC) was used to analyse the data. Different assays were adjusted for starting parasitemias and growth curves were generated using GraphPad Prism version 7.

2.2.3 Calcium release assays

Changes in the levels of intracellular free Ca²⁺ were measured in Fluo-4-AM loaded mature *P. falciparum* schizonts in the presence of the PDE inhibitor, Zaprinast, or the calcium ionophore, A23187. Fluo-4-AM is a non-fluorescent acetoxymethyl ester, which is cell permeable. De-esterification of Fluo-4-AM traps Fluo-4 inside the cell. Fluo-4 acts as a calcium indicator since it fluoresces upon binding to free Ca²⁺.

Mature schizonts from RAP- and DMSO-treated cultures were Percoll enriched and ~1.25x10⁸ cells from each condition were incubated for 45 minutes in 1 ml of phenol

red free RPMI containing 10 μM Fluo-4-AM (Invitrogen). The parasites were washed twice in pre-warmed phenol red free RPMI, then incubated for 20 minutes to allow for de-esterification of the AM ester. The parasites were washed twice more, then resuspended in phenol red free RPMI at 1.25×10^8 parasites/ml. 100 μl of resuspended parasites were added to wells on the bottom half of a 96-well plate. 3 wells containing phenol red free RPMI were also included as a control. Baseline Fluo-4 fluorescence in each well was read at 22 second intervals for 3 minutes using a Spectramax M3 plate reader (Molecular Devices) pre-warmed to 37°C with excitation and emission wavelengths of 483 and 525 nm, respectively. The plate was removed from the reader and the parasites were transferred to wells containing test compounds at a final concentration of 75 μM for Zaprinast and 20 μM for A23187. Control wells containing DMSO only were also included as a control. The plate was placed back in the reader and read at 22 second intervals for a further 5 minutes. All samples were run in triplicate. Relative fluorescence units from reads at each time point and condition were averaged and baseline and DMSO control values subtracted. Plots were generated using GraphPad Prism version 7.

2.2.4 Measurement of intracellular cAMP and cGMP levels

Intracellular cyclic nucleotide levels in mature *P. falciparum* schizonts were measured using ELISA-based high-sensitivity direct cAMP and cGMP colorimetric assay kits (Enzo). Mature schizonts from RAP- and DMSO-treated cultures that were treated with 1.5 μM compound (C2) overnight were used for the cyclic nucleotide detection assays. Around 1.25×10^8 cells from each condition were incubated for 3 minutes in RPMI containing 1.5 μM C2 only or in the presence of 75 μM Zaprinast (Sigma) to inhibit PDE activity. Parasites were pelleted at 9,000 x g, resuspended in 100 μl of 0.1 M HCl and incubated for 10 minutes at room temperature with intermittent vortexing to complete cell lysis. The samples were pelleted at 9,000 x g and the supernatant collected and frozen at -80°C . Once all biological replicates were collected, each sample was diluted by adding 400 μl of 0.1 M HCl. Samples and standards were acetylated in order to improve sensitivity, according to the manufacturer's instructions.

The detection ranges were 0.078 - 20 and 0.08 - 50 pmol/ml for the cAMP and cGMP assays, respectively. All samples and standards were set up in duplicate. Absorbance was measured at 405 nm using a Spectramax M3 plate reader (Molecular Devices). The

standards were used to plot a standard curve from which the concentrations of cyclic nucleotides in the parasite samples could be determined. Plots were generated using GraphPad Prism version 7.

2.2.5 Egress timepoint assays

Mature segmented schizonts treated with 1.5 μM C2 overnight were Percoll enriched and washed several times in pre-warmed RPMI. Parasites were resuspended in RPMI at 3.25×10^8 parasites/ml and 65 μl aliquots were dispensed in 5 eppendorf tubes. To harvest samples at each time point, parasites were pelleted at 9,000 x g and culture supernatants were purified using 0.22 μm Costar Spin-X centrifuge filters (Corning). The parasite pellet from the first time point was retained as a parasite loading control. Samples were subject to western blot analysis, and probed with an α -SERA5 antibody as a measure of schizont egress.

2.2.6 Extraction of proteins by their solubility profile

Saponin-lysed parasite pellets were repeatedly freeze/thawed after resuspending the parasite pellets in 4 volumes of hypotonic buffer containing 5 mM Tris and 2 mM MgCl_2 (pH 8) supplemented with cOmplete EDTA-free protease inhibitor (Roche) and 1 mM PMSF. The parasite lysates were centrifuged at 12,000 x g for 10 minutes at 4°C and the supernatants collected and stored on ice. The parasite pellet was washed twice in hypotonic buffer, then lysed in co-immunoprecipitation (CoIP) buffer containing 150 mM NaCl, 10 mM Tris (pH 7.5), 0.5 mM EDTA and 1% NP40 that was supplemented with cOmplete EDTA-free protease inhibitor (Roche) and 1 mM PMSF. The parasite lysates were centrifuged at 12,000 x g for 10 minutes at 4°C and the supernatants collected and stored on ice. The hypotonic and NP40 lysates were subjected to western blot analysis.

2.2.7 RNA extraction and reverse transcription quantitative PCR (RT-qPCR)

RNA from saponin-lysed mature schizonts treated with 1.5 μM C2 was extracted with TRIzol Reagent (Invitrogen) and purified using a Direct-zol RNA Miniprep Plus kit (Zymo Research) according to the manufacturer's instructions. In-column deoxyribonuclease I treatment (Zymo Research) was performed to remove contaminating genomic DNA. RNA yields were determined using a Nanodrop spectrophotometer (Thermo Fisher Scientific). Complementary DNA (cDNA) synthesis was performed using 500 ng of RNA from each

condition using All-in-One cDNA Synthesis SuperMix (Biotool) according to the manufacturer's protocol and diluted 1:20 using nuclease-free water. qPCR was performed using an ABI PRISM 7500 Fast PCR System (Thermo Fisher Scientific). Each reaction contained 2 μ l of cDNA, 300 nM of each primer and 1x SYBR Green PCR Master Mix (Biotool) in a total volume of 20 μ l. Samples were set up in triplicate, using two different primer sets specific for MyoA and PDE α that were selected using the Primer3 online tool (Kõressaar et al., 2018). For each experiment, genomic DNA was set up as a series of 10-fold serial dilutions (1×10^6 – 1×10 copies) in triplicate, to be used as a standard for absolute quantification of cDNA. The qPCR programme used was 95°C for 10 minutes followed by 40 cycles of 95°C for 15 seconds and 60°C for 60 seconds. Single amplicons were detected for each primer pair by thermal melt assay. Under the conditions used, the primer pair efficiencies were 97.6% and 91.4% for the MyoA and PDE α primer pairs, respectively when tested on a gDNA standard ranging from 1×10^6 to 1×10 copies. Using the gDNA standard, absolute quantities of MyoA and PDE α in each sample were calculated and MyoA levels normalised to PDE α levels. Parasite samples were then normalised to their matched untreated control.

2.3 Microscopy

2.3.1 Imaging Giemsa-stained blood films

An Olympus BX51 microscope fitted with an Olympus SC30 digital colour camera through a 100x oil immersion objective was used to image Giemsa-stained blood films. Images were processed in Graphic (Picta, Inc.).

2.3.2 Live parasite imaging

To image live parasites, a small amount of culture material at 50% hematocrit was added to a microscope slide and covered with a coverslip and images were acquired using an EVOS FL cell imaging system. To visualise nuclei, parasites were treated with 1 μ -g/ml Hoechst 33342 for 5 minutes at 37°C before imaging. Parasites were incubated for 5 minutes with 5 μ g/ml wheat germ agglutinin (WGA) conjugated to Alexa Fluor 488 (Invitrogen) to stain erythrocyte membranes. To stain female gametes, α -Pfs25 antibody conjugated to Cy3, kindly provided by Michael Delves (LSHTM, London, UK) was used at 0.5 μ g/ml to stain gametes overnight as previously described (Delves et al., 2013).

2.3.3 Time-lapse video microscopy

Egress and gametocyte rounding up were monitored by differential interference contrast (DIC) alone or coupled with fluorescence microscopy using using a Nikon Eclipse Ti fluorescence microscope with a 60x oil immersion objective and fitted with a Hamamatsu C11440 digital camera. For egress videos, segmented schizonts treated with 1.5 μ M C2 overnight were Percoll enriched and resuspended in warm CM at 0.4% hematocrit then transferred to pre-warmed Poly-L-Lysine μ -Slide VI 0.4 (IBIDI) imaging chambers and imaged on a temperature-controlled microscope stage held at 37°C. For gametocyte rounding up videos, mature stage V gametocytes were Percoll enriched and resuspended in room temperature CM containing 100 μ M XA (Sigma) at 0.8 to 1.2% hematocrit then transferred to Poly-L-Lysine μ -Slide VI 0.4 (IBIDI) imaging chambers and imaged at room temperature. Images were taken every 2 seconds for a total of 20-30 minutes, and the resulting videos were processed and analysed in ICY bioimage analysis software (icy.bioimageanalysis.org). Plots were generated using GraphPad Prism version 7.

2.3.4 *In vitro* motility assays

Motility assays were performed as previously described (Butt et al., 2010). Motility assay buffer (AB) containing 25 mM imidazole-HCL, 25 mM KCl, 1 mM EGTA and 4 mM MgCl₂ (pH 7.4) was repeatedly degassed and flushed with nitrogen and stored in a hypodermic syringe to prevent oxygen contamination which could lead to photobleaching (Swoboda et al., 2012). Merozoite and saponin released schizont pellets were lysed in 4 volumes of ColP buffer containing 150 mM NaCl, 10 mM Tris (pH 7.5), 0.5 mM EDTA and 1% NP40 that was supplemented with cOmplete EDTA-free protease inhibitor (Roche) and 1 mM PMSF. Samples were incubated on ice for 10 minutes then centrifuged at 12,000 x g for 10 minutes at 4°C and the supernatant collected and stored on ice while the motility assay flow-cell chambers were prepared.

Custom flow-cell chambers with an internal volume of ~10 μ l were constructed by adhering nitrocellulose-coated cover slips to microscope slides with strips of double-sided tape. α -mCherry antibody (ab183628, Abcam) was diluted 1:50 to 7 μ g/ml in AB and was applied in the flow-cell for 5 minutes. Unbound antibody was washed out with AB then blocked for 5 minutes with AB containing 0.5 mg/ml BSA (AB/BSA). Parasite lysates were applied into the flow-cell and incubated for 5 minutes to capture MyoA-mCherry

complexes. Unbound material was washed out twice with AB/BSA. AB containing 0.1 μ M rhodamine-phalloidin-labelled F-actin was applied to the flow-cell and incubated for 2 minutes. Unbound actin filaments were washed out using AB/BSA. Imaging buffer (IB) was made using AB/BSA containing 20 mM DTT, 0.2 mg/ml glucose oxidase, 0.5 mg/ml catalase, 3 mg/ml glucose to scavenge oxygen and prevent photobleaching. The flow-cell was washed twice with IB then viewed by fluorescence microscopy to check for actin binding. This was done using an Axioskop 40 fluorescence microscope with a Zeiss PlanNeofluar x100, 1.3 numeric aperture objective lens. Fluorescence was excited by a mercury arc lamp using a rhodamine filter set (excitation filter HQ535/50, dichroic mirror Q565LP, and emission filter HQ605/75; Chroma Technology), and light emitted from the rhodamine-phalloidin-labeled actin filament specimen was imaged using an IC-310 image-intensified charge-coupled device camera (Photon Technology International). In order to activate the myosin motors, IB containing 2 mM ATP and 1% methylcellulose (IB/ATP) was applied to the flow-chamber. Sequences of video frames were captured every 40 ms using a frame grabber card (Multipix Imaging Limited). Each image sequence was saved as a median of five consecutive image blocks, and filaments were manually tracked with GMimPro (Mashanov and Molloy, 2007). Non-motile or short tracks were removed from the analysis. From the resulting velocities, frequency distribution histograms were calculated (bin size of 0.02), and a Gaussian curve was fitted with GraphPad Prism version 7.

2.4 Immunocytochemistry

2.4.1 Immunofluorescence analysis (IFA)

Thin blood smears were fixed using high-quality methanol-free 4% formaldehyde (Thermo Scientific) in 1x PBS for 20 minutes, followed by two PBS washes then permeabilized with 0.1% Triton X-100 in 1x PBS for 10 minutes. Detergent was washed off twice in PBS and slides were blocked in 3% bovine serum albumin (BSA) in 1x PBS for 1 hour and subsequently probed with primary antibodies in blocking solution for 1 hour. Slides were washed 3 times with PBS then probed with secondary antibodies in blocking solution for 1 hour. Slides were washed 3 times before being mounted in ProLong Gold Antifade Mountant containing DAPI (Thermo Fisher Scientific). Images were acquired using either a Nikon Eclipse Ti fluorescence microscope fitted with a Hamamatsu C11440 digital cam-

era, or an EVOS FL Cell Imaging System and overlaid in ICY bioimage analysis software (icy.bioimageanalysis.org). All antibodies used for IFA in this study are presented in table 1.

Primary Antibodies			
Target	Species	Dilution	Provider/manufacturer
α -HA (Clone 3F10)	Rat	1:250	Roche
α -mCherry (ab183628)	Rabbit	1:500	Abcam
α -RFP (5F8)	Rat	1:1,000	Chromotek
α -GAP45	Rabbit	1:1,000	Judith Green (Francis Crick Institute, London UK) (Ridzuan et al., 2012)
α -GAP50	Rabbit	1:2,000	Judith Green (Francis Crick Institute, London UK) (Ridzuan et al., 2012)
α -MTIP	Rabbit	1:2,000	Judith Green (Francis Crick Institute, London UK) (Ridzuan et al., 2012)
α -Pfs16	Mouse	1:1,000	David Baker (LSHTM, London UK) (Baker et al., 1994)
α -Pfs25 (4B7 from MR4 coupled to Cy3)	Mouse	1:500	Michael Delves (LSHTM, London UK) (Delves et al., 2013)
Secondary Antibodies			
Target	Conjugate	Dilution	Provider/manufacturer
α -Rat IgG heavy and light chains	Alexa Fluor 488	1:500	Invitrogen Molecular Probes
α -Mouse IgG heavy and light chains	Alexa Fluor 488	1:500	Invitrogen Molecular Probes
α -Rabbit IgG heavy and light chains	Alexa Fluor 594	1:500	Invitrogen Molecular Probes

Table 1. List of primary and secondary antibodies used for immunofluorescence analysis

2.4.2 Western blot analysis

Saponin-released parasite pellets were lysed in 4 volumes of ColP buffer containing 150 mM NaCl, 10 mM Tris (pH 7.5), 0.5 mM EDTA and 1% NP40 that was supplemented with cOmplete EDTA-free protease inhibitor (Roche) and 1 mM PMSF and incubated on ice for 10 minutes. Samples were centrifuged at 12,000 x g for 10 minutes at 4°C and the supernatant collected. Reducing sample buffer was added to NP40-lysed parasite samples or culture supernatants and proteins were resolved on 4%-15% Mini-PROTEAN TGX Stain-Free Precast Gels (Bio-Rad) or 3%-8% NuPAGE Tris-Acetate Protein Gels (Thermo Fisher Scientific) for high molecular weight proteins. Proteins were transferred

onto nitrocellulose membranes using a semidry Trans-Blot Turbo Transfer System (Bio-Rad) and blocked using 10% skimmed milk in PBS containing 0.1% Tween-20 (PBST) for 1 hour. Antibody incubations were carried out in 1% skimmed milk in PBST. After probing with primary antibodies for at least 1 hour, membranes were washed 3 times for 5 minutes in PBST followed by incubation with secondary antibodies conjugated to near infrared (NIR) dyes for 1 hour. Membranes were washed 3 times for 5 minutes in PBST followed by a single wash in PBS. Membranes were dried between Whatman 3MM blotting papers and images using an Azure c600 Imaging System (Azure Biosystems) or a ChemiDoc Imaging System (Bio-Rad). Densitometry quantifications were performed using ImageJ and plotted in GraphPad Prism version 7. All antibodies used for western blot in this study are presented in table 2.

2.5 Molecular biology techniques

2.5.1 Identifying Cas9 targeting sites

Two online guide RNA (gRNA) prediction tools, Protospacer Workbench (Macpherson and Scherf, 2015) and Bechnling's CRISPR gRNA design software (www.benchling.com), were used to identify suitable CRISPR/Cas9 targeting sites in the *P. falciparum* genome based on the sequences deposited in PlasmoDB for Myosin A (PF3D7_1342600) and GC α (PF3D7_1138400). gRNA sequences were selected based on lowest probability of off-target cleavage and closest proximity to the homology regions used to repair the double stranded break. A list of gRNAs used in this study along with their on target and off target scores is available in table 3 in the appendix.

2.5.2 Primer design

Primers were ordered from integrated DNA technologies (IDT). The online tool, OligoCalc (Kibbe, 2007) was used to determine the annealing temperatures of the primers and assess self-hybridisation and hairpin formation. Primers used in this study are listed in table 4 in the appendix.

2.5.3 Synthetic gene design

Genes and gene fragments were manually recodonised, and the online tool Resite finder (resitefinder.appspot.com) was used to introduce restriction enzyme sites without chan-

Primary Antibodies			
Target	Species	Dilution	Provider/manufacturer
α -HA (Clone 3F10)	Rat	1:5,000	Roche
α -PKG	Rabbit	1:1,000	ENZO life sciences
α -GFP (Clones 7.1 and 13.1)	Mouse	1:5,000	Roche
α -mCherry (ab183628)	Rabbit	1:2,500	Abcam
α -RFP (6G6)	Rat	1:5,000	Chromotek
α -mNeon Green (32F6)	Mouse	1:1,000	Chromotek
α -GAP45	Rabbit	1:2,000	Judith Green (Francis Crick Institute, London UK) (Ridzuan et al., 2012)
α -GAP50	Rabbit	1:5,000	Judith Green (Francis Crick Institute, London UK) (Ridzuan et al., 2012)
α -MTIP	Rabbit	1:5,000	Judith Green (Francis Crick Institute, London UK) (Ridzuan et al., 2012)
α -MyoA	Rat	1:10,000	Judith Green (Francis Crick Institute, London UK) (Ridzuan et al., 2012)
α -pS19 MyoA	Rabbit	1:1,000	Custom antibody raised against 'N'-RRV[pS]NVEAFDKC peptide generated by Genosphere Biotechnologies (Alam et al., 2015)
α -GAPDH	Mouse	1:30,000	Claudia Daubenberger (Swiss Tropical and Public Health Institute, Basel Switzerland)
α -SERA5	Rabbit	1:5,000	Mike Blackman (Francis Crick Institute, London UK)
Secondary Antibodies			
Target	Conjugate	Dilution	Provider/manufacturer
α -Rabbit IgG heavy and light chains	DyLight 680	1:5,000	Invitrogen Molecular Probes
α -Rabbit IgG heavy and light chains	DyLight 800	1:5,000	Invitrogen Molecular Probes
α -Mouse IgG heavy and light chains	DyLight 680	1:10,000	Invitrogen Molecular Probes
α -Mouse IgG heavy and light chains	DyLight 800	1:5,000	Invitrogen Molecular Probes
α -Rat IgG heavy and light chains	IRDye 680RD	1:5,000	LI-COR Odyssey

Table 2. List of primary and secondary antibodies used for western blot analysis.

ging the coding sequence. Large genes were ordered using the GeneArt Gene Synthesis Service (Invitrogen), while smaller fragments were ordered as gBlocks (IDT).

2.5.4 Polymerase chain reaction (PCR)

DNA used for cloning was amplified using proofreading Q5 DNA polymerase 2x mix (NEB) or CloneAmp HiFi PCR 2x premix (TaKaRa), according to the supplier's instructions. Either *P. falciparum* genomic DNA or plasmid DNA were used as PCR templates and primers were used at 500 nM. PCRs were carried out in a C1000 Touch Thermal Cycler (Bio-Rad). A typical PCR reaction consisted of 25 to 35 cycles of denaturation at 98°C for 10 seconds, followed by annealing at 55-60°C for 10 seconds, and extension at 68-72°C. The duration of the extension step was dependent on the size of the amplicon. PCR products generated were purified using the MinElute kit (Qiagen) after confirming successful amplification by agarose gel electrophoresis.

2.5.5 Restriction digests

Restriction digests were set up using enzymes from New England Biolabs (NEB), Promega or Fermentas according to the manufacturer's protocol. Plasmid digests for cloning were purified using the MinElute kit (Qiagen) and the resulting DNA fragments were used in subsequent cloning steps. Restriction enzymes used to linearise DNA fragments for transfections were heat denatured according to the manufacturer's instructions.

2.5.6 Ligation-based cloning

Digested plasmid vectors were first treated with Antarctic phosphatase (NEB), purified, and subsequently ligated to digested inserts with complementary overhangs using T4 DNA ligase (NEB).

2.5.7 Ligation-independent cloning

The In-Fusion HD cloning kit (TaKaRa) was used for ligation-independent cloning steps, according to the recommended protocol. Inserts for cloning were designed with 15 bp overlaps with either end of the linearised vector.

2.5.8 Transformation of chemocompetent bacteria

E. coli Stellar competent cells (TaKaRa) were used for In-Fusion cloning while *E. coli* XL10-Gold Ultracompetent cells (Agilent) were used for ligation cloning and for the propagation of plasmid DNA. Competent cells were transformed by heatshock according to the supplier's guidelines then spread onto Luria-Bertani (LB) agar plates supplemented with 100 µg/ml ampicillin or 50 µg/ml kanamycin. Plates were incubated overnight at 37°C.

2.5.9 Plasmid DNA isolation

Single *E. coli* colonies were grown overnight in LB medium supplemented with 100 µg/ml ampicillin or 50 µg/ml kanamycin while shaking at 37°C. Plasmids were isolated for small or large-scale preparations using either a MiniPrep kit (Qiagen) or a MidiPrep kit (Macherey-Nagel). DNA yields were determined using a Nanodrop spectrophotometer (Thermo Fisher Scientific).

2.5.10 Sequencing of DNA

Sanger sequencing was performed by EuroFins (formerly GATC) on amplicons from parasite genomic DNA to verify correct integration and on plasmids to validate plasmid construction.

2.5.11 Parasite genomic DNA isolation

DNA was isolated from saponin-released parasite pellets, which were at least 5 µl in volume, using the QIAmp DNA Blood Mini Kit (Qiagen) according to the manufacturer's instructions. DNA yields were determined using a Nanodrop spectrophotometer (Thermo Fisher Scientific).

3 GC α is an essential "bifunctional" Guanylyl Cyclase expressed in the asexual blood stage

cGMP signalling plays a vital role across all stages of the life cycle. During the asexual blood stages, inhibition of this signalling pathway by using reversible PKG-specific inhibitors such as compound 2 (C2), leads to a block in Ca²⁺ release and the secretion of micronemes and exonemes (Collins et al., 2013b; Brochet et al., 2014). As a result, merozoites are unable to egress from the host erythrocyte. Despite the importance of cGMP signalling during this stage, it remains unclear how this pathway is activated in mature blood stage schizonts.

GC α is thought to be responsible for synthesising cGMP during the blood stages of the infection, however it remains poorly characterised in *Plasmodium* parasites. Furthermore, previous attempts to detect GC activity by recombinant expression of the PfGC α catalytic domains in *E. coli* were unsuccessful, with activity only detectable using the catalytic domain of GC β (Carucci et al., 2000). GC α is also refractory to deletion, despite several attempts to disrupt this gene in *Plasmodium* parasites (Taylor et al., 2008; Moon et al., 2009; Kenthirapalan et al., 2016). Other than its predicted role in synthesising cGMP, the N-terminal portion of GC α encodes a P-type ATPase domain, which lacks key residues for ion transport, but is closely related to putative aminophospholipid transporters which are predicted to be involved in flipping phosphatidylserine (PS) or phosphatidylethanolamine (PE) (Baker, 2004). The unique bifunctional structure of GC α is conserved across GCs found in other alveolates including *Toxoplasma*, *Tetrahymena* and *Paramecium*, which may signify a functional link between these two domains. The aim of this chapter was to functionally characterise GC α in *P. falciparum* parasites during the asexual blood stages, and generate a conditional ATPase and GC domain knockout using the dimerisable Cre recombinase (DiCre) system (Collins et al., 2013a) to dissect the function of this protein.

3.1 Results

3.1.1 GC α is expressed during the asexual blood stages of the life cycle

In order to generate a GC α -tagged parasite line, a construct was made to introduce by single homologous crossover a triple *hemagglutinin* (3xHA) epitope tag at the 3' end of the

endogenous GC α gene, along with a *human dihydrofolate reductase (hDHFR)* selection cassette, which confers resistance to WR99210, flanked by two *loxP* sites (Figure 3.1.A). The construct was transfected into 3D7 1G5 DiCre parasites (Collins et al., 2013a), which constitutively express the dimerisable Cre recombinase (DiCre) as two separate subunits, each fused to a rapamycin binding domain. After obtaining WR99210 resistant parasites, four rounds of drug cycling were performed, to enrich the proportion of parasites in which integration had occurred. Upon successful detection of integration in the population by PCR (data not shown), parasites were treated with 100 nM rapamycin for 3 hours in order to excise the floxed *hDHFR* cassette, leaving a single *loxP* site downstream of the *3xHA* epitope tag. This was done so that the selection cassette could be repurposed in future transfections. Parasites were then cloned by limiting dilution (Thomas et al., 2016) and two clones called GC α :HA clone 1 and clone 2 were obtained. Work up until this point was done by Christian Flueck (LSHTM, London UK), prior to the start of my PhD. Genomic DNA was extracted from GC α :HA clone 1 and integration of the *3xHA* tag and excision of the *hDHFR* cassette were confirmed by PCR (Figure 3.1.B). The growth of GC α :HA clone 1 parasites in the presence of 2.5 nM WR99210 over 3 cycles demonstrated that this line was sensitive to the drug, confirming excision of the *hDHFR* cassette and absence of episomes (Figure 3.1.C). GC α :HA clone 1 was used in subsequent experiments and is referred to as GC α :HA.

According to the transcriptional profile of GC α (López-Barragán et al., 2011; Zanghì et al., 2018), it is expressed in late trophozoites and schizonts, with maximal transcripts detected around 40-48 hours post invasion (hpi). Western blot analysis of samples harvested from GC α :HA parasites every 4 hours from early trophozoites (24 hpi) to late schizonts (48 hpi) using an α -HA antibody revealed that tagged GC α could be detected as early as 36 hpi with maximal expression detected at around 44-48 hpi (Figure 3.2.A). However, full length GC α , which is predicted to migrate at ~499 kDa, could not be detected. Instead, two species migrating at ~175 kDa and ~125 kDa were observed. Interestingly, there was a shift from the 125 kDa form to the 175 kDa form over time. However, western blot analysis of unmodified 3D7 DiCre schizonts probed with the α -HA antibody revealed that the 125 kDa band is a non-specific band (Figure 3.2.B), likely due to cross reactivity of the antibody with a protein found in the parental parasite line. Although it is unclear whether the 175 kDa fragment is a result of degradation or physiological proteolytic processing of

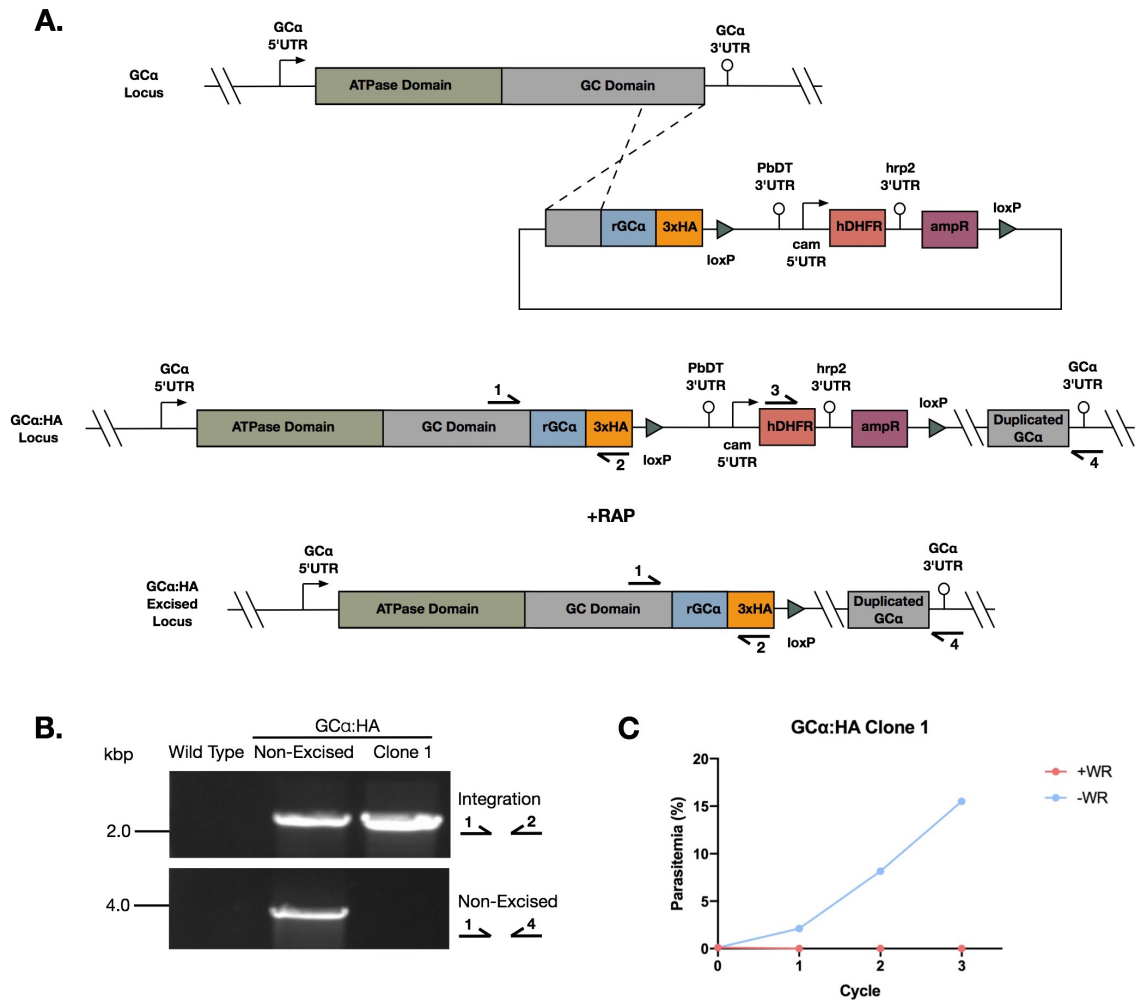


Figure 3.1. Generation of a GC α :HA tagged line. **A.** Schematic representation of the single homology crossover approach used to tag the 3' end of the endogenous GC α gene with a 3xHA tag, and subsequent RAP-mediated excision of the *hDHFR* cassette. Arrows represent the relative position of oligonucleotide primers used for diagnostic PCR screens. **B.** Diagnostic PCR analysis confirming successful integration of the 3xHA tag, and efficient excision of the floxed *hDHFR* tag in a GC α :HA clone. **C.** Growth curve showing GC α :HA clone 1 parasites are sensitive to treatment with 2.5 nM WR99210, consistent with successful excision of the *hDHFR* cassette. Data presented are from counting parasites on Giemsa-stained blood smears. At least 100 parasites were counted per condition.

GC α , a similar phenomenon is also observed in *Toxoplasma* where TgGC predominantly migrates at ~125 kDa and ~75 kDa instead of at 460 kDa which would represent the full length protein (Jia et al., 2017; Yang et al., 2019; Bisio et al., 2019; Brown and Sibley, 2018). In some studies, full-length TgGC could also be detected, however this accounted for only a small proportion of the total population of TgGC (Yang et al., 2019; Brown and Sibley, 2018). Therefore it is possible that full-length GC α is below the detection limit in this experiment. Mapping of the 175 kDa fragment to the predicted domain structure of GC α suggests that this fragment would comprise both C1 and C2 domains along with 12 transmembrane domains (Figure 3.2.C). IFA analysis of GC α :HA C2-blocked mature schizonts revealed that GC α localises to the parasite periphery and partially co-localises with GAP45, an IMC-specific protein which forms part of the glideosome (Figure 3.2.D). The IMC and plasma membrane are separated by ~20-40 nm, therefore it is difficult to distinguish between them. However, late in schizogony, when individual merozoites are pinched off, the residual body remains encapsulated by plasma membrane but not IMC (Ridzuan et al., 2012). Upon close examination, it is apparent that the residual body is surrounded by faint α -HA signal but not α -GAP45 signal. This is indicative of a plasma membrane localisation for GC α , consistent with it being an integral plasma membrane protein. Unlike TgGC which localises to the apical end of tachyzoites, in *P. falciparum* GC α is found across the entire surface of the parasite.

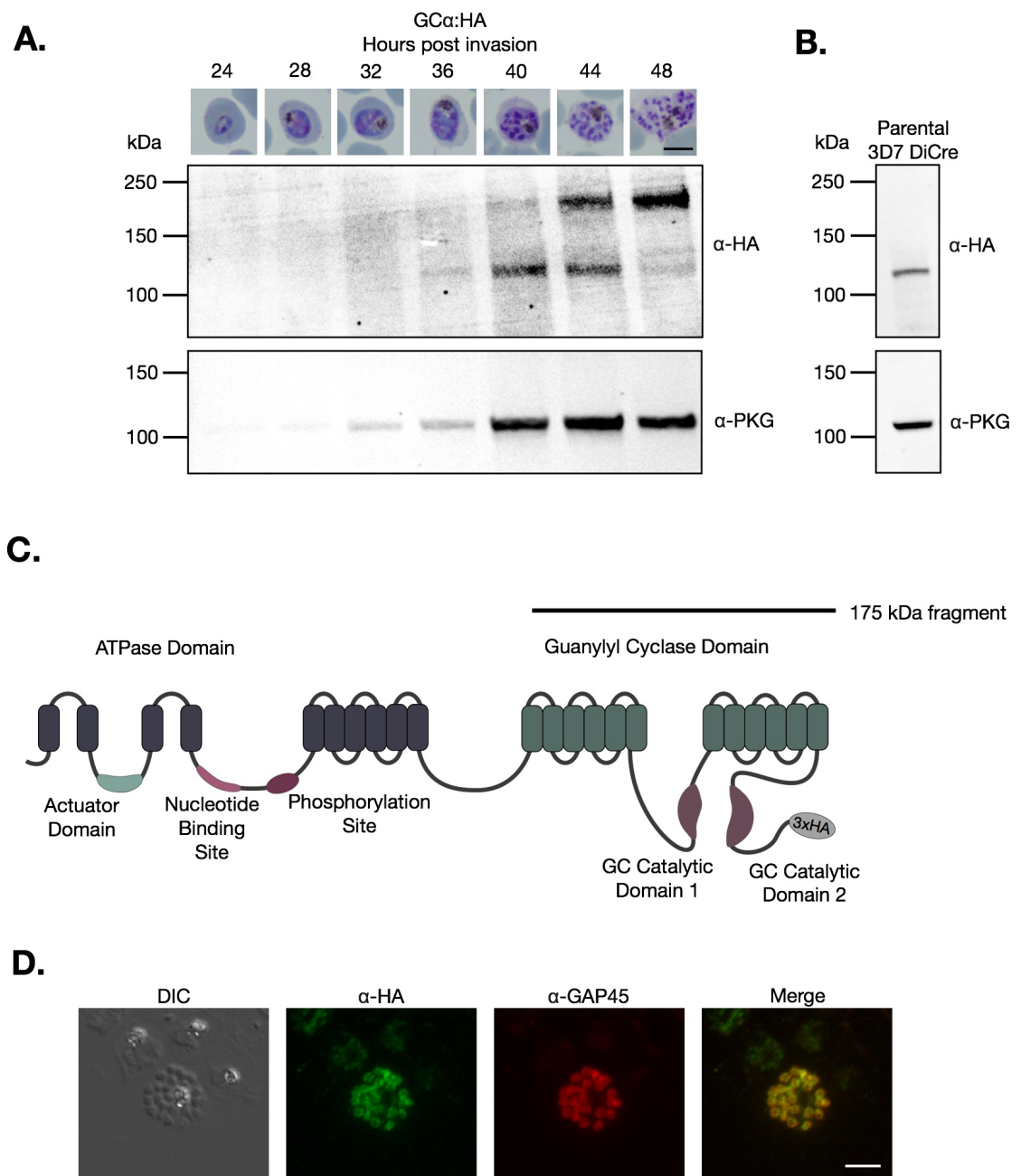


Figure 3.2. GC α is expressed in blood stage schizonts and localises to the plasma membrane. **A.** Western blot showing a time course of GC α :HA expression in *P. falciparum* blood stages. Parasites were harvested at the timing indicated, with representative microscopy images shown above each sample. Scale bar, 5 μ m. PKG was used as a loading control. GC α :HA migrated as several fragments, while full length protein (~499 kDa) could not be detected. **B.** Western blot analysis of unmodified 3D7 DiCre parasites showing that the α -HA antibody cross reacts with a protein at ~125 kDa. **C.** Schematic representation of the domain architecture of GC α . Horizontal lines with corresponding molecular weights show approximate fragments observed by western blot. **D.** IFA analysis of mature GC α :HA schizonts showing colocalisation of GC α :HA (green) with the IMC marker GAP45 (red). Scale bar, 5 μ m.

3.2 GC α is essential for asexual blood stage growth and is required for egress

To determine the function of GC α and whether it is essential for asexual growth, a conditional knockout (cKO) line was generated using marker-free CRISPR/Cas9-mediated gene editing to introduce a second *loxP* site into GC α :HA parasites, which already possess a single *loxP* site downstream of the *3xHA* epitope tag, by introducing an artificial intron based on a PfSERA2 intron, harbouring a *loxP* site (*loxPint*) Jones et al. (2016) within the ATPase domain of GC α . This was achieved by transfecting GC α :HA parasites with a linearised repair template to introduce the *loxPint* sequence, along with a pool of three different pDC2-Cas9-hDHFR plasmids Lim et al. (2017), each harbouring a different gRNA to maximise editing efficiency of the locus (Figure 3.3.A). Parasites were then cultured in the presence of 2.5 nM WR99210 for 9 days to select for parasites harbouring one or more of the pDC2-Cas9-hDHFR plasmids. Parasites were observed two weeks post transfection. gDNA was extracted from these parasites and PCR analysis confirmed successful integration of the *loxPint* (Figure 3.3.B). Since the wild type locus could still be detected in the population, the parasites were cloned by limiting dilution (Thomas et al., 2016). Two clones were obtained called GC α :HA:cKO clone 1 and clone 2, and PCR analysis confirmed *loxPint* integration and the absence of the wild type locus in both clones (Figure 3.3.C). GC α :HA:cKO clone 1 was subsequently used in all further experiments.

Addition of rapamycin to the GC α :HA:cKO line would lead to the excision of DNA sequences encoding part of the ATPase domain and the entire GC domain of GC α (Figure 3.4.A), disrupting the activity of both these domains. Early ring stage GC α :HA:cKO parasites were treated with either 50 nM RAP or the equivalent volume of DMSO for two hours, and gDNA was extracted once the parasites had developed into mature schizonts. PCR analysis revealed that RAP-mediated excision was highly efficient, since a band was not amplified in the integration specific PCR following RAP treatment (Figure 3.4.B). Furthermore, western blot analysis revealed that the ~175 kDa GC α band could no longer be detected in RAP-treated GC α :HA:cKO schizonts, while the non-specific ~125 kDa band could still be detected (Figure 3.4.C). Therefore it appears that treatment of GC α :HA:cKO parasites with rapamycin leads to efficient excision of the GC α gene.

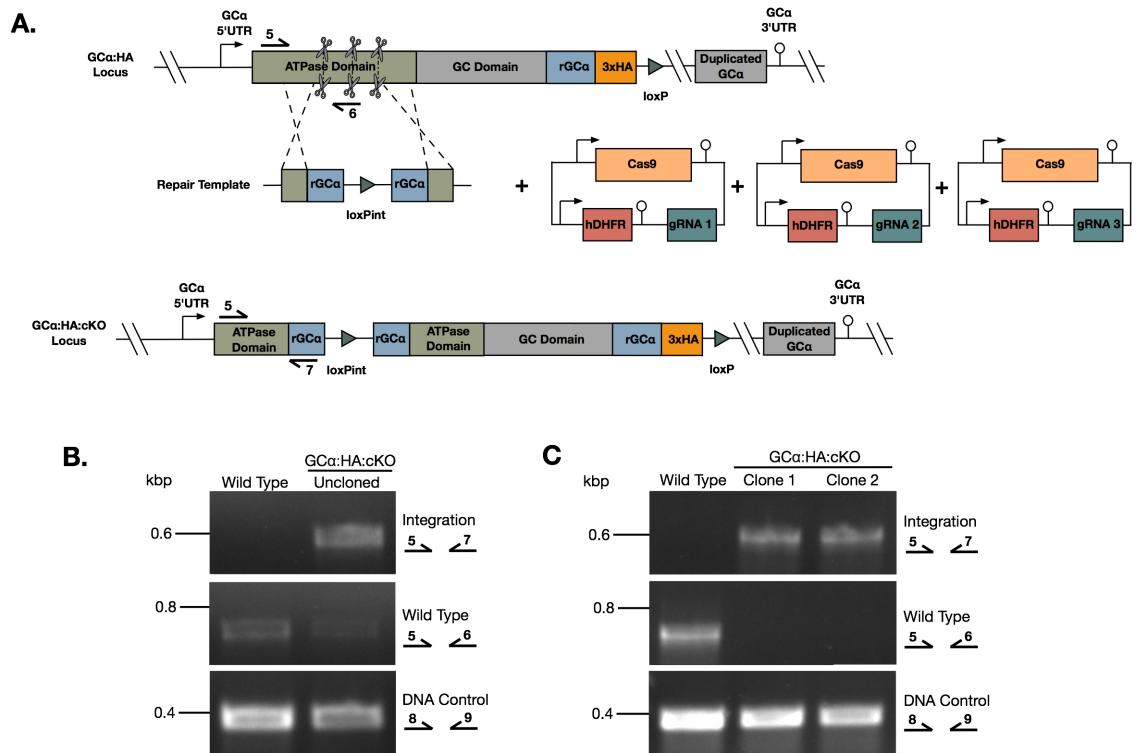


Figure 3.3. Generation of a GC α :HA:cKO line. **A.** Schematic representation of the marker-free CRISPR/Cas9-mediated approach used to introduce the *loxPint* into the ATPase domain of GC α in GC α :HA parasites to generate the GC α :HA:cKO line. Scissors indicate CRISPR/Cas9 cleavage sites, while arrows represent the relative position of oligonucleotide primers used for diagnostic PCR screens. **B.** Diagnostic PCR analysis showing successful integration of the *loxPint* in the uncloned GC α :HA:cKO parasite population, however wild type locus could still be detected. A DNA control PCR was included, which amplified a small segment at an independent locus to test the quality of the DNA used. **C.** Diagnostic PCR analysis confirming successful integration of the *loxPint* and absence of wild type locus in two GC α :HA:cKO clones. A DNA control PCR was included, which amplified a small segment at an independent locus to test the quality of the DNA used.

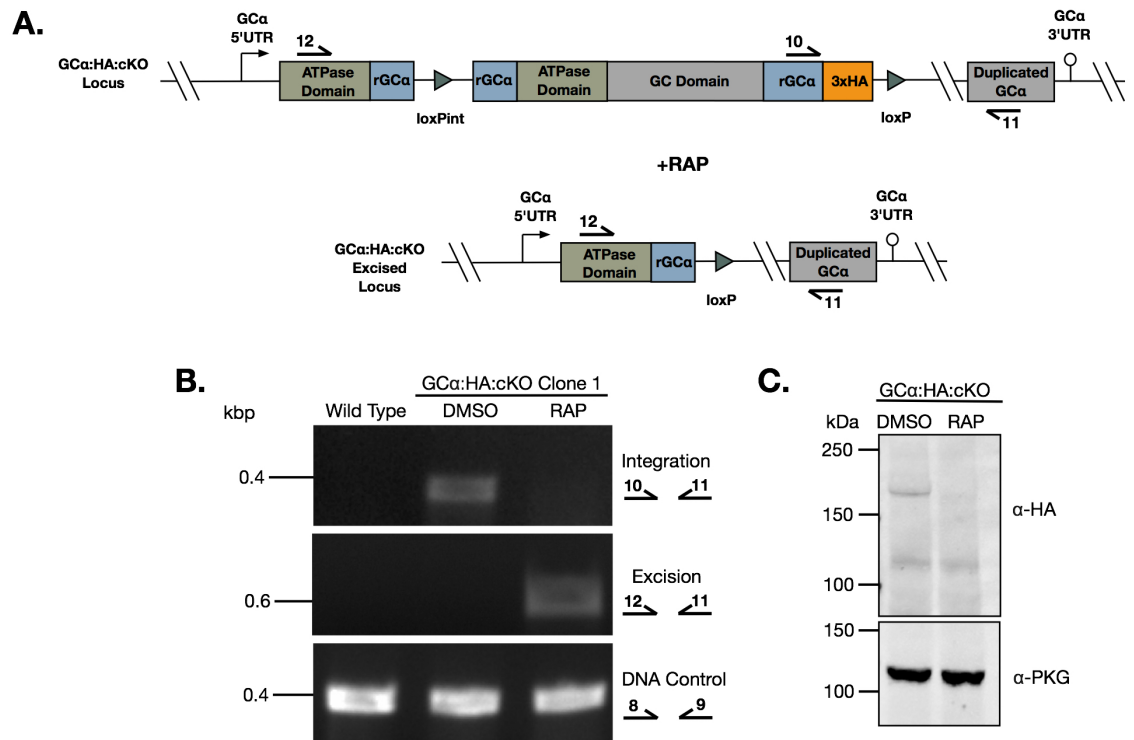


Figure 3.4. Effective conditional disruption of GC α expression. **A.** Schematic representation of RAP-mediated excision of a portion of the ATPase domain and the entire GC domain. Arrows represent the relative position of oligonucleotide primers used for diagnostic PCR screens. **B.** Diagnostic PCR analysis of DMSO- and RAP-treated GC α :HA:cKO parasites showing efficient excision of the GC α gene following RAP treatment. A DNA control PCR was included, which amplified a small segment at an independent locus to test the quality of the DNA used. **C.** Western blot analysis of DMSO- and RAP-treated GC α :HA:cKO and 3D7 DiCre schizonts probed using an α -HA antibody, showing a loss of the ~175 kDa band in the RAP-treated parasites, while the non-specific ~125 kDa band can still be observed in both samples. The blot was also probed using an α -PKG antibody to serve as a loading control.

In order to assess the impact of GC α disruption on parasite viability and growth, a flow cytometry-based replication assay was performed on DMSO- and RAP-treated GC α :HA:cKO parasites over 3 cycles. This revealed a complete arrest in parasite growth resulting from the disruption of the GC α locus (Figure 3.5.A). Close examination of Giemsa-stained GC α :HA:cKO parasites in the excision cycle (cycle 0) revealed that both DMSO- and RAP-treated parasites developed normally and were able to form mature segmented schizonts. However, there appeared to be an accumulation of schizonts and an absence of ring stage parasites in GC α -deficient cultures (Figure 3.5.B), indicating that GC α is required for egress. Live time-lapse microscopy performed on mature DMSO- and RAP-treated schizonts released from a C2 block (Figure 3.6.A), confirming that GC α knockout parasites were unable to egress (Figure 3.6.B). Consistent with this result, examination of culture supernatants from DMSO- and RAP-treated C2 released mature schizonts revealed that the PV-resident serine repeat antigen 5 (SERA5), which is released into the culture supernatant during egress, could not be detected in supernatant samples obtained from RAP-treated cultures (Figure 3.6.C). Collectively, these results establish that GC α is required for merozoite egress and that it plays an essential role during the asexual cycle.

Although GC α :HA:cKO parasites displayed a complete arrest in parasite growth in the flow cytometry-based assay, after around 16 days post rapamycin treatment parasites could be observed in culture. However, subsequent PCR analysis showed that these parasites were not GC α knockouts since the GC α locus was intact. Owing to the fact that the 1G5 DiCre parasite line has a tendency to lose the DiCre expression cassette (personal communication Mike Blackman, Francis Crick Institute London, UK) it is most likely that these parasites are DiCre revertants that have lost the ability to excise the floxed GC α locus. Consistent with this, treatment of GC α :HA:cKO 'revertants' with rapamycin did not result in excision of GC α by PCR (Figure 3.7.A) and had no effect on parasite growth in a flow cytometry-based replication assay (Figure 3.7.B).

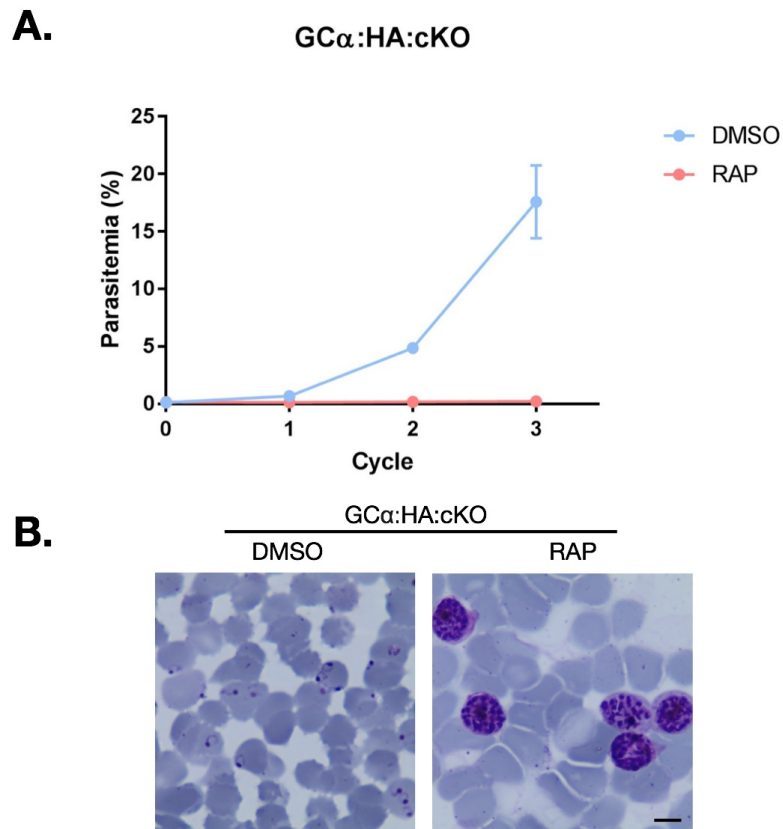


Figure 3.5. GC α is required for asexual growth. A. Growth curves showing parasitemias of GC α :HA:cKO parasites treated with either DMSO or RAP, measured by flow cytometry-based sorting of SYBR Green positive cells. Data points plotted are means from two repeat experiments, each performed in triplicate. Error bars represent the standard deviation. **B.** Representative microscopy images of Giemsa-stained parasites from DMSO- and RAP-treated GC α :HA:cKO cultures, showing the accumulation of schizonts in RAP-treated samples. Scale bar, 5 μ m.

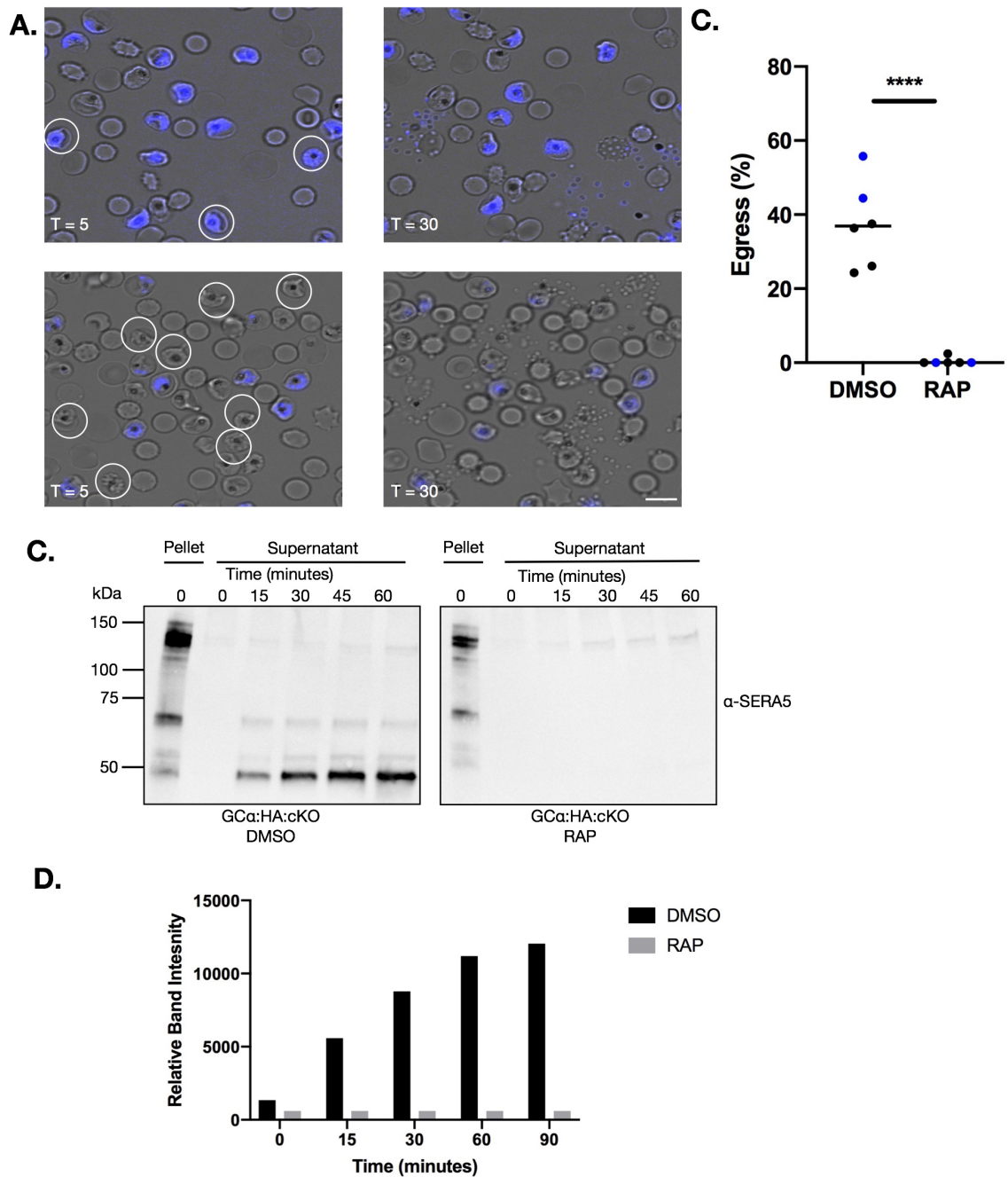


Figure 3.6. GC α disruption results in a complete egress block. **A.** DIC and fluorescence images from time lapse video microscopy of DMSO- and RAP-treated GC α :HA:cKO schizonts taken at 5 minutes and 30 minutes after releasing from a C2 block. In each experiment, one subset of parasites was treated with Hoechst to stain the nuclei so that DMSO- and RAP-treated parasites could be viewed side by side in the same imaging chamber. In the top panel, DMSO-treated parasites are Hoechst stained, while in the bottom panel, RAP-treated parasites are Hoechst stained. Schizonts from the first frame that rupture over the course of the video are circled in white. Scale bar, 10 μ m. **B.** Quantification of the percentage of for DMSO- and RAP-treated schizonts that egress in each 30 minute video. Data are collected from 6 videos, with Hoechst-treated samples depicted in blue. Statistical significance was measured by unpaired t-test, where **** signifies $p < 0.0001$. **C.** Western blot analysis monitoring the release of SERA5 into the culture supernatant of DMSO- and RAP-treated GC α :HA:cKO schizonts, as a measurement of egress over time. Pellet samples were included as loading controls. The lack of SERA5 signal in supernatants from RAP-treated samples indicates impaired egress in GC α -deficient parasites. **D.** Densitometry analysis of the egress assay western blot samples shown in Figure 3.6.C., showing there is a significant difference in levels of SERA5 release into the supernatant between DMSO- and RAP-treated GC α :HA:cKO parasites.

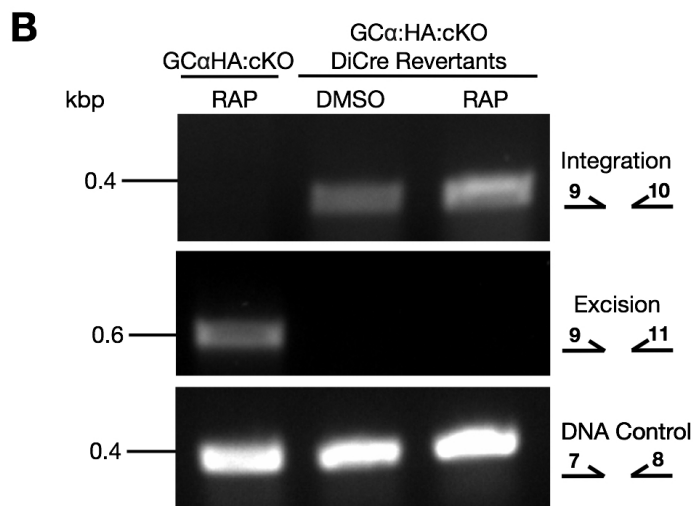
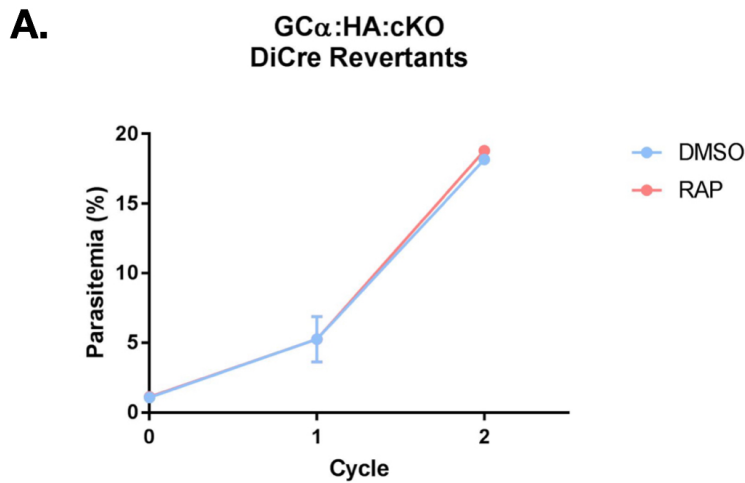


Figure 3.7. GC α :HA:cKO parasites are susceptible to losing the DiCre cassette. A. Growth curves showing parasitemias of GC α :HA:cKO DiCre revertant parasites treated with either DMSO or RAP, measured by flow cytometry-based sorting of SYBR Green positive cells. Data points plotted are means from two repeat experiments, each performed in triplicate. Error bars represent the standard deviation. RAP-treatment had no effect on parasite growth. **B.** Diagnostic PCR analysis of DMSO- and RAP-treated GC α :HA:cKO DiCre revertant parasites showing the GC α gene was not excised following RAP treatment. A RAP-treated GC α :HA:cKO sample was also included as a positive control for RAP-mediated excision. A DNA control PCR reaction was included, which amplified a small segment at an independent locus to test the quality of the DNA used.

3.2.1 GC α displays guanylyl cyclase activity and is responsible for cGMP production in asexual blood stages

To evaluate the impact of GC α deletion on cyclic nucleotide production, cAMP and cGMP assays were performed on extracts from DMSO- and RAP-treated GC α :HA:cKO mature schizonts held in a C2 block. Parasites were blocked in C2 to prevent egress and ensure a similar number of schizonts were used in each assay. Although no discernible changes in cAMP levels were detected between the samples (Figure 3.8.A), deletion of GC α led to a 94.5% reduction in cGMP levels (Figure 3.8.B). Addition of the PDE inhibitor Zaprinast, which would block hydrolysis of cGMP, resulted in an increase in cGMP levels in DMSO- but not RAP-treated parasites (Figure 3.8.B), confirming that schizonts are unable to synthesise cGMP in the absence of GC α .

Since GC α -deficient parasites are unable to synthesise cGMP, it is likely that PKG is not active in these parasites. Consistent with this, the egress phenotype of GC α knockout parasites is indistinguishable from the egress block observed when wild type parasites are treated with the PKG-specific inhibitor C2 (Figure 3.9.A). To determine whether Ca²⁺ release, a PKG-dependent process (Brochet et al., 2014), is affected in GC α knockout parasites, Zaprinast-induced Ca²⁺ release was measured in DMSO- and RAP-treated GC α :HA:cKO parasites. While Zaprinast treatment led to a 5% increase in Ca²⁺ levels in DMSO-treated parasites, no measurable increase could be detected in RAP-treated parasites (Figure 3.9.B). Despite this, DMSO- and RAP-treated parasites showed similar response levels to the calcium ionophore A23187, which allows Ca²⁺ ions to cross cell membranes; indicating that internal calcium stores were unaffected (Figure 3.9.C). These results confirm that GC α is a functional GC and is the only GC capable of synthesising cGMP during the asexual blood stage of the lifecycle and that GC α activity is required PKG-dependent Ca²⁺ release.

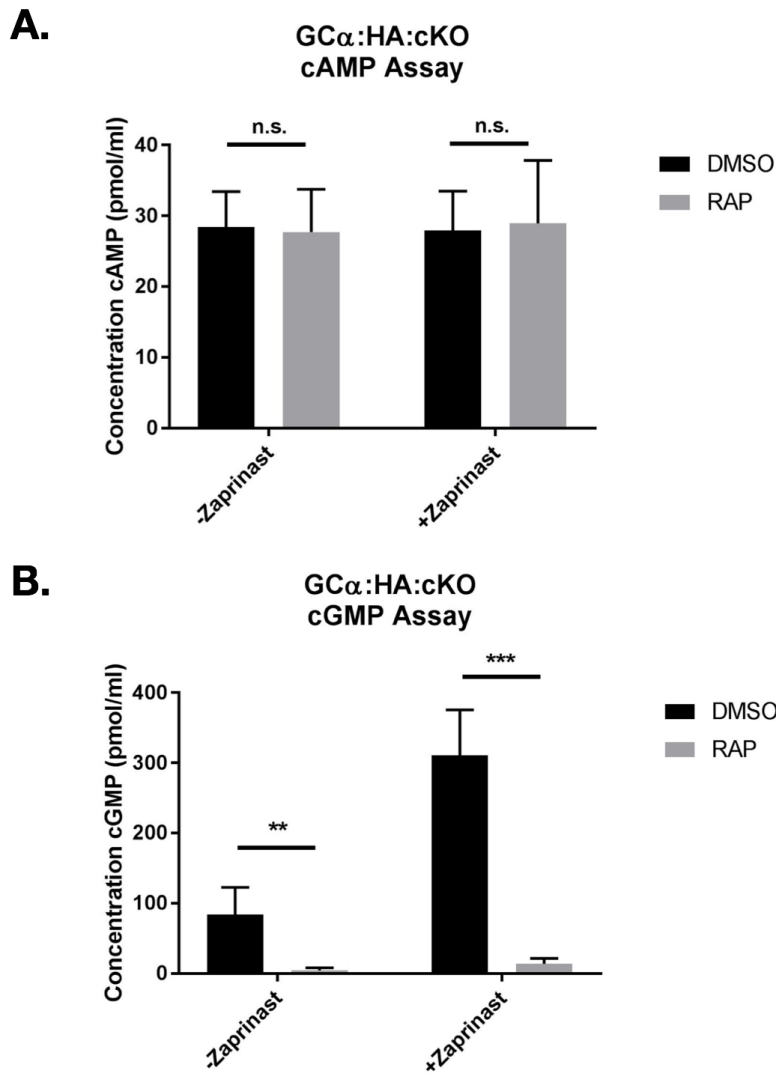


Figure 3.8. GC α disruption leads to a complete loss of cGMP production. A. Absolute levels of cAMP in mature DMSO- and RAP-treated GC α :HA:cKO schizonts that were blocked in 1.5 μ M C2. Data presented is from four independent experiments, each performed in duplicate. Error bars represent the standard deviation. Statistical significance was measured by unpaired t-test, n.s. indicates not significant ($p > 0.05$). cAMP levels remain unchanged, even when treated with 75 μ M Zaprinast for 3 minutes. **B.** Absolute levels of cGMP in mature DMSO- and RAP-treated GC α :HA:cKO schizonts. Data presented is from four independent experiments, each performed in duplicate. Error bars represent the standard deviation. Statistical significance was measured by unpaired t-test, ** signifies $p < 0.01$ whereas *** signifies $p < 0.001$. There is a significant reduction of cGMP synthesis in RAP-treated samples compared to DMSO-treated samples. This difference becomes more significant when parasites are treated with 75 μ M Zaprinast for 3 minutes.

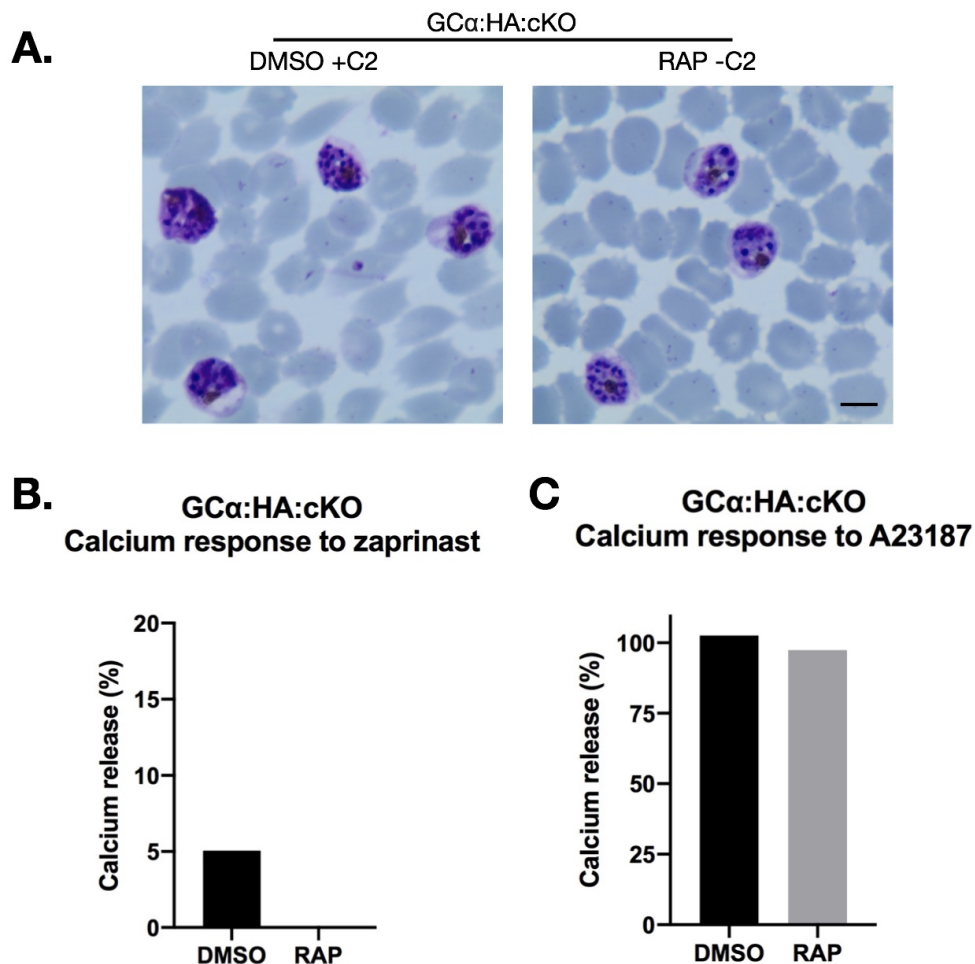


Figure 3.9. GC α disruption phenotypically resembles chemical inhibition of PKG and results in a block in calcium release. **A.** Representative images of Giemsa-stained parasites from DMSO-treated GC α :Ha:cKO parasites in the presence of 1.5 μ M C2, and RAP-treated GC α :HA:cKO parasites. PKG inhibition leads to a similar phenotype to that observed in GC α knockout parasites. Scale bar, 5 μ m. **B.** Determination of calcium release using 75 μ M Zaprinast in synchronous Fluo-4-loaded mature DMSO- and RAP-treated GC α :HA:cKO parasites measured by fluorimetry. Signals were normalised to DMSO (0% signal) and 20 μ M A23187 ionophore (100%). Data plotted is from one experiment, performed in triplicate. **C.** Determination of calcium stores using 20 μ M A23187 ionophore in synchronous Fluo-4-loaded mature DMSO- and RAP-treated GC α :HA:cKO parasites measured by fluorimetry. Signals were normalised to the DMSO-treated GC α :HA:cKO levels (100% signal). Data plotted is from one experiment, performed in triplicate.

3.2.2 Chemical complementation of GC α knockout parasites with PET-cGMP rescues the egress defect

Since the egress phenotype observed in GC α -deficient parasites is most likely due to their inability to produce cGMP to activate PKG, bypassing the need for cGMP synthesis by directly activating PKG could potentially rescue the egress defect and give rise to a second phenotype that arises due to loss of the ATPase domain. To test this, either cGMP or cGMP analogues were added to RAP-treated GC α :HA:cKO schizonts. The cGMP analogues 1-NH₂-cGMP and PET-cGMP were selected since they display a high affinity for recombinant PfPKG and effectively activate the enzyme (Paul Bowyer, unpublished work) and the latter displays good membrane permeability. Mature RAP-treated GC α :HA:cKO schizonts were smeared after incubating for one hour in the presence of varying concentrations of cGMP, 1-NH₂-cGMP and PET-cGMP. As can be seen in figure 3.10., PET-cGMP was highly effective at rescuing the egress block, resulting in the release of merozoites at all concentrations tested. While rings with normal morphology could be observed in the 62.5 and 31.2 μ M samples, parasites incubated in higher concentrations of PET-cGMP appeared as intracellular and extracellular pyknotic forms, indicating that higher concentrations may be toxic. Some rings were also observed in the cGMP and 1-NH₂-cGMP-treated samples, however these compounds were not as effective as PET-cGMP at rescuing the egress defect of GC α -deficient parasites.

To determine the ideal concentration of PET-cGMP that can be used to sustain growth in RAP-treated GC α :HA:cKO treated parasites, a SYBR Green growth assay was performed to test parasite growth at varying concentrations of PET-cGMP over 72 hours. However, none of the concentrations tested could rescue GC α knockout parasites (Figure 3.11.), even at the concentrations that could induce egress. The assay was also performed using DMSO-treated parasites to determine the EC₅₀ of PET-cGMP against asexual parasite replication *in vitro*. This revealed that PET-cGMP is toxic at high concentrations with an EC₅₀ of 12.49 \pm 0.06 μ M. Therefore it is likely that premature activation of PKG in early stage parasites, when PKG is inactive due to insufficient levels of cGMP, is lethal.

To determine whether short-term incubation of mature schizonts with PET-cGMP can be tolerated, 30 μ M PET-cGMP was added to mature DMSO- and RAP-treated GC α -

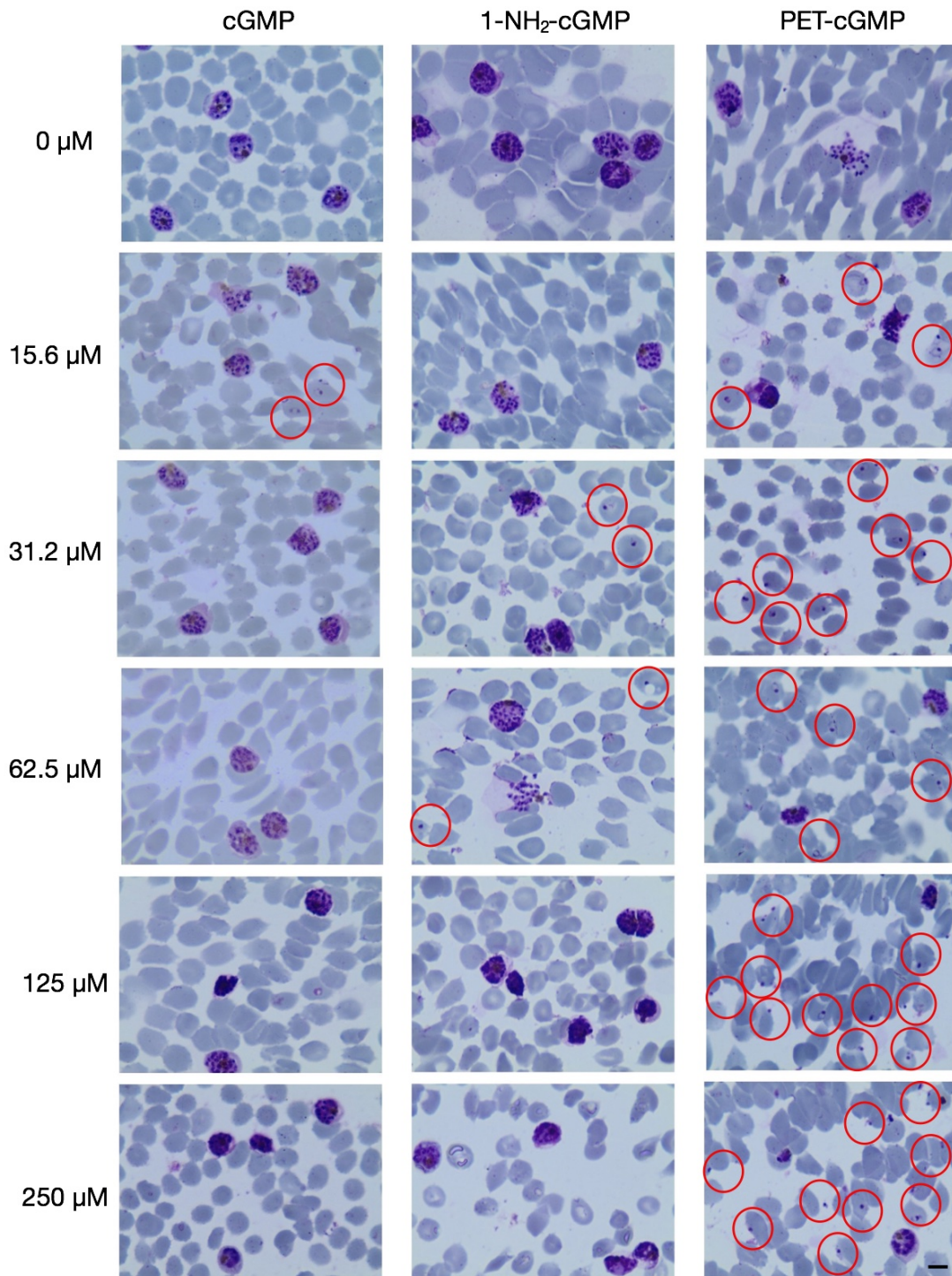


Figure 3.10. Reversing the egress block phenotype of mature GC α knockout schizonts by using cGMP analogues. Representative images of Giemsa-stained parasites from RAP-treated GC α :Ha:cKO parasites in the presence of varying concentrations of cGMP, 1-NH₂-cGMP and PET-cGMP. Released merozoites and rings are circled in red. Scale bar, 5 μ m.

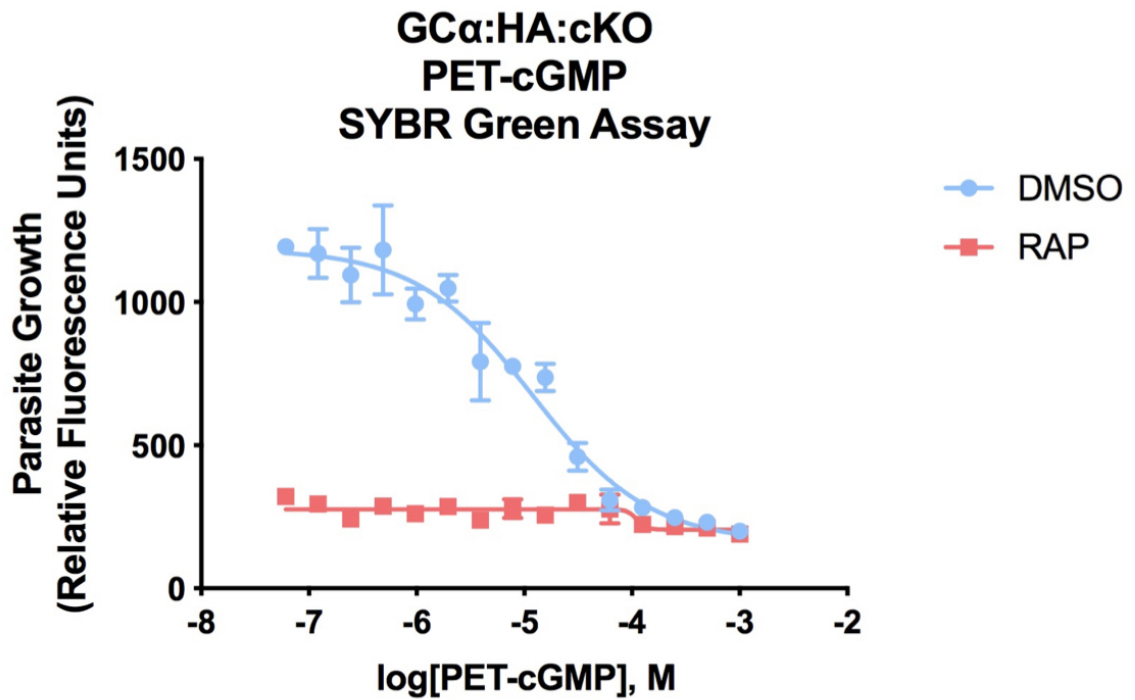


Figure 3.11. Continuous PET-cGMP treatment is toxic and does not rescue GC α knockout parasite growth. Growth curves of DMSO- and RAP-treated GC α :HA:cKO parasites at different concentrations of PET-cGMP as measured in a 72 hour SYBR Green growth assay. Assays were repeated twice and the EC₅₀ of PET-cGMP was measured as 12.49 ± 0.06 μ M using wild type parasites.

:HA:cKO schizonts and was washed off ~10 hours later, once most of the schizonts had ruptured and formed rings. This resulted in a marked decrease in toxicity, allowing RAP-treated GC α :HA:cKO parasites to mature and form schizonts (data not shown). Therefore it appears that PET-cGMP is not toxic when added to mature schizonts when PKG is supposed to be active, however it is important to wash it off to prevent premature activation of PKG in the following cycle. A flow cytometry-based replication assay was performed to quantify the level of rescue that could be achieved over 1 growth cycle using DMSO- and RAP-treated GC α :HA:cKO parasites. Parasites were treated with 30 μ M PET-cGMP once mature segmented schizonts had appeared in culture. After ~10 hours, PET-cGMP was washed off and samples were harvested the following day when parasites were unsegmented schizonts. This assay revealed that PET-cGMP treatment resulted in a 3.6-fold increase in parasitemia in RAP-treated parasites, while untreated parasites were unable to expand (Figure 3.12.A.). Furthermore, positive growth could be sustained over several cycles (Figure 3.12.B.). However, the resulting parasitemias at the end of the assay were significantly lower than those of DMSO-treated controls. Therefore it is possible to chemically complement the egress defect observed in GC α knockout

parasites by bypassing cGMP synthesis. Surprisingly, PET-cGMP rescue did not reveal a second ATPase knockout-related phenotype. This suggests that the ATPase domain is either not required for asexual blood stage growth or that it is involved in mediating cGMP synthesis, in which case chemical complementation is sufficient to bypass loss of both ATPase and GC domains.

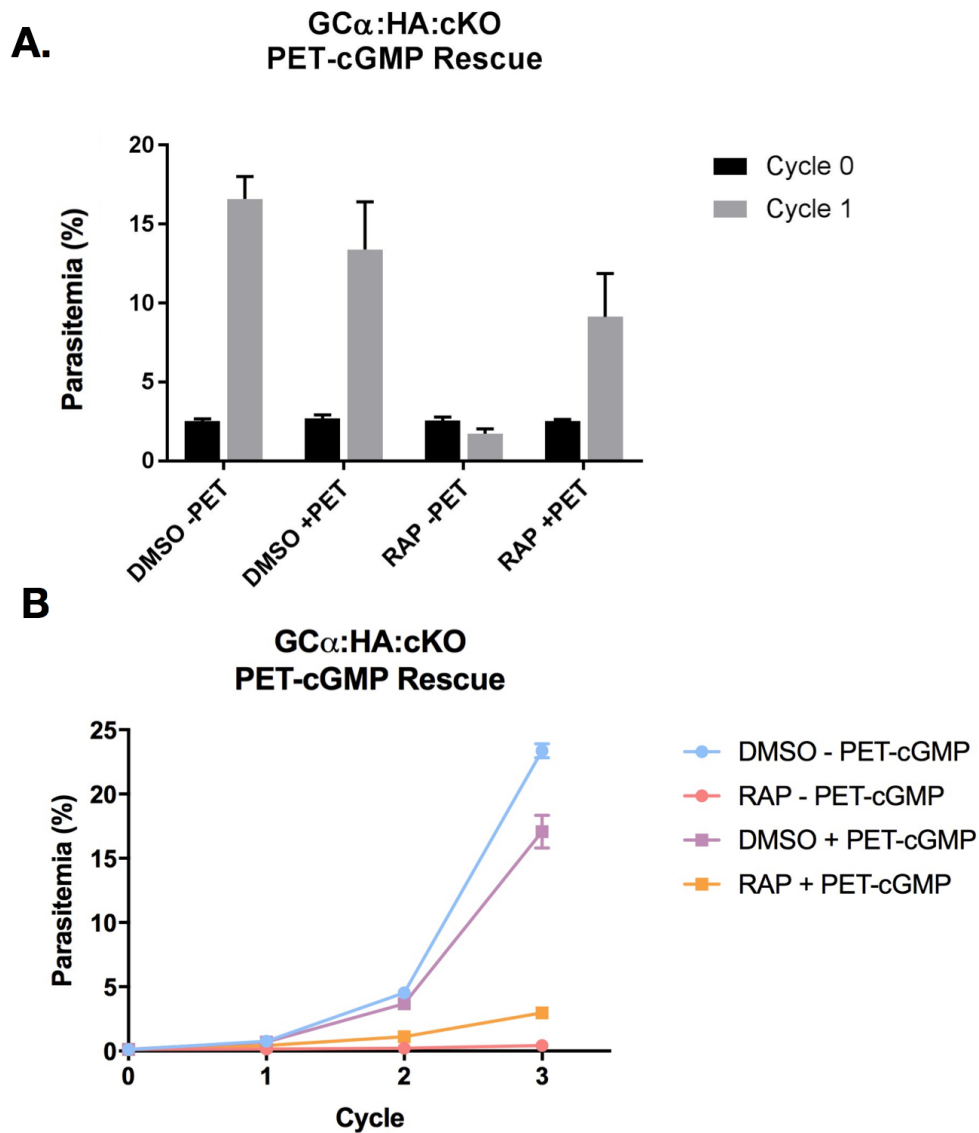


Figure 3.12. PET-cGMP treatment can bypass the need of cGMP synthesis by GC α . **A.** Parasitemias of DMSO- and RAP-treated GC α :HA:cKO DiCre parasites cultured in the presence of 30 μ M PET-cGMP or the equivalent volume of water, as measured by flow cytometry-based sorting of SYBR Green positive cells. PET-cGMP was added when schizonts appeared in culture, and was washed off around 10 hours later, once rings had formed. Data points plotted are means from two repeat experiments, each performed in triplicate. Error bars represent the standard deviation. **B.** Growth curves showing parasitemias of DMSO- and RAP-treated GC α :HA:cKO DiCre parasites over 3 cycles when treated with 30 μ M PET-cGMP or the equivalent volume of water, as measured by flow cytometry-based sorting of SYBR Green positive cells. PET-cGMP was added when schizonts appeared in culture, and was washed off around 10 hours later, once rings had formed. Data points plotted are the means from triplicate values from one experiment. Error bars represent the standard deviation.

3.2.3 The ATPase domain is essential for parasite survival

The N-terminal portion of GC α encodes a putative type IV P-type ATPase (P4-ATPase), which shares closest homology to putative aminophospholipid transporters (Baker, 2004), which are predicted to flip phospholipids from the outer to the inner leaflet of a lipid bilayer. The typical domain architecture of P4-ATPases consists of a transmembrane domain with sets of 6 and 4 transmembrane helices, which span the lipid bilayer and interact with the transported ligand; a nucleotide binding domain, which binds to ATP; a phosphorylation domain, which contains an aspartate residue within a conserved DKTGT motif which gets phosphorylated to form an aspartyl phosphate intermediate; and an actuator domain, which dephosphorylates the phosphorylation domain (Kühlbrandt, 2004; Montigny et al., 2015). GC α contains the conserved DKTGT motif in the phosphorylation domain, which is critical for ATPase activity as well as other residues conserved in P4-ATPases predicted to function as aminophospholipid flippases (Figure 3.13.).

To investigate whether the ATPase domain of GC α is essential for parasite survival, marker free CRISPR/Cas9-mediated gene editing was employed to introduce mutations in the conserved aspartate residue (D756) to block formation of the aspartyl phosphate intermediate and ablate its activity. 3D7a parasites were transfected with a pool of three different pDC2-Cas9-hDHFR plasmids, which were used to introduce the loxPint into the ATPase domain of GC α to generate the GC α :HA:cKO line, along with a repair template that would introduce the D756N mutation (Figure 3.14.A). A control transfection was also performed using a repair template that would introduce shield mutations but not change the wild type amino acid sequence to confirm that editing of the GC α locus had occurred. Parasites were treated with 2.5 nM WR99210 for one week to select for parasites that had taken up one or more of the pDC2-Cas9-hDHFR plasmids. Although parasites appeared in control transfections 2 weeks post transfection, parasites were never observed when transfected with the D756N repair template, even after 6 weeks post transfection. Transfections were repeated twice, with the same outcome. Integration was confirmed in D756 parasites from transfections 1 (T1) and 2 (T2) by integration-specific PCR (Figure 3.14.B) confirming that the phosphorylation domain had been successfully edited in both parasite lines. The failure to obtain parasites harbouring the D756N mutation after multiple attempts, strongly suggests that an active ATPase domain is required for parasite

```

ATP8B1 NTKFLCIKESK-----YANNAIKTYKNAFTFIPMNLFEQPKRAANLYFLALLILOAVQISITLAWYTTLVPLLVVLGVTAIKDLVDVVAHAKMKEINNRCEVTKDGR--FKVAKWKE
FETa --RFLNLF-----YDNNIKTSKYGFNPLMNLFEQPKRANAYFLLLFLQLVQVQISSLAWYTTVPLLVVLSITGVKDAIDDDVKKRHSDDQINNRSVLIVNGR--VEEIKWRN
Drs2p EPRVIHINDSLANSSPGYSDNHSITRYNFATFLPKFLQEFKSKYANFLPFLTSAIQQVHVSPTRNYTTIGTLVVLVIVSAMKCEIEDIKRANSKDELANNSTAEIFSEAHDDFVEKRWID
PFGCα PFSNKICSKNYGKYSFIPKGLYEQFLRLPNIFLLISLLEPIQ4SNMYYSKHSFFLLIPFIC5KNIYEDSRRSNIYQINNRCLHMLDGFNSQLKAVRWME
PFGCβ not great align RIYNSFLYFIRR-LISFDAILVYSFLFTVYIFSEINHGETTKRYLFDITAIPLFFNIILLIVIESLFLBKLLKDKVKNANSQYYLRIVPKMS----YFEKVMTKD
Actuator domain
ATP8B1 IQVGDVIRLKNKDFPADILLSSSEPNLCYVETAEILGETNLKFKMSLEITDQYLOREDTATFDGFIETCEPPNRLDKFTGTFLWRNTSFLDADKILLRGCVIRNTDFCHGLVIFAG
FETa VQVGDIIKLENNHPTADMILLSSSEPYGLTYIETADLIGETNLKVKQALVTSAMEDNLELSSFNQGEVRCDDPPNKLDFSGTLSYLGNTYLLNHERLLRGCVIRNTDWCYGLVYVYG
Drs2p IRVGGDIIRVKEEPIADTIISSSEPEGLCYIETANLIGETNLKIKQSRVETAKPID-VKTKMNGKVVSEQPNSSLYTYEGMTLNDRQIPLSPQMI LRGATLRNTAMIFGLVIFTG
PFGCα LSVGSIIRLIENEQVPADILLSCNNEGVVYIETSLNIGETNLKIKYVAVDKYIKDKDYLMKLEINGVIRCELPNKNI PCQGNFLDKHPRSLNLF3ALQSSVLKGAEYIDAVVYVYG
PFGCβ IKVGNIIIRIFQGEFPADVILYVKNN-ANAIVDSFKIILFLRKBKIKYAVDKYIKDKDYLMKLEINGVIRCELPNKNI PCQGNFLDKHPRSLNLF3ALQSSVLKGAEYIDAVVYVYG
TM3 TM4
ATP8B1 ADTKIMKNS-GKTRFKRTKIDYLMNYMVTYIFVLLISAGLAIGHAYWQAQVGN--SSWYLDGEDDTPSYRGLIFWGYIILVNTMVPISLYSVVIRLQGSHPINWDLQMYAEKDT
FETa QDQKMLQNS-GRSTFKRTHIDHLMNVVWVIMFLLGGMCFLLSIGHGIVNSRGYQAFPLPKHYITSSATSSALIFWGYIILVNTMVPISLYSVVIRLQGSYYINWDRKMYEAKPMN
Drs2p IRVGGDIIRVKEEPIADTIISSSEPEGLCYIETANLIGETNLKIKQSRVETAKPID-VKTKMNGKVVSEQPNSSLYTYEGMTLNDRQIPLSPQMI LRGATLRNTAMIFGLVIFTG
PFGCα NDTKIMKNI-SNNKHLGYVKNELN-SYTIIGLIFTFCVFSVLFKWTEDDKFRNGSHFLTYKDN--ICESVVKY--LILVNTMVPISLYSVVIRLQGSHPINWDLQMYAEKDT
PFGCβ ADTKIMKNI-ENKNTFCIKMNIIVYVLIIMYFVVLVSIKTIKIPFKHKNFQ---NSRDSPL--MLEDFVGLY----LILVNTMVPISLYSVVIRLQGSHPINWDLQMYAEKDT
Phosphorylation domain
ATP8B1 PAKARTTLENEQLQIHYIFSDKTGTLTQNIHTFKKCCINGQIYGDHRDASQHNHKK--IQEVDFSWNTYADGKLAFYDHYLIEIQISGKPEVROQDLDIFANTRTLCICLYEIEEK
FETa PAQARTTLENEQLQVQVYFSDKTGTLTENVIMFNKCSINGKTYGYSYDNGEYVFKSPKDKYDFVSNHLDAPKFSFYDKTIVLVAVKS--EDPLVYLLPCLCLSICHTMSEKVEGELV
Drs2p IRVGGDIIRVKEEPIADTIISSSEPEGLCYIETANLIGETNLKIKQSRVETAKPID-VKTKMNGKVVSEQPNSSLYTYEGMTLNDRQIPLSPQMI LRGATLRNTAMIFGLVIFTG
PFGCα YQSSSLEDECLYSSFLGYRLVLRNKTMCIE--IDGSFNKWTIIGVNEINRRKMSIVVK-PDSM4LLYVKGSDSSLSL 247 LEKQARFVSKGLRSMIFAFRVLSE
PFGCβ NLKSKKYNVNEEILNKNVLTSEVKSQITIG2EDSQKNIQSVKIBL1FLQGGCNR1IINYSKSLDISMNEYKSDNFMET23SHDDENINSLEYEDICLYNI1R4QKVYFLTYCH
Nucleotide-binding domain
ATP8B1 YQASPPDEGALVNAARNPQFAFLARTQNTITIS--ELCTERTYVNLAILLNSDRKMSIIVTPEGNIKLYCKGADTVIYERLHR-MNPTKQETFLAVCHTVMVD-RTDQGLN
FETa YQASPPDEGALVYATRNQVFCRSRTPETITVI--EMKIRVYVRLALILFENKRRMSIVTPEGRVMLFCQKADTVIYELLLHPCASLSEVYEMHDDDFASGELRLMVAVRELDKA
Drs2p YQASPPDEGALVQGGADLQYKFIIRKPNSTVYVLEETGEEKYLINLCEHSNDRKMSIIVTPEGRVMLFCQKADTVIYERLHR-MNPTKQETFLAVCHTVMVD-RTDQGLN
PFGCα YQSSSLEDECLYSSFLGYRLVLRNKTMCIE--IDGSFNKWTIIGVNEINRRKMSIVVK-PDSM4LLYVKGSDSSLSL 247 LEKQARFVSKGLRSMIFAFRVLSE
PFGCβ NLKSKKYNVNEEILNKNVLTSEVKSQITIG2EDSQKNIQSVKIBL1FLQGGCNR1IINYSKSLDISMNEYKSDNFMET23SHDDENINSLEYEDICLYNI1R4QKVYFLTYCH
Phosphorylation domain
ATP8B1 EFTWNNKFFMAASVASTNRDEALDKVYEEIEKDLILLGATAIEDKLDQGVPEITSLAKADIKIIVWLDGDKKTAENIGFACELLTDDTTICGEDINSLLHARMENQRNRGGVYAKFAP
FETa YFQTWIKKHGEAWLLENREKRALVYEEIERDMLGATAIEDKLDQGVPEITSLAKADIKIIVWLDGDKKTAENIGFACELLTDDTTICGEDINSLLHARMENQRNRGGVYAKFAP
Drs2p EYEEWNIYNEAATLDNRKAEKLEAANLEKRLIILGATAIEDKLDQGVPEITSLAKADIKIIVWLDGDKKTAENIGFACELLTDDTTICGEDINSLLHARMENQRNRGGVYAKFAP
PFGCα ETTKYRMYDACSISYLNKQRLKVAEVEFERDILYLTIGVKNLQEKVPTIDILNQSIRIIVWLDGDNVYSLHVSPLCKFNLKHKIIPHAALENS----NAKKLREGMAYELF
PFGCβ DFLRSNRFPMCLKCCY2NNEKEGGLYVRYDFNLPYISKEKNNIKIKNVIKTYLNYLKVITLCKKQISNEDIKRYIILKSIKLLSKFVYDLKFLFYDLVLEIGIIGLKNQRLR
Phosphorylation domain
ATP8B1 PVQESFFPPGGNRLIITGWSLNEIILEKTKRKNILKLFPRTEERRMRTQSKRRLEAKKQORQKNEVDLACECSAVICCRVTPKOKAMVVDLVKRYKKAITLAI CDGANDVMIKTA
FETa --ESLLESDP-----IN-----MYLARKPKMP--FKSLDEVANGNYLIVISQSLAYALEGSELEPELLRTACMCKGVVCCRMFLQKAAQVVDLVKRYKVVYLAICDGANDVMIKAA
Drs2p -----K--IN-----ALNEHQLS--THDMNTLA-----LVLIDKDLGALPELEEDYLLTVAKLCKAVICCRVSPQKALVVMYKRSKSSLLLAICDGANDVMIKAA
PFGCα QLEKEEKKPYENLCLLVNQRNLQTLFNYTDLQTHFLNMACTCDVV-----IACHITAKQKALVQLKRNRYLNTLAICDGANDVMIKAA
PFGCβ CKLQNETKGIIRTYLAL3KLTVLGIGTTLNDV4LLKYS
TM5 TM6
ATP8B1 HIGVIGSQEGMQAVMSDDYFAQFRYLQRLLLVHGRWSYIRMKCFLYFPMKNSNFAFTLVHFWYFNFNGYSAQTAYEDWFTITLVNLYTSLPVLMLGLLDQVSDKLSLRFPLYIVGQR
FETa HIGVIGSQEGMQAVLSSDFEFCQFHLQRLLLVHGRWSYIRMKCFLYFPMKNSNFAFTLVHFWYFNFNGYSAQTAYEDWFTITLVNLYTSLPVLMLGLLSEKDVNWSLCLPELYEPGQH
Drs2p HVGVIGSQEGMQAARGADLAVGQPKFLKLLLVHGRWSYIRSVAILYSFMKNTALYMQVWYVAFANSGQSIMESWTMSFNFYFTVWPFVIVGVDQVSSRLLERYPQLYKLGQK
PFGCα NIGVIMTSDCIISAGYSDYCIKPKCYLRKLLFIYGSKHLTYTISILLYNFKKNTLILPFIFFYQAYASWSCVKIYPELLYTFEFSIFWVFIPIIYYMFLQHNLYDILYNIPLFYALSRR
PFGCβ SISVFLSLNEHV2YNIISDYVLEQFKFISELLIL-GRN2LCKVFLMIIYIKLVVSVYFFHFDNYFSGSSASSLITQTTFALLHYFLIIAFSAYE1-DLPYKFRVRLPYIYQLSRR
Lysine in TM5 conserved in all P4-ATPases
TM7 TM8 TM9
ATP8B1 DLLFNKRFVSLHGVLTSMILFPIPLGAYLQTVGQDGE-APSDYQSFVAVTASALVITVNFQIGLDSYWTVFNAPSIFGSIAYLFGIMDFHSAGIHVLPFSAFOFTGTASNALRQF
FETa NLYFNKKEFVKLLHGILYNSFVLPFVPMGTVFNSENRNDG-DISDFQSFLLVQVTTLIGVMTQIALRTSWTMINHTFTWGSGLYFCILLLCSDGCLRYPISFNLGVARNLSQF
Drs2p CQFFSVYIFWGWINGFFHSALVPIGTLIYRYGFAALNHGELADHWSGVTVYTTSVIIIVLGAALVNTWTKFTLAIAPGSL-LFPWLIFFPIYAS-IFPHANISREYVGVKHTYSGG
PFGCα RYNNMCKFLPWIFEAIFYSMIYFPAYAAKENSHELLN-GEVITNTFGNICFGLLISILRPLEGSLWSPSILITCFGCFLEVPFPPSLLFCFAYLSNEYIREVFRQTFWAPLYV
PFGCβ KYFLNNNIILITIEAILISLTSYIILRLNVFHLITHREFTFHFILNVPITTEKILLLSKTWHIYF-----IMAVLIIIGILLYNIFTLVDCIKNGKGEFSLPQENIYFWTSLFP
TM10
ATP8B1 YIWLTIILAVAGCLLPVVAIRFLSMTIWPSESDKIQKH-----RKLKAEQWQRQVFRAGVSTRRSAYAFSHQRGADLISGGRSIRKKRSP-----
FETa QIWLCLILSTLTCMPLIGYELRPLRPLWIPNADKVLN-----RIHFLCKHPIPTQVQKIKHPSLRSAYAFSHKQCFGALITSGKTLKS-----
Drs2p VEWLTLIIVLPIFALVDFELMKYKRYEPEYHVIQEMQKYNISDRPHVQPNQAIKRVQVQKMKQRQCFAPSAQAEQGEKIVRMYYDTQKRGYQELQDASANPPDNNGLGSNDP
PFGCα LILLWFSTCIISYIFINETSILEPNIYVNVHMLFQYQEKHNKNIYFS
PFGCβ LIYINIFDKLMKYIKNRIYDIDSYLRKYFLRRCCHNNDKFLSQRIKIGINKPVNEKNDILKYIPTPKIYKIKDDPTTYNKSRSKFLYDTFRKVIDINVKYRQNLNLEYKTYEK

```

Figure 3.13. The ATPase domain of PfGC α possesses several conserved residues required for ATPase activity. Alignment of PfGC α and PfGC β amino acid sequences with human ATP8B1, mouse FETa and yeast Drs2p, which are probable aminophospholipid transporters. The actuator, phosphorylation and nucleotide binding domains are highlighted in red, green and blue boxes, respectively. Transmembrane domains are highlighted in grey. Highlighted yellow numbers indicate the number of amino acids not included in the analysis, while dashes represent gaps in the amino acid sequence. Several key residues required for ATPase activity are conserved in GC α , however in GC β , which possesses a pseudo-ATPase, several of these residues are missing. Alignments were done by David Baker (LSHTM, London UK).

survival. These data combined with the ability to sustain positive growth of GC α knockout parasites over several cycles by chemical complementation with PET-cGMP indicate that the ultimate role of the ATPase domain is linked to cGMP synthesis.

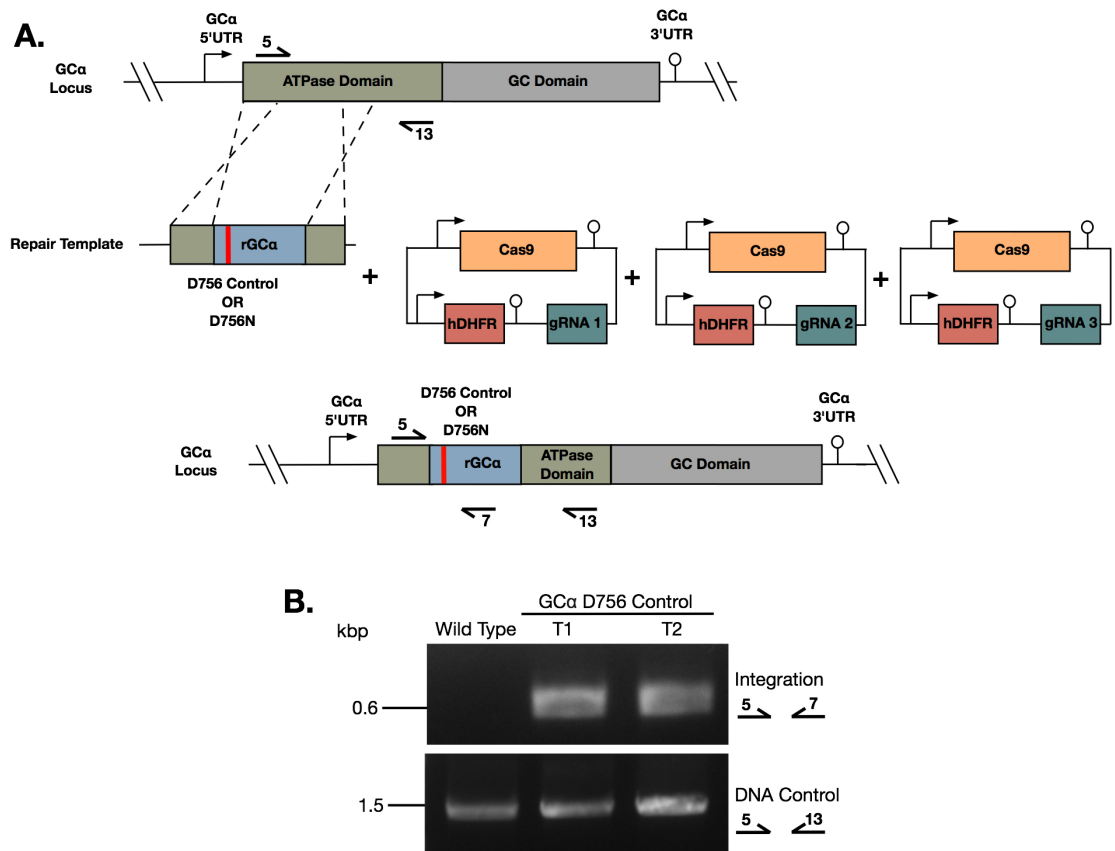


Figure 3.14. Failure to mutate the D756 residue required for ATPase activity indicates the ATPase domain is essential. **A.** Schematic representation of the marker-free CRISPR/Cas9-mediated approach used to introduce the D756N mutation, or the D756 control wild type sequence into the actuator domain of the ATPase of GC α . Scissors indicate CRISPR/Cas9 cleavage sites, while arrows represent the relative position of oligonucleotide primers used for diagnostic PCR screens. **B.** Diagnostic PCR analysis confirming integration of the D756 control wild type sequence in two independent transfections, T1 and T2 confirming successful editing of the locus. A DNA control PCR was included, which amplified a small segment at an independent locus to test the quality of the DNA used. The inability to obtain parasites harbouring the D756N mutation indicates that the ATPase is essential for parasite survival.

3.2.4 Functional analysis of the ATPase domain of GC α

Although the ATPase domain of GC α appears to be vital for parasite survival, it remains unclear what its functional role is. As previously mentioned, it is predicted that the ATPase is involved in flipping phosphatidylserine (PS) or phosphatidylethanolamine (PE). To test this, GC α :HA:cKO parasites were transfected with a plasmid (made by Avnish Patel, LSHTM London, UK) containing an expression cassette to drive constitutive expression of annexin V, a protein which binds to PS, fused to an mNeon Green tag. If GC α flips PS onto the inner leaflet of the plasma membrane, it would be expected that deletion of GC α would lead to an accumulation of PS on the outer leaflet of the plasma membrane. Therefore it would be predicted that in DMSO-treated GC α :HA:cKO parasites, annexin V would bind to the PM (Figure 3.15.A), while in RAP-treated GC α :HA:cKO parasites, annexin V would remain diffuse (Figure 3.15.B). However, since the expression levels of annexinV-mNeonGreen were very high, it was difficult to determine by microscopy whether the distribution of cytosolic vs. membrane-bound annexinV-mNeonGreen changed in DMSO- and RAP-treated mature schizonts and merozoites (data not shown). Therefore sequential protein extraction was performed by hypotonic lysis of DMSO- and RAP-treated GC α :HA:cKO schizonts to separate cytosolic proteins from membranous and membrane-bound proteins, which were then extracted by using a detergent-containing buffer. Western blot analysis of these fractions revealed that annexinV-mNeonGreen was mainly found in the cytosolic fraction of the RAP-treated sample, but a much fainter band was detected in the DMSO-treated parasites (Figure 3.15.C). This would suggest that there is less PS on the inner leaflet of the PM in the RAP-treated sample than the DMSO-treated sample. However, since there was no increase in mNeon Green signal in the membrane fraction of the DMSO-treated sample, the results of this experiment are difficult to interpret. Therefore it remains unclear whether the ATPase domain of GC α displays PS flipping activity.

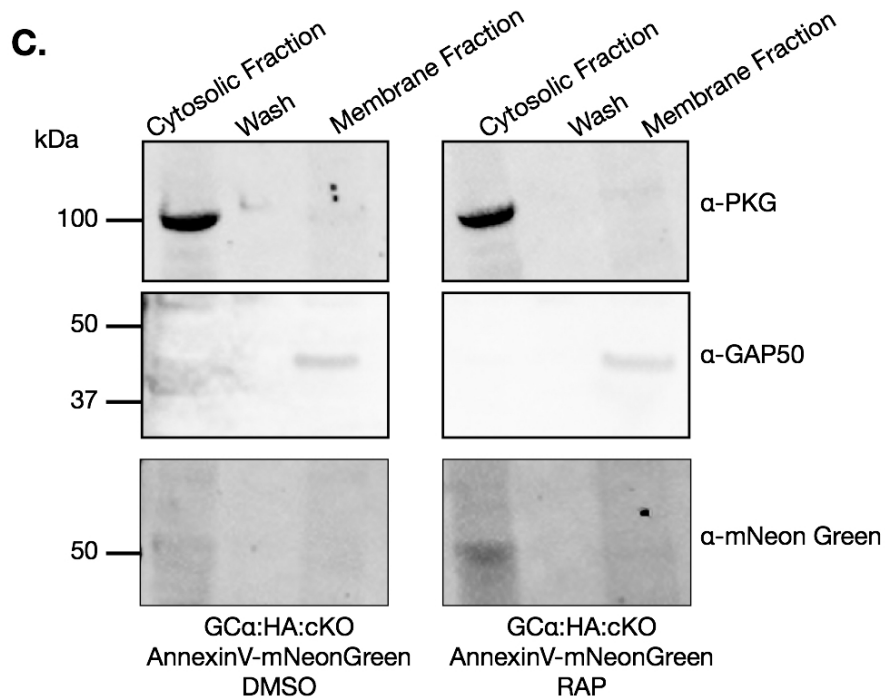
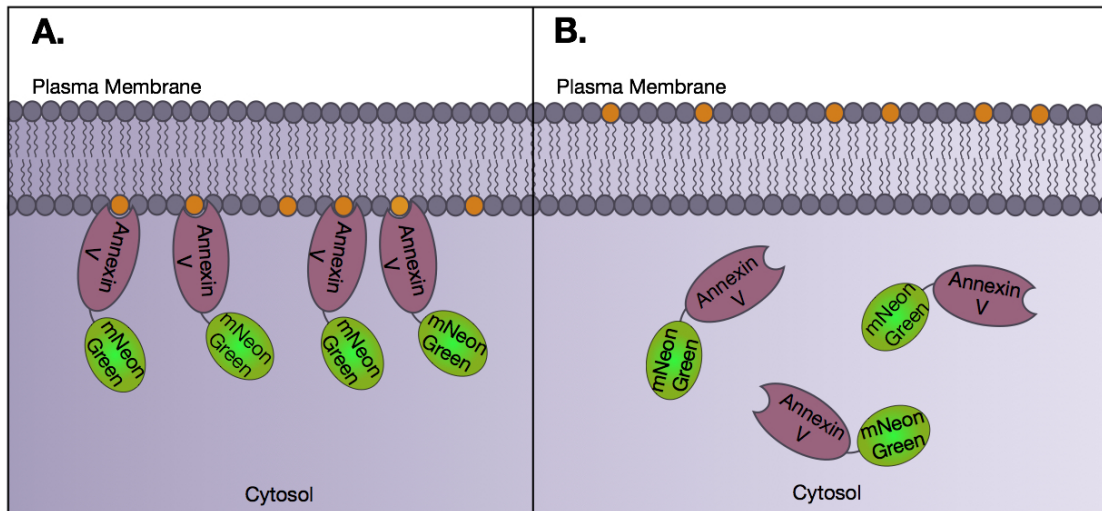


Figure 3.15. Phosphatidylserine flipping may be catalysed by GC α . If GC α is capable of flipping phosphatidylserine (depicted in yellow) it is expected that **A. in DMSO-treated GC α :HA:cKO parasites, AnnexinV-mNeonGreen would localise to the plasma membrane, while **B.** in RAP-treated GC α :HA:cKO parasites, AnnexinV-mNeonGreen would display a cytosolic localisation. **C.** Western blot analysis of the cytosolic and membrane fractions of DMSO- and RAP-treated GC α :HA:cKO parasites expressing AnnexinV-mNeonGreen. PKG and GAP50 were used as controls for the cytosolic and membrane compartments, respectively. A small amount of PKG is also observed in the membrane fractions, consistent with previous reports (Hopp et al., 2012). mNeon Green signal is mainly observed in the cytosolic fraction at the predicted molecular weight of the AnnexinV-mNeonGreen fusion protein (~63 kDa) for both DMSO- and RAP-treated samples, with a greater amount detected in the latter.**

3.3 Discussion

Recent whole genome screens in both *P. falciparum* (Zhang et al., 2018) and *P. berghei* (Bushell et al., 2017) predict that GC α is dispensable for asexual growth, however previous attempts to disrupt GC α in *Plasmodium* parasites have been unsuccessful (Taylor et al., 2008; Moon et al., 2009; Kenthirapalan et al., 2016), indicating that it plays an essential role in the asexual blood stage of infection. The data described in this chapter confirm that GC α is indeed expressed in blood stage schizonts, where it localises to the parasite periphery. Furthermore, using the conditional DiCre system, this study has definitively demonstrated that GC α is essential for asexual parasite growth. Despite deletion of both ATPase and GC domains, the phenotype observed in GC α knockout parasites was consistent with inhibition of PKG activity with mature GC α knockout schizonts unable to egress, similar to a C2 block. Indeed, GC α -deficient parasites are unable to synthesise cGMP and release Ca²⁺ from internal stores, consistent with PKG not being activated. Chemical complementation with PET-cGMP led to a substantial rescue of GC α knockout parasite growth, demonstrating that GC α could be bypassed by directly activating PKG. Surprisingly, this growth could be sustained over several cycles, despite deletion of the ATPase domain, which appears to be essential for parasite growth. Therefore chemical complementation of the GC domain is sufficient to bypass the loss of the ATPase domain, indicating that the ultimate role of the ATPase is in cGMP synthesis, potentially through regulating the activity of the GC domain.

Despite attempting to determine whether the ATPase is involved in flipping phosphatidylserine across the plasma membrane, it remains unclear whether GC α is indeed a phospholipid flippase. Studies in *Toxoplasma* have shown that TgGC does not display PS flipping activity (Bisio et al., 2019). Instead several studies have shown that the ATPase domain is required for sensing pH, K⁺ and phosphatidic acid (PA) levels, which leads to the release of Ca²⁺ (Yang et al., 2019; Bisio et al., 2019). Further work will be required to determine whether GC α also plays a role in sensing pH, K⁺ and PA levels.

Interestingly, full length GC α could not be detected by western blot analysis. Instead, it appears to migrate as a smaller band at around 175 kDa. A similar phenomenon is also observed in *Toxoplasma* (Jia et al., 2017; Bisio et al., 2019; Brown and Sibley, 2018) and

in recombinant *Paramecium* GC expressed in insect cells (Linder et al., 1999). However, Brown and Sibley have shown that the ATPase and GC domains must be expressed on the same polypeptide in order for efficient microneme secretion to take place in *Toxoplasma*. Furthermore, the ATPase domain seems to be required for correct localisation of the GC domain to the apical end of tachyzoites (Brown and Sibley, 2018; Bisio et al., 2019). The results from these studies in *Toxoplasma* would suggest that the fragments observed are likely an artefact due to protein degradation. It remains unclear whether separation of the ATPase domain from the GC domain would also ablate GC activity in *P. falciparum*. However, genetic complementation of the GC α :HA:cKO parasite line with a version of GC α which expresses each domain on a separate polypeptide could be done in the future to address this question. In *Toxoplasma* two chaperones are required for correct GC localisation and activity. This includes a cell division control 50 (CDC50) and a unique GC organiser (UGO) protein which chaperone the ATPase and GC domains, respectively (Bisio et al., 2019). Although *P. falciparum* encodes three putative CDC50s, it is unclear whether a UGO protein is encoded in the genome. BLAST analysis revealed that a conserved protein of unknown function (PF3D7_1003000) shows closest homology to UGO, however these proteins share only ~30% identity. Pulldowns using the GC α :HA tagged line will be required to identify GC α interaction partners.

4 Inducible knockdown of Myosin A using the *glmS* ribozyme

Initiation of the erythrocytic stage of the malaria parasite life cycle, responsible for disease pathology, requires active invasion of red blood cells by merozoites. This process involves substrate-dependent motility powered by Myosin A (MyoA), a motor protein which forms part of the glideosome. Typically, myosins are comprised of three domains (Sellers, 2000); the head domain, which binds to actin filaments and hydrolyses ATP; the neck domain, which acts as a linker for transducing force generated by the head domain and contains IQ motifs which are binding sites for myosin light chains; and a tail domain, which binds to cargo and can also have a regulatory role. Myosins generate force through a power stroke mechanism, which couples ATP hydrolysis to conformational changes that lead to the motor binding further along the actin filament (Tyska and Warshaw, 2002). Most myosins move along the actin filament toward the barbed (+) end, however myosin VI moves toward the pointed (-) end.

MyoA belongs to class XIV myosins, a unique group of single-headed myosins specific to apicomplexans and some ciliates. Of the 6 myosins encoded by *Plasmodium* parasites, only MyoA is well conserved across apicomplexans (Wall et al., 2019). At the start of this PhD project, there were no published reports of a MyoA knockout in *Plasmodium* parasites. Two whole genome screens in *P. falciparum* (Zhang et al., 2018) and *P. berghei* (Bushell et al., 2017) indicate that MyoA is essential for blood stage growth. In *Toxoplasma*, TgMyoA is important for egress and gliding motility and invasion (Meissner et al., 2002; Andenmatten et al., 2013), however it is not essential since its function can be compensated for by Myosin C (Egarter et al., 2014; Fréna1 et al., 2014). However, disruption of GAP45 in *P. falciparum* parasites revealed that the actomyosin motor is required for merozoite invasion, but not egress (Perrin et al., 2018). Therefore it is likely that MyoA is also required for merozoite invasion of host erythrocytes.

Currently, it is unclear how the activity of MyoA is regulated, since it lacks a TEDS consensus sequence (Heintzelman and Schwartzman, 1997), a phosphorylatable motif which regulates the mechanochemical activity of the motor (Bement and Mooseker,

1995). As mentioned earlier in the introduction, MyoA is phosphorylated in a PKG-dependent manner at a single site, Ser19 (Alam et al., 2015). Phosphorylation of TgMyoA at Ser21, the equivalent residue in *Toxoplasma gondii*, appears to be important for efficient gliding motility and egress from the host cell (Tang et al., 2014; Gaji et al., 2015). It is possible that similar to *Toxoplasma*, phosphorylation of MyoA at Ser19 may also serve as a mechanism to regulate the actomyosin motor activity in *Plasmodium* parasites. Prior to investigating the effect of phosphorylation of PfMyoA on motor activity and parasite viability, the aim of this chapter was to generate a *Plasmodium falciparum* MyoA conditional knockdown line using the *glmS* ribozyme system in order to determine whether MyoA is essential during the blood stages of infection.

The *glmS* ribozyme, found in Gram-positive bacteria, is located in the 5' untranslated region (UTR) of the *glmS* gene, which encodes the enzyme that synthesises glucosamine-6-phosphate (GlcN6P) from glutamine and glucose-6-phosphate. The ribozyme is a genetic regulatory element which binds to small molecules and regulates the expression of genes at the mRNA level (Serganov and Nudler, 2013). When physiological levels of GlcN6P are high, this small molecule binds to and activates the latent self-cleavage activity of the ribozyme, resulting in degradation of the mRNA and down-regulation of *glmS* expression and GlcN production (Watson and Fedor, 2011). In 2013, Prommana et al. showed that the *glmS* ribozyme could be used in *P. falciparum* to conditionally modulate gene expression. This can be achieved by placing the *glmS* sequence in the 3'UTR of a target gene and adding GlcN to the culture medium. Reporter genes in transgenic parasites harbouring the ribozyme sequence in the 3'UTR were successfully disrupted upon addition of GlcN leading to a knockdown in mRNA and protein levels. Several studies have since successfully used the *glmS* ribozyme to generate conditional gene knockdowns (Parkyn Schneider et al., 2017; Counihan et al., 2017; Cobb et al., 2017; Ghosh et al., 2018) with some genes showing almost complete reduction in protein levels. This system therefore provides a conditional reverse genetic tool which allows for the study of essential genes which otherwise cannot be directly disrupted. Since this system is reversible and the level of knockdown can be regulated by the amount of GlcN added to parasite cultures, it offers a more modular approach in comparison to the DiCre system which completely disrupts gene expression and is irreversible. However, the *glmS* ribozyme has had varying degrees of success, with some genes displaying only mild

reductions in protein levels (Florentin et al., 2017).

4.1 Results

4.1.1 Generating conditional Myosin A knockdown parasite lines

In order to generate a MyoA conditional knockdown parasite line, CRISPR/Cas9-mediated gene editing was used to introduce the *glmS* sequence into the 3'UTR of the endogenous *MyoA* gene (Figure 4.1.A). 3D7a parasites were transfected with the pUF1-Cas9 plasmid (Ghorbal et al., 2014), which contains the *Cas9* expression cassette and the *yeast dihydroorotate dehydrogenase (yDHODH)* selection marker conferring resistance to DSM1, a potent inhibitor of the parasite DHODH; along with a linearised construct containing the sgRNA and the repair template comprising of two homology regions flanking the cleavage site, and a recodonised region that would insert an mCherry gene sequence at the 3' end of the endogenous *MyoA* gene and introduce the *glmS* sequence just after the stop codon. The repair template would also replace the endogenous 3'UTR with the *PbDT* 3'UTR and introduce a *hDHFR* cassette which confers resistance to WR99210 in order to select for integration. The repair template was linearised in order to prevent episome formation and to ensure that drug pressure would select for parasites where integration of the repair template containing the *hDHFR* cassette into the *MyoA* locus had occurred.

After transfection, parasites were treated for one week with 1.5 μ M DSM1 to select for the pUF1-Cas9 plasmid, and 2.5 nM WR99210 to select for integration of the repair template. Parasites were subsequently cycled on/off WR99210 three times in order to enrich the population for parasites where integration of the repair template had occurred. Upon confirming successful integration by PCR, the resulting parasite line was cloned by limiting dilution (Thomas et al., 2016). Two clones were obtained and called MyoA:mCherry:glmS clone 1 and clone 2. Genomic DNA (gDNA) was extracted from the clones and integration was confirmed by PCR while a control PCR which would only amplify a product in the absence of integration confirmed that the clones did not contain any wild type DNA (Figure 4.1.B). Sanger sequencing was performed across the *glmS* sequence to confirm that the clones did not harbour any mutations that might affect GlcN-mediated knockdown.

A second parasite line called MyoA:mCherry, which lacks the *glmS* sequence, was gen-

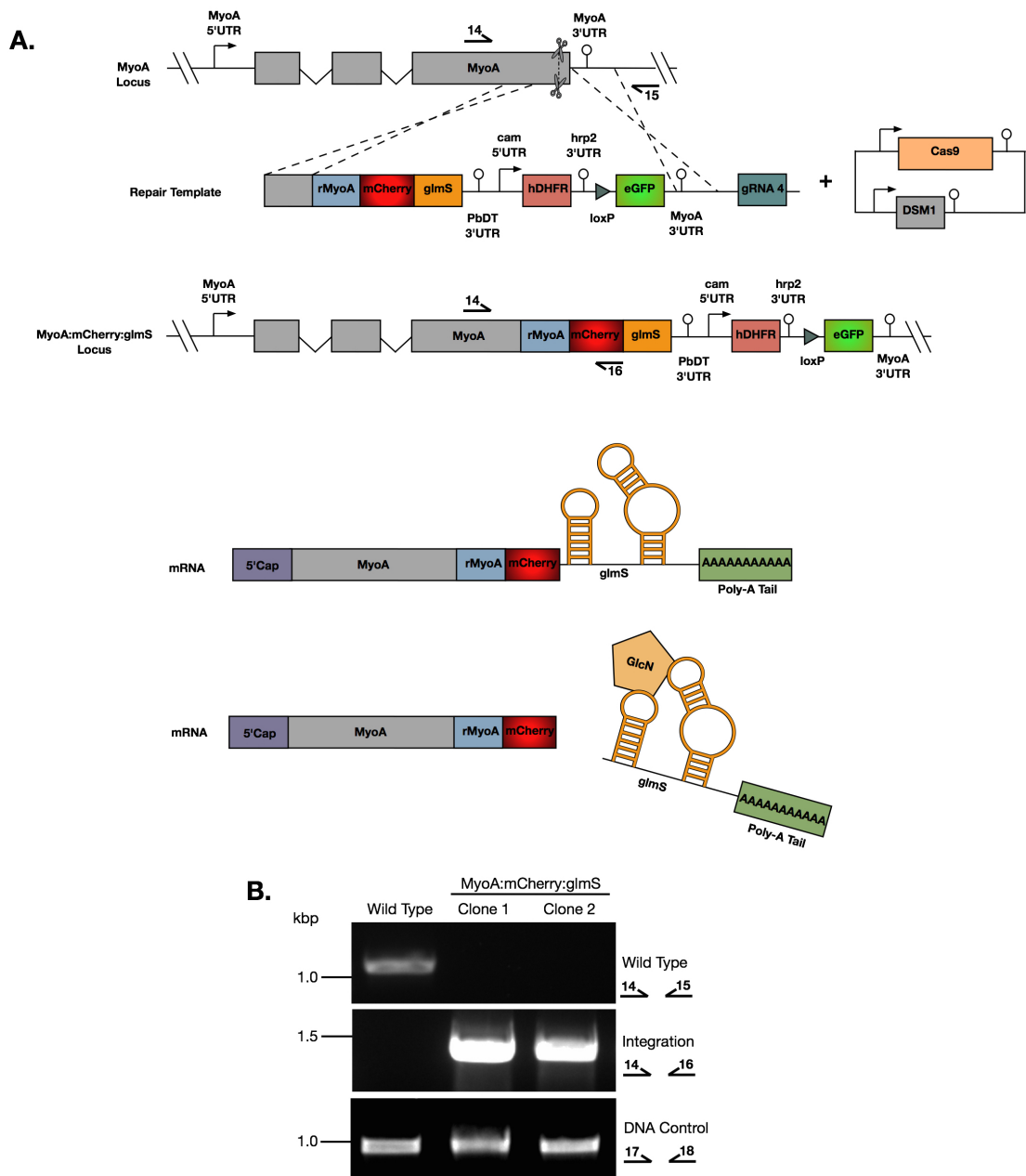


Figure 4.1. Generation of a MyoA:mCherry:glmS conditional knockdown line. A.

Schematic representation of the CRISPR/Cas9-based approach used to introduce an *mCherry* tag at the 3' end of the endogenous *MyoA* gene and install the *glmS* ribozyme in the 3'UTR. In the absence of GlcN, *MyoA* mRNA is transcribed and translated. Upon addition of GlcN, activation of the latent self-cleavage activity of the *glmS* ribozyme results in degradation of the mRNA, and knockdown of protein expression. Scissors indicate CRISPR/Cas9 cleavage sites, while arrows represent the relative position of oligonucleotide primers used for diagnostic PCR screens. **B.** Diagnostic PCR analysis confirming successful tagging of the *MyoA* locus in two independent clones, and absence of WT locus. A DNA control PCR was included, which amplified a small segment at an independent locus to test the quality of the DNA used for PCR.

erated in a similar manner to serve as a negative control for *glimS*-mediated knockdown experiments (Figure 4.2.A). gDNA was extracted from the generated line and integration was confirmed by PCR (Figure 4.2.B). Since the wild type locus could not be detected by PCR, the uncloned population was used in subsequent experiments.

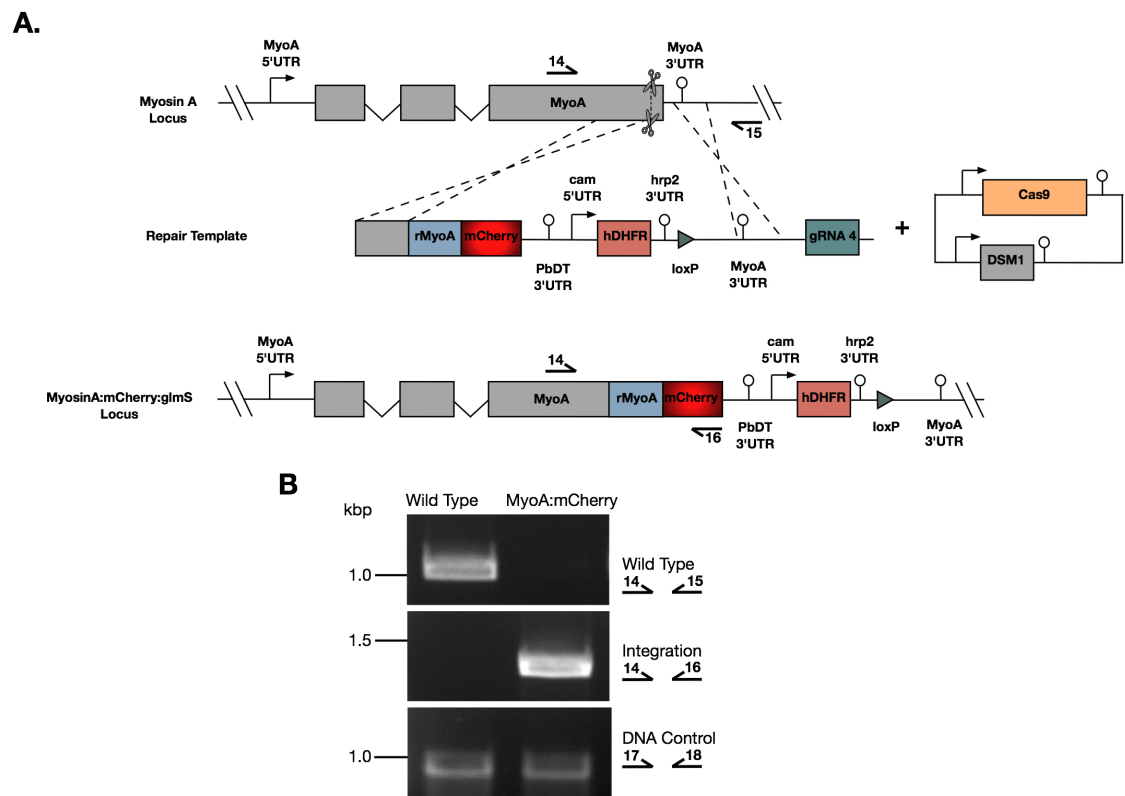


Figure 4.2. Generation of a control *MyoA:mCherry* line. **A.** Schematic representation of the CRISPR/Cas9-based approach used to introduce an *mCherry* tag at the C-terminal end of the endogenous *MyoA* gene. Scissors indicate CRISPR/Cas9 cleavage sites, while arrows represent the relative position of oligonucleotide primers used for diagnostic PCR screens. **B.** Diagnostic PCR analysis confirming successful tagging of the *MyoA* locus, and absence of WT locus. A DNA control PCR was included, which amplified a small segment at an independent locus to test the quality of the DNA used for PCR.

4.2 Glucosamine displays toxicity when used at high concentrations

When using a compound on parasite cultures, it is important to determine whether it displays any toxic effects. In the original paper, Prommana et al. used GlcN at concentrations ranging from 2.5 mM to 10 mM. Despite this, the EC_{50} of GlcN for *P. falciparum* was not reported and the effect of GlcN on wild type parasite survival and viability was not assessed. To determine whether the concentrations used in the paper showed any

toxicity, the growth of MyoA:mCherry parasites grown in the absence of GlcN or in the presence of 5 mM or 10 mM GlcN was assessed using a flow cytometry-based replication assay over two replication cycles. Culture media and GlcN were replenished every day since GlcN is not stable at 37°C. The results from this assay revealed that treatment of parasites with 5 mM GlcN showed no considerable reduction in parasitemia compared to the untreated control, while parasites treated with 10 mM GlcN showed a 65% reduction in parasitemia at the end of the assay (Figure 4.3.). Since the MyoA:mCherry line lacks the *glmS* sequence, the reduction in replication observed in the presence of 10 mM GlcN can be attributed to the toxic effects of this compound on the parasites. Therefore 5 mM GlcN was subsequently used in all further experiments.

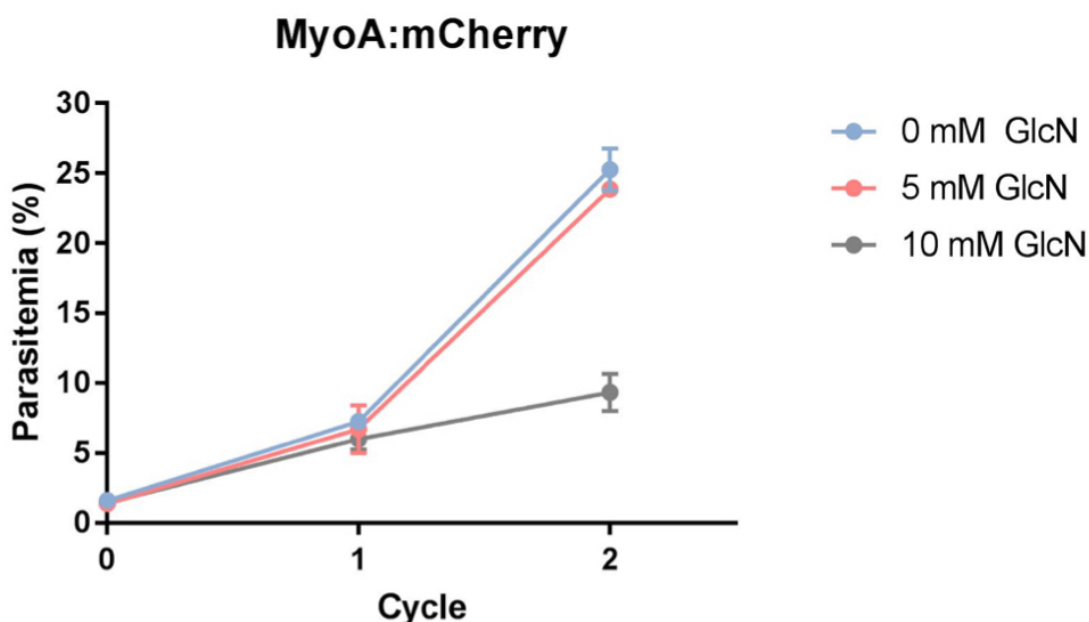


Figure 4.3. Testing MyoA:mCherry parasite growth in the presence of 5 mM and 10 mM GlcN. Flow cytometry-based growth curves showing the replication of MyoA:mCherry parasites in either the absence of GlcN or in presence of 5 mM or 10 mM GlcN over two replication cycles. 10 mM GlcN led to a marked reduction in parasite growth, while the growth of parasites in 5 mM GlcN was similar to that of the 0 mM control. Results are the mean of two independent experiments, each performed in triplicate. Error bars represent the standard deviation.

4.2.1 A partial knockdown of Myosin A results in a slight growth defect

To determine whether addition of GlcN resulted in the knockdown of MyoA at the mRNA level, RT-qPCR analysis was performed on the MyoA:mCherry control line and the MyoA:mCherry:*glmS* clones. All three cultures were tightly synchronised to a two hour window the cycle before. Early stage rings were then diluted to the desired parasitemia and treated

with or without GlcN. Parasites were also treated with 1.5 μ M compound 2 (C2), a PKG-specific inhibitor that blocks egress, in order to ensure similar staging across all parasite cultures. RNA was then harvested from these parasites at around 48 hours post invasion. RT-qPCR was then performed on these samples using primers 9 and 19 to amplify the MyoA gene and primers 20 and 21 to amplify the PDE α gene. Primer sequences are listed in table 4 in the appendix. The relative copy number of MyoA cDNA was determined by normalising against the PDE α gene (PF3D7_1209500), which has a similar expression profile to MyoA and shows little variation in mRNA levels at 40-48 hpi when MyoA is maximally expressed (Otto et al., 2010). Interestingly, addition of 5 mM GlcN to the control MyoA:mCherry line resulted in a 25% increase in relative MyoA transcripts when compared to the untreated sample (Figure 4.4.). This could have resulted either from the upregulation of MyoA expression, or a downregulation of PDE α expression in the presence of GlcN. However, both MyoA:mCherry:glmS clones showed a reduction in relative MyoA transcript levels to varying degrees following treatment with GlcN (Figure 4.4.). Clone 1 displayed a statistically significant reduction of 53% when compared to the untreated sample, while the 29% reduction displayed by clone 2 was not statistically significant.

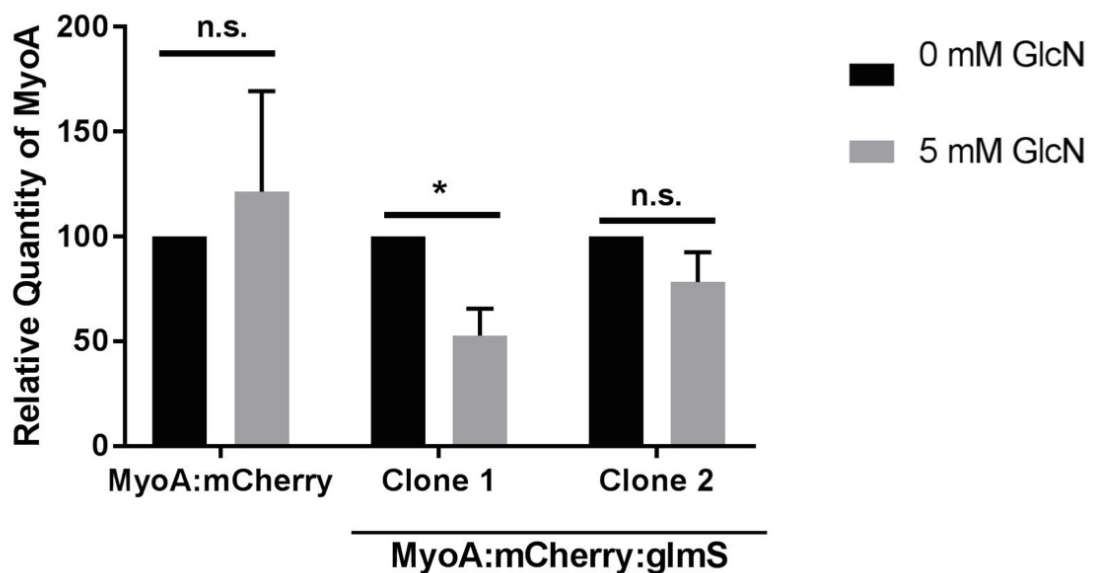


Figure 4.4. Analysis of MyoA cDNA levels in response to GlcN treatment. qRT-PCR analysis of MyoA cDNA levels. The bars represent the ratio of relative MyoA transcript levels in parasites treated with with or without 5 mM GlcN. The results from each parasite line were normalised to the matched untreated control. The data presented represent the mean of two independent experiments, each performed in duplicate. Values are normalised for PDE α (PF3D7_1209500) transcripts. Error bars represent the standard deviation. Statistical significance was measured by Welch corrected t-test, * signifies $p < 0.05$ whereas n.s. indicates not significant ($p > 0.05$).

To determine whether a knockdown of MyoA could be achieved at the protein level by adding GlcN, western blot analysis was performed using MyoA:mCherry and MyoA:mCherry:glmS parasite material harvested from C2 arrested schizonts treated with or without GlcN for 46 hours. An α -mCherry antibody was used to probe for MyoA, while α -GAPDH antibody was used as a loading control. Relative quantities of MyoA were estimated by densitometry analysis of data from three independent experiments. MyoA levels in each sample were normalised to glyceraldehyde 3-phosphate dehydrogenase (GAPDH) levels and expressed as a percentage of the corresponding untreated sample. When the data from the three biological replicates was collated, there was no significant reduction of MyoA at the protein level in any of the samples (Figure 4.5.), including MyoA:mCherry:glmS clone 1 which displayed a significant knockdown at the mRNA level.

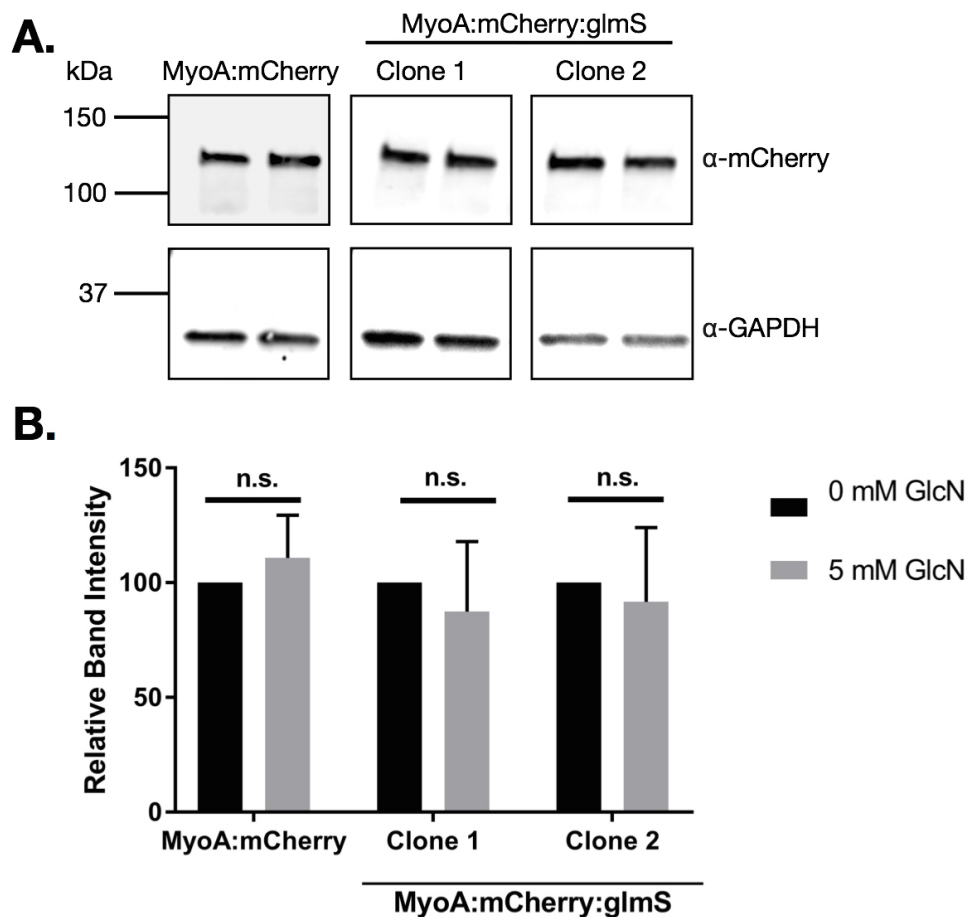


Figure 4.5. Ribozyme-mediated knockdown of MyoA expression. **A.** A representative western blot of the MyoA:mCherry control line and MyoA:mCherry:glmS clones treated with or without 5 mM GlcN probed with an α -mCherry antibody to determine levels of MyoA and an α -GAPDH antibody to serve as a loading control. **B.** Densitometry analysis of three biological replicates showing the relative band intensity of mCherry in each sample. This was calculated by normalising the α -mCherry band intensity to the α -GAPDH band intensity. Relative intensities were normalised to the matched untreated control. Statistical significance was measured by Welch corrected t-test, where n.s. indicates not significant ($p > 0.05$).

The growth of MyoA:mCherry and MyoA:mCherry:glmS parasites in the presence or absence of 5 mM GlcN was measured in a flow-cytometry based replication assay across two cycles. MyoA:mCherry:glmS clone 1 and clone 2 showed a 28% and 45% reduction in parasitemia respectively, while the growth of the control MyoA:mCherry parasites was unaffected (Figure 4.6.). Therefore despite GlcN resulting in a partial downregulation of MyoA at the mRNA and protein level in the MyoA:mCherry:glmS clones, growing parasites in the presence of GlcN over several cycles resulted in a significant decrease in parasite replication rate that was not observed in the control line. The reduction in parasite growth did not correspond to the reduced levels seen in the RT-qPCR experiments since clone 1 showed the biggest decrease in mRNA levels, but had less of a growth defect when compared to clone 2.

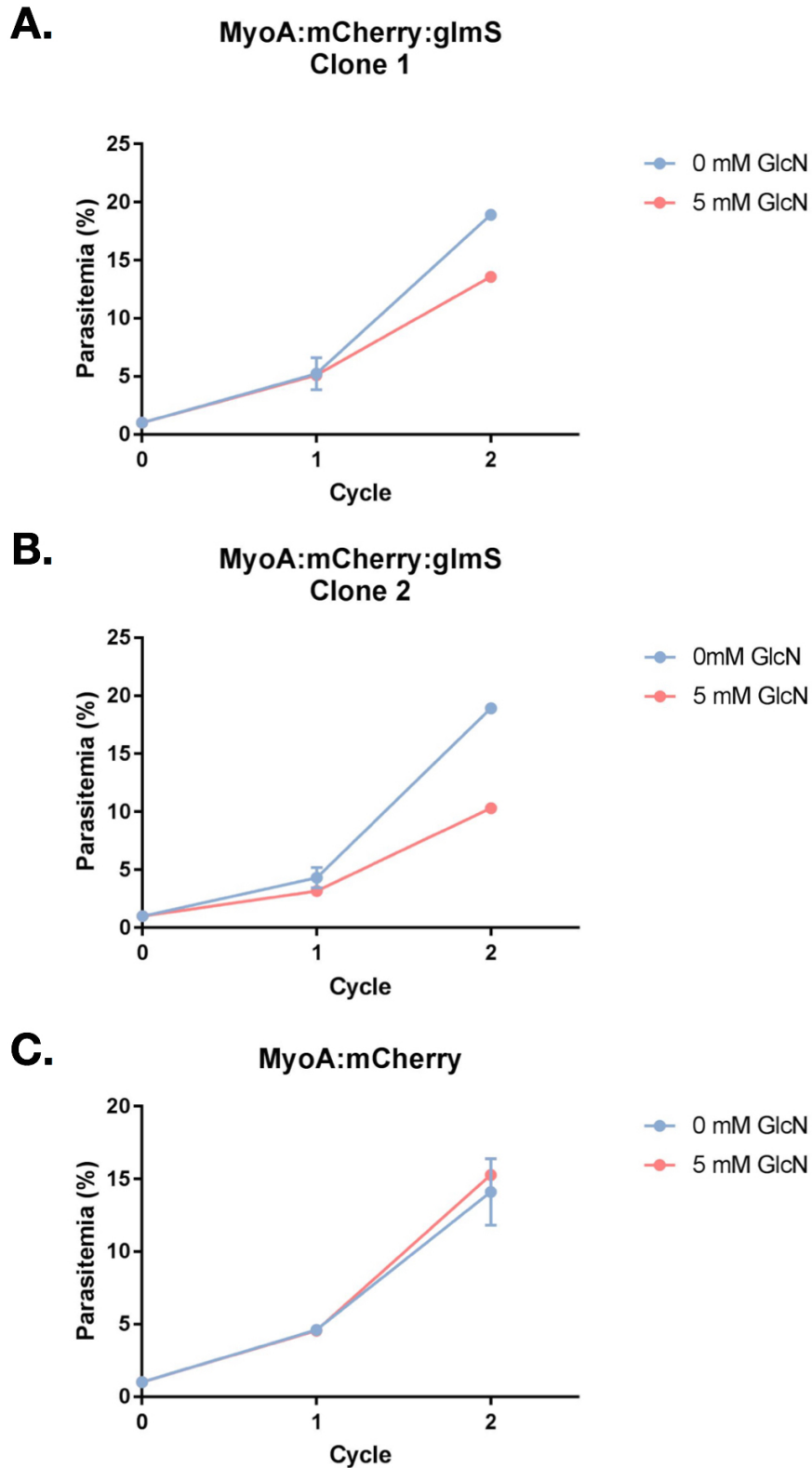


Figure 4.6. Ribozyme-mediated knockdown of MyoA expression. A-C. Flow cytometry-based growth curves showing the replication of MyoA:mCherry and MyoA:mCherry:glmS clones 1 and 2 in response to 5 mM GlcN over two replication cycles. The control MyoA:mCherry line showed no growth defect in the presence of 5 mM GlcN, while MyoA:mCherry:glmS clone 1 and clone 2 showed a marked reduction in parasitemia at the end of the assay, by 25% and 45%, respectively. Results are the mean of two independent experiments, performed in triplicate. Error bars represent the standard deviation.

4.3 Discussion

In *P. falciparum* parasites, Myosin A, which forms part of the glideosome, is thought to be the motor that helps power invasion of erythrocytes during the asexual blood stages of the lifecycle. Several attempts at generating a direct MyoA knockout in *P. falciparum* have been unsuccessful, including a recent global insertional mutagenesis screen in *P. falciparum* (Zhang et al., 2018) along with a genome-wide mutagenesis screen in *P. berghei* (Gomes et al., 2015; Bushell et al., 2017), providing evidence to suggest that MyoA is essential. Therefore, to study the role of MyoA, a *P. falciparum* line containing the the *glmS* ribozyme sequence in the 3'UTR of the *MyoA* gene was generated to conditionally knockdown MyoA by adding GlcN to the culture medium. Although the inducible *glmS* knockdown system has been a valuable reverse genetic tool allowing for the conditional knockdown of some *P. falciparum* genes, the data presented in this chapter demonstrate that this system is only partially effective at knocking down MyoA at the mRNA and protein level. As mentioned previously, this system has shown varying degrees of success (Florentin et al., 2017), however it remains unclear why certain genes are amenable to GlcN-mediated knockdown while others are not.

Furthermore, the *glmS* system showed marked differences in the degree of effectiveness between the MyoA:mCherry:*glmS* clones, and discrepancies between different types of experiments. Although a protein level knockdown was not detected in cycle 0, a growth defect became apparent after treating the clones for several cycles in the presence of GlcN. Ultimately the role of MyoA could not be elucidated using this system. Therefore, other reverse genetic approaches, such as the Cre recombinase-mediated conditional deletion system (Collins et al., 2013a), will be required to understand the role of MyoA in host cell invasion.

5 Myosin A is vital for blood stage merozoite invasion but is dispensible for gametocyte development and gametogenesis

Since the level of GlcN-mediated knockdown of MyoA in the MyoA:mCherry:glmS parasite line described in the previous chapter were not sufficient to investigate the role of MyoA, an alternative approach was adopted to generate a conditional PfMyoA knockout line. This was achieved using the conditional dimerisable Cre recombinase (DiCre) system (Collins et al., 2013a) which was also used to generate the GC α knockout line described in Chapter 3.

5.1 Results

5.1.1 Generation of a *P. falciparum* Myosin A conditional knockout line

To generate a MyoA conditional knockout (cKO) using the DiCre system, a two step approach was taken. First, a *loxP* site was introduced in the 5' untranslated region (UTR) of the endogenous *MyoA* gene, just upstream of the start codon using marker-free CRISPR/Cas9-mediated gene editing. 3D7a parasites harbouring the DiCre cassette in the *Pfs47* locus (a gift from Marta Tiburcio, Francis Crick Institute London, UK) were transfected with a linearised repair template consisting of two homology arms flanking a *loxP* site, along with a pool of two different pDC2-Cas9-hDHFR plasmids (Lim et al., 2017), each harbouring a different gRNA to maximise editing efficiency of the locus (Figure 5.1.A). Transfected parasites were cultured in the presence of 2.5 nM WR99210 for 9 days to select for parasites harbouring at least one of the pDC2-Cas9-hDHFR plasmids. Parasites were detected after around 4 weeks and gDNA was extracted. Integration of the repair template would lead to the removal of the two endogenous introns, effectively making the *MyoA* coding sequence shorter in *loxP:MyoA* parasites. This was exploited for PCR analysis to confirm successful integration of the *loxP* site. Indeed, the PCR amplification product obtained from the transfectants was smaller than that from the parental line (Figure 5.1.B), confirming integration of the *loxP* site. Since the pDC2-Cas9-hDHFR plasmids do not encode a negative selection cassette, the resulting *loxP:MyoA* line was cultured in the absence of WR99210 for 1 month to promote loss of the pDC2-Cas9-

hDHFR plasmids so that the *hDHFR* cassette could be recycled in future transfections. The parasites were cloned by limiting dilution (Thomas et al., 2016) and the resulting loxP:MyoA clone was WR99210 sensitive, and the *hDHFR* cassette could not be amplified by PCR (data not shown).

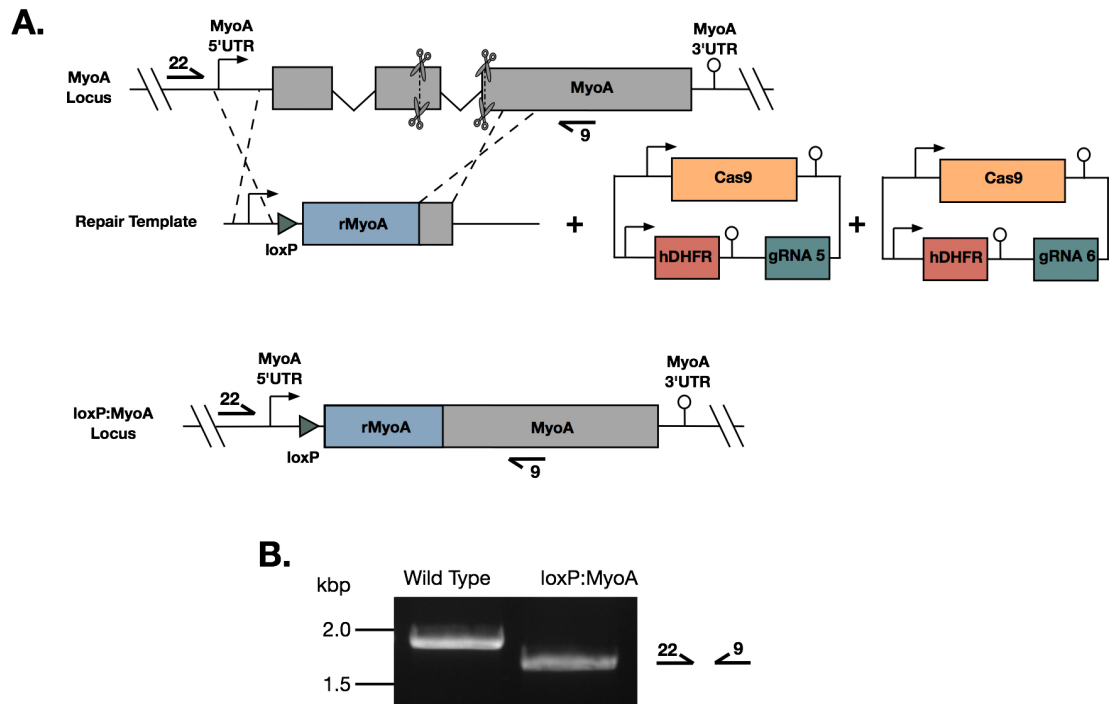


Figure 5.1. Introduction of a *loxP* site in the *MyoA* 5'UTR. **A.** Schematic representation of the marker-free CRISPR/Cas9-mediated approach used to introduce a *loxP* site into the 5'UTR of the *MyoA* gene, 6 basepairs upstream of the start codon. Scissors indicate CRISPR/Cas9 cleavage sites, while arrows represent the relative position of oligonucleotide primers used for diagnostic PCR screens. **B.** Diagnostic PCR analysis showing amplification of a smaller PCR product in loxP:MyoA parasites compared to parental wild type parasites, confirming successful integration of the repair template and deletion of the endogenous introns in loxP:MyoA parasites.

A second CRISPR/Cas9-mediated gene editing step was carried out to introduce an mCherry tag at the 3' end of the *MyoA* gene followed by a second *loxP* site (Figure 5.2.A). The repair template would also replace the endogenous 3'UTR with the *PbDT* 3'UTR and introduce a *hDHFR* cassette to select for integration. This was achieved by transfecting clonal loxP:MyoA parasites with the linear repair template used to generate the control *MyoA*:mCherry line described in Chapter 4, along with the pUF1-Cas9 plasmid (Ghorbal et al., 2014). Following transfection, parasites were treated with 1.5 μ M DSM1 to select for the pUF1-Cas9 plasmid, and 2.5 nM WR99210 for 9 days to select for integration of the repair template. Parasites were subsequently cycled on/off WR99210 three times, in order to enrich the population for parasites where integration of the repair template had

occurred. PCR analysis confirmed integration of the mCherry tag and absence of wild type locus in the resulting *MyoA*:mCherry:cKO line (Figure 5.2.B).

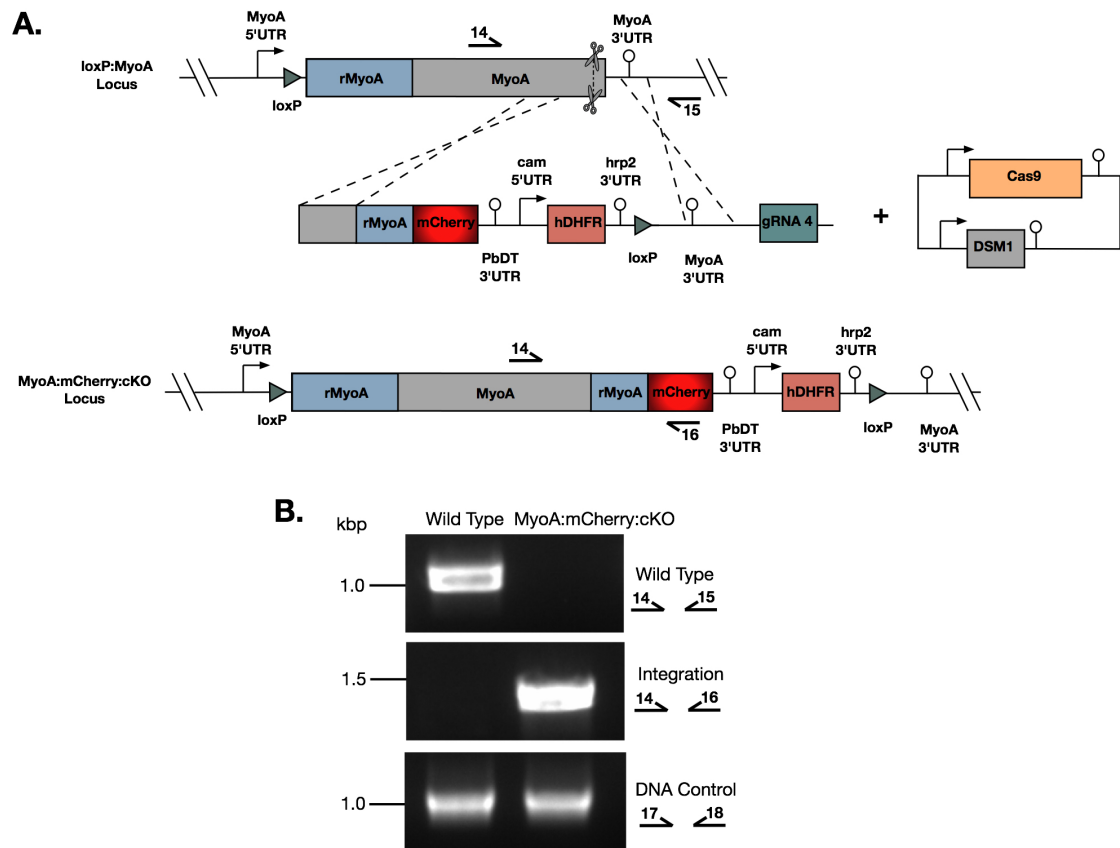


Figure 5.2. Generation of a *MyoA*:mCherry:cKO line. **A.** Schematic representation of the CRISPR/Cas9-mediated approach used to introduce an *mCherry* fluorescent tag gene at the 3' end of the endogenous *MyoA* gene, along with an *hDHFR* cassette and a second *loxP* site. Scissors indicate CRISPR/Cas9 cleavage sites, while arrows represent the relative position of oligonucleotide primers used for diagnostic PCR screens. **B.** Diagnostic PCR analysis confirming integration of the mCherry tag in *MyoA*:mCherry:cKO parasites and absence of wild type locus. A DNA control PCR was included, which amplified a small segment at an independent locus to test the quality of the DNA used.

5.1.2 Myosin A is essential for parasite invasion but not egress

The strategy was designed so that rapamycin-mediated activation of the DiCre subunits would lead to the excision of the entire *MyoA* gene, and loss of mCherry signal in the *MyoA*:mCherry:cKO line (Figure 5.3.A). Early ring stage *MyoA*:mCherry:cKO parasites were treated with either 100 nM rapamycin or the equivalent volume of DMSO for four hours. gDNA was harvested from the parasites once they became segmented schizonts and PCR analysis confirmed that RAP treatment led to the excision of the *MyoA* gene, however a faint integration band could still be detected in the RAP-treated sample, in-

dicating that excision was not 100% effective (Figure 5.3.B). Western blot analysis revealed an 81% reduction in MyoA-mCherry at the protein level (Figure 5.3.C) confirming that RAP-mediated excision was effective but incomplete. Immunofluorescence imaging also confirmed the loss of RFP signal in RAP-treated parasites, while in DMSO-treated parasites, MyoA colocalises with GAP45 at the periphery of intracellular merozoites as expected (Figure 5.3.D). Despite several attempts to improve the excision efficiency of MyoA:mCherry:cKO parasites by testing different concentrations of rapamycin, treatment times and by treating at different stages of the lifecycle, there was always a substantial proportion of unexcised parasites (data not shown).

A flow cytometry-based growth assay was performed on DMSO- and RAP-treated MyoA:mCherry:cKO parasites to assess the impact of MyoA disruption on parasite growth. MyoA-deficient parasites displayed a significant growth defect and were unable to proliferate in culture, confirming that MyoA is essential for parasite growth (Figure 5.4.A). Examination of Giemsa-stained blood smears from MyoA:mCherry:cKO cultures from cycle 1 post excision showed that in RAP-treated cultures, there was an accumulation of free merozoites and an absence of ring stage parasites, demonstrating a defect in RBC invasion (Figure 5.4.B). Although MyoA knockout parasites appear to egress normally, it is possible that they may display minor changes in egress kinetics compared to wild type parasites.

To determine whether there were any changes in the egress kinetics in MyoA-deficient parasites, live time-lapse DIC and fluorescence microscopy was performed on mature DMSO- and RAP-treated MyoA:mCherry:cKO schizonts released from a C2 block that were mixed and imaged in the same imaging chamber. As can be seen in figure 5.5.A, both DMSO- and RAP-treated parasites were able to rupture, with no statistical difference in the rate of egress between RAP- and DMSO-treated parasites (Figure 5.5.B). Consistent with this, examination of culture supernatants from rupturing DMSO- and RAP-treated schizonts confirmed that there were no changes in the release of the PV-resident serine repeat antigen 5 (SERA5), which is released into the culture supernatant during egress (Figure 5.5.C). Together, these results confirm that MyoA is not required for egress, consistent with the results observed when GAP45 is disrupted in *P. falciparum* parasites (Perrin et al., 2018).

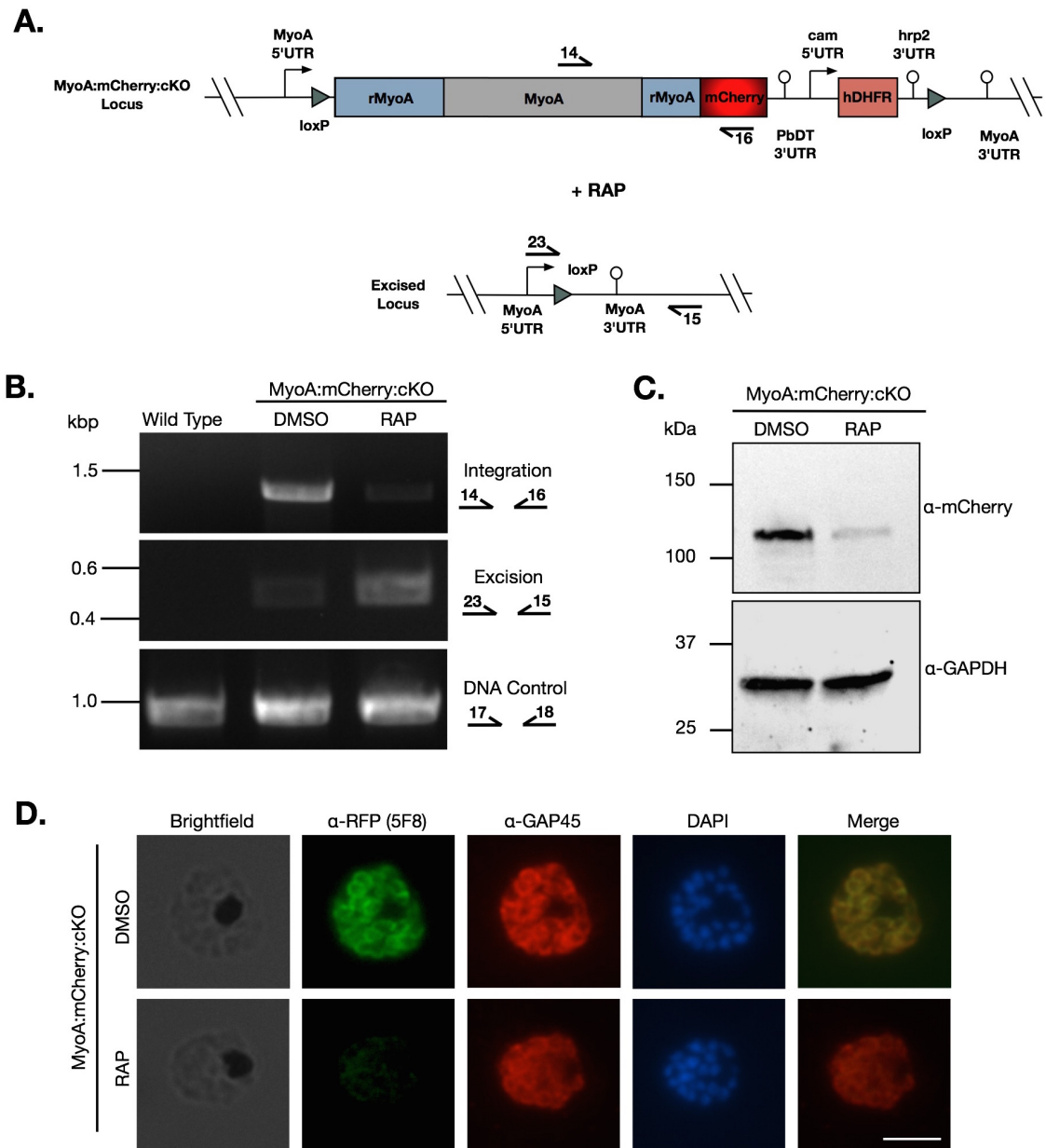


Figure 5.3. RAP treatment of MyoA:mCherry:cKO parasites results in a loss of MyoA-mCherry expression. **A.** Schematic representation of RAP-mediated excision of the entire *MyoA* gene. Arrows represent the relative position of oligonucleotide primers used for diagnostic PCR screens. **B.** Diagnostic PCR analysis of DMSO- and RAP-treated MyoA:mCherry:cKO parasites showing efficient yet incomplete excision of the *MyoA* gene following RAP treatment. A DNA control PCR was included, which amplified a small segment at an independent locus to test the quality of the DNA used. **C.** Western blot analysis of DMSO- and RAP-treated MyoA:mCherry:cKO parasites probed with an α -mCherry antibody (ab183628) confirming tagging of MyoA in the DMSO control samples and RAP-induced reduction in MyoA expression levels. Blots were also probed with an α -GAPDH antibody to serve as a loading control. **D.** IFA showing colocalisation of RFP and GAP45 signals at the periphery of individual merozoites in DMSO-treated MyoA:mCherry:cKO parasites, and ablation of RFP signal by RAP-treatment. Scale bar, 5 μ m.

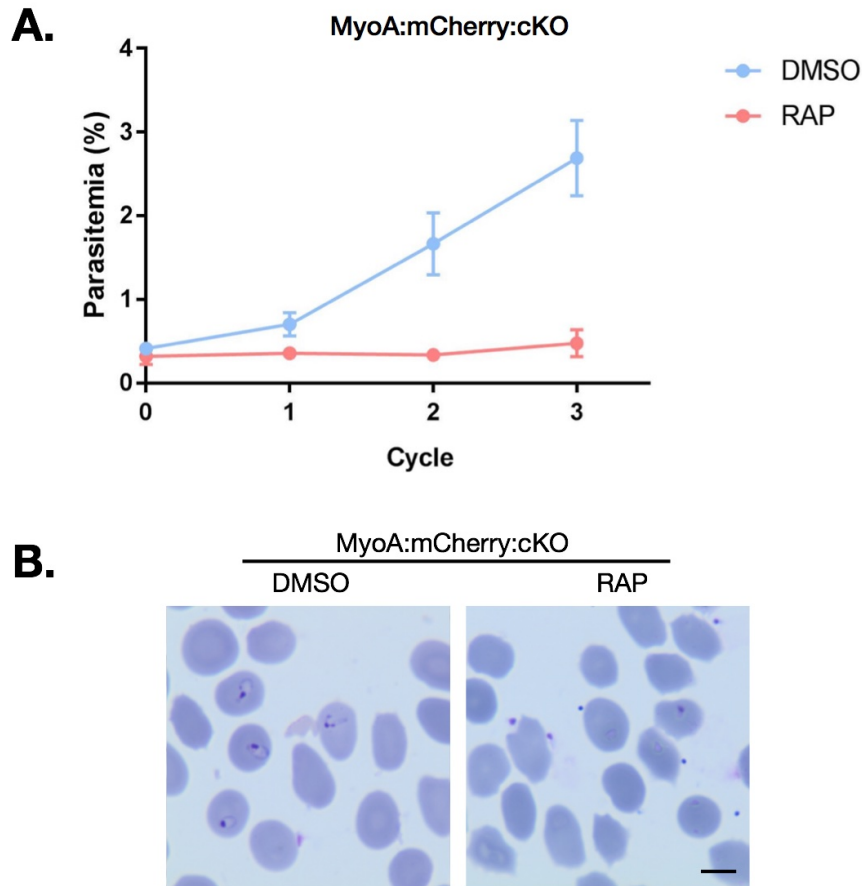


Figure 5.4. Ablation of MyoA expression leads to a severe growth defect and the inability of merozoites to invade host erythrocytes. **A.** Growth curves showing parasitemias of MyoA:mCherry:cKO parasites treated with either DMSO or RAP, measured by flow cytometry-based sorting of SYBR Green positive cells. Data points plotted are means from two repeat experiments, each performed in triplicate. Error bars represent the standard deviation. RAP-treatment resulted in a severe growth defect in MyoA:mCherry:cKO parasites. **B.** Representative microscopy images of Giemsa-stained parasites from DMSO- and RAP-treated MyoA:mCherry:cKO cultures, showing the presence of rings in DMSO-treated samples and the absence of rings in RAP-treated samples, where merozoites appeared attached to erythrocytes, indicating an invasion defect. Scale bar, 5 μ m.

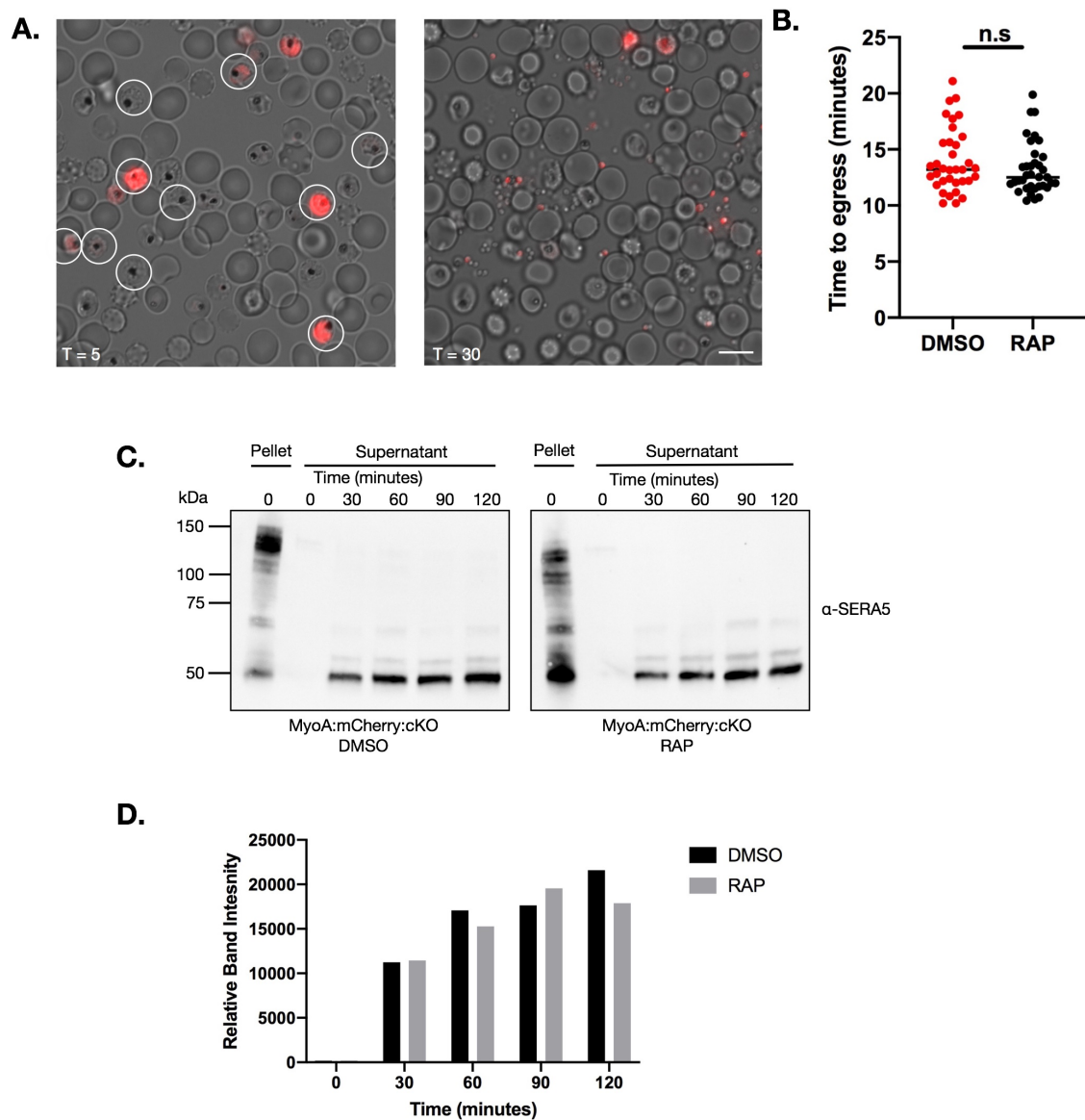


Figure 5.5. Egress kinetics are not altered in *MyoA* knockout parasites. **A.** DIC and fluorescence images from time lapse video microscopy of DMSO- and RAP-treated *MyoA:mCherry:cKO* schizonts taken at 5 minutes and 30 minutes after releasing from a C2 block. DMSO-treated parasites are mCherry positive, while RAP-treated parasites are mCherry negative due to excision of the *MyoA:mCherry* sequence. Schizonts from the first frame that rupture over the course of the video are circled in white. Scale bar, 10 μ m. **B.** Quantification of the time taken for DMSO- and RAP-treated schizonts to egress. Data are collected from 3 videos. The average time for DMSO-treated parasites to egress was 14 minutes while for RAP-treated parasites it was 13.26 minutes. Statistical significance was measured by unpaired t-test, where n.s. indicates not significant ($p > 0.05$). **C.** Western blot analysis monitoring the release of SERA5 into the culture supernatant of DMSO- and RAP-treated *MyoA:mCherry:cKO* schizonts, as a measurement of egress over time. Pellet samples were included as loading controls. **D.** Densitometry analysis of the egress assay western blot samples shown in figure 5.5.C., showing that no significant changes in SERA5 release into the supernatant between DMSO- and RAP-treated *MyoA:mCherry:cKO* parasites.

5.1.3 Deletion of Myosin A does not disrupt expression of other glideosome components or formation of the IMC

IFA (Figure 5.6.A) and western blot analysis (Figure 5.6.B) performed on DMSO- and RAP-treated MyoA:mCherry:cKO parasites revealed that both localisation and expression levels of Myosin A-tail interacting protein (MTIP) and glideosome-associated protein 45 and 50 (GAP45 and GAP50) were not affected upon depletion of MyoA, suggesting that glideosome stability and assembly is not reliant on the presence of the motor protein. On the other hand, as reported by Perrin et al., deletion of GAP45 leads to a significant reduction in MTIP and MyoA levels, indicating that the stability of these proteins is reliant on expression of GAP45, which may serve as a mechanism for degrading excess MyoA that is not actively engaged with the glideosome to prevent it from binding to actin and blocking interaction of MyoA that has formed an active complex with the glideosome.

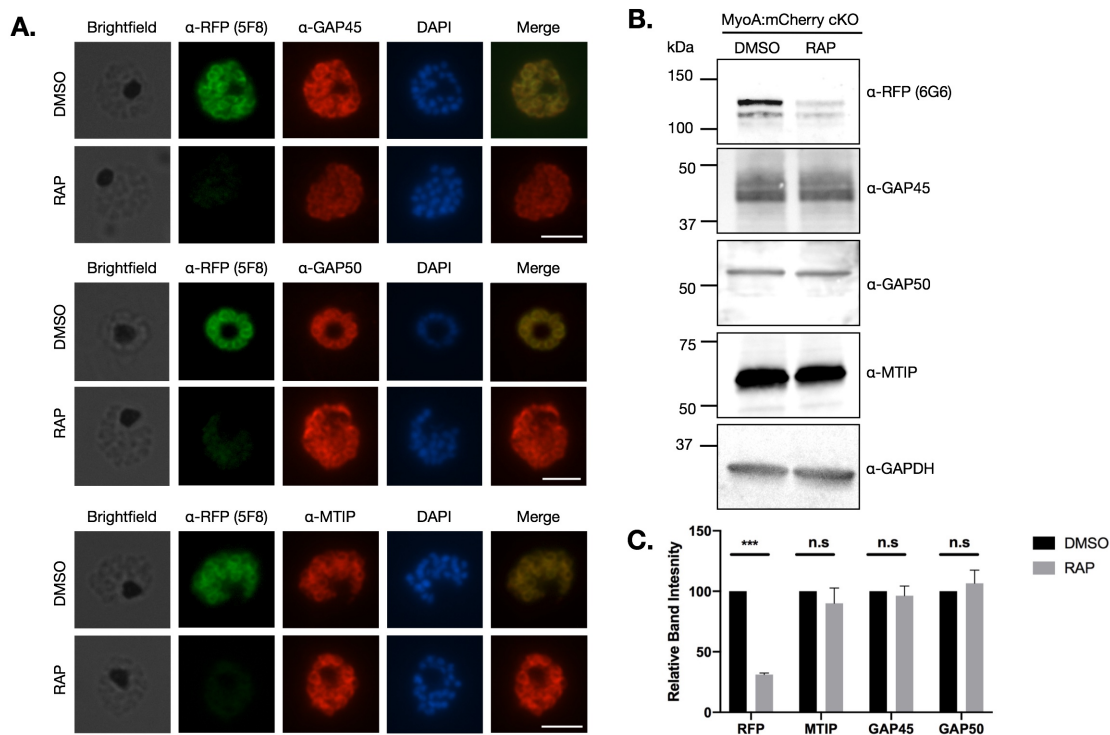


Figure 5.6. Glideosome assembly and stability is not affected in MyoA-deficient parasites.

A. IFA showing colocalisation of RFP signal with other glideosome components including GAP45, GAP50 and MTIP in DMSO-treated MyoA:mCherry:cKO parasites. RAP-mediated deletion of MyoA did not disrupt the peripheral localisation of GAP45, GAP50 or MTIP. Scale bars, 5 μ m. **B.** Representative western blot analysis showing the expression levels of MyoA-mCherry, GAP45, GAP50, MTIP in DMSO and RAP-treated MyoA:mCherry:cKO parasites. Blots were also probed with an α -GAPDH antibody to serve as a loading control. **C.** Densitometry analysis of the western blot samples shown in Figure 6B. Relative band intensities were calculated by normalising samples to the matched GAPDH signal. Samples were then normalised to their matched DMSO-treated controls. Data presented are means from two independent experiments. Error bars represent standard deviation. Results indicate that there were no significant changes in expression levels of MTIP, GAP45 or GAP50 upon RAP-mediated excision of MyoA. RAP treatment led to a significant reduction in RFP levels, consistent with deletion of MyoA-mCherry. Statistical significance was measured by unpaired t-test, where n.s. indicates not significant ($p > 0.05$) whereas *** signifies $p < 0.001$.

5.1.4 Genetic complementation of MyoA:mCherry:cKO parasites rescues the growth defect when the endogenous MyoA gene is deleted

To confirm that the growth defect observed upon RAP treatment of MyoA:mCherry:cKO parasites was specifically due to deletion of MyoA and not due to rapamycin treatment or any unidentified genomic alterations in these parasites, an "inducible expression" genetic complementation approach was employed. This approach, developed by Avnish Patel (LSHTM London, UK), has previously been used to rescue PKA knockout parasites by RAP-activated expression of a second ectopic copy inserted into the *p230p* locus (Patel et al., 2019). MyoA:mCherry:cKO parasites were transfected with the pDC2-p230p-Cas9-gRNA plasmid which would introduce a double strand break in the *p230p* locus (Knuepfer et al., 2017; Mogollon et al., 2016) and a linearised repair template which would integrate a promoterless second copy of the *MyoA* gene tagged at the 3' end with the *enhanced green fluorescent protein (eGFP)* gene (Figure 5.7.A). The repair template would also introduce an expression cassette consisting of a *MyoA* promoter followed by a floxed coding sequence which would express cytosolic eGFP and confer resistance to blasticidin S (BSD). The *eGFP* and *blasticidin S deaminase (BSDr)* genes were separated by a T2A peptide, a self-cleaving peptide which would allow the two genes to be expressed as separate polypeptides. Two days after transfection, parasites were treated with 5 µg/ml BSD (Sigma) for one week to select for integration. BSD resistant parasites, were observed around 4 weeks post transfection and the resulting line was called MyoA:mCherry:cKO + p230p:MyoA(WT):eGFP. Live fluorescence microscopy confirmed that these parasites were both mCherry and GFP positive, with the mCherry signal localising to the periphery of individual merozoites, while the GFP signal was diffuse and encompassed the parasite cytosol (Figure 5.7.B).

The strategy was designed so that RAP treatment of MyoA:mCherry:cKO + p230p:MyoA(WT):eGFP parasites would lead to deletion of the endogenous *MyoA:mCherry* and the floxed *eGFP-T2A-BSDr* coding sequences, placing the ectopic *MyoA:GFP* sequence under the control of the *MyoA* promoter (Figure 5.8.A). Early ring stage parasites were treated with 100 nM RAP or the equivalent volume of DMSO for 3 hours and segmented schizonts from the excision cycle were examined by live fluorescence microscopy. This revealed that RAP-treated parasites displayed a loss in mCherry signal and a change in

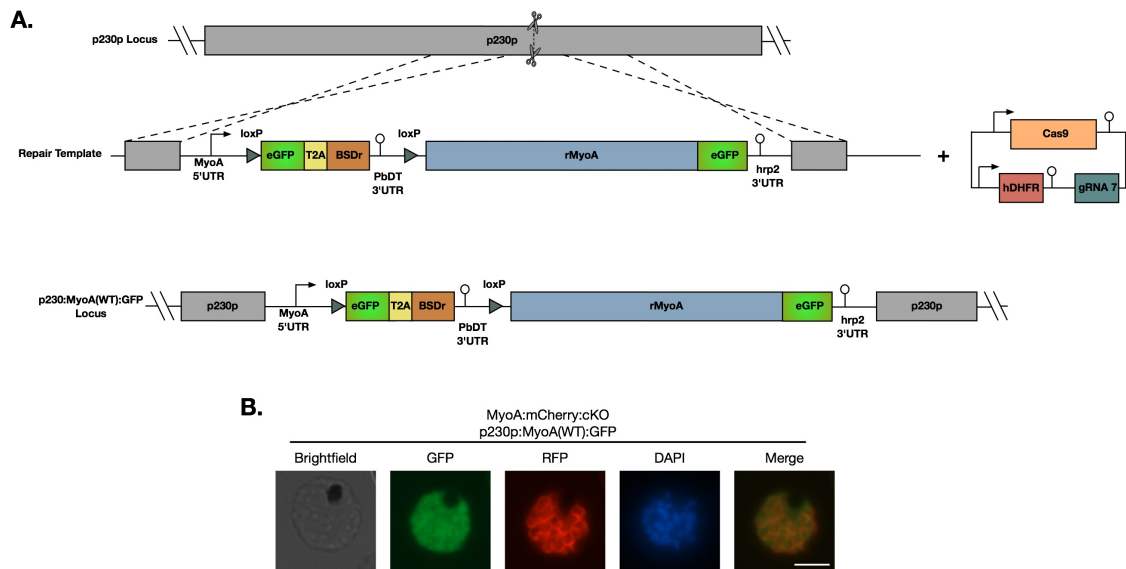


Figure 5.7. Generation of a genetically complemented *MyoA:mCherry:cKO* line. A. Schematic representation of the CRISPR/Cas9-mediated approach used to generate an inducible genetically complemented *MyoA:mCherry:cKO* line. Integration would lead to the expression of cytosolic eGFP and BSDr, under the control of the *MyoA* promoter. Scissors indicate CRISPR/Cas9 cleavage sites. **B.** Live fluorescence microscopy confirming cytosolic expression of eGFP in *MyoA:mCherry:cKO* + *p230p:MyoA(WT):eGFP* parasites, confirming successful integration of the repair template. The GFP and mCherry signals do not overlap, confirming that expression of *MyoA(WT)-eGFP* could not be detected prior to RAP treatment. Scale bar, 5 μm .

GFP pattern from cytosolic to peripheral, confirming deletion of the endogenous *MyoA:mCherry* and expression of *MyoA-GFP* from the *p230p* locus (Figure 5.8.B). Western blot analysis also confirmed that RAP treatment resulted in a reduction but not total loss of *MyoA-mCherry* expression and induction of *MyoA-GFP* expression (Figure 5.8.C). However, cytosolic eGFP which would migrate as a ~ 30 kDa band could not be detected in either DMSO- or RAP-treated samples. A flow cytometry-based growth assay demonstrated that RAP-treated *MyoA:mCherry:cKO* + *p230p:MyoA(WT):eGFP* parasites replicated at the same rate as control DMSO-treated parasites (Figure 5.8.D), confirming efficient genetic complementation of endogenous *MyoA* gene deletion. These results therefore confirm that the growth defect observed in RAP-treated *MyoA:mCherry:cKO* parasites is due to loss of *MyoA* expression and not due to any off target effects of RAP treatment or any genetic abnormalities of the parasite line.

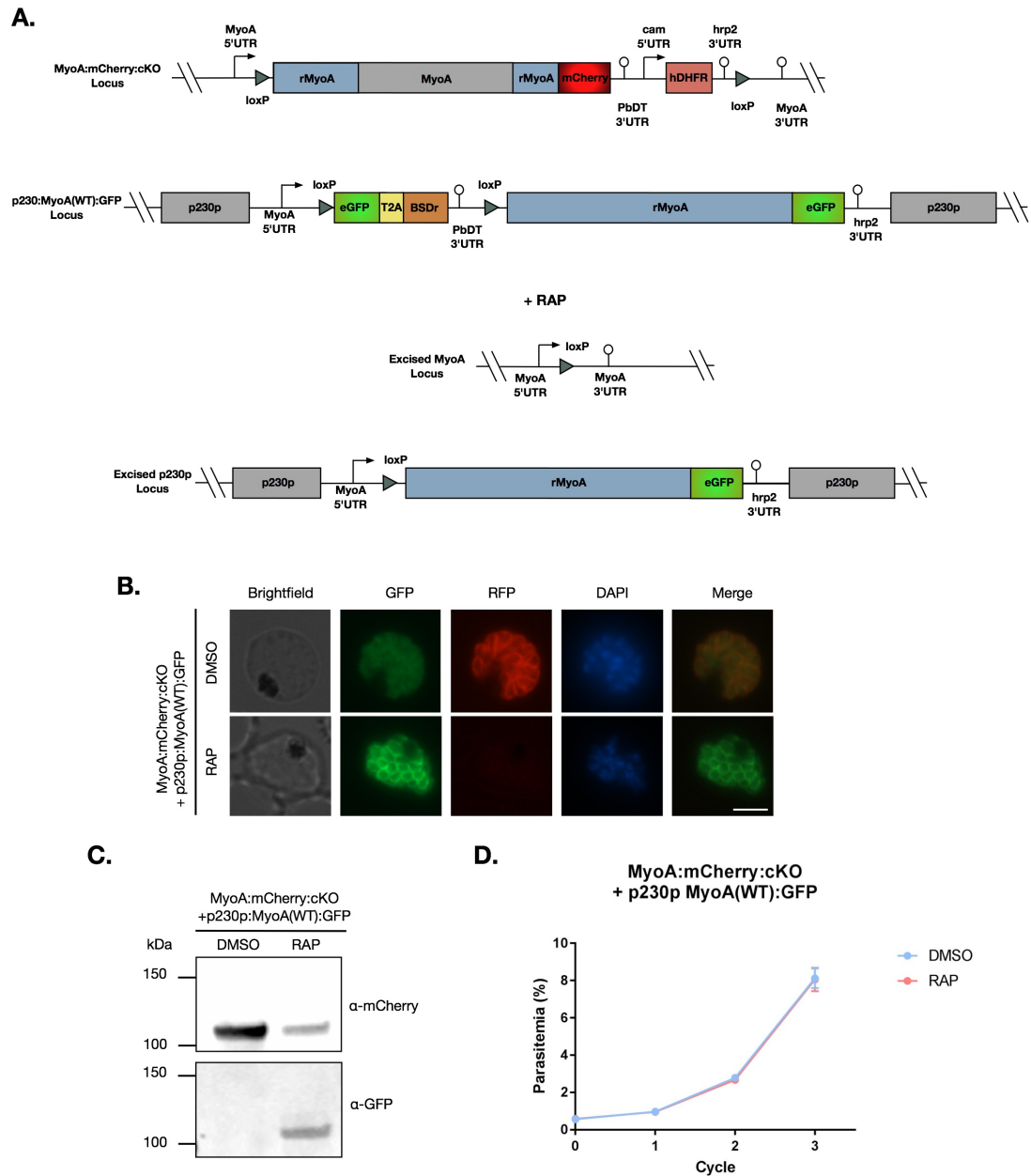


Figure 5.8. RAP-induced transgenic expression of wild type MyoA-GFP is able to rescue the growth defect resulting from deletion of the endogenous *MyoA* gene. **A.** Schematic representation of RAP-induced deletion of the *MyoA:mCherry* at the endogenous locus and and deletion of *eGFP:T2A:BSDr* at the *p230p* locus leading to expression of the *MyoA:GFP* transgene under the control of the *MyoA* promoter. **B.** Live fluorescence microscopy of *MyoA:mCherry:cKO* + *p230p:MyoA(WT):eGFP* showing loss of mCherry signal in RAP-treated parasites, along with a change of eGFP localisation from cytosolic to peripheral, indicating a switch in expression from eGFP to MyoA-eGFP. Scale bar, 5 μ m. **C.** Western blot analysis showing the RAP-inducible switch of expression of MyoA-mCherry from the endogenous locus to expression of MyoA-GFP from the *p230p* locus. A GFP-positive band at the predicted molecular weight of MyoA-GFP (~120 kDa) could not be detected in the DMSO-treated sample, confirming that there is no leaky expression of MyoA-GFP from the *p230p* locus prior to RAP treatment. **D.** Growth curves showing parasitemias of *MyoA:mCherry:cKO* + *p230p:MyoA(WT):eGFP* parasites treated with either DMSO or RAP, measured by flow cytometry-based sorting of SYBR Green positive cells. Data points plotted are means from two repeat experiments, each performed in triplicate. Error bars represent the standard deviation. Results show that RAP-induced MyoA-GFP expression rescues the growth defect observed in *MyoA:mCherry* deficient parasites.

5.1.5 Myosin A displays a striking stripy pattern in gametocytes

P. falciparum gametocytes undergo remarkable morphological changes as they progress from spherical stage I to crescent-shaped stage V gametocytes, as highlighted in the Introduction (Figure 1.2). Little is known concerning how this transformation occurs, however, ultrastructural changes coincide with the formation of the sub-pellicular membrane complex (SMC), which is analogous to the IMC of blood stage merozoites. The SMC is deposited as 13 disk-like structures that associate with microtubules and extend laterally across the gametocyte as it develops. Disruption of photosensitized 5-[125I]iodonaphthalene-1-azide labeled protein-1 (PhIL1) or PhIL1 interacting protein 1 (PIP1), two SMC proteins expressed in gametocytes, leads to a block in gametocyte elongation and development beyond stage III (Parkyn Schneider et al., 2017), demonstrating that these SMC proteins play an important role in gametocyte development. Other glideosome proteins including GAP50, GAP45, MTIP and MyoA are also expressed in gametocytes (Dearnley et al., 2011), however, it is unclear whether these proteins play a role in gametocyte development or gametogenesis. Addition of cytochalasin D, which inhibits actin polymerisation, does not affect gametocyte development, suggesting that elongation of the gametocyte is not driven by the actomyosin motor (Dearnley et al., 2011). However, it is possible that MyoA may perform a structural role during gametocyte development or may be involved in mediating rounding up and emergence from the host erythrocyte during gametogenesis.

Having generated the MyoA:mCherry:cKO line, the localisation of MyoA throughout gametocyte development as well as in rounded up gametes was monitored by IFA (Figure 5.9.). In early stage IIa gametocytes, MyoA-mCherry staining appeared diffuse, consistent with MyoA localisation previously reported by Dearnley et al. using an α -MyoA antibody. However, in stage III and IV gametocytes, a striated pattern reminiscent of PhIL1 was observed, consistent with MyoA localising to the SMC. In stage V gametocytes, the striated pattern was less apparent, which is likely due to the disassembly of the microtubular network, which gives the SMC a more relaxed structure (Parkyn Schneider et al., 2017). In rounded-up gametes, MyoA-mCherry localised to the periphery of the parasite, showing a dramatic rearrangement of the SMC.

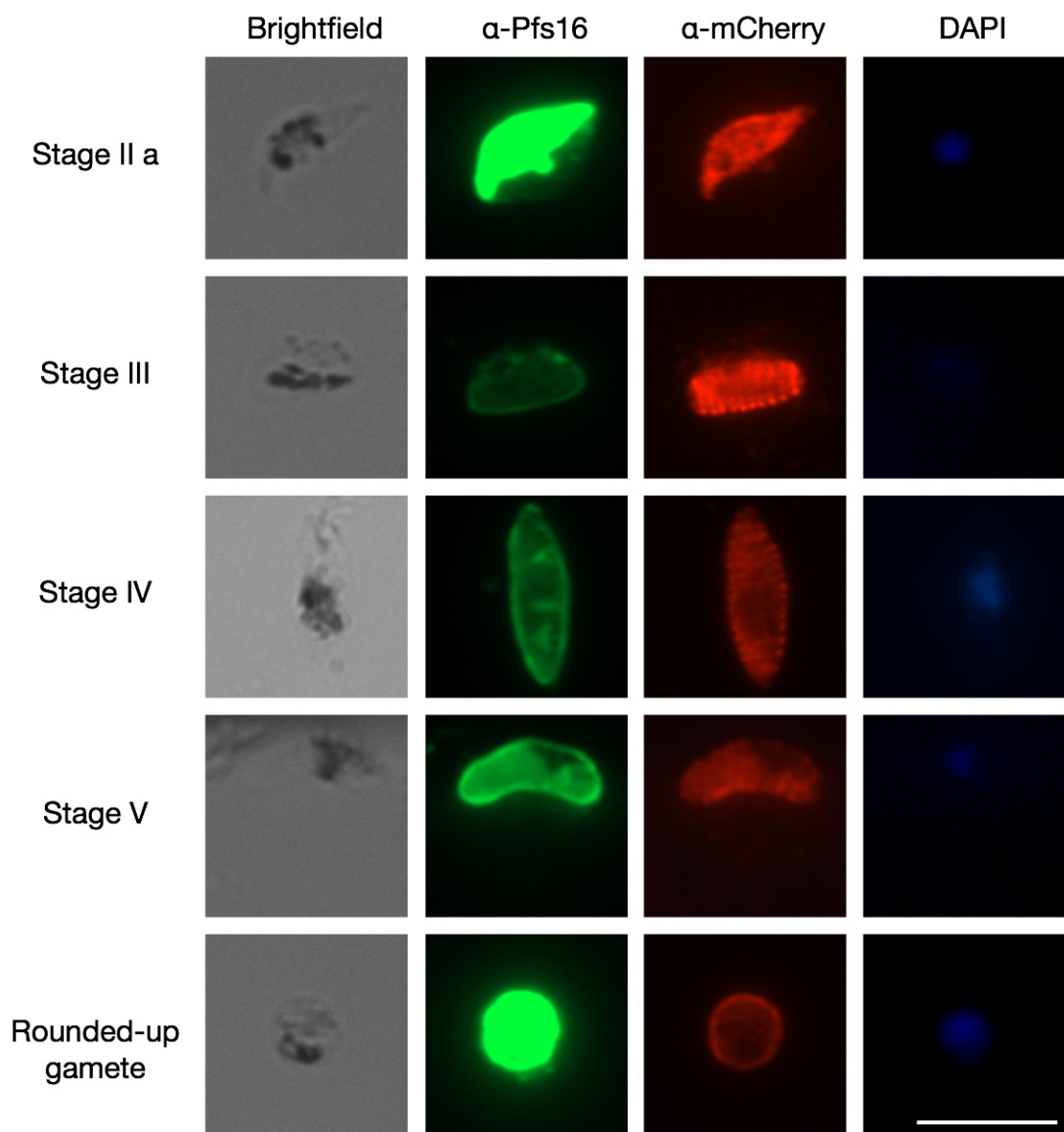


Figure 5.9. MyoA shows a striking striated pattern in gametocytes which transitions to the periphery once they form rounded-up gametes. IFA showing localisation of MyoA-mCherry along with Pfs16, a gametocyte-specific PVM protein, across several stages of gametocyte development and in rounded-up gametes from the MyoA:mCherry:cKO parasite line. In stage IIa, MyoA appears diffuse, however a pronounced striated pattern can be observed in stage III and IV gametocytes. In rounded-up gametes, MyoA-mCherry localises to the periphery of the parasite and no longer displays a striated pattern. Scale bar, 10 μ m.

5.1.6 Myosin A is not required for gametocyte development or rounding up and emerging from RBCs during gametogenesis.

To determine whether MyoA plays a role in gametocyte development or gametogenesis, MyoA knockout gametocytes were generated by treating sexually committed MyoA:mCherry:cKO rings with 100 nM RAP for 2 hours. Live fluorescence microscopy revealed that mCherry signal could still be detected in RAP-treated stage IIa gametocytes, appearing as a row of puncta that is reminiscent of the nascent IMC plates. However mCherry signal was no longer observed beyond this stage (Figure 5.10.A). MyoA-deficient parasites were able to form mature stage V gametocytes, with no discernible differences in gametocyte numbers when compared to the DMSO-treated control. Therefore MyoA does not appear to be required for gametocyte development.

To examine whether ablation of MyoA expression would affect gametogenesis, mature DMSO and RAP-treated stage V gametocytes were incubated at room temperature in the presence 100 μ M XA to induce rounding up and emergence from the host erythrocyte, and parasites were stained using α -Pfs25 antibody conjugated to Cy3, which specifically binds to the surface of female gametes. Parasites were incubated overnight to ensure maximal Pfs25 staining. To visualise erythrocytes, samples were stained for 5 minutes with wheat germ agglutinin (WGA) conjugated to Alexa Fluor 488. Live fluorescence microscopy revealed that both DMSO and RAP-treated gametocytes were able to round up and emerge from host erythrocytes (Figure 5.10.B). Since Pfs25 is only expressed by female gametes, male gametes would not be stained by α -Pfs25. However parasites that were not stained by WGA or α -Pfs25 could be observed, and are highlighted by white circles. Although Pfs25 negative gametes are likely males, a male specific marker would be required to confirm this. However, it appears that neither male nor female gametogenesis is affected by the deletion of MyoA.

Collectively, these results demonstrate that MyoA is not necessary gametocyte development, consistent with cytochalasin D treatment having no effect on gametocyte morphology, and is not required for XA-mediated rounding up and emergence from RBCs. However, this study did not assess whether exflagellation was affected in MyoA knockout parasites, therefore it remains possible that MyoA is required for this process. It is also likely that MyoA will be involved in mediating gliding motility observed in ookinetes.

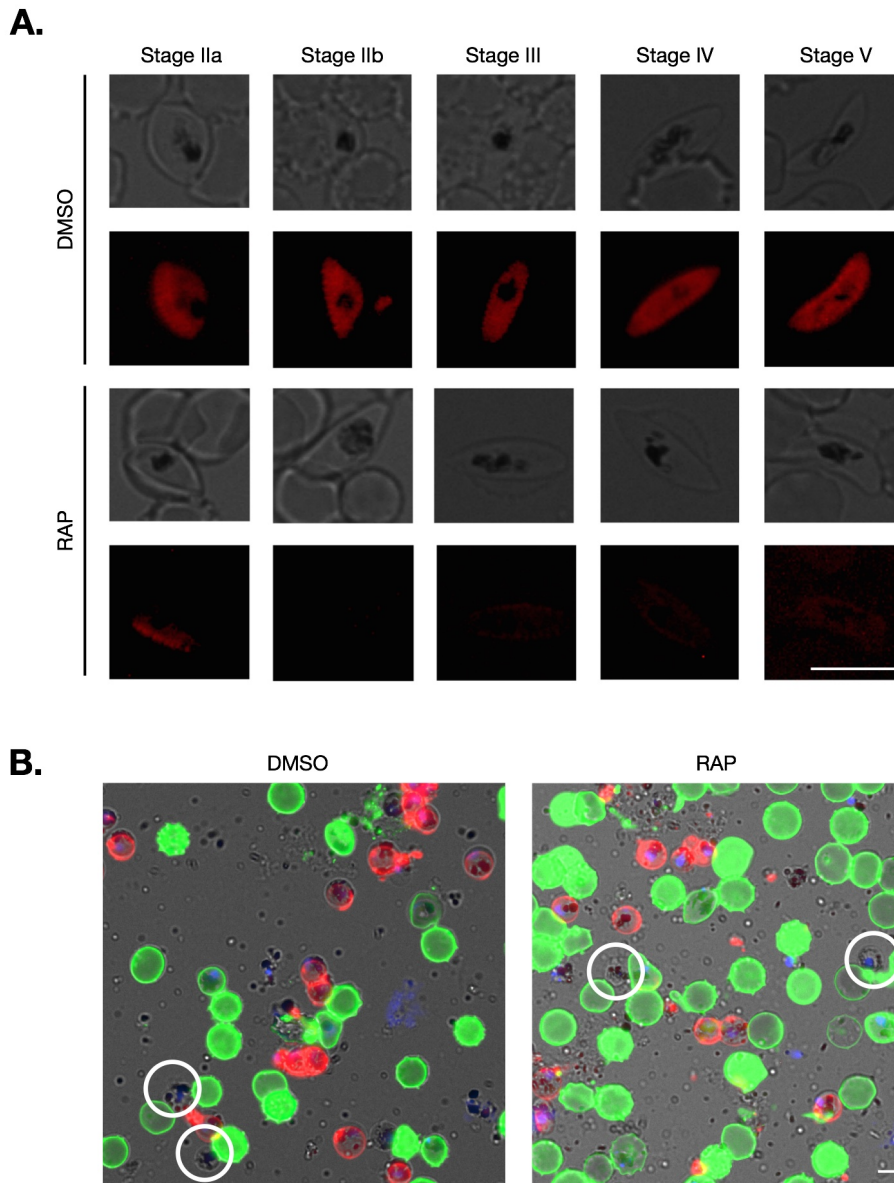


Figure 5.10. MyoA deletion does not cause defects in gametocyte development or the ability to round up and emerge. A. Live fluorescence microscopy showing mCherry signal in DMSO- and RAP-treated MyoA:mCherry:cKO parasites in different stages of gametocyte development. Although mCherry signal could be detected in RAP-treated stage IIa gametocytes, this signal disappeared as the gametocytes developed. Both DMSO and RAP-treated samples were able to form mature stage V gametocytes. Scale bar, 10 μ m. **B.** Merged live fluorescence microscopy images of brightfield (grey), Hoechst (blue), WGA (green) and Pfs25 (red) staining of XA-induced rounded up DMSO and RAP-treated MyoA:mCherry:cKO gametes. Pfs25-stained female emerged gametes can be observed in both samples, as well as Pfs25-negative WGA-negative gametes, circled in white, which are likely male gametes, since Pfs25 is a female-specific protein. Scale bar, 10 μ m.

5.2 Discussion

The work conducted in this chapter set out to establish whether MyoA is required for asexual blood stage growth by generating a conditional PfMyoA knockout line using the DiCre system. At the start of this project, there were no published reports of a MyoA knockout line in *Plasmodium* parasites, however pharmacological evidence revealed that inhibition of actin polymerisation with cytochalasin D led to a block in merozoite invasion, suggesting that the motor is required for active invasion of host erythrocytes (Miller et al., 1979). Conditional disruption of PfGAP45, an essential component of the glideosome which recruits the MyoA:MTIP complex to the IMC, confirmed that the actomyosin motor is indeed required for invasion (Perrin et al., 2018). Unlike in *Toxoplasma*, where disruption of MyoA expression leads to an egress defect (Meissner et al., 2002; Andenmatten et al., 2013), GAP45-deficient parasites were still able to egress, indicating that this process is not reliant on activity of the actomyosin motor.

Using the MyoA:mCherry:cKO line, this study confirms that similar to GAP45, MyoA is not required for egress but is essential for merozoite invasion of RBCs. However, unlike GAP45 which is required for the stable expression of other glideosome components and glideosome assembly, deletion of MyoA did not affect the formation of the IMC or expression levels of other glideosome components such as GAP45, GAP50 and MTIP. Genetic complementation of the MyoA knockout line confirmed that the growth phenotype observed in MyoA-deficient parasites is indeed due to loss of MyoA expression and not due to genetic abnormalities in the MyoA:mCherry:cKO line.

The work presented in this chapter also attempted to elucidate the role of MyoA in gametocyte development and rounding up and emergence from the host erythrocyte during gametogenesis. Although disruption of other SMC proteins, such as PhIL1 and PIP1 leads to a stall in gametocyte development, MyoA-deficient gametocytes showed no abnormalities and were able to form mature stage V gametocytes. Therefore, MyoA is not needed for the structural integrity of the SMC in gametocytes. Furthermore, MyoA-deficient parasites were able to round up and emerge upon XA induction, indicating that MyoA is not involved in either of these processes. This study did not test whether exflagellation was affected in MyoA knockout parasites, therefore it is possible that MyoA may

be required for exflagellation, however it remains unclear what the functional role of MyoA is during this stage of the lifecycle.

Recently, a PfMyoA conditional knockout line has been published (Robert-Paganin et al., 2019). Consistent with the results reported here, the study by Robert-Paganin et al. also demonstrated that MyoA is essential for asexual blood stage growth and is required for invasion. Both the published MyoA knockout line and the one reported here failed to show 100% excision efficiency, despite the 5' *loxP* sites being placed in different locations. Therefore it is possible that the *MyoA* gene is not always accessible to the Cre recombinase, which could be due to nucleosome occupancy or other chromatin features of this locus.

6 PKG-dependent phosphorylation of Myosin A modulates motor activity and is important for efficient parasite growth

Having demonstrated that Myosin A (MyoA) is essential for *P. falciparum* asexual blood stage growth in Chapter 5, the aim of this chapter was to investigate the role of MyoA serine 19 (S19) phosphorylation on motor activity and determine whether this phosphorylation event is critical for parasite survival. As mentioned previously, S19 is phosphorylated in a PKG-dependent manner, since treatment of parasites with PKG-specific inhibitors such as C2 leads to a drastic reduction in phosphorylation of this residue (Alam et al., 2015; Flueck et al., 2019). However, it is not known whether MyoA is a direct substrate of PKG or whether it is phosphorylated by a protein kinase that acts downstream of PKG. In *Toxoplasma*, phosphorylation of the equivalent residue (serine 21) in TgMyoA is important for parasite survival, with mutations that ablate phosphorylation of this residue leading to inefficient motility and a 30% and 23% reduction in egress and invasion, respectively (Tang et al., 2014; Gaji et al., 2015). Due to the close conservation of MyoA between *Plasmodium* and *Toxoplasma*, it is predicted that phosphorylation of PfMyoA S19 may also be important for modulating motor activity in the malaria parasite.

In *Toxoplasma*, phosphorylation of TgMyoA S21 is mediated by calcium-dependent protein kinase 3 (TgCDPK3) (Gaji et al., 2015) however, it remains unclear which kinase is responsible for phosphorylation of MyoA S19 in *Plasmodium* parasites. Although it was originally thought that PKAc is responsible for MyoA phosphorylation (Lasonder et al., 2015), conditional deletion of PKAc does not disrupt MyoA phosphorylation (Patel et al., 2019), indicating that another kinase can carry out this function. Furthermore, although MyoA S19 phosphorylation is dependent on PKG activation (Alam et al., 2015), premature elevation of cAMP levels by disruption of PDE β led to phosphorylation of MyoA S19, even in the presence of C2 (Flueck et al., 2019), which specifically inhibits PKG. Therefore it is likely that MyoA S19 is phosphorylated by a CDPK, since these kinases act downstream of PKG activation (Absalon et al., 2018), and treatment of mature schizonts with BAPTA-AM, a membrane-permeable calcium chelator, dramatically reduces MyoA S19 phosphorylation (Flueck et al., 2019).

6.1 Results

6.1.1 Myosin A S19 is rapidly phosphorylated upon activation of PKG, achieving maximal levels of phosphorylation in merozoites

Several studies have shown that phosphorylation of MyoA S19 in mature schizonts occurs in a PKG-dependent manner, since phosphorylation of this residue is drastically reduced in schizonts treated with PKG-specific inhibitors such as C2 (Alam et al., 2015; Flueck et al., 2019). To test whether this could be recapitulated, mature MyoA:mCherry schizonts were treated with either 1.5 μ M C2 to specifically inhibit PKG, or with 40 μ M E64, a protease inhibitor which blocks merozoite egress downstream of PKG activation and PVM rupture (Hale et al., 2017) (Figure 6.1.A). Western blot analysis using a pan-MyoA antibody to probe for total MyoA, and an antibody specific for MyoA phosphorylated at S19 confirmed that this phosphorylation event was dependent on PKG activity since phosphorylation could not be detected in the C2-blocked sample (Figure 6.1.B). To determine how quickly MyoA S19 is phosphorylated upon PKG activation, a western blot time course was performed on C2-blocked mature MyoA:mCherry schizonts that were released into an E64 block (Figure 6.1.C). This revealed that MyoA S19 was rapidly phosphorylated following PKG activation, with maximal levels detected 14-18 minutes following release of the C2 block (Figure 6.1.D).

To investigate whether there are any changes in phosphorylation levels of MyoA S19 at different stages of the asexual blood stage, the phospho-status of MyoA:mCherry E64-blocked schizonts, purified merozoites and newly formed rings at around 0-4 hours post invasion (Figure 6.2.A) was analysed by western blot. This revealed remarkable changes in the phospho-status of MyoA as the parasites transition from schizonts to merozoites and then rings (Figure 6.2.B), with a 6-fold increase in MyoA S19 phosphorylation in merozoites, followed by a 10-fold reduction in rings (Figure 6.2.C). This dramatic increase in phosphorylation during the free merozoite stage, where the actomyosin motor is required for invasion, could point towards a regulatory role of this phosphorylation event.

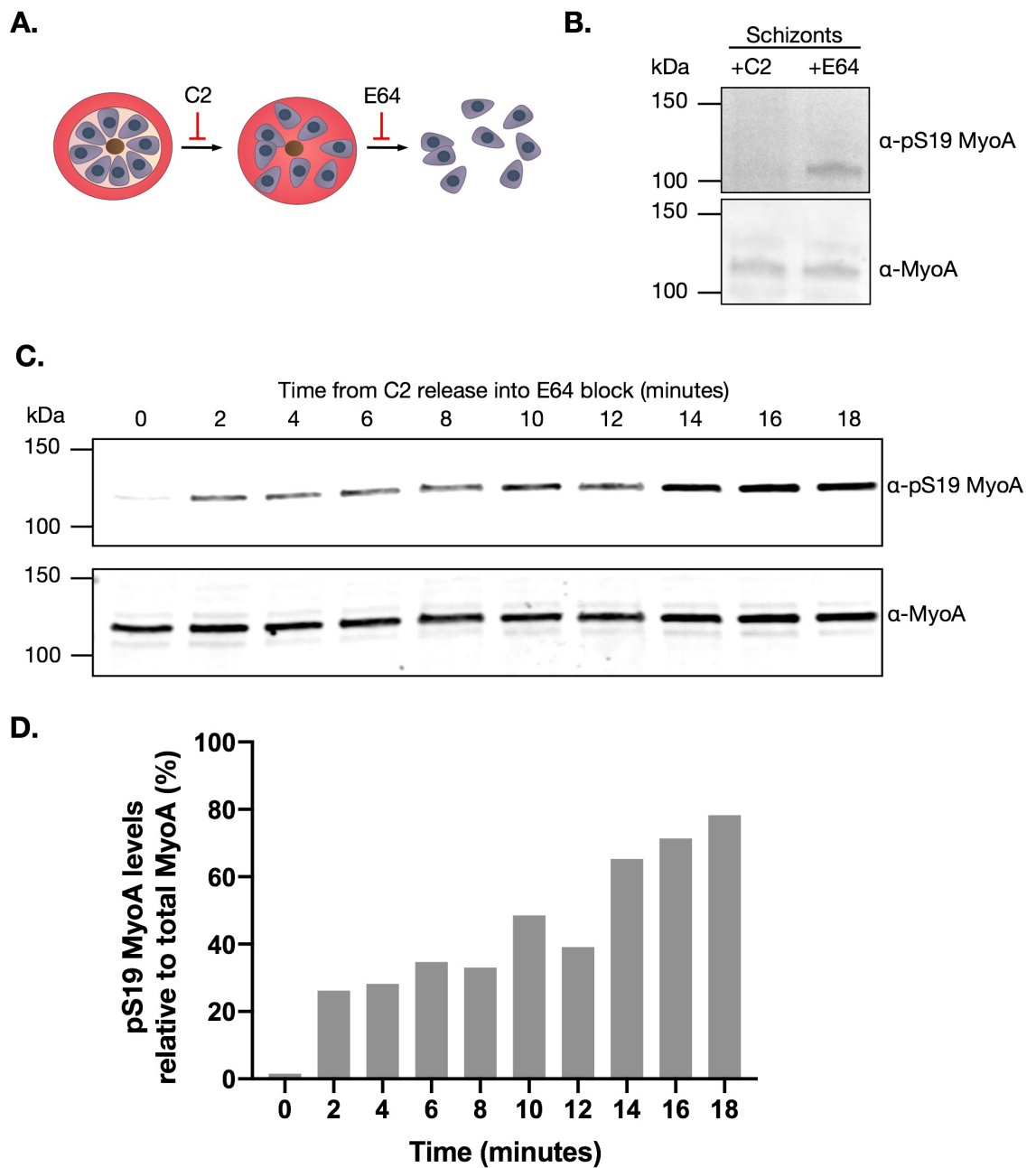


Figure 6.1. MyoA S19 is rapidly phosphorylated upon PKG activation. **A.** Schematic representation showing stages at which C2 and E64 treatment block schizont rupture. **B.** Western blot analysis of MyoA:mCherry C2 and E64-blocked schizont samples probed with a phosphoS19-specific MyoA antibody and a pan-specific MyoA antibody to determine relative levels of phosphorylation in each sample. **C.** Densitometry analysis of the western blot samples shown in Figure 1B. Relative band intensities were calculated by normalising pS19 MyoA to total MyoA signal in each sample. **D.** Western blot showing a time course of MyoA S19 phosphorylation in MyoA:mCherry schizonts released from a C2 block into an E64 block. The blot was probed with a phosphoS19-specific MyoA antibody and a pan-specific MyoA antibody to determine relative levels of phosphorylation in each sample. **E.** Densitometry analysis of the western blot samples shown in Figure 1D showing MyoA S19 is rapidly phosphorylated upon PKG activation. Relative band intensities were calculated by normalising pS19 MyoA to total MyoA signal in each sample.

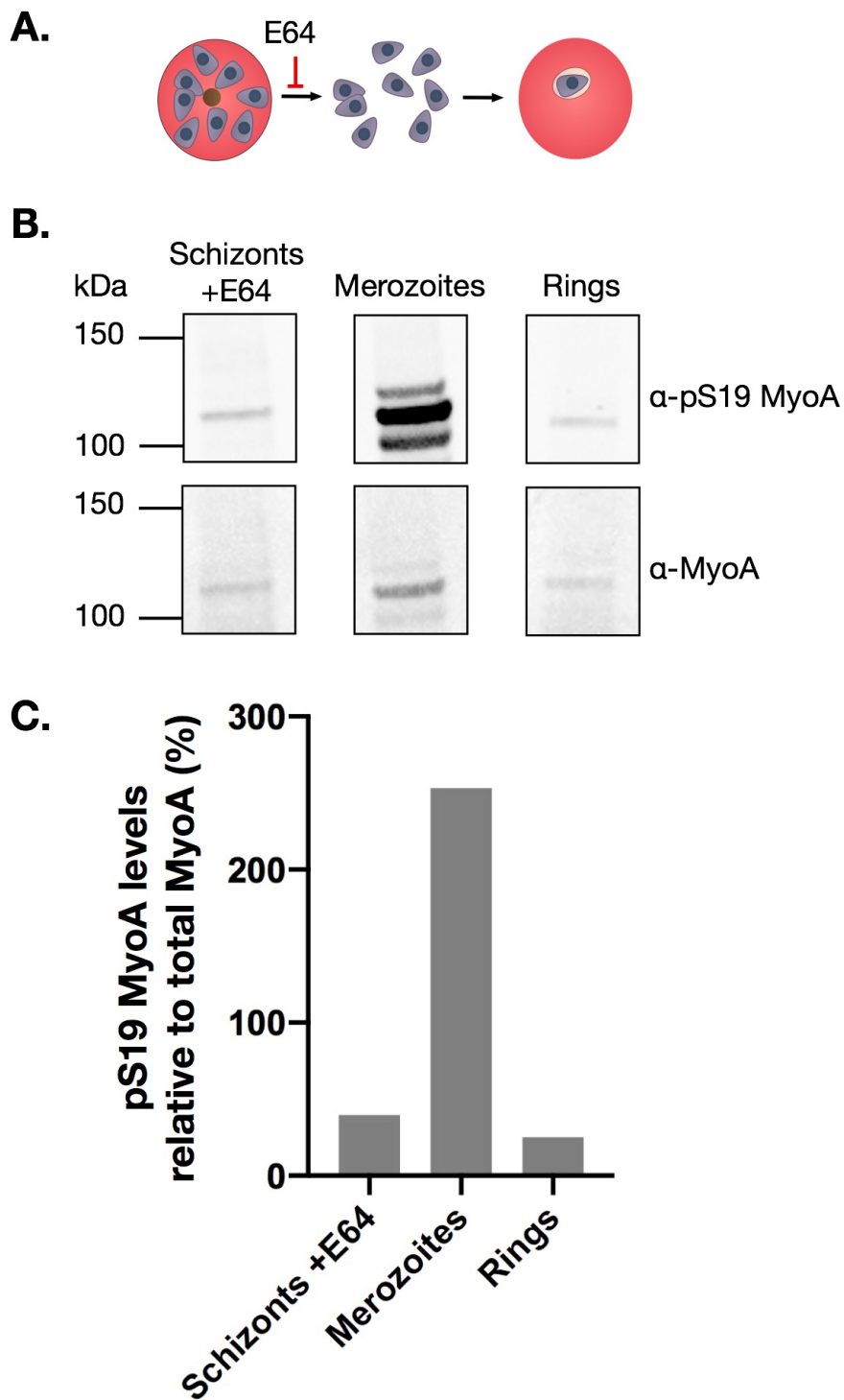


Figure 6.2. MyoA S19 undergoes pronounced stage-dependent changes in phosphorylation during egress and invasion. **A.** Schematic representation of the parasite samples analysed. **B.** Western blot analysis of MyoA:mCherry E64-blocked schizonts, merozoites and ring stage samples probed with a phosphoS19-specific MyoA antibody and a pan-specific MyoA antibody to determine relative levels of phosphorylation in each sample. **C.** Densitometry analysis of the western blot samples shown in figure 6.2.B showing dynamic changes in MyoA S19 phosphorylation as the parasites transition from schizonts to merozoites then rings. Relative band intensities were calculated by normalising pS19 MyoA to total MyoA signal in each sample.

6.1.2 Introducing mutations into the endogenous Myosin A locus to mimic or ablate Myosin A S19 phosphorylation

To determine whether phosphorylation of MyoA S19 is critical for *P. falciparum* asexual blood stage growth, marker free CRISPR/Cas9-mediated gene editing was employed to attempt to introduce mutations which would either mimic or ablate phosphorylation of this residue. While substitution of the serine residue with an aspartic acid residue (S19D), a negatively charged residue which would mimic the negative charge introduced by phosphorylation; substitution with an alanine residue (S19A) would prevent phosphorylation at this site. To introduce these mutations into the parasite genome, the repair template used to introduce the loxP site upstream of the *MyoA* start codon in Chapter 5 was modified to install the S19A or S19D mutations into the endogenous *MyoA* locus. 3D7a parasites were transfected with a pool of two pDC2-Cas9-hDHFR plasmids (Lim et al., 2017), each harbouring a different gRNA to maximise editing efficiency, along with each of these repair templates, which were delivered as linearised plasmids (Figure 6.3.A). The original repair template used to generate the loxP:MyoA line, which would not change the coding sequence, was also transfected to serve as a positive control for integration. Parasites were then treated with 2.5 nM WR99210 for 9 days to select for parasites harbouring at least one of the pDC2-Cas9-hDHFR plasmids. Around 4 weeks post transfection, parasites were observed for all transfections. gDNA was extracted from the parasites and subject to PCR analysis to determine whether the repair template had integrated. Integration would lead to the amplification of a smaller PCR product (~1.6 kb) compared to wild type parasites (~2 kb), since integration of the repair template would result in the deletion of two endogenous introns found in the *MyoA* gene. This revealed that both the S19 control and S19D mutations had successfully integrated into the endogenous *MyoA* locus, however integration could not be detected in the parasites transfected with the repair template that would introduce the S19A mutation (Figure 6.3.B). Instead, amplification of a larger PCR product indicated that parasites in the S19A transfection were wild type parasites. Transfections were repeated twice, however integration of the S19A mutation could not be achieved indicating that this mutation may be lethal or lead to a fitness cost, allowing wild type parasites to outgrow any parasites harbouring the S19A mutation. Despite generating a parasite line harbouring the S19D mutations, the growth of these parasites in comparison to wild type parasites was not compared in a growth-based assay.

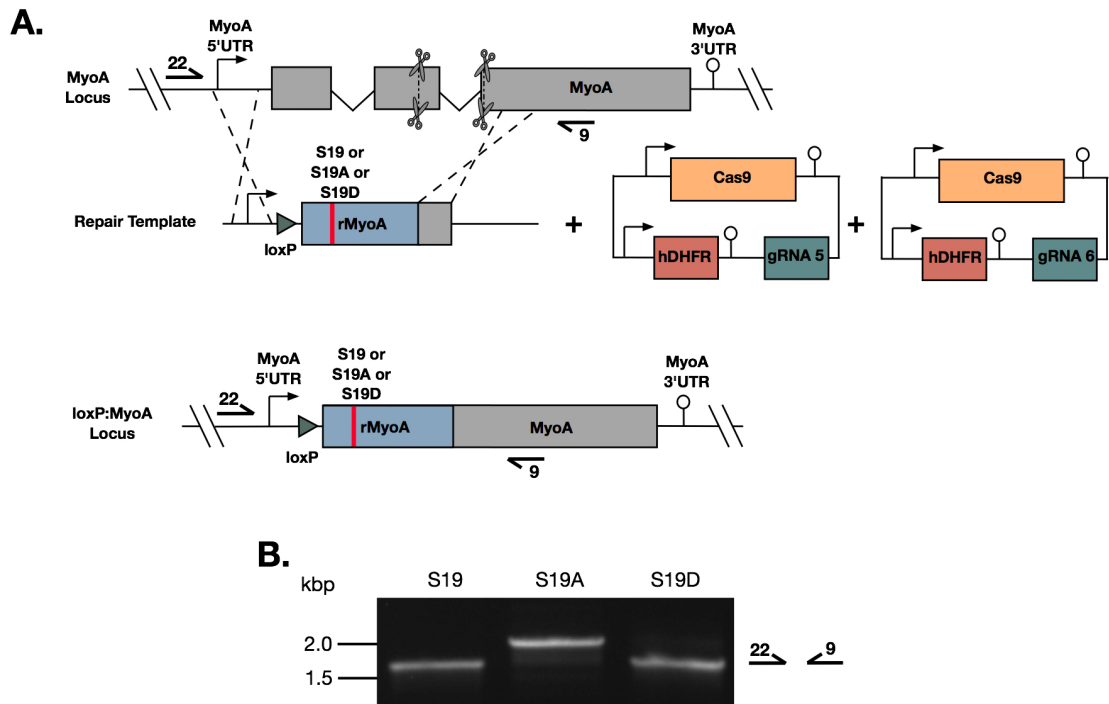


Figure 6.3. Mutation of the endogenous *MyoA* locus to generate parasites expressing phosphomutant (S19A) and phosphomimetic (S19D) *MyoA*. **A.** Schematic representation of the marker-free CRISPR/Cas9-mediated approach used to introduce the S19A or S19D mutations, or the S19 control wild type sequence into the endogenous *MyoA* locus. Scissors indicate CRISPR/Cas9 cleavage sites, while arrows represent the relative position of oligonucleotide primers used for diagnostic PCR screens. **B.** Diagnostic PCR analysis confirming integration of the S19 control and S19D phosphomimetic mutation by amplification of a smaller 1.6 kb product. Amplification of a larger 2 kb product in parasites transfected with the repair construct that would integrate the S19A phosphomutation confirms presence of wild type unedited locus and failure to integrate this mutation.

6.1.3 Genetic complementation of MyoA:mCherry:cKO parasites with MyoA(S19A) or MyoA(S19D) leads to a significant growth defect in asexual blood stages

Since the S19A phosphomutation could not be directly introduced into the endogenous MyoA locus, the approach used to conditionally complement MyoA:mCherry:cKO parasites with RAP-inducible *MyoA:GFP* in Chapter 5 was modified so that RAP treatment would lead excision of the endogenous *MyoA* gene and concomitant induction of expression of MyoA(S19A):GFP or MyoA(S19D):GFP. To achieve this, MyoA:mCherry:cKO parasites were transfected with the pDC2-p230p-Cas9-gRNA plasmid to introduce a double strand break in the p230p locus (Knuepfer et al., 2017; Mogollon et al., 2016) and linearised repair templates designed to integrate a promoterless second copy of the *MyoA* gene harbouring either an S19A or S19D mutation, fused to the *enhanced green fluorescent protein (eGFP)* gene (Figure 6.4.A). Two days after transfection, parasites were treated with 5 µg/ml BSD (Sigma) for one week to select for integration. BSD-resistant parasites were observed around 4 weeks post transfection and the resulting phosphomutant and phosphomimic lines were called MyoA:mCherry:cKO + p230p:MyoA(S19A):eGFP and MyoA:mCherry:cKO + p230p:MyoA(S19D):eGFP, respectively. Live fluorescence microscopy confirmed that parasites from these lines were both mCherry and GFP positive, with the mCherry signal localising to the periphery of individual merozoites, consistent with MyoA localisation; while the GFP signal was diffuse, encompassing the parasite cytosol (Figure 6.4.B).

This strategy was designed so that RAP treatment of MyoA:mCherry:cKO + p230p:MyoA(S19A):eGFP and MyoA:mCherry:cKO + p230p:MyoA(S19D):eGFP parasites would give rise to deletion of the endogenous *MyoA:mCherry* and the floxed *eGFP:T2A:BSDr* coding sequences in the *p230p* locus, placing the respective *MyoA:GFP* mutant sequences under the control of the ectopic *MyoA* promoter (Figure 6.5.A). Live fluorescence microscopy revealed that RAP treatment resulted in a loss in mCherry signal and a change in GFP pattern from cytosolic to peripheral, confirming deletion of the endogenous *MyoA:mCherry* sequence and expression of the ectopic MyoA-GFP mutants in each line (Figure 6.5.B). Western blot analysis also confirmed RAP treatment led to a reduction but not total loss of MyoA-mCherry expression and induction of MyoA-GFP expression in both parasite lines

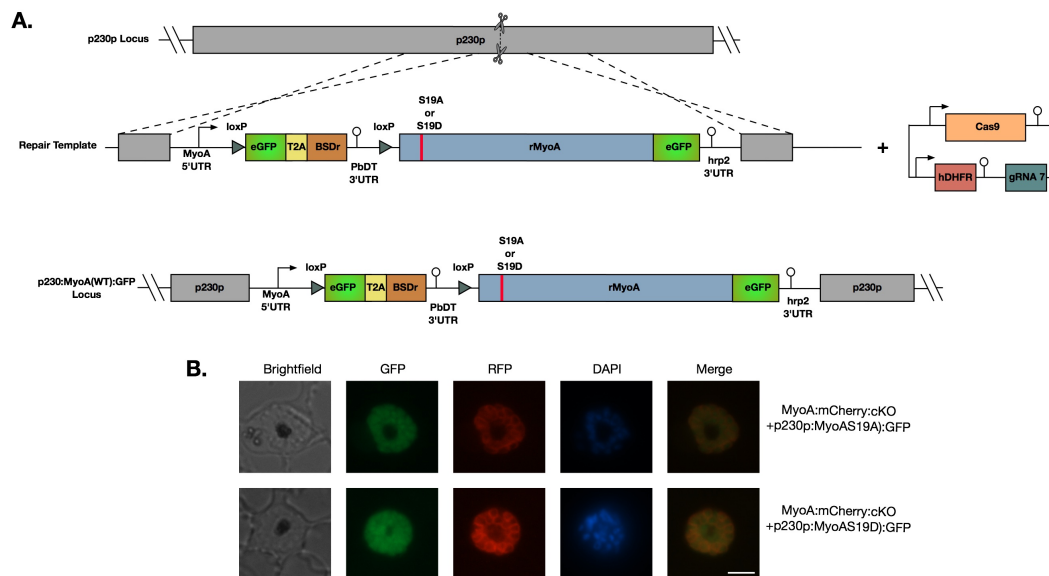


Figure 6.4. Generation of MyoA:mCherry:cKO parasite lines genetically complemented with RAP-inducible MyoA(S19A):GFP and MyoA(S19D):GFP. **A.** Schematic representation of the CRISPR/Cas9-mediated approach used to generate conditional MyoA(S19A):GFP and MyoA(S19D):GFP lines. Integration into the *p230p* locus leads to the expression of cytosolic eGFP and BSD, under the control of the *MyoA* promoter. Scissors indicate CRISPR/Cas9 cleavage sites. **B.** Live fluorescence microscopy showing cytosolic expression of eGFP in MyoA:mCherry:cKO + p230p:MyoA(S19A):eGFP and MyoA:mCherry:cKO + p230p:MyoA(S19D):eGFP parasites, confirming successful integration of the repair templates. The GFP and mCherry signals do not overlap, confirming that expression of MyoA(S19A)-eGFP and MyoA(S19D)-eGFP could not be detected prior to RAP treatment. Scale bar, 5 μ m.

(Figure 6.5.C). Surprisingly, a ~30 kDa band, the predicted molecular weight of eGFP, could not be detected in either the DMSO- or RAP-treated samples.

To assess whether dependence on expression of the S19 phosphomutant or phosphomimetic versions of MyoA-GFP had an effect on parasite growth, flow cytometry-based growth assays were performed on DMSO- and RAP-treated MyoA:mCherry:cKO + p230p:MyoA(S19A):eGFP and MyoA:mCherry:cKO + p230p:MyoA(S19D):eGFP parasites. Complementation of the MyoA knockout with MyoA(S19A)-GFP and MyoA(S19D)-GFP resulted in a 63% and 60% rescue in growth, respectively (Figure 6.6.). As shown in Chapter 5, complementation with GFP-tagged wild type MyoA, using the exact same set up, fully rescued MyoA knockout parasites. These data therefore demonstrate that mutations, which ablate or mimic phosphorylation of MyoA S19, lead to reduced growth during the asexual blood stages of the life cycle. Therefore, phosphorylation and dephosphorylation of MyoA S19 is important but not absolutely essential for parasite survival in vitro. Interestingly, although both mutations led to a similar growth defect in inducible complementation experiments, only the S19A mutation failed to directly integrate

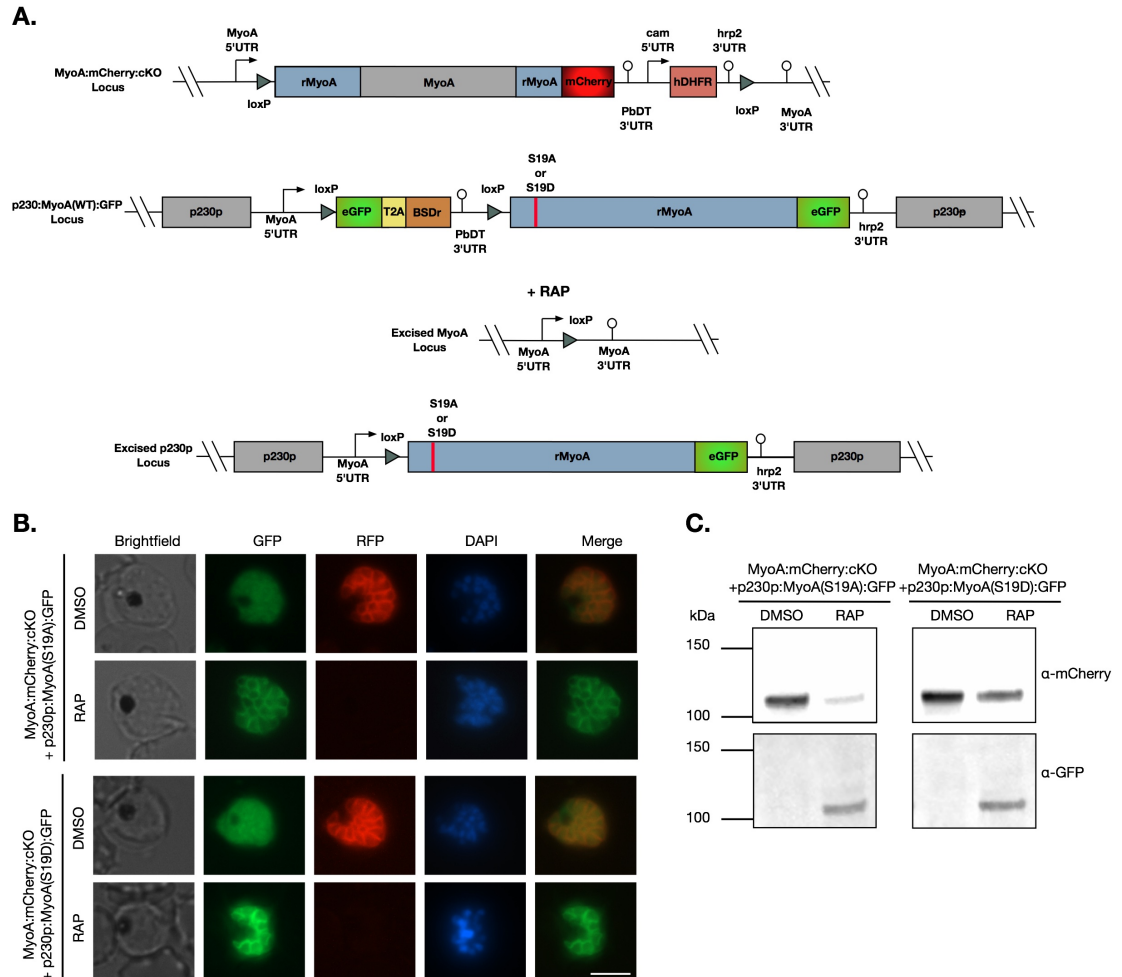


Figure 6.5. RAP treatment leads to the transgenic expression of either the MyoA(S19A)-GFP phosphomutant or the MyoA(S19D)-GFP and loss of MyoA-mCherry expression. **A.** Schematic representation of RAP-induced deletion of *MyoA-mCherry* at the endogenous locus and deletion of *eGFP:T2A:BSDr* at the *p230p* locus leading to expression of MyoA(S19A)-GFP and MyoA(S19D)-GFP in MyoA:mCherry:cKO + p230p:MyoA(S19A):eGFP and MyoA:mCherry:cKO + p230p:MyoA(S19D):eGFP parasites, respectively. **B.** Live fluorescence microscopy showing cytosolic expression of eGFP in MyoA:mCherry:cKO + p230p:MyoA(S19A):eGFP and MyoA:mCherry:cKO + p230p:MyoA(S19D):eGFP parasites, confirming successful integration of the repair templates. The GFP and mCherry signals do not overlap, confirming that expression of MyoA(S19A)-eGFP and MyoA(S19D)-eGFP could not be detected prior to RAP treatment. Scale bar, 5 μ m. **C.** Western blot analysis showing RAP-inducible expression of the MyoA-GFP mutants from the *p230p* locus by probing with an α -GFP antibody, and reduction in MyoA-mCherry expression by probing with an α -mCherry antibody.

into the endogenous MyoA locus (Figure 6.3.B). Phosphomimetic mutations simulating phosphorylated serine are not always successful, since the chemical environment created by negatively charged amino acids such as aspartic acid is different to the chemical environment of phospho-serine (Hunter, 2012). Therefore, it is possible that the MyoA S19D mutation mimics non-phosphorylated rather than phosphorylated MyoA S19. This could explain why the growth rates of both lines are very similar, however it is also conceivable that constitutive phosphorylation of MyoA could have a negative impact on growth. Testing a different phosphomimetic substitution, such as glutamic acid instead of aspartic acid, could be attempted in the future to test whether the S19E mutation is better at mimicking phosphorylated S19.

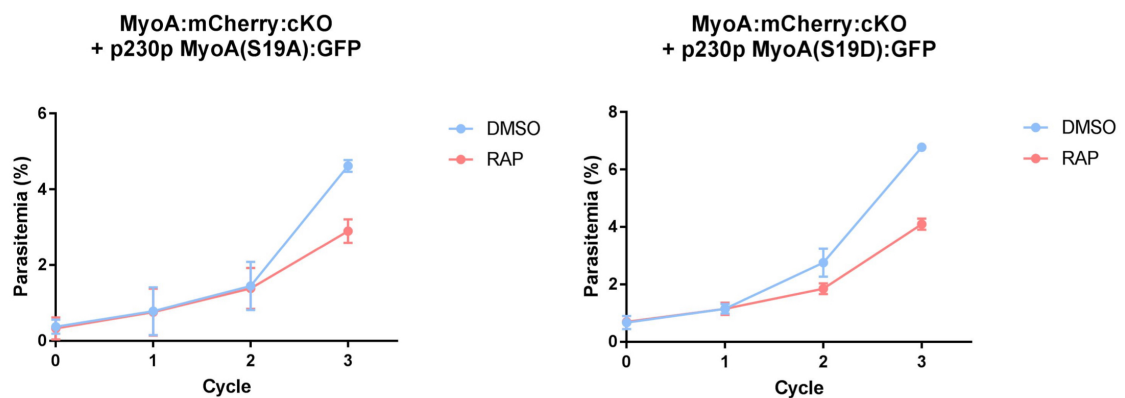


Figure 6.6. RAP-induced transgenic expression of either the MyoA(S19A)-GFP phosphomutant or the MyoA(S19D)-GFP phosphomimetic leads to a moderate but incomplete rescue following deletion of *MyoA:mCherry* from the endogenous locus. Growth curves showing parasitemias of MyoA:mCherry:cKO + p230p:MyoA(S19A):eGFP and MyoA:mCherry:cKO + p230p:MyoA(S19D):eGFP parasites treated with either DMSO or RAP, measured by flow cytometry-based sorting of SYBR Green positive cells. Data points plotted are means from two repeat experiments, each performed in triplicate. Error bars represent the standard deviation.

Several other approaches were also attempted to conditionally switch from expressing wild type MyoA-mCherry to MyoA-GFP harbouring either the S19A or S19D mutations, however these approaches either failed or showed only partial success and are described in further detail in the appendix.

6.1.4 Phosphorylation of Myosin A modulates motor activity by increasing the motor speed

Having demonstrated that mutations that mimic or ablate MyoA S19 phosphorylation led to a defect in parasite growth, *in vitro* motility assays were performed using parasite-

derived MyoA to determine whether MyoA S19 phosphorylation is involved in modulating the activity of the motor. Motility assays were set up as described in section 2.3.4 and involved tracking ATP-driven movement of rhodamine-phalloidin-labelled rabbit actin filaments over glass cover slips coated in mCherry-tagged MyoA captured from mature schizont or merozoite lysates with an α -mCherry antibody (Figure 6.7.A). To ensure that actin binding was specific to MyoA captured via the α -mCherry antibody, actin was added to flow cells that were or were not pre-coated with α -mCherry antibody. Actin filaments could only be detected in the antibody-coated flow cells, confirming that actin binding was due to the capture of MyoA-mCherry from parasite lysates (data not shown). In the absence of ATP, actin filaments remained bound to the surface and did not display any motility (Figure 6.7.B). Upon addition of ATP-containing buffer to the flow cell, and activation of the captured MyoA motors, actin filament motility could readily be observed (Figure 6.7.B), confirming that active myosin motors could be isolated from parasite lysates.

Motility assays were performed using MyoA:mCherry C2- and E64-blocked schizonts and purified merozoites to test whether blocking PKG-dependent phosphorylation of MyoA S19 had an effect on filament motility (Figure 6.8.A). The average filament velocity for C2-treated samples was 0.398 $\mu\text{m/s}$, while E64-treated samples moved 13% faster with an average velocity of 0.455 $\mu\text{m/s}$ (Figure 6.8.B). Merozoite samples displayed an average filament velocity of 0.636 $\mu\text{m/s}$, 38% and 29% faster than C2- and E64-blocked samples, respectively. Therefore there appears to be a correlation between motor speed and phosphorylation levels of MyoA S19 since merozoite samples display highest levels of S19 phosphorylation and actin displacement velocities, followed by E64 then C2-blocked samples. However, since MyoA co-precipitates with other components of the glideosome, including GAP40 and GAP45 (Green et al., 2017), which are also phosphorylated in a PKG-dependent manner (Alam et al., 2015), it is possible that this change in actin filament velocity could be due to the altered phospho-status of these other components and not solely due to the changed phospho-status of MyoA S19.

To overcome this issue and to ensure that the only difference between samples was the phospho-status of MyoA, wild type 3D7 parasites were transfected with plasmids driving episomal expression of MyoA(S19)-mCherry, MyoA(S19A)-mCherry or MyoA(S19D)-mCherry, while the endogenous MyoA locus was left unaltered (Figure 6.9.A). Since

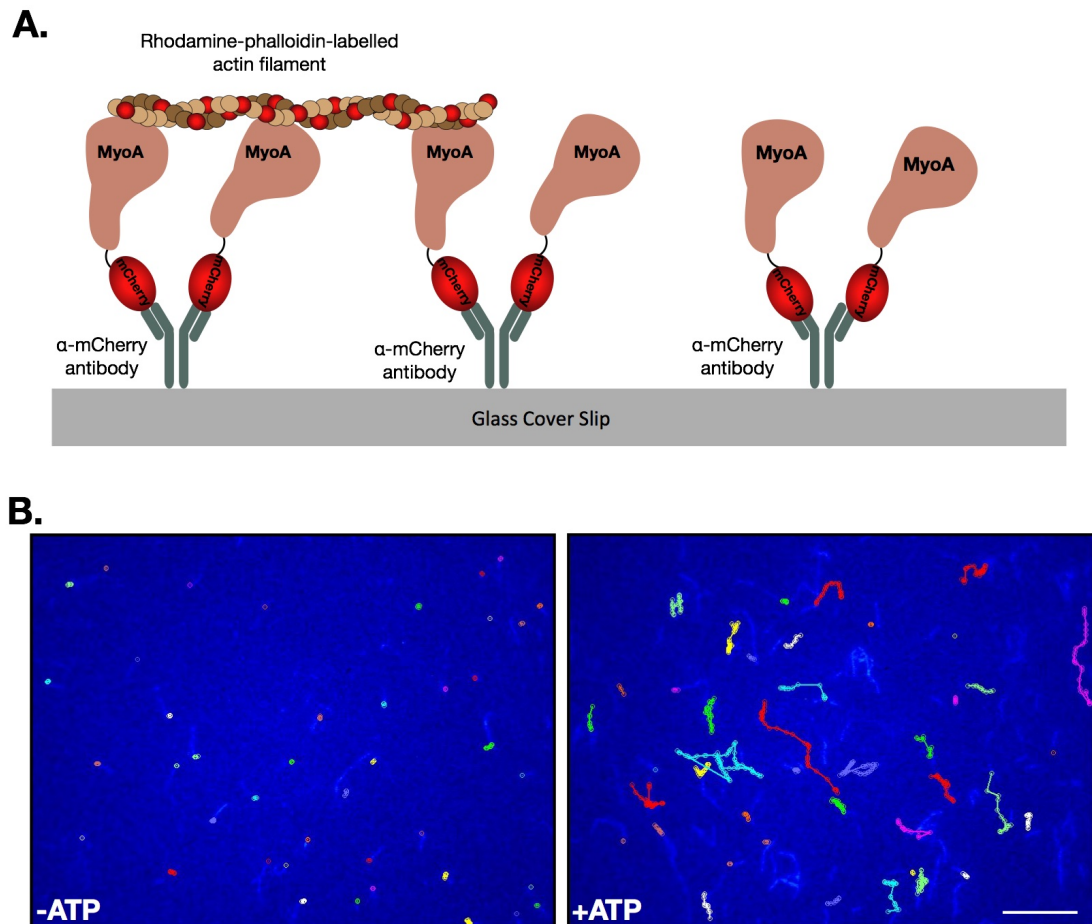


Figure 6.7. *In vitro* motility of actin over parasite-derived MyoA-mCherry. **A.** Schematic representation of the flow cell set up, showing fluorescently-labelled actin moving over parasite-derived MyoA-mCherry captured via an α -mCherry antibody on glass cover slips. **B.** In the absence of ATP, actin filaments remain bound, and no motility is observed, however addition of ATP-containing imaging buffer leads to the activation of the MyoA motors and movement of the actin filaments can be observed. Motility tracks for each filament are highlighted in different colours. Scale bar, 30 μ m.

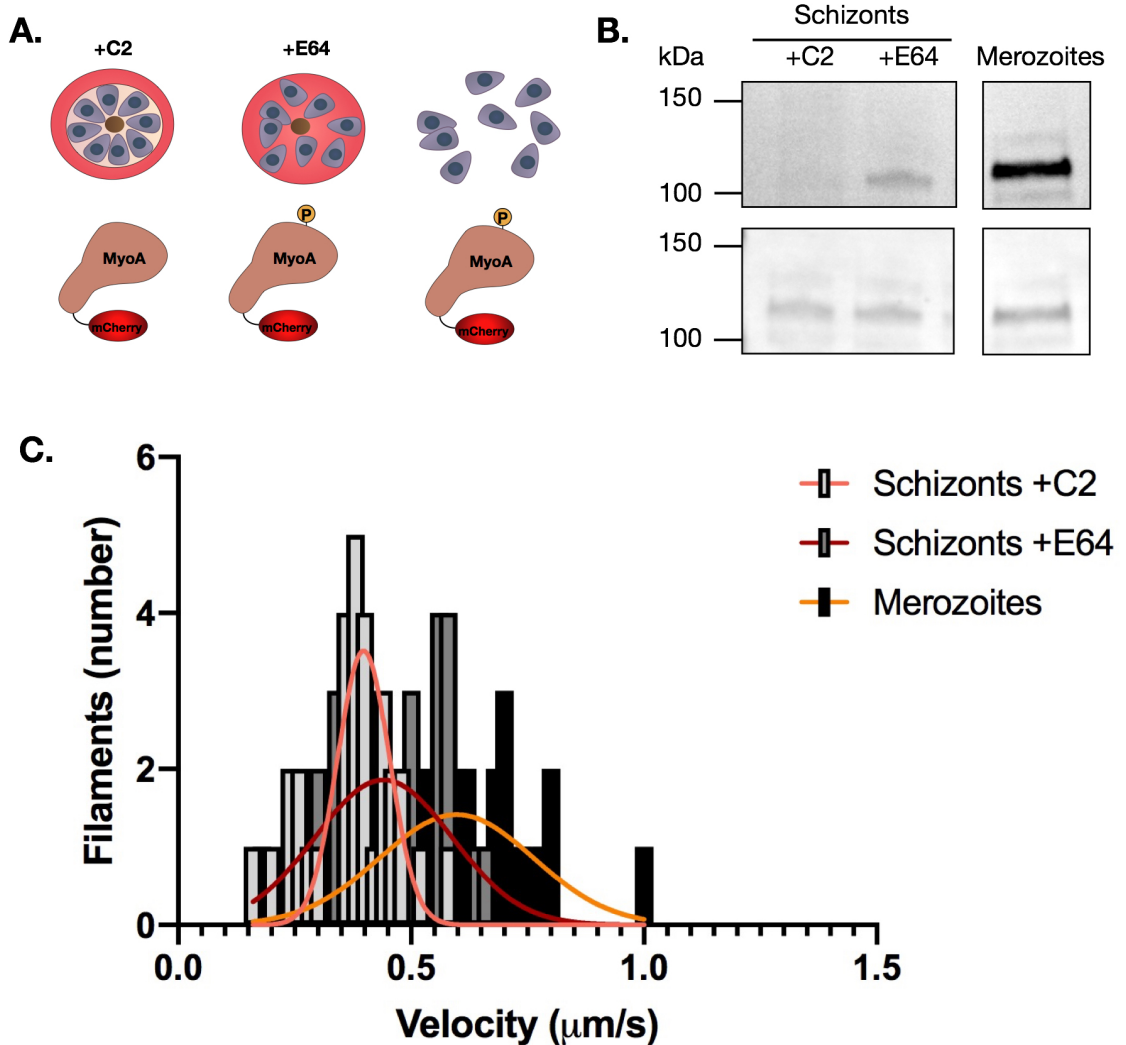


Figure 6.8. PKG-dependent phosphorylation of MyoA S19 increases the motor's speed. **A.** Schematic representation of the motility assay samples used, where non-phosphorylated MyoA-mCherry was obtained from C2-blocked schizonts, while phosphorylated MyoA-mCherry was obtained from E64-blocked schizonts and purified merozoites. **B.** Western blot analysis of the samples used in the gliding assay, confirming MyoA-mCherry from C2-blocked schizonts was non-phosphorylated at S19, while MyoA-mCherry from E64-blocked schizonts and purified merozoites was phosphorylated at S19. Blots were probed using a phosphoS19-specific MyoA antibody and a pan-specific MyoA antibody to determine relative levels of phosphorylation in each sample. **C.** Speed distributions from *in vitro* motility assays using MyoA-mCherry from C2- or E64-blocked schizonts or released merozoites.

MyoA expressed from the endogenous locus is untagged in these lines, only MyoA-mCherry expressed from the respective episomes is expected to be precipitated onto the slide. The expression plasmids also encoded a BSDr cassette to select for episome formation. After transfection, parasites were treated with 2.5 $\mu\text{g/ml}$ BSD, and resistant parasites for all transfections were observed within 3 weeks after transfection. Purified merozoite samples were harvested for all lines, however motility assays were only performed on the wild type phosphorylatable MyoA(S19)-mCherry and phosphomutant MyoA(S19A)-mCherry samples. The average filament velocity for MyoA(S19)-mCherry samples was 0.603 $\mu\text{m/s}$, while MyoA(S19A)-mCherry samples moved 24% slower with an average velocity of 0.457 $\mu\text{m/s}$ (Figure 6.9.B).

Therefore by using chemical or genetic approaches, these data demonstrate that non-phosphorylated MyoA S19 displays reduced motility compared to phosphorylated MyoA S19. This confirms that phosphorylation of residue plays an important role in modulating the speed of the actomyosin motor.

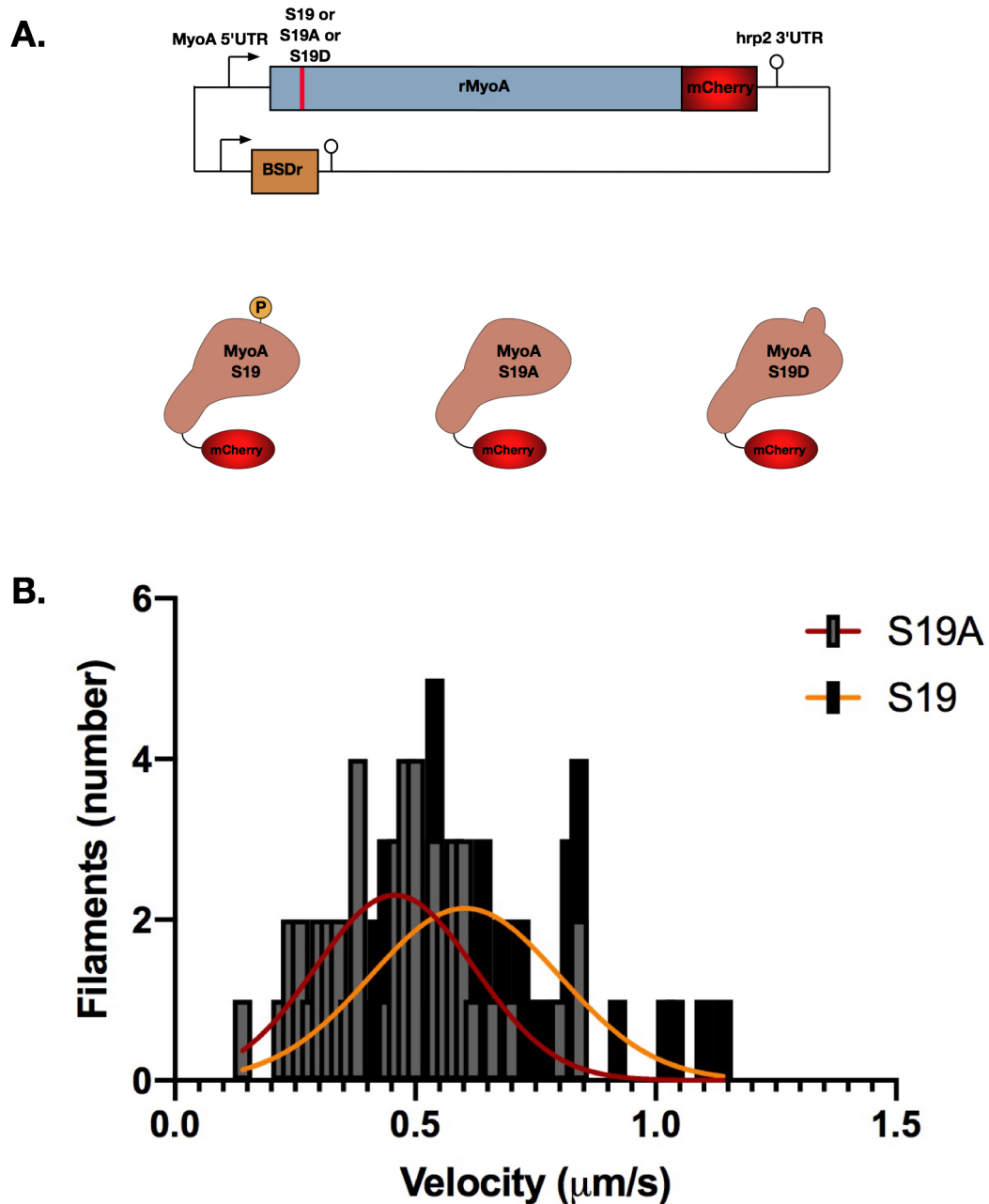


Figure 6.9. MyoA(S19A)-mCherry displays reduced motility compared to wild type MyoA(S19)-mCherry. **A.** Schematic representation of the plasmid used to episomally express either MyoA(S19A)-mCherry or MyoA(S19D)-mCherry mutants or wild type MyoA(S19)-mCherry in wild type 3D7 parasites. **B.** Speed distributions from *in vitro* motility assays using episomally expressed wild type MyoA(S19)-mCherry or phosphomutant MyoA(S19A)-mCherry from merozoites.

6.1.5 Motor activity is not altered when PKAc is knocked out

Since PKAc knockout parasites display an invasion defect (Patel et al., 2019), similar to that of MyoA knockout parasites, it is possible that the MyoA motor shows reduced activity when PKAc is depleted. To test this, MyoA(S19)-mCherry was episomally expressed in the published RAP-inducible PKAc knockout line, PKAc-HA:loxP (Patel et al., 2019). DMSO- and RAP-treated PKAc-HA:loxP merozoites expressing MyoA(S19)-mCherry were harvested and used in *in vitro* gliding motility assays as described earlier. The average filament velocity for DMSO and RAP-treated samples was 0.619 and 0.6346 $\mu\text{M/s}$, respectively (Figure 6.10.). Therefore it appears that motor function is not impaired in PKAc-deficient parasites, and is not the reason why PKAc-deficient parasites are unable to invade.

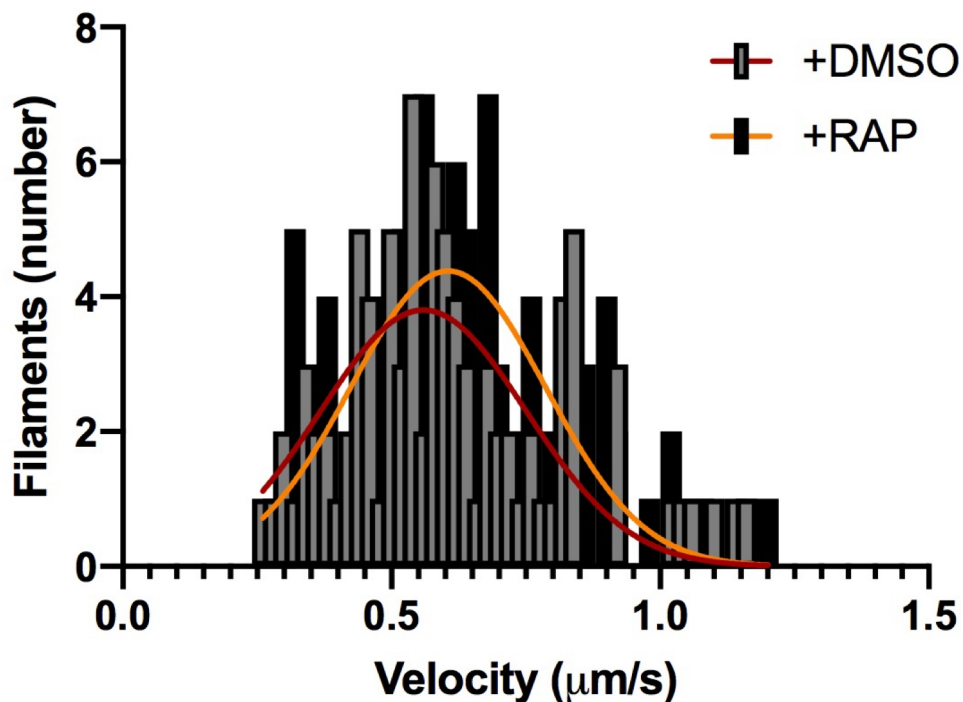


Figure 6.10. Deletion of PKAc does not affect motor speed or activity. Speed distributions from *in vitro* motility assays using episomally expressed wild type MyoA-mCherry from DMSO- and RAP-treated PKA conditional knockout merozoites.

6.2 Discussion

Phosphorylation is an important post-translation modification that can influence the properties and function of proteins. Activation of cAMP and cGMP signalling culminates in the phosphorylation of a large number of proteins in *P. falciparum* schizonts, as evidenced by recent phosphoproteomic studies (Alam et al., 2015; Flueck et al., 2019). Understanding which of these individual phosphorylation events bring about the changes observed upon activation of cyclic nucleotide and calcium signalling will be important for expanding our understanding of how these intricate signalling networks function.

One cGMP-dependent phosphorylation event that particularly stands out is phosphorylation of MyoA S19. This is the only phosphorylation site in MyoA that can be detected across schizont, merozoite and salivary gland sporozoite phosphoproteomes (Solyakov et al., 2011; Treeck et al., 2011; Lasonder et al., 2012; Pease et al., 2013; Alam et al., 2015; Swearingen et al., 2017). Phosphorylation of only one other site at MyoA S29 in merozoite samples has been identified (Lasonder et al., 2012), however this site has not been detected in any of the other phosphoproteomes.

The main aim of this chapter was to determine whether phosphorylation of MyoA S19 is required for asexual blood stage growth. Complementation of the MyoA:mCherry:cKO line described in Chapter 5 with RAP-inducible MyoA-GFP mutants which either mimic (S19D) or ablate (S19A) phosphorylation demonstrated that phosphorylation is important but not essential for asexual blood stage growth. Complementation with either mutant led to around a 40% reduction in growth when compared to parasites expressing wild type phosphorylatable MyoA. Therefore, not only is MyoA S19 phosphorylation important, but it appears that the motor also needs to be dephosphorylated, since the phosphomimetic mutation also resulted in a growth defect. *In vitro* motility assays using MyoA(S19A) isolated from merozoites revealed that the phosphomutation led to reduced motor speed when compared to wild type phosphorylatable MyoA. Furthermore non-phosphorylated MyoA harvested from PKG-inhibited schizonts also showed slower velocities when compared to phosphorylated MyoA from E64-blocked schizonts. Together these data demonstrate that blocking phosphorylation of MyoA S19 either chemically or genetically leads to reduced motility. Future *in vitro* motility assays will be performed using MyoA(S19D),

which have been harvested, in order to determine whether this mutation is able to mimic phosphorylation and achieve speeds comparable to wild type MyoA.

The work described in this chapter has also provided greater resolution into the timing of MyoA S19 phosphorylation during the asexual blood stages of infection. Prior to PKG activation, MyoA S19 is predominantly non-phosphorylated. Once cGMP signalling is triggered, MyoA S19 is rapidly phosphorylated, however maximal phosphorylation levels are only achieved once merozoites egress. Shortly after merozoites have invaded and formed rings, MyoA S19 phosphorylation intensity decreases. It remains unclear how these changes in MyoA S19 phosphorylation are achieved. Although it was previously thought that MyoA S19 is phosphorylated by PKAc (Lasonder et al., 2015), conditional disruption of PKAc revealed that this phosphorylation event is not affected (Patel et al., 2019). Consistent with this, in vitro motility assays demonstrated that MyoA isolated from PKAc-deficient merozoites displayed similar actin displacement velocities to wild type parasites. Future work identifying the kinase and phosphatase responsible for phosphorylation and dephosphorylation of MyoA S19 will provide a better understanding of how this dynamic phosphorylation event is regulated.

Overall the data presented in this chapter demonstrate that phosphorylation of MyoA S19 plays an important role in modulating motor activity. Since ablating phosphorylation of MyoA S19 leads to a slower motor, future work involving time-lapse video microscopy capturing MyoA(S19A) mutant parasites invading erythrocytes will be required in order to determine whether these parasites take a longer time to invade RBCs than wild type parasites. Previous work has shown that the invasive capacity of *P. falciparum* merozoites declines relatively quickly following merozoite egress (Boyle et al., 2010), therefore a slower motor could explain the growth defect observed in MyoA knockout parasites complemented with MyoA(S19A)-GFP.

In a recently published paper, which demonstrated that MyoA deletion leads to an invasion defect during asexual blood stage growth, the crystal structure of PfMyoA was also solved (Robert-Paganin et al., 2019). This revealed that the phosphorylated S19 residue, which is located on an unusual N-terminal extension, is able to interact with the positively charged K764 residue, which forms part of the converter domain. Typic-

ally, converter domains influence the kinetic properties of the motor (Swank et al., 2002), therefore this interaction could point toward the involvement of MyoA S19 phosphorylation in modulating the activity of the motor. Robert-Paganin et al. also performed motility assays using recombinant PfMyoA expressed in Sf9 cells harbouring either the S19A or K764E mutations, which would ablate the interaction formed by these two residues. Each of these mutations led to a two-fold reduction in motor speed, consistent with the in vitro motility data presented in this chapter. Furthermore, the recombinant PfMyoA S19A and K764E mutants were able to generate two-fold more force than wild type MyoA. From these data, the authors propose a model where MyoA S19 is expected to be dephosphorylated in merozoites such that the parasite is able to generate sufficient force for parasite entry, while in sporozoites the motor needs to be phosphorylated to achieve high gliding velocities.

If the model is true, it is unclear why MyoA S19 is so highly phosphorylated in merozoites. Although the literature suggests that merozoites do not display gliding motility (Baum et al., 2005), recent work has provided evidence that *Plasmodium* merozoites do indeed display gliding motility (personal communication Melissa Hart LSHTM, London UK). Although gliding motility is more prominent and noticeable in *P. knowlesi* merozoites, which are larger than *P. falciparum* merozoites, gliding motility can also be observed to some extent in *P. falciparum*. Therefore, it is possible that in merozoites phosphorylation of MyoA S19 could be important for gliding motility to help the parasite find an erythrocyte to invade. Although work in this chapter has demonstrated that in ring stage parasites MyoA S19 is dephosphorylated, it remains unclear when dephosphorylation occurs. Probing the phosphostatus of MyoA S19 in tightly synchronised ring stage parasites may help reveal this.

7 Conclusions

Cell signalling is a fundamental process which allows cells to sense their surroundings and mediate internal responses (Uings and Farrow, 2000). Accordingly, signalling pathways regulate critical events across all stages of the malaria parasite lifecycle (Brochet and Billker, 2016; Baker et al., 2017a). Recent advances have been made using reverse genetic techniques to unravel the complexities of the signalling pathways employed by the malaria parasite, revealing that cGMP, cAMP and calcium signalling interact with one another, forming complex networks. The essential nature of these pathways make them attractive areas of research, since a deeper understanding of how they operate may help inform the discovery of novel antimalarial compounds through the identification of novel druggable targets. Recent adaptation of the DiCre system and CRISPR/Cas9 gene editing for use in *Plasmodium falciparum* has paved the way for a new era of research, allowing the study of genes that were previously not amenable to direct knockout.

Activation of cGMP signalling during the asexual blood stages of infection leads to release of internal Ca^{2+} stores (Brochet et al., 2014), triggering calcium signalling; and the secretion of proteins from specialised organelles including micronemes and exonemes (Collins et al., 2013b). This culminates in the egress of merozoites from infected erythrocytes and the activation of cAMP signalling, which is vital for invasion and the establishment of a new replication cycle leading to exponential parasite growth (Patel et al., 2019). To further our understanding of how cGMP signalling governs important events during egress and invasion, this study investigates two integral components of this signalling cascade during the intraerythrocytic stages of *Plasmodium falciparum* parasites. Firstly, this includes $\text{GC}\alpha$, a predicted guanylyl cyclase thought to be essential for cGMP synthesis during the asexual blood stages; and secondly Myosin A, an actomyosin motor protein that is phosphorylated as a result of activation of this signalling pathway (Alam et al., 2015).

7.1 GC α - a tale of two domains that cooperate to mediate asexual blood stage egress

Prior to the start of this project, very little was known regarding GC α . This large, seemingly bifunctional protein encodes an N-terminal putative type IV P-type ATPase, predicted to be involved in flipping aminophospholipids from the outer to the inner leaflet of a lipid bilayer based on sequence homology to other flippases; as well as a C-terminal guanylyl cyclase domain. However, it was unknown whether PfGC α was in fact a guanylyl cyclase, since GC activity could not be detected by performing assays on recombinant catalytic domains of GC α expressed in *E. coli* (Carucci et al., 2000). Furthermore, previous efforts to detect GC α in schizonts using immunoelectron microscopy were unsuccessful (Carucci et al., 2000). Despite this, the transcriptional profile of GC α (López-Barragán et al., 2011; Zanghì et al., 2018) coupled with the fact that GC β is not required for blood stage growth (Hirai et al., 2006; Taylor et al., 2008; Moon et al., 2009; Gao et al., 2018) are consistent with GC α being the cyclase responsible for cGMP production to initiate cGMP signalling in asexual blood stage schizonts and in gametocytes during gametogenesis. We therefore hypothesised that GC α would be essential for asexual blood stage growth, and predicted that disruption would lead to the abrogation of cGMP production and the inability of mature schizonts to egress from erythrocytes. Using a combination of mutagenesis and conditional disruption, work presented in this thesis has definitively demonstrated that GC α is indeed expressed during the asexual blood stages and is essential for survival. Disruption of GC α results in the ablation of cGMP synthesis, consistent with this protein being the sole GC in blood stage schizonts. As a result, PKG remains inactive and schizonts are unable to release Ca²⁺ from internal stores or egress from the host erythrocyte. It is predicted that microneme and exoneme secretion is also impeded in the absence of GC α , and future IFA experiments will be done to determine whether this is indeed the case.

Failure to recover parasites harbouring mutations in a conserved residue in the ATPase domain strongly suggests that activity of this domain is required for parasite survival. Despite the disruption of both ATPase and GC domains, the phenotype observed in GC α -deficient parasites was consistent with loss of the GC domain, with no obvious additional phenotype arising due to loss of the ATPase domain. In an attempt to override the

egress defect and discern the phenotype that arises due to loss of the ATPase domain, GC α -deficient parasites were chemically complemented with PET-cGMP, a membrane permeable cGMP analogue, to bypass cGMP production. To our surprise, PET-cGMP was able to stimulate egress in GC α -null parasites and even resulted in the formation of ring stage parasites. Furthermore, we found that PET-cGMP could sustain GC α -deficient parasite growth over several cycles with no obvious second phenotype arising due to lack of the ATPase domain. Although previous reports have shown that in *Toxoplasma*, PET-cGMP could trigger microneme release in TgGC-deficient parasites, the study did not report whether parasite growth was rescued (Brown and Sibley, 2018). The work presented here demonstrates that in *P. falciparum*, the ATPase domain is ultimately involved in cGMP production by potentially mediating or regulating the activity of the GC domain, however it remains unclear how the ATPase domain achieves this. In *Toxoplasma*, release of Ca²⁺ from internal stores can be triggered by increased levels of phosphatidic acid (PA) or decreases in pH or K⁺ levels in a TgGC-dependent manner (Bisio et al., 2019; Yang et al., 2019). The authors of these studies suggest that the ATPase domain is able to sense these changes, triggering the synthesis of cGMP. Although it is possible that *Plasmodium* GC α also senses changes in pH, K⁺ or PA levels, preliminary data from Abigail Perrin (personal communication, Francis Crick Institute London UK) has demonstrated that PA does not trigger schizont egress. Furthermore, since cGMP signalling is activated prior to egress, it remains unclear how parasites would experience changes in pH or K⁺ levels from within the erythrocyte. To address this, future work using genetic complementation of the GC α knockout line with the GC domain only, using the conditional expression approach used for MyoA described in this thesis, may help elucidate the role of the ATPase during the asexual blood stage.

Since the transcriptional profile of GC α also suggests that it is the predominant GC found in gametocytes, it will be interesting to determine the role this protein plays during gametogenesis when cGMP signalling is activated. Previous studies have shown that in the presence of a PKG-specific inhibitor, mature stage V gametocytes are unable to round up and emerge from the host erythrocyte following stimulation with xanthurenic acid (XA) coupled with a decrease in temperature (McRobert et al., 2008). Therefore, it is likely that GC α -deficient gametocytes will be unable to round up and emerge, similar to inhibition of PKG. Since addition of XA to gametocyte membrane preparations led to an increased

synthesis of cGMP (Muhia et al., 2001), it is possible that XA may directly stimulate GC α activity. To test whether this is the case, cGMP enzyme activity assays can be performed with immunoprecipitated GC α from stage V gametocytes following addition of XA. It will also be interesting to determine whether a drop in temperature is also important for cGMP production. Unfortunately the 3D7 1G5 DC line that was used to generate the GC α knock-out parasites is unable to generate viable stage V gametocytes (personal communication Eloise Walker, previously at LSHTM). Therefore to address these questions, a new GC α knockout line will have to be made in a gametocyte producing 3D7 background.

7.2 Phosphorylation of Myosin A S19 puts the motor in "turbo" mode

Activation of cGMP signalling leads to the phosphorylation of many downstream proteins involved in a myriad of different processes ranging from egress and invasion to chromatin and transcriptional regulation (Alam et al., 2015). Understanding which of these individual phosphorylation events bring about the changes observed upon activation of cGMP signalling will be important for expanding our understanding of how this signalling pathway functions and how it forms networks with other signalling pathways. The second half of the work presented in this thesis involved investigation of PKG-dependent phosphorylation of MyoA S19. Previous studies have shown that phosphorylation of TgMyoA S21, the equivalent residue in *Toxoplasma*, appears to be important for tachyzoite egress from the infected host cell, and is required for efficient gliding motility (Tang et al., 2014; Gaji et al., 2015). At the outset of this PhD, it was thought that PfMyoA is essential for asexual blood stage growth, with pharmacological evidence suggesting that it most likely plays a role in powering invasion (Miller et al., 1979; Mizuno et al., 2002). Despite the fact that unlike *Toxoplasma* tachyzoites, *Plasmodium* merozoites are not thought to display gliding motility (Baum et al., 2005), we hypothesised that PKG-dependent phosphorylation of MyoA S19 would be required for activating the motor prior to invasion. Prior to testing this hypothesis, the role of MyoA in egress and invasion had to be established. Conditional disruption of PfMyoA revealed that unlike in *Toxoplasma*, the motor is not required for merozoite egress and instead plays a vital role in erythrocyte invasion, as MyoA-deficient parasites are unable to invade. These results are consistent with recent work showing

that disruption of GAP45, a structural component of the glideosome that links the IMC to the PPM, also leads to a block in merozoite invasion, but has no effect on egress (Perrin et al., 2018). However, unlike GAP45, MyoA is not required for glideosome assembly, consistent with its non-structural role.

Inducible complementation of the conditional MyoA knockout line with a mutant non-phosphorylatable version of MyoA harbouring an S19A mutation, revealed that phosphorylation of S19 is important for parasite growth. However, parasites harbouring the MyoA S19A mutation were still able to proliferate, albeit at a slower rate compared to wild type parasites. *In vitro* motility assays using parasite-derived wild type MyoA(S19) or non-phosphorylatable MyoA(S19A) revealed that blocking phosphorylation of the motor leads to reduced motility, suggesting that this phosphorylation event modulates the activity of the actomyosin motor. Consistent with the work presented in this thesis, a very recent publication has shown that recombinant MyoA(S19A) displays reduced motility compared to wild type parasites (Robert-Paganin et al., 2019). Interestingly, Robert-Paganin et al. also reported that MyoA(S19A) is able to generate more force than wild type MyoA. Therefore contrary to the original hypothesis instead of activating the motor, phosphorylation of MyoA S19 appears to be involved in fine tuning the activity of the motor. Interestingly, we observed that MyoA S19 becomes hyper-phosphorylated in released merozoites. Since it is likely that a CDPK is responsible for phosphorylating MyoA S19, it is possible that the hyper-phosphorylation observed in merozoites is due to the calcium flux experienced by the parasites upon RBC attachment (Singh et al., 2010; Gao et al., 2013) which promotes further activation of CDPKs. Identifying the kinases responsible for phosphorylating MyoA S19 could provide further insight into how this phosphorylation event is regulated. This could be achieved by N-terminally tagging MyoA with a proximity-dependent labelling protein such as BioID.

Perhaps surprisingly, MyoA knockout parasites complemented with MyoA(S19D), a mutant version which mimics phosphorylation, demonstrated a similar growth defect to parasites depending on MyoA(S19A). It was predicted that complementation with the phospho-mimic would lead to a complete rescue, however it is feasible that the S19D substitution does not effectively mimic phospho-serine. To address whether this is the case, *in vitro* motility assays using parasite-derived MyoA(S19D) will help determine whether the motor

displays normal or reduced speeds similar to wild type MyoA or MyoA(S19A), respectively. However, it is also possible that constitutive phosphorylation of MyoA leads to a growth defect. Consistent with this model, MyoA S19 appears to be dephosphorylated in ring stage parasites shortly after or during invasion. Furthermore, in PDE β knockout parasites, which display a 70% reduction in invasion, MyoA S19 is prematurely phosphorylated (Flueck et al., 2019). It is therefore conceivable that over stimulation of the motor contributes to the invasion defect observed in PDE β -null parasites. Future work will be required to address the exact timing of MyoA S19 dephosphorylation during or shortly after invasion and whether blocking this results in a growth defect similar to PDE β -null parasites.

7.3 Morphological changes observed during gametocyte development and gametogenesis do not require Myosin A

P. falciparum parasites undergo remarkable changes in morphology as they develop from stage I to stage V gametocytes. Recent work has shown that subpellicular membrane complex (SMC) proteins are required for this process (Parkyn Schneider et al., 2017). Having generated the conditional MyoA knockout line, the involvement of the motor in driving the elongation of gametocytes was assessed. This revealed that the motor is not required for gametocyte development. Furthermore, MyoA-deficient mature stage V gametocytes were able to round up and emerge from the host erythrocyte upon XA-stimulated gametogenesis. It remains unclear why this motor is expressed in gametocytes, however future experiments assessing whether exflagellation is impaired in MyoA knockout parasites will help rule out the requirement of the motor in this stage. With the establishment of a transmission lab at LSHTM, it will be possible to assess whether MyoA is required during the mosquito stages of the life cycle. It is likely that MyoA-deficient parasites will display a defect in the ookinete stage, which requires gliding motility to penetrate the midgut of the mosquito.

7.4 Final conclusions

The work performed over the course of this PhD has helped expand our understanding of cGMP signalling in *Plasmodium falciparum* parasites, by confirming the central role that GC α plays in initiating this signalling cascade, and by elucidating the effect of phosphorylation on a downstream effector of this pathway. Future work on other proteins which are phosphorylated in a PKG-dependent manner will be required to further expand our knowledge of how cGMP signalling regulates events required for egress and invasion. Of particular interest are other signalling proteins, including GC α , PDE β , AC β and CDPK1, which are phosphorylated in a PKG-dependent manner, pointing towards a potential means of cross talk between these different signalling pathways.

8 Appendix

CRISPR/Cas9 gRNAs				
Number	Target	Off target score(%)	On target score(%)	Sequence
1	GC α	99	46	TTTAATATGTGTTCTATAGC AGG
2	GC α	94	30	CCT AATGATTATGATGAATATG
3	GC α	99	47	TCTATAGCAGGAAAAACATAT GG
4	MyoA	100	25	CCTTCTCTTTT GAGAGTACAAGC
5	MyoA	100	61	CCATAC GATATTGATCCA ACTCA
6	MyoA	99	70	GTTGTACAAATTGATCCAC CCGG
7	p230p	98	46	GAATATTATTCTAATGATA AAGG

Table 3. List of gRNAs used for CRISPR/Cas9-mediated gene editing. Protospacer adjacent motifs are highlighted in bold. On and Off target scores are from Bechnling's CRISPR gRNA design software (www.benchling.com). Higher on and off target values indicate better gRNAs

Primers	
Number	Nucleotide sequence
1	ATTGAACATAATGAAGAAGATTACA
2	ATAACTTCGTATAATGTATGCTATAC
3	CCCTTTAAAGGTCGATTCTTCTCA
4	TTATTTTTACCGTTCCATGGTCGGAAAAATATTCATGTG-CATAAAT
5	GTATTAAAAGTAAAATTAATCTATATCACAATCAAATACT
6	AGTCTTATCAGTGAAAATGAAATCTACATTTCTAAATC-TCCAT
7	CGTCGTAGTCGTTCAAATTGT
8	ACCCAAATTCAACAGAGGTAAGT
9	TAGAGGATCCCCATGGAGCTTTACATAAGGAAGATTTCA-ACAC
10	AGAAGTAGAATCATCAAACCACTC
11	CTACCTTAAGTACGTAAGTAGTACTT
12	GACGGCCAGTGAATTCCTCTGAAGATTCATCAAATAAT-AAATATAACAG
13	GACGGCCAGTGAATTCATTCCATGAAGAGCTAGATTTGTACTT
14	AAAAGACATGGGGTCTACTTGAGA
15	GTATATATAAGTAAATAAGGGCATTCTT
16	GCCATATCCCTCCCCGGGTACTTGTACAGCTCGTCCA-TGC
17	CGTTTATAGATATTTTTTCAGCGAAC
18	TTTTACCGTTCCATGGGCACCGTCTCTGTTTTTGTGG-TATC
19	ACACACCCATATCCTCATCCA
20	TTCAACCCAAGTTTTATGTGGA
21	TCCATGTCTGATTTCTTTTTAGCTT
22	GCAGGTGAATTCTATTTATTTTTTTTTGTGAACCATACGG
23	AAAAAAAAAAGGATCCATAACTTCGTATAG

Table 4. List of oligonucleotide primers used in this study.

8.1 Failed approaches used to generate *P. falciparum* lines which conditionally express MyoA harbouring mutations which ablate or mimic phosphorylation of MyoA S19.

Several attempts were made to generate a *P. falciparum* parasite line which would enable conditional deletion of the endogenous MyoA:mCherry gene and switch to the expression of a second MyoA:GFP gene harbouring mutations that would either mimic (S19D) or ablate (S19A) phosphorylation of MyoA S19 to determine whether this phosphorylation event is required for parasite survival. In total, four different approaches were employed, with the successful approach described in Chapter 6. The other three approaches, which either failed or only worked for some of the mutations, are detailed below.

CRISPR/Cas9-mediated gene editing was used to modify the loxP:MyoA line generated in chapter 5 to introduce an mCherry tag at the 3' end of the endogenous *MyoA* gene, replace the endogenous 3'UTR with the *PbDT* 3'UTR and introduce a *hDHFR* cassette which confers resistance to WR99210 in order to select for integration. The repair template would also introduce a second loxP site followed by a promoterless second copy of *MyoA* fused to an *eGFP tag*. Three different version of the repair template were generated to introduce either S19A or S19D mutations or the wild type S19 sequence (Figure 8.1.A). Rapamycin treatment of the resulting line, termed MyoA:mCherry:cMutMyoA:GFP, would lead to the excision of the endogenous *MyoA:mCherry* gene, and place the *MyoA:GFP* gene under the control of the endogenous promoter, allowing for conditional expression of the second copy of *MyoA* (Figure 8.1.B). However, after several attempts to integrate all three repair templates, the only repair template that integrated correctly was the wild type MyoA(S19):GFP version (Figure 8.1.C). Although the mutant MyoA(S19A):GFP and MyoA(S19D):GFP versions also integrated, there was a truncation of the integrated repair template in both these lines as evident by PCR and live fluorescence microscopy since these two lines were not mCherry positive. Surprisingly, treatment of the MyoA:mCherry:cMutMyoA(S19):GFP did not lead to ablation of MyoA-mCherry levels, however MyoA-GFP expression was activated following treatment (data not shown). It remains unclear how both copies were expressed simultaneously, since there is only one promoter, and no leaky MyoA-GFP expression could be detected prior to RAP treatment. Since it was possible that MyoA-mCherry expression was being driven from the looped

out floxed DNA, it would be expected that after several cycles in culture, the floxed DNA would be lost. However, after maintaining RAP-treated *MyoA:mCherry:cMutMyoA(S19):GFP* parasites in culture for 8 cycles *MyoA:mCherry* and *MyoA:GFP* could still be observed by live fluorescence microscopy (data not shown). Due to the various problems encountered with this line, further experiments were not performed to characterise them.

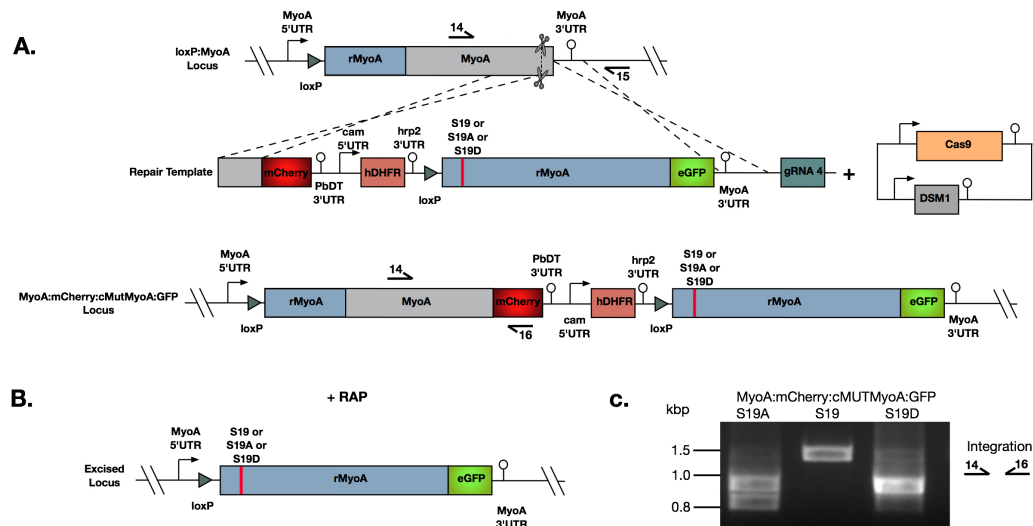


Figure 8.1. First approach used to generate conditional *MyoA* mutant parasite lines using CRISPR/Cas9-mediated gene editing. **A.** Schematic representation of the CRISPR/Cas9-based approach used to simultaneously introduce an *mCherry* tag and a *loxP* site downstream of the endogenous *MyoA* gene and install a second promoterless copy of *GFP*-tagged *MyoA* downstream of the endogenous gene. Scissors indicate CRISPR/Cas9 cleavage sites, while arrows represent the relative position of oligonucleotide primers used for diagnostic PCR screens. **B.** RAP treatment would lead to excision of the endogenous *MyoA:mCherry* sequence and place the *MyoA:GFP* sequence harbouring the S19 mutations under the control of the endogenous promoter. **C.** Diagnostic PCR analysis confirming integration of the repair template in all parasite lines, however only the *MyoA(S19)-GFP* sequence resulted in the amplification of a PCR product of the correct predicted size (~1.5 kb). The amplification of smaller PCR products at around 0.9 and 0.8 kb in the parasite lines transfected with the *MyoA(S19A):GFP* and *MyoA(S19D):GFP* repair templates indicates a truncation in the integrated repair templates somewhere between the *MyoA* and *mCherry* interface.

Since the CRISPR/Cas9 based approach to integrate a second *MyoA* gene downstream of the endogenous one was unsuccessful, another approach using selection-linked integration (SLI) (Birnbaum et al., 2017) to integrate the second *MyoA* gene was adopted. This approach relies on single homologous recombination integrating a plasmid of interest which would result in the introduction of a *T2A* skip peptide gene and a *neomycin resistance (NeoR)* cassette, which confers resistance to G418, at the 3' end of a gene of interest. Expression from the *NeoR* cassette can only be achieved once the plasmid has integrated, however presence of the *T2A* peptide ensures that the *NeoR* gene is trans-

lated as a separate polypeptide from the gene of interest. SLI plasmids were generated to tag the endogenous *MyoA* locus of loxP:*MyoA* parasites with an *mCherry* tag, and introduce a second loxP site followed by the promoterless second *MyoA* gene fused to *GFP* (Figure 8.2.). Versions that would integrate *MyoA:GFP* harbouring either S19A or S19D mutations or wild type S19 were generated. After transfecting loxP:*MyoA* parasites with the SLI plasmids, parasites were treated with 2.5 nM WR99210 to select for episome formation. After around 4 weeks, WR99210 resistant parasites for all three lines were obtained. However, no parasites could be observed up to 6 weeks following treatment with 400 µg/ml G418, indicating that integration was unsuccessful.

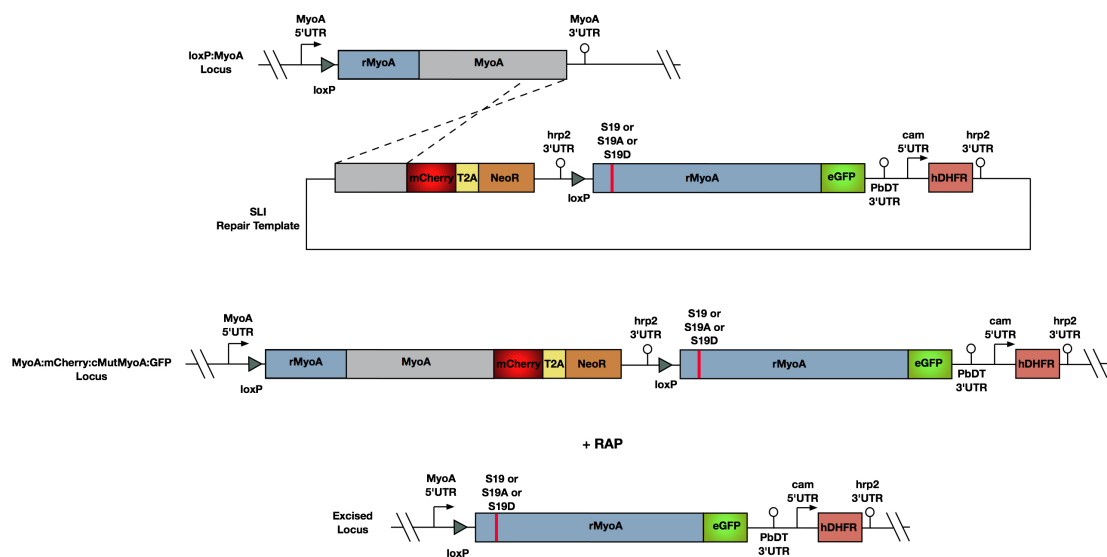


Figure 8.2. Second approach used to generate conditional *MyoA* mutant parasite lines using SLI. **A.** Schematic representation of the approach used to introduce an *mCherry* tag and a loxP site downstream of the endogenous *MyoA* gene and install a second promoterless copy of *GFP*-tagged *MyoA* downstream of the endogenous gene via single homologous cross over. Integration would lead to the expression of the *NeoR* gene, conferring resistance to G418. **B.** RAP treatment would lead to excision of the endogenous *MyoA*:*mCherry* sequence and place the *MyoA*:*GFP* sequence harbouring the S19 mutations under the control of the endogenous promoter.

After generating the *MyoA*:*mCherry*:cKO line, described in Chapter 5, a third approach was attempted, whereby *MyoA*:*mCherry*:cKO parasites were complemented with episomally expressed *MyoA*(S19)-*GFP*, *MyoA*(S19A)-*GFP* or *MyoA*(S19D)-*GFP*. To do this, expression plasmids were generated, encoding a BSDr cassette to select for episome formation, and placing the the second *MyoA* gene fused to *GFP* under the control of the *MyoA* promoter to ensure correct timing of expression hyperlinkAP3(Figure 8.3.A). *MyoA*:*mCherry*:cKO parasites were transfected with the expression plasmids encoding

either *MyoA(S19):GFP*, *MyoA(S19A):GFP* or *MyoA(S19D):GFP*. Parasites were treated with 2.5 g/ml BSD, and resistant parasites for all transfections were observed within 5 weeks post transfection. However, while most of the *MyoA:mCherry:cKO+MyoA(S19):GFP* and *MyoA:mCherry:cKO+MyoA(S19D):GFP* appeared to express MyoA-GFP, only a very small proportion of the *MyoA:mCherry:cKO+MyoA(S19A):GFP* line were GFP positive. This indicates that there could be a dominant negative effect as a result of expressing the S19A MyoA phosphomutant. Therefore despite the system working well to complement *MyoA:mCherry:cKO* parasites with wild type S19 and phosphomimetic S19D versions of MyoA [hyperlinkAP3](#)(Figure 8.3.B), this approach was unsuccessful for the S19A phosphomutant.

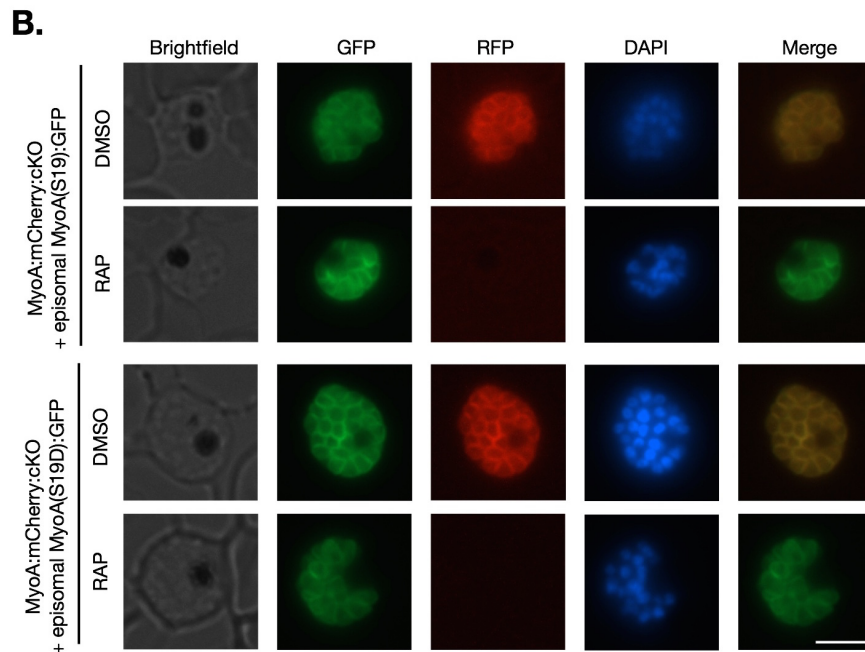
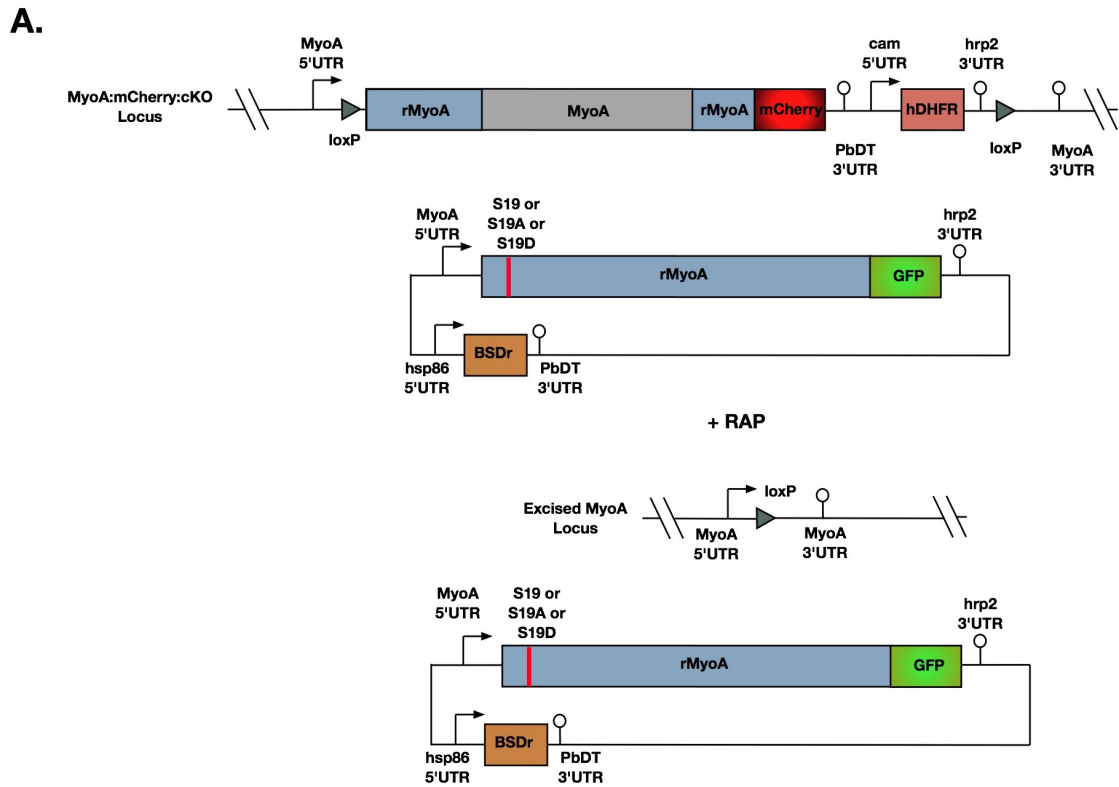


Figure 8.3. Third approach used to generate conditional *MyoA* mutant parasite lines by complementing *MyoA*:mCherry:cKO parasites with episomally expressed *MyoA*-GFP harbouring either S19A or S19D mutations or the wild type S19 sequence. **A. Schematic representation of the method used to complement the *MyoA*:mCherry:cKO line with episomally expressed *MyoA*-GFP mutants. Prior to RAP treatment, parasites would express both *MyoA*-mCherry and mutant *MyoA*-GFP. RAP treatment would lead to excision of the endogenous *MyoA*:mCherry sequences, leaving parasites reliant on the *MyoA*-GFP mutants. **B.** Live fluorescence microscopy of *MyoA*:mCherry:cKO+ episomal *MyoA*(S19):GFP and *MyoA*:mCherry:cKO+ episomal *MyoA*(S19D):GFP parasites. In DMSO treated parasites, both mCherry and GFP signals overlap and localise to the parasite periphery, consistent with *MyoA* localisation. In RAP-treated parasites, mCherry signal is no longer detected, confirming deletion of *MyoA*-mCherry. Scale bar, 5 μ m.**

9 References

- Absalon, S., Blomqvist, K., Rudlaff, R. M., DeLano, T. J., Pollastri, M. P., and Dvorin, J. D. 2018. Calcium-Dependent Protein Kinase 5 Is Required for Release of Egress-Specific Organelles in *Plasmodium falciparum*. *mBio*, 9(1):1–16.
- Alam, M. M., Solyakov, L., Bottrill, A. R., Flueck, C., Siddiqui, F. a., Singh, S., Mistry, S., Viskaduraki, M., Lee, K., Hopp, C. S., Chitnis, C. E., Doerig, C., Moon, R. W., Green, J. L., Holder, A. a., Baker, D. a., and Tobin, A. B. 2015. Phosphoproteomics reveals malaria parasite Protein Kinase G as a signalling hub regulating egress and invasion. *Nature Communications*, 6:7285.
- Alves, E., Bartlett, P. J., Garcia, C. R., and Thomas, A. P. 2011. Melatonin and IP3-induced Ca²⁺ release from intracellular stores in the malaria parasite *Plasmodium falciparum* within infected red blood cells. *Journal of Biological Chemistry*, 286(7):5905–5912.
- Amino, R., Thiberge, S., Martin, B., Celli, S., Shorte, S., Frischknecht, F., and Ménard, R. 2006. Quantitative imaging of *Plasmodium* transmission from mosquito to mammal. *Nature Medicine*, 12(2):220–224.
- Andenmatten, N., Egarter, S., Jackson, A. J., Jullien, N., Herman, J.-P., and Meissner, M. 2013. Conditional genome engineering in *Toxoplasma gondii* uncovers alternative invasion mechanisms. *Nature methods*, 10(2):125–7.
- Anders, R. F. and Smythe, J. A. 1989. Polymorphic Antigens in *Plasmodium falciparum*. *Blood*, 74(6):1865–1875.
- Andersen, J. P., Vestergaard, A. L., Mikkelsen, S. A., Mogensen, L. S., Chalat, M., and Molday, R. S. 2016. P4-ATPases as phospholipid flippases-structure, function, and enigmas. *Frontiers in Physiology*, 7(JUL):1–23.
- Ashley, E. A., Dhorda, M., Fairhurst, R. M., Amaratunga, C., Lim, P., Suon, S., Sreng, S., Anderson, J. M., Mao, S., Sam, B., Sopha, C., Chuor, C. M., Nguon, C., Sovannaroeth, S., Pukrittayakamee, S., Jittamala, P., Chotivanich, K., Chutasmit, K., Suchatsoonthorn, C., Runcharoen, R., Hien, T. T., Thuy-Nhien, N. T., Thanh, N. V., Phu, N. H., Htut, Y., Han, K.-T., Aye, K. H., Mokuolu, O. A., Olaosebikan, R. R., Folaranmi, O. O., Mayxay, M., Khanthavong, M., Hongvanthong, B., Newton, P. N., Onyamboko, M. A.,

- Fanello, C. I., Tshefu, A. K., Mishra, N., Valecha, N., Phyto, A. P., Nosten, F., Yi, P., Tripura, R., Borrmann, S., Bashraheil, M., Peshu, J., Faiz, M. A., Ghose, A., Hossain, M. A., Samad, R., Rahman, M. R., Hasan, M. M., Islam, A., Miotto, O., Amato, R., MacInnis, B., Stalker, J., Kwiatkowski, D. P., Bozdech, Z., Jeeyapant, A., Cheah, P. Y., Sakulthaew, T., Chalk, J., Intharabut, B., Silamut, K., Lee, S. J., Vihokhern, B., Kunasol, C., Imwong, M., Tarning, J., Taylor, W. J., Yeung, S., Woodrow, C. J., Flegg, J. A., Das, D., Smith, J., Venkatesan, M., Plowe, C. V., Stepniewska, K., Guerin, P. J., Dondorp, A. M., Day, N. P., and White, N. J. 2014. Spread of Artemisinin Resistance in Plasmodium falciparum Malaria . *New England Journal of Medicine*, 371(5):411–423.
- Baker, D. A. 2004. Adenylyl and guanylyl cyclases from the malaria parasite Plasmodium falciparum. *IUBMB Life*, 56(9):535–540.
- Baker, D. A., Drought, L. G., Flueck, C., Nofal, S. D., Patel, A., Penzo, M., and Walker, E. M. 2017a. Cyclic nucleotide signalling in malaria parasites. *Cellular Microbiology*, 7.
- Baker, D. A. and Kelly, J. M. 2004. Purine nucleotide cyclases in the malaria parasite. *Trends in Parasitology*, 20(5).
- Baker, D. A., O, D., McCrossan, M. V., Harmer, J., and Targett, G. A. T. 1994. Subcellular localization of Pfs16, a Plasmodium falciparum gametocyte antigen. *Parasitology*, 108(2):108.
- Baker, D. A., Stewart, L. B., Large, J. M., Bowyer, P. W., Ansell, K. H., Jiménez-Díaz, M. B., El Bakkouri, M., Birchall, K., Dechering, K. J., Bouloc, N. S., Coombs, P. J., Whalley, D., Harding, D. J., Smiljanic-Hurley, E., Wheldon, M. C., Walker, E. M., Desens, J. T., Lafuente, M. J., Sanz, L. M., Gamo, F. J., Ferrer, S. B., Hui, R., Bousema, T., Angulo-Barturén, I., Merritt, A. T., Croft, S. L., Gutteridge, W. E., Kettleborough, C. A., and Osborne, S. A. 2017b. A potent series targeting the malarial cGMP-dependent protein kinase clears infection and blocks transmission. *Nature Communications*, 8(1):1–9.
- Bakkouri, M. E., Kouidmi, I., Wernimont, A. K., Amani, M., Hutchinson, A., Loppnau, P., Kim, J. J., Flueck, C., Walker, J. R., Seitova, A., Senisterra, G., Kakihara, Y., Kim, C., Blackman, M. J., Calmettes, C., Baker, D. A., and Hui, R. 2019. Structures of the cGMP-dependent protein kinase in malaria parasites reveal a unique structural relay mechanism for activation. *Proceedings of the National Academy of Sciences of the United States of America*, 116(28):14164–14173.

- Bancells, C., Llorà-Batlle, O., Poran, A., Nötzel, C., Rovira-Graells, N., Elemento, O., Kafsack, B. F., and Cortés, A. 2019. Revisiting the initial steps of sexual development in the malaria parasite *Plasmodium falciparum*. *Nature Microbiology*, 4(1):144–154.
- Bansal, A., Molina-cruz, A., Brzostowski, J., Mu, J., and Miller, L. H. 2017. *Plasmodium falciparum* Calcium-Dependent Protein Kinase 2 Is Critical for Male Gametocyte Exflagellation but Not essential for Asexual Proliferation. *mBio*, 8(5):1–17.
- Bartoloni, A. and Zammarchi, L. 2012. Clinical aspects of uncomplicated and severe malaria. *Mediterranean Journal of Hematology and Infectious Diseases*, 4(1).
- Baruch, D. I., Gormley, J. A., Howard, R. J., and Paloske, B. L. 1996. *Plasmodium falciparum* erythrocyte membrane protein 1 is parasitized erythrocyte receptor for adherence to CD36 , thrombospondin , and intercellular adhesion molecule 1. *Proceedings of the National Academy of Sciences*, 93:3497–3502.
- Baum, J., Chen, L., Healer, J., Lopaticki, S., Boyle, M., Triglia, T., Ehlgren, F., Ralph, S. A., Beeson, J. G., and Cowman, A. F. 2009. Reticulocyte-binding protein homologue 5 - An essential adhesin involved in invasion of human erythrocytes by *Plasmodium falciparum*. *International Journal for Parasitology*, 39(3):371–380.
- Baum, J., Richard, D., Healer, J., Rug, M., Krnajski, Z., Gilberger, T.-W., Green, J. L., Holder, A. A., and Cowman, A. F. 2005. A Conserved Molecular Motor Drives Cell Invasion and Gliding Motility across Malaria Life Cycle Stages and Other Apicomplexan Parasites. *Journal of Biological Chemistry*, 281(8):5197–5208.
- Beck, J. R., Muralidharan, V., Oksman, A., and Goldberg, D. E. 2014. HSP101/PTEX mediates export of diverse malaria effector proteins into the host erythrocyte. *Nature*, 511(7511):592.
- Bement, W. M. and Mooseker, M. S. 1995. TEDS rule: A molecular rationale for differential regulation of myosins by phosphorylation of the heavy chain head. *Cell Motility and the Cytoskeleton*, 31(2):87–92.
- Bergman, L. W. 2003. Myosin A tail domain interacting protein (MTIP) localizes to the inner membrane complex of *Plasmodium* sporozoites. *Journal of Cell Science*, 116(1):39–49.

- Beshir, K. B., Sepúlveda, N., Bharmal, J., Robinson, A., Mwanguzi, J., Busula, A. O., De Boer, J. G., Sutherland, C., Cunningham, J., and Hopkins, H. 2017. Plasmodium falciparum parasites with histidine-rich protein 2 (pfrhp2) and pfrhp3 gene deletions in two endemic regions of Kenya. *Scientific Reports*, 7(1):1–10.
- Bhatt, S., Weiss, D. J., Cameron, E., Bisanzio, D., Mappin, B., Dalrymple, U., Battle, K. E., Moyes, C. L., Henry, A., Eckhoff, P. A., Wenger, E. A., Briët, O., Penny, M. A., Smith, T. A., Bennett, A., Yukich, J., Eisele, T. P., Griffin, J. T., Fergus, C. A., Lynch, M., Lindgren, F., Cohen, J. M., Murray, C. L., Smith, D. L., Hay, S. I., Cibulskis, R. E., and Gething, P. W. 2015. The effect of malaria control on Plasmodium falciparum in Africa between 2000 and 2015. *Nature*, 526(7572):207–211.
- Billker, O., Dechamps, S., Tewari, R., Wenig, G., Franke-Fayard, B., and Brinkmann, V. 2004. Calcium and a calcium-dependent protein kinase regulate gamete formation and mosquito transmission in a malaria parasite. *Cell*, 117(4):503–514.
- Billker, O., Lindo, V., Panico, M., Etienne, A. E., Paxton, T., Dell, A., Rogers, M., Sinden, R. E., and Morris, H. R. 1998. Identification of xanthurenic acid as the putative inducer of malaria development in the mosquito. *Nature*, 392(6673):289–292.
- Billker, O., Shaw, M. K., Margos, G., and Sinden, R. E. 1997. The roles of temperature, pH and mosquito factors as triggers of male and female gametogenesis of Plasmodium berghei in vitro. *Parasitology*, 115(1):1–7.
- Birnbaum, J., Flemming, S., Reichard, N., Soares, A. B., Mesén-Ramírez, P., Jonscher, E., Bergmann, B., and Spielmann, T. 2017. A genetic system to study Plasmodium falciparum protein function. *Nature Methods*, 14(4):450–456.
- Bisio, H., Lunghi, M., Brochet, M., and Soldati-Favre, D. 2019. Phosphatidic acid governs natural egress in Toxoplasma gondii via a guanylate cyclase receptor platform. *Nature Microbiology*, 4(3):420–428.
- Blasco, B., Leroy, D., and Fidock, D. A. 2017. Antimalarial drug resistance: linking Plasmodium falciparum parasite biology to the clinic. *Nature Medicine*, 8(23):917–928.
- Bookwalter, C. S., Tay, C. L., Mccrorie, R., Previs, M. J., Lu, H., Kremmentsova, B., Fagnant, P. M., Baum, J., and Trybus, K. M. 2017. Reconstitution of the core of the malaria parasite glideosome with recombinant Plasmodium class XIV myosin A and Plasmodium actin. *Journal of Biological Chemistry*, 292:19290–19303.

- Bootman, M. D., Hall, W., and Keynes, M. 2015. Calcium Signalling and Regulation of Cell Function. *John Wiley & Sons, Ltd.*, (October).
- Bousema, T. and Drakeley, C. 2011. Epidemiology and Infectivity of Plasmodium falciparum and Plasmodium vivax Gametocytes in Relation to Malaria Control and Elimination. *Clinical Microbiology Reviews*, 24(2):377–410.
- Bousema, T., Okell, L., Shekalaghe, S., Griffin, J. T., Omar, S., Sawa, P., Sutherland, C., Sauerwein, R., Ghani, A. C., and Drakeley, C. 2010. Revisiting the circulation time of Plasmodium falciparum gametocytes : molecular detection methods to estimate the duration of gametocyte carriage and the effect of gametocytocidal drugs. *Malaria Journal*, 9(136):1–11.
- Boyle, M. J., Wilson, D. W., Richards, J. S., Riglar, D. T., Tetteh, K. K., Conway, D. J., Ralph, S. A., Baum, J., and Beeson, J. G. 2010. Isolation of viable Plasmodium falciparum merozoites to define erythrocyte invasion events and advance vaccine and drug development. *Proceedings of the National Academy of Sciences of the United States of America*, 107(32):14378–14383.
- Brancucci, N. M., Gerdt, J. P., Wang, C. Q., De Niz, M., Philip, N., Adapa, S. R., Zhang, M., Hitz, E., Niederwieser, I., Boltryk, S. D., Laffitte, M. C., Clark, M. A., Grüning, C., Ravel, D., Blancke Soares, A., Demas, A., Bopp, S., Rubio-Ruiz, B., Conejo-Garcia, A., Wirth, D. F., Gendaszewska-Darmach, E., Duraisingh, M. T., Adams, J. H., Voss, T. S., Waters, A. P., Jiang, R. H., Clardy, J., and Marti, M. 2017. Lysophosphatidylcholine Regulates Sexual Stage Differentiation in the Human Malaria Parasite Plasmodium falciparum. *Cell*, 171(7):1532–1544.e15.
- Brochet, M. and Billker, O. 2016. Calcium signalling in malaria parasites. *Molecular Microbiology*, 100(3):397–408.
- Brochet, M., Collins, M. O., Smith, T. K., Thompson, E., Sebastian, S., Volkmann, K., Schwach, F., Chappell, L., Gomes, A. R., Berriman, M., Rayner, J. C., Baker, D. A., Choudhary, J., and Billker, O. 2014. Phosphoinositide Metabolism Links cGMP-Dependent Protein Kinase G to Essential Ca²⁺ Signals at Key Decision Points in the Life Cycle of Malaria Parasites. *PLoS Biology*, 12(3).
- Brown, K. M. and Sibley, L. D. 2018. Essential cGMP Signaling in Toxoplasma Is Initiated

- by a Hybrid P-Type ATPase-Guanylate Cyclase. *Cell Host and Microbe*, 24(6):804–816.e6.
- Bruce, M. C., Alano, P., S. D., and Carter, R. 1990. Commitment of the malaria parasite *Plasmodium falciparum* to sexual and asexual development. *Parasitology*, 100(2):191–200.
- Bullen, H. E., Charnaud, S. C., Kalanon, M., Riglar, D. T., Dekiwadia, C., Kangwanrangsan, N., Torii, M., Tsuboi, T., Baum, J., Ralph, S. A., Cowman, A. F., De Koning-Ward, T. F., Crabb, B. S., and Gilson, P. R. 2012. Biosynthesis, localization, and macromolecular arrangement of the *Plasmodium falciparum* translocon of exported proteins (PTEX). *Journal of Biological Chemistry*, 287(11):7871–7884.
- Bushell, E., Gomes, A. R., Sanderson, T., Anar, B., Girling, G., Herd, C., Metcalf, T., Modrzynska, K., Schwach, F., Martin, R. E., Mather, M. W., McFadden, G. I., Parts, L., Rutledge, G. G., Vaidya, A. B., Wengelnik, K., Rayner, J. C., and Billker, O. 2017. Functional Profiling of a *Plasmodium* Genome Reveals an Abundance of Essential Genes. *Cell*, 170(2).
- Butt, T., Mufti, T., Humayun, A., Rosenthal, P. B., Khan, S., Khan, S., and Molloy, J. E. 2010. Myosin motors drive long range alignment of actin filaments. *Journal of Biological Chemistry*, 285(7):4964–4974.
- Cabrera, A., Herrmann, S., Warszta, D., Santos, J. M., John Peter, A. T., Kono, M., Debrouver, S., Jacobs, T., Spielmann, T., Ungermann, C., Soldati-Favre, D., and Gilberger, T. W. 2012. Dissection of minimal sequence requirements for rhoptry membrane targeting in the malaria parasite. *Traffic*, 13(10):1335–1350.
- Cao, J., Kaneko, O., Thongkukiatkul, A., Tachibana, M., Otsuki, H., Gao, Q., Tsuboi, T., and Torii, M. 2009. Rhoptry neck protein RON2 forms a complex with microneme protein AMA1 in *Plasmodium falciparum* merozoites. *Parasitology International*, 58(1):29–35.
- Carucci, D. J., Witney, a. a., Muhia, D. K., Warhurst, D. C., Schaap, P., Meima, M., Li, J. L., Taylor, M. C., Kelly, J. M., and Baker, D. a. 2000. Guanylyl cyclase activity associated with putative bifunctional integral membrane proteins in *Plasmodium falciparum*. *The Journal of biological chemistry*, 275(29):22147–56.

- Chandramohanadas, R., Davis, P. H., Beiting, D. P., Harbut, M. B., Darling, C., Velmourougane, G., Lee, M. L., Greer, P. A., Roos, D. A., and Greenbaum, D. C. 2009. Apicomplexan Parasites Co-Opt Host Calpains to Facilitate Their Escape from Infected Cells. *Science*, 324(5298):794–797.
- Chaubey, S., Grover, M., and Tatu, U. 2014. Endoplasmic reticulum stress triggers gametocytogenesis in the malaria parasite. *Journal of Biological Chemistry*, 289(24):16662–16674.
- Chen, L., Lopaticki, S., Riglar, D. T., Dekiwadia, C., Uboldi, A. D., Tham, W. H., O'Neill, M. T., Richard, D., Baum, J., Ralph, S. A., and Cowman, A. F. 2011. An egf-like protein forms a complex with pfrh5 and is required for invasion of human erythrocytes by plasmodium falciparum. *PLoS Pathogens*, 7(9).
- Child, M. A., Harris, P. K., Collins, C. R., Withers-Martinez, C., Yeoh, S., and Blackman, M. J. 2013. Molecular determinants for subcellular trafficking of the malarial sheddase PfSUB2. *Traffic*, 14(10):1053–1064.
- Choudhary, H. H., Gupta, R., and Mishra, S. 2019. PKAc is not required for the preerythrocytic stages of Plasmodium berghei. *Life Science Alliance*, 2(3):1–11.
- Claessens, A., Affara, M., Assefa, S. A., Kwiatkowski, D. P., and Conway, D. J. 2017. Culture adaptation of malaria parasites selects for convergent loss-of-function mutants. *Scientific Reports*, 7:1–8.
- Clyde, D. F., McCarthy, V. C., Miller, R. M., and Hornick, R. B. 1973. Specificity of protection of man immunized against sporozoite-induced falciparum malaria. *The American Journal of the Medical Sciences*, 266(6):398–404.
- Cobb, D. W., Florentin, A., Fierro, M. A., and Krakowiak, M. 2017. The Exported Chaperone PfHsp70x Is Dispensable for the Plasmodium falciparum Intraerythrocytic Life Cycle. *mSphere*, 2(5):1–15.
- Cogswell, F. B. 1992. The hypnozoite and relapse in primate malaria. *Clinical Microbiology Reviews*, 5(1):26–35.
- Collins, C. R., Das, S., Wong, E. H., Andenmatten, N., Stallmach, R., Hackett, F., Herman, J.-p., Müller, S., Meissner, M., and Blackman, M. J. 2013a. Robust inducible Cre recombinase activity in the human malaria parasite Plasmodium falciparum enables

- efficient gene deletion within a single asexual erythrocytic growth cycle. *Molecular Microbiology*, 88(March):687–701.
- Collins, C. R., Hackett, F., Atid, J., Tan, M. S. Y., and Blackman, M. J. 2017. *The Plasmodium falciparum pseudoprotease SERA5 regulates the kinetics and efficiency of malaria parasite egress from host erythrocytes*, volume 13.
- Collins, C. R., Hackett, F., Strath, M., Penzo, M., Withers-martinez, C., Baker, D. A., and Blackman, M. J. 2013b. Malaria Parasite cGMP-dependent Protein Kinase Regulates Blood Stage Merozoite Secretory Organelle Discharge and Egress. *PLoS Pathogens*, 9(5).
- Corran, P., Coleman, P., Riley, E., and Drakeley, C. 2007. Serology: a robust indicator of malaria transmission intensity? *Trends in Parasitology*, 23(12):575–582.
- Counihan, N. A., Chisholm, S. A., Bullen, H. E., Srivastava, A., Sanders, P. R., Jonsdottir, T. K., Weiss, G. E., Ghosh, S., Crabb, B. S., Creek, D. J., Gilson, P. R., and de Koning-Ward, T. F. 2017. Plasmodium falciparum parasites deploy RhopH2 into the host erythrocyte to obtain nutrients, grow and replicate. *eLife*, 6:1–31.
- Cox-Singh, J., Davis, T. M. E., Lee, K. S., Shamsul, S. S. G., Matusop, A., S, R., Rahman, H. A., Conway, D. J., and Singh, B. 2008. Plasmodium knowlesi malaria in humans is widely distributed and potentially life threatening. *Clinical Infectious Diseases*, 46(2):165–171.
- Crosnier, C., Bustamante, L. Y., Bartholdson, S. J., Bei, A. K., Theron, M., Uchikawa, M., Mboup, S., Ndir, O., Kwiatkowski, D. P., Duraisingh, M. T., Rayner, J. C., and Wright, G. J. 2012. Basigin is a receptor essential for erythrocyte invasion. *Nature*, 480(7378):534–537.
- Das, S., Hertrich, N., Perrin, A. J., Withers-Martinez, C., Collins, C. R., Jones, M. L., Watermeyer, J. M., Fobes, E. T., Martin, S. R., Saibil, H. R., Wright, G. J., Treeck, M., Epp, C., and Blackman, M. J. 2015. Processing of Plasmodium falciparum Merozoite Surface Protein MSP1 Activates a Spectrin-Binding Function Enabling Parasite Egress from RBCs. *Cell Host and Microbe*, 18(4):433–444.
- Davies, H. M., Nofal, S. D., Mclaughlin, E. J., and Osborne, A. R. 2017. Repetitive sequences in malaria parasite proteins. *FEMS Microbiology Reviews*, 3(April):1–18.

- Dawn, A., Singh, S., More, K. R., Siddiqui, F. A., Pachikara, N., Ramdani, G., Langsley, G., and Chitnis, C. E. 2014. The Central Role of cAMP in Regulating Plasmodium falciparum Merozoite Invasion of Human Erythrocytes. *PLoS Pathogens*, 10(12).
- Day, K. P. and Marsh, K. 1991. Naturally acquired immunity to Plasmodium falciparum. *Immunology Today*, 12(3):68–71.
- de Koning-ward, T. F., Gilson, P. R., Boddey, J. a., Rug, M., Smith, B. J., Papenfuss, A. T., Sanders, P. R., Lundie, R. J., Maier, A. G., Cowman, A. F., Crabb, B. S., de Koning-ward, T. F., Gilson, P. R., Boddey, J. a., Rug, M., Smith, B. J., Papenfuss, A. T., Sanders, P. R., Lundie, R. J., Maier, A. G., Cowman, A. F., Crabb, B. S., Koning-ward, T. F. D., Gilson, P. R., Boddey, J. a., Rug, M., Smith, B. J., Papenfuss, A. T., Sanders, P. R., Lundie, R. J., Maier, A. G., Cowman, A. F., and Crabb, B. S. 2009. A novel protein export machine in malaria parasites. *Nature*, 459(7249):945–949.
- Dearnley, M. K., Yeoman, J. A., Hanssen, E., Kenny, S., Turnbull, L., Whitchurch, C. B., Tilley, L., and Dixon, M. W. A. 2011. Origin , composition , organization and function of the inner membrane complex of Plasmodium falciparum gametocytes. *Journal of Cell Science*, 125:2053–2063.
- Delves, M. J., Ruecker, A., Straschil, U., Lelièvre, J., Marques, S., López-Barragán, M. J., Herreros, E., and Sinden, R. E. 2013. Male and female Plasmodium falciparum mature gametocytes show different responses to antimalarial drugs. *Antimicrobial Agents and Chemotherapy*, 57(7):3268–3274.
- Deng, W. and Baker, D. A. 2002. A novel cyclic GMP-dependent protein kinase is expressed in the ring stage of the Plasmodium falciparum life cycle. *Molecular Microbiology*, 44(5):1141–1151.
- Deng, W., Parbhu-Patel, A., Meyer, D. J., and Baker, D. A. 2003. The role of two novel regulatory sites in the activation of the cGMP-dependent protein kinase from Plasmodium falciparum. *Biochemical Journal*, 374(2):559–565.
- Dini, S., Zaloumis, S., Cao, P., Price, R. N., Fowkes, F. J. I., van der Pluijm, R. W., McCaw, J. M., and Simpson, J. 2018. Investigating the Efficacy of Triple Artemisinin-Based Combination Therapies for Treating Plasmodium falciparum Malaria Patients Using Mathematical Modeling. *Antimicrobial Agents and Chemotherapy*, 62(11):1–11.

- Donald, R. G., Zhong, T., Wiersma, H., Nare, B., Yao, D., Lee, A., Allocco, J., and Liberator, P. A. 2006. Anticoccidial kinase inhibitors: Identification of protein kinase targets secondary to cGMP-dependent protein kinase. *Molecular and Biochemical Parasitology*, 149(1):86–98.
- Dondorp, A. M., Kager, P. A., Vreeken, J., and White, N. J. 2000. Abnormal blood flow and red blood cell deformability in severe malaria. *Parasitology Today*, 16(6):228–232.
- Doolan, D. L., Dobaño, C., and Baird, J. K. 2009. Acquired immunity to Malaria. *Clinical Microbiology Reviews*, 22(1):13–36.
- Draper, S. J., Sack, B. K., King, C. R., Nielsen, C. M., Rayner, J. C., Higgins, M. K., Long, C. A., and Seder, R. A. 2018. Malaria Vaccines: Recent Advances and New Horizons. *Cell Host and Microbe*, 24(1):43–56.
- Dvorin, J. D., Martyn, D. C., Patel, S. D., Grimley, J. S., Collins, R., Hopp, C. S., Bright, A. T., Westenberger, S., Blackman, M. J., Baker, D. A., Wandless, T. J., and Manoj, T. 2011. A Plant-Like Kinase in *Plasmodium falciparum* Regulates Parasite Egress From Erythrocytes. *Science*, 328(5980):910–912.
- Eckly-Michel, A., Martin, V., and Lugnier, C. 1997. Involvement of cyclic nucleotide-dependent protein kinases in cyclic AMP-mediated vasorelaxation. *British Journal of Pharmacology*, 122(1):158–164.
- Egarter, S., Andenmatten, N., Jackson, A. J., Whitelaw, J. A., Pall, G., Black, J. A., Ferguson, D. J. P., Tardieux, I., Mogilner, A., and Meissner, M. 2014. The *Toxoplasma* Acto-MyoA Motor Complex Is Important but Not Essential for Gliding Motility and Host Cell Invasion. *PLoS ONE*, 9(3):e91819.
- Eksi, S., Morahan, B. J., Haile, Y., Furuya, T., Jiang, H., Ali, O., Xu, H., Kiattibutr, K., Suri, A., Czesny, B., Adeyemo, A., Myers, T. G., Sattabongkot, J., zhuan Su, X., and Williamson, K. C. 2012. *Plasmodium falciparum* Gametocyte Development 1 (Pfgdv1) and Gametocytogenesis Early Gene Identification and Commitment to Sexual Development. *PLoS Pathogens*, 8(10).
- Elsworth, B., Matthews, K., Nie, C. Q., Kalanon, M., Charnaud, S. C., Sanders, P. R., Chisholm, S. A., Counihan, N. A., Shaw, P. J., Pino, P., Chan, J. A., Azevedo, M. F., Rogerson, S. J., Beeson, J. G., Crabb, B. S., Gilson, P. R., and De Koning-Ward, T. F.

2014. PTEX is an essential nexus for protein export in malaria parasites. *Nature*, 511(7511):587–591.
- Falae, A., Combe, A., Amaladoss, A., Carvalho, T., Menard, R., and Bhanot, P. 2010. Role of Plasmodium berghei cGMP-dependent protein kinase in late liver stage development. *Journal of Biological Chemistry*, 285(5):3282–3288.
- Fang, H., Gomes, A. R., Klages, N., Pino, P., Maco, B., Walker, E. M., Zenonos, Z. A., Angrisano, F., Baum, J., Doerig, C., Baker, D. A., Billker, O., and Brochet, M. 2018. Epistasis studies reveal redundancy among calcium-dependent protein kinases in motility and invasion of malaria parasites. *Nature Communications*, 9(1):1–14.
- Farrell, A., Thirugnanam, S., Lorestani, A., Dvorin, J. D., Eidell, K. P., Ferguson, D. J. P., Anderson-White, B. R., Duraisingh, M. T., Marth, G. T., and Marc-Jan, G. 2012. A DOC2 Protein Identified by Mutational Profiling is Essential for Apicomplexan Parasite Exocytosis. *Science*, 335(6065):218–221.
- Ferreira, M. U., Nunes, S., and Wunderlich, G. 2004. Antigenic Diversity and Immune Evasion by Malaria Parasites. *Minireviews*, 11(6):987–995.
- Filarsky, M., Fraschka, S. A., Niederwieser, I., Brancucci, N. M. B., Carrington, E., Carrió, E., Moes, S., Jenoe, P., Bártfai, R., and Voss, T. S. 2018. GDV1 induces sexual commitment of malaria parasites by antagonizing HP1-dependent gene silencing. *Science*, 359:1259–1263.
- Fivelman, Q. L., McRobert, L., Sharp, S., Taylor, C. J., Saeed, M., Swales, C. A., Sutherland, C. J., and Baker, D. A. 2007. Improved synchronous production of Plasmodium falciparum gametocytes in vitro. *Molecular and Biochemical Parasitology*, 154(1):119–123.
- Flannery, E., Chatterjee, A., and Winzeler, E. 2003. Antimalarial Drug Discovery: Approaches and Progress towards New Medicines. *Nature Reviews Microbiology*, 11(12):1–28.
- Florentin, A., Cobb, D. W., Fishburn, J. D., Cipriano, M. J., Kim, P. S., Fierro, M. A., Striepen, B., and Muralidharan, V. 2017. PfClpC Is an Essential Clp Chaperone Required for Plastid Integrity and Clp Protease Stability in Plasmodium falciparum. *Cell Reports*, 21(7):1746–1756.

- Flueck, C., Drought, L. G., Jones, A., Patel, A., Perrin, A. J., Walker, E. M., Nofal, S. D., Snijders, A. P., Blackman, M. J., and Baker, D. A. 2019. *Phosphodiesterase beta is the master regulator of camp signalling during malaria parasite invasion*, volume 17.
- Foy, B. D., Alout, H., Seaman, J. A., Rao, S., Magalhaes, T., Wade, M., Parikh, S., Soma, D. D., Sagna, A. B., Fournet, F., Slater, H. C., Bougma, R., Drabo, F., Diabaté, A., Couliadiaty, A. G. V., Rouamba, N., and Dabiré, R. K. 2019. Efficacy and risk of harms of repeat ivermectin mass drug administrations for control of malaria (RIMDAMAL): a cluster-randomised trial. *The Lancet*, 393(10180):1517–1526.
- Frénal, K., Marq, J. B., Jacot, D., Polonais, V., and Soldati-Favre, D. 2014. Plasticity between MyoC- and MyoA-Glideosomes: An Example of Functional Compensation in *Toxoplasma gondii* Invasion. *PLoS Pathogens*, 10(11).
- Frénal, K., Polonais, V., Marq, J. B., Stratmann, R., Limenitakis, J., and Soldati-Favre, D. 2010. Functional dissection of the apicomplexan glideosome molecular architecture. *Cell Host and Microbe*, 8(4):343–357.
- Frevert, U., Engelmann, S., Zougbedé, S., Stange, J., Ng, B., Matuschewski, K., Liebes, L., and Yee, H. 2005. Intravital observation of plasmodium berghei sporozoite infection of the liver. *PLoS Biology*, 3(6):1034–1046.
- Gaji, R. Y., Johnson, D. E., Treeck, M., Wang, M., Hudmon, A., and Arrizabalaga, G. 2015. Phosphorylation of a Myosin Motor by TgCDPK3 Facilitates Rapid Initiation of Motility during *Toxoplasma gondii* egress. *PLoS Pathogens*, 11(11):1–20.
- Ganter, M., Goldberg, J. M., Dvorin, J. D., Paulo, J. A., King, J. G., Tripathi, A. K., Paul, A. S., Yang, J., Coppens, I., Jiang, R. H., Elsworth, B., Baker, D. A., Dinglasan, R. R., Gygi, S. P., and Duraisingh, M. T. 2017. Erratum: Plasmodium falciparum CRK4 directs continuous rounds of DNA replication during schizogony. *Nature microbiology*, 2:17038.
- Gao, H., Yang, Z., Wang, X., Qian, P., Hong, R., Chen, X., zhuan Su, X., Cui, H., and Yuan, J. 2018. ISP1-Anchored Polarization of GC β /CDC50A Complex Initiates Malaria Ookinete Gliding Motility. *Current Biology*, 28(17):2763–2776.e6.
- Gao, X., Gunalan, K., Yap, S. S. L., and Preiser, P. R. 2013. Triggers of key calcium signals during erythrocyte invasion by Plasmodium falciparum. *Nature Communications*, 4:1–11.

- Gaskins, E., Gilk, S., DeVore, N., Mann, T., Ward, G., and Beckers, C. 2004. Identification of the membrane receptor of a class XIV myosin in *Toxoplasma gondii*. *Journal of Cell Biology*, 165(3):383–393.
- Ghorbal, M., Gorman, M., Macpherson, C. R., Martins, R. M., Scherf, A., and Lopez-Rubio, J.-J. 2014. Genome editing in the human malaria parasite *Plasmodium falciparum* using the CRISPR-Cas9 system. *Nature Biotechnology*, 32(8):819–821.
- Ghosh, S., Chisholm, S. A., Dans, M., Lakkavaram, A., Kennedy, K., Ralph, S. A., Counihan, N. A., and De Koning-Ward, T. F. 2018. The cysteine protease dipeptidyl aminopeptidase 3 does not contribute to egress of *Plasmodium falciparum* from host red blood cells. *PLoS ONE*, 13(3):1–16.
- Gilson, P. R. and Crabb, B. S. 2009. Morphology and kinetics of the three distinct phases of red blood cell invasion by *Plasmodium falciparum* merozoites. *International Journal for Parasitology*, 39(1):91–96.
- Ginsburg, H., Krugliak, M., Eidelman, O., and Cabantchik, Z. I. 1983. New permeability pathways induced in membranes of *Plasmodium falciparum* infected erythrocytes. *Science*, 8:177–190.
- Goldberg, D. E., Slater, A. F., Cerami, A., and Henderson, G. B. 1990. Hemoglobin degradation in the malaria parasite *Plasmodium falciparum*: an ordered process in a unique organelle. *Proceedings of the National Academy of Sciences*, 87(8):2931–2935.
- Gomes, A. R., Bushell, E., Schwach, F., Girling, G., Anar, B., Quail, M. A., Herd, C., Pfander, C., Modrzynska, K., Rayner, J. C., and Billker, O. 2015. A genome-scale vector resource enables high-throughput reverse genetic screening in a malaria parasite. *Cell Host and Microbe*, 17(3):404–413.
- Gomes, F. M. and Barillas-Mury, C. 2018. Infection of anopheline mosquitoes with *Wolbachia*: Implications for malaria control. *PLoS Pathogens*, 14(11):1–6.
- Govindasamy, K., Jebiwott, S., Jaijyan, D. K., Davidow, A., Ojo, K. K., Van Voorhis, W. C., Brochet, M., Billker, O., and Bhanot, P. 2016. Invasion of hepatocytes by *Plasmodium* sporozoites requires cGMP-dependent protein kinase and calcium dependent protein kinase 4. *Molecular Microbiology*, 102(2):349–363.

- Green, J. L., Martin, S. R., Fielden, J., Ksagoni, A., Grainger, M., Yim Lim, B. Y. S., Molloy, J. E., and Holder, A. A. 2006. The MTIP-myosin A complex in blood stage malaria parasites. *Journal of Molecular Biology*, 355(5):933–941.
- Green, J. L., Wall, R. J., Vahokoski, J., Yusuf, N. A., Mohd Ridzuan, M. A., Stanway, R. R., Stock, J., Knuepfer, E., Brady, D., Martin, S. R., Howell, S. A., Pires, I. P., Moon, R. W., Molloy, J. E., Kursula, I., Tewari, R., and Holder, A. A. 2017. Compositional and expression analyses of the glideosome during the Plasmodium life cycle reveal an additional myosin light chain required for maximum motility. *Journal of Biological Chemistry*, 292(43):17857–17875.
- Greenwood, B. 2010. Anti-malarial drugs and the prevention of malaria in the population of malaria endemic areas. *Malaria Journal*, 9(SUPPL. 3).
- Günay-Esiyok, Ö., Scheib, U., Noll, M., and Gupta, N. 2019. An unusual and vital protein with guanylate cyclase and P4-ATPase domains in a pathogenic protist. *Life Science Alliance*, 2(3):e201900402.
- Gurnett, A. M., Liverator, P. A., Dulski, P. M., Salowe, S. P., Donald, R. G. K., Anderson, J. W., Wiltsie, J., Diaz, C. A., Harris, G., Chang, B., Darkin-Rattray, S. J., Nare, B., Crumley, T., Blum, P. S., Misura, A. S., Tamas, T., Sardana, M. K., Yuan, J., Biftu, T., and Schmatz, D. M. 2002. Purification and Molecular Characterization of cGMP-dependent Protein Kinase from Apicomplexan Parasites. A NOVEL CHEMOTHERAPEUTIC TARGET. *Journal of Biological Chemistry*, 277(18):15913–15922.
- Hale, V. L., Watermeyer, J. M., Hackett, F., Vizcay-barrena, G., Ooij, C. V., and Thomas, J. A. 2017. Parasitophorous vacuole poration precedes its rupture and rapid host erythrocyte cytoskeleton collapse in Plasmodium falciparum egress. *Proceedings of the National Academy of Sciences*, 114(13):3439–3444.
- Harris, P. K., Yeoh, S., Dluzewski, A. R., O'Donnell, R. A., Withers-Martinez, C., Hackett, F., Bannister, L. H., Mitchell, G. H., and Blackman, M. J. 2005. Molecular identification of a malaria merozoite surface sheddase. *PLoS Pathogens*, 1(3):0241–0251.
- Hawking, F., Wilson, M. E., and Gammage, K. 1971. Evidence for cyclic development and short-lived maturity in the gametocytes of Plasmodium falciparum. *Transactions of the Royal Society of Tropical Medicine and Hygiene*, 65(5):549–559.

- Heintzelman, M. B. and Schwartzman, J. D. 1997. A novel class of unconventional myosins from *Toxoplasma gondii*. *Journal of molecular biology*, 271(1):139–146.
- Hemingway, J., Ranson, H., Magill, A., Kolaczinski, J., Fornadel, C., Gimnig, J., Coetzee, M., Simard, F., Roch, D. K., Hinzoumbe, C. K., Pickett, J., Schellenberg, D., Gething, P., Hoppé, M., and Hamon, N. 2016. Averting a malaria disaster: Will insecticide resistance derail malaria control? *The Lancet*, 387(10029):1785–1788.
- Hirai, M., Arai, M., Kawai, S., and Matsuoka, H. 2006. PbGC β is essential for *Plasmodium* ookinete motility to invade midgut cell and for successful completion of parasite life cycle in mosquitoes. *Journal of Biochemistry*, 140(5):747–757.
- Hoffman, S., Goh, L., Luke, T., Schneider, I., Le, T., Doolan, D., Sacchi, J., de la Vega, P., Dowler, M., Paul, C., Gordon, D., Stoute, J., Church, L., Sedegah, M., Heppner, D., Ballou, W., and Richie, T. 2002. Protection of Humans against Malaria by Immunization with Radiation-Attenuated *Plasmodium falciparum* Sporozoites. *The Journal of Infectious Diseases*, 185(8):1155–1164.
- Hopp, C. S., Chiou, K., Ragheb, D. R., Salman, A. M., Khan, S. M., Liu, A. J., and Sinnis, P. 2015. Longitudinal analysis of plasmodium sporozoite motility in the dermis reveals component of blood vessel recognition. *eLife*, 4(AUGUST2015):1–21.
- Hopp, C. S., Flueck, C., Solyakov, L., Tobin, A., and Baker, D. A. 2012. Spatiotemporal and Functional Characterisation of the *Plasmodium falciparum* cGMP-Dependent Protein Kinase. *PLoS ONE*, 7(11):1–9.
- Hovlid, M. L. and Winzeler, E. A. 2016. Phenotypic Screens in Antimalarial Drug Discovery. *Trends in Parasitology*, 32(9):697–707.
- Howes, R. E., Dewi, M., Piel, F. B., Monteiro, W. M., Battle, K. E., Messina, J. P., Sakuntabhai, A., Satyagraha, A. W., Williams, T. N., Baird, J. K., and Hay, S. I. 2013. Spatial distribution of G6PD deficiency variants across malaria-endemic regions. *Malaria Journal*, 12(1):1–15.
- Hughes, G. L., Koga, R., Xue, P., Fukatsu, T., and Rasgon, J. L. 2011. *Wolbachia* Infections Are Virulent and Inhibit the Human Malaria Parasite *Plasmodium Falciparum* in *Anopheles Gambiae*. *PLoS Pathogens*, 7(5):3–10.

- Humphreys, G. S., Merinopoulos, I., Ahmed, J., Whitty, C. J., Mutabingwa, T. K., Sutherland, C. J., and Hallett, R. L. 2007. Amodiaquine and artemether-lumefantrine select distinct alleles of the *Plasmodium falciparum* *mdr1* gene in Tanzanian children treated for uncomplicated malaria. *Antimicrobial Agents and Chemotherapy*, 51(3):991–997.
- Hunter, T. 2012. Why nature chose phosphate to modify proteins. *Philosophical Transactions of the Royal Society B: Biological Sciences*, 367(1602):2513–2516.
- Idro, R., Marsh, K., John, C. C., and Newton, C. R. J. 2011. Europe PMC Funders Group Cerebral Malaria ; Mechanisms Of Brain Injury And Strategies For Improved Neuro-Cognitive Outcome. *Journal of Neuroscience Methods*, 68(4):267–274.
- Inselburg, J. and Banyal, H. S. 1984. *Plasmodium falciparum*: Synchronization of asexual development with aphidicolin, a DNA synthesis inhibitor. *Experimental Parasitology*, 57(1):48–54.
- Ishino, T., Orito, Y., Chinzei, Y., and Yuda, M. 2006. A calcium-dependent protein kinase regulates *Plasmodium* ookinete access to the midgut epithelial cell. *Molecular Microbiology*, 59(4):1175–1184.
- Ishizuka, A. S., Lyke, K. E., DeZure, A., Berry, A. A., Richie, T. L., Mendoza, F. H., Enama, M. E., Gordon, I. J., Chang, L. J., Sarwar, U. N., Zephir, K. L., Holman, L. A., James, E. R., Billingsley, P. F., Gunasekera, A., Chakravarty, S., Manoj, A., Li, M., Ruben, A. J., Li, T., Eappen, A. G., Stafford, R. E., Natasha, K. C., Murshedkar, T., DeCederfelt, H., Plummer, S. H., Hendel, C. S., Novik, L., Costner, P. J., Saunders, J. G., Laurens, M. B., Plowe, C. V., Flynn, B., Whalen, W. R., Todd, J. P., Noor, J., Rao, S., Sierra-Davidson, K., Lynn, G. M., Epstein, J. E., Kemp, M. A., Fahle, G. A., Mikolajczak, S. A., Fishbaugher, M., Sack, B. K., Kappe, S. H., Davidson, S. A., Garver, L. S., Björkström, N. K., Nason, M. C., Graham, B. S., Roederer, M., Kim Lee Sim, B., Hoffman, S. L., Ledgerwood, J. E., and Seder, R. A. 2016. Protection against malaria at 1 year and immune correlates following PfSPZ vaccination. *Nature Medicine*, 22(6):614–623.
- Jacot, D., Tosetti, N., Pires, I., Stock, J., Graindorge, A., Hung, Y.-F., Han, H., Tewari, R., Kursula, I., and Soldati-Favre, D. 2016. An Apicomplexan Actin-Binding Protein Serves as a Connector and Lipid Sensor to Coordinate Motility and Invasion. *Cell Host & Microbe*, 20(6):731–743.

- Janse, C. J., van der Klooster, P. F., van der Kaay, H. J., van der Ploeg, M., and Prosper Overdulve, J. 1986. DNA synthesis in *Plasmodium berghei* during asexual and sexual development. *Molecular and Biochemical Parasitology*, 20(2):173–182.
- Jia, Y., Marq, J., Bisio, H., Jacot, D., Mueller, C., Yu, L., Choudhary, J., Brochet, M., and Soldati-Favre, D. 2017. Crosstalk between PKA and PKG controls pH dependent host cell egress of *Toxoplasma gondii*. *The EMBO Journal*, 36(21):3250–3267.
- Joice, R., Nilsson, S. K., Montgomery, J., Dankwa, S., Morahan, B., Seydel, K. B., Bertucini, L., Alano, P., Kim, C., Duraisingh, M. T., Taylor, T. E., and Milner, D. A. 2014. Levels and changes of HDL cholesterol and apolipoprotein A-I in relation to risk of cardiovascular events among statin-treated patients; a meta-analysis. *Circulation*, 6(244):1–16.
- Jones, M. L., Das, S., Belda, H., Collins, C. R., Blackman, M. J., and Treeck, M. 2016. A versatile strategy for rapid conditional genome engineering using loxP sites in a small synthetic intron in *Plasmodium falciparum*. *Scientific Reports*, 6(November 2015):21800.
- Kafsack, B. F. C., Rovira-graells, N., Clark, T. G., and Bancells, C. 2014. A transcriptional switch underlies commitment to sexual development in human malaria parasites. *Nature*, 507(7491):248–252.
- Kapulu, M. C., Da, D. F., Miura, K., Li, Y., Blagborough, A. M., Churcher, T. S., Nikolaeva, D., Williams, A. R., Goodman, A. L., Sangare, I., Turner, A. V., Cottingham, M. G., Nicosia, A., Straschil, U., Tsuboi, T., Gilbert, S. C., Long, C. A., Sinden, R. E., Draper, S. J., Hill, A. V., Cohuet, A., and Biswas, S. 2015. Comparative assessment of transmission-blocking vaccine candidates against *plasmodium falciparum*. *Scientific Reports*, 5(June):1–15.
- Kaushal, D. C., Carter, R., Miller, L. H., and Krishna, G. 1980. Gametocytogenesis by malaria parasites in continuous culture. *Nature*, 286:490–492.
- Kawamoto, F., Alejo-Blanco, R., Fleck, S. L., and Sinden, R. E. 1991. *Plasmodium berghei*: Ionic regulation and the induction of gametogenesis. *Experimental Parasitology*, 72(1):33–42.
- Kenthirapalan, S., Waters, A. P., Matuschewski, K., and Kooij, T. W. A. 2016. Functional profiles of orphan membrane transporters in the life cycle of the malaria parasite. *Nature Communications*, 7(JANUARY):10519.

- Kibbe, W. A. 2007. OligoCalc: An online oligonucleotide properties calculator. *Nucleic Acids Research*, 35(SUPPL.2):43–46.
- Kim, J. J., Flueck, C., Franz, E., Sanabria-figueroa, E., Herberg, W., and Kim, C. 2015. Crystal Structures of the Carboxyl cGMP Binding Domain of the Plasmodium falciparum cGMP-dependent Protein Kinase Reveal a Novel Capping Triad Crucial for Merozoite Egress. *PLoS Pathogens*, pages 1–22.
- Kleinschmidt, I., Bradley, J., Knox, T. B., Mnzava, A. P., Kafy, H. T., Mbogo, C., Ismail, B. A., Bigoga, J. D., Adechoubou, A., Raghavendra, K., Cook, J., Malik, E. M., Nkuni, Z. J., Macdonald, M., Bayoh, N., Ochomo, E., Fondjo, E., Awono-Ambene, H. P., Etang, J., Akogbeto, M., Bhatt, R. M., Chourasia, M. K., Swain, D. K., Kinyari, T., Subramaniam, K., Massougbdji, A., Okê-Sopoh, M., Ogouyemi-Hounto, A., Kouambeng, C., Abdin, M. S., West, P., Elmardi, K., Cornelie, S., Corbel, V., Valecha, N., Mathenge, E., Kamau, L., Lines, J., and Donnelly, M. J. 2018. Implications of insecticide resistance for malaria vector control with long-lasting insecticidal nets: a WHO-coordinated, prospective, international, observational cohort study. *The Lancet Infectious Diseases*, 18(6):640–649.
- Knuepfer, E., Napiorkowska, M., Van Ooij, C., and Holder, A. A. 2017. Generating conditional gene knockouts in Plasmodium - A toolkit to produce stable DiCre recombinase-expressing parasite lines using CRISPR/Cas9. *Scientific Reports*, 7(1):1–12.
- Kobylinski, K. C., Foy, B. D., and Richardson, J. H. 2012. Ivermectin inhibits the sporogony of Plasmodium falciparum in Anopheles gambiae. *Malaria Journal*, 11(1):1.
- Koch, M., Wright, K. E., Otto, O., Herbig, M., Salinas, N. D., Tolia, N. H., Satchwell, T. J., Guck, J., Brooks, N. J., and Baum, J. 2017. Plasmodium falciparum erythrocyte-binding antigen 175 triggers a biophysical change in the red blood cell that facilitates invasion. *Proceedings of the National Academy of Sciences*, page 201620843.
- Kõressaar, T., Lepamets, M., Kaplinski, L., Raime, K., Andreson, R., and Remm, M. 2018. Primer3-masker: Integrating masking of template sequence with primer design software. *Bioinformatics*, 34(11):1937–1938.
- Koussis, K., Withers-Martinez, C., Yeoh, S., Child, M., Hackett, F., Knuepfer, E., Juliano, L., Woehlbier, U., Bujard, H., and Blackman, M. J. 2009. A multifunctional ser-

- ine protease primes the malaria parasite for red blood cell invasion. *EMBO Journal*, 28(6):725–735.
- Krishna, S., Woodrow, C., Webb, R., Penny, J., Takeyasu, K., Kimura, M., and East, J. M. 2001. Expression and Functional Characterization of a Plasmodium falciparum Ca²⁺-ATPase (PfATP4) Belonging to a Subclass Unique to Apicomplexan Organisms. *Journal of Biological Chemistry*, 276(14):10782–10787.
- Kühlbrandt, W. 2004. Biology, structure and mechanism of P-type ATPases. *Nature Reviews Molecular Cell Biology*, 5(4):282–295.
- Kumar, P., Tripathi, A., Ranjan, R., Halbert, J., Gilberger, T., Doerig, C., and Sharma, P. 2014. Regulation of Plasmodium falciparum development by calcium-dependent protein kinase 7 (PfCDPK7). *Journal of Biological Chemistry*, 289(29):20386–20395.
- Kyrou, K., Hammond, A. M., Galizi, R., Kranjc, N., Burt, A., Beaghton, A. K., Nolan, T., and Crisanti, A. 2018. A CRISPR-Cas9 gene drive targeting doublesex causes complete population suppression in caged Anopheles gambiae mosquitoes. *Nature biotechnology*, 36(11):1062–1066.
- Lacerda, M. V. G., Llanos-Cuentas, A., Krudsood, S., Lon, C., Mohammed, R., Yilma, D., Pereira, D. B., Espino, F. E. J., Mia, R. Z., Chuquiyauri, R., Val, F., Casapía, M., Monteiro, W. M., Brito, M. A. M., Costa, M. R. F., Buathong, N., Noedl, H., Diro, E., Getie, S., Wubie, K. M., Abdissa, A., Zeynudin, A., Abebe, C., Tada, M. S., Mohamed, K., Clover, D. D., Fletcher, K., Breton, J. J., Ugwuegbulam, C. O., Green, J. A., and Koh, G. C. K. W. 2019. Single-Dose Tafenoquine to Prevent Relapse of Plasmodium vivax Malaria. *New England Journal of Medicine*, 380(3):215–228.
- Lakshmanan, V., Fishbaugher, M. E., Morrison, B., Baldwin, M., Macarulay, M., Vaughan, A. M., Mikolajczak, S. A., and Kappe, S. H. 2015. Cyclic GMP balance is critical for malaria parasite transmission from the mosquito to the mammalian host. *mBio*, 6(2):1–10.
- Lamarque, M., Besteiro, S., Papoin, J., Roques, M., Vulliez-Le Normand, B., Morlon-Guyot, J., Dubremetz, J. F., Fauquenoy, S., Tomavo, S., Faber, B. W., Kocken, C. H., Thomas, A. W., Boulanger, M. J., Bentley, G. A., and Lebrun, M. 2011. The RON2-AMA1 interaction is a critical step in moving junction-dependent invasion by apicomplexan parasites. *PLoS Pathogens*, 7(2).

- Lambros, C. and Vanderberg, J. P. 1979. Synchronization of Plasmodium Falciparum Erythrocytic Stages in Culture. *Journal of Parasitology*, 65(3):418–420.
- Langreth, S. G. and Peterson, E. 1985. Pathogenicity, stability, and immunogenicity of a knobless clone of Plasmodium falciparum in Colombian owl monkeys. *Infection and Immunity*, 47(3):760–766.
- Lasonder, E., Green, J. L., Camarda, G., Talabani, H., Holder, A. a., Langsley, G., and Alano, P. 2012. The plasmodium falciparum schizont phosphoproteome reveals extensive phosphatidylinositol and cAMP-protein kinase A signaling. *Journal of Proteome Research*, 11(11):5323–5337.
- Lasonder, E., Green, J. L., Grainger, M., Langsley, G., and Holder, A. A. 2015. Extensive differential protein phosphorylation as intraerythrocytic Plasmodium falciparum schizonts develop into extracellular invasive merozoites. *Proteomics*, 15(15):2716–2729.
- Leech, B. Y. J. H., Barnwell, J. W., Miller, L. H., and Howard, R. J. 1984. Identification of strain-specific malarial antigen exposed on the surface of Plasmodium falciparum-infected erythrocytes. *Journal of Experimental Medicine*, 159(June):1567–1575.
- Lees, R. S., Gilles, J. R., Hendrichs, J., Vreysen, M. J., and Bourtzis, K. 2015. Back to the future: the sterile insect technique against mosquito disease vectors. *Current Opinion in Insect Science*, 10:156–162.
- Lehmann, C., Tan, M. S. Y., de Vries, L. E., Russo, I., Sanchez, M. I., Goldberg, D. E., and Deu, E. 2018. *Plasmodium falciparum* dipeptidyl aminopeptidase 3 activity is important for efficient erythrocyte invasion by the malaria parasite, volume 14.
- Levine, N. D. 1970. Taxonomy of the Sporozoa. *The Journal of Parasitology*, 56(4):1–389.
- Leykauf, K., Treeck, M., Gilson, P. R., Nebl, T., Bräulke, T., Cowman, A. F., Gilberger, T. W., and Crabb, B. S. 2010. Protein Kinase A Dependent Phosphorylation of Apical Membrane Antigen 1 Plays an Important Role in Erythrocyte Invasion by the Malaria Parasite. *PLoS Pathogens*, 6(6):e1000941.
- Lim, C., Hansen, E., Desimone, T. M., Moreno, Y., Junker, K., Bei, A., Brugnara, C., Buckee, C. O., and Duraisingh, M. T. 2013. Expansion of host cellular niche can drive

- adaptation of a zoonotic malaria parasite to humans. *Nature Communications*, 4:1638–1639.
- Lim, M. Y.-X., LaMonte, G., Lee, M. C. S., Reimer, C., Tan, B. H., Corey, V., Tjahjadi, B. F., Chua, A., Nachon, M., Wintjens, R., Dedek, P., Malleret, B., Renia, L., Bonamy, G. M. C., Ho, P. C.-L., Yeung, B. K. S., Chow, E. D., Lim, L., Fidock, D. A., Diagona, T. T., Winzeler, E. A., and Bifani, P. 2017. UDP-galactose and Acetyl-CoA transporters as Plasmodium multidrug resistance genes. *Nature Microbiology*, 546(7660):651–655.
- Linder, J. U., Engel, P., Reimer, A., Krüger, T., Plattner, H., Schultz, A., and Schultz, J. E. 1999. Guanylyl cyclases with the topology of mammalian adenylyl cyclases and an N-terminal P-type ATPase-like domain in Paramecium, Tetrahymena and Plasmodium. *EMBO Journal*, 18(15):4222–4232.
- Loomis, W. F. 2014. Cell signaling during development of Dictyostelium. *Developmental Biology*, 391(1):1–16.
- Lopaticki, S., Maier, A. G., Thompson, J., Wilson, D. W., Tham, W. H., Triglia, T., Gout, A., Speed, T. P., Beeson, J. G., Healer, J., and Cowman, A. F. 2011. Reticulocyte and erythrocyte binding-like proteins function cooperatively in invasion of human erythrocytes by malaria parasites. *Infection and Immunity*, 79(3):1107–1117.
- López-Barragán, M. J., Lemieux, J., Quiñones, M., Williamson, K. C., Molina-Cruz, A., Cui, K., Barillas-Mury, C., Zhao, K., and Su, X.-z. 2011. Directional gene expression and antisense transcripts in sexual and asexual stages of Plasmodium falciparum. *BMC Genomics*, 12(1):587.
- Lourido, S., Shuman, J., Zhang, C., Shokat, K. M., Hui, R., and Sibley, L. D. 2010. Calcium-dependent protein kinase 1 is an essential regulator of exocytosis in Toxoplasma. *Nature*, 465(7296):359–362.
- Macpherson, C. R. and Scherf, A. 2015. correspondence Flexible guide-RNA design for CRISPR applications using Protospacer Workbench. *Nature Publishing Group*, 33(8):805–806.
- Mair, G. R., Braks, J. A. M., Garver, L. S., Dimopoulos, G., Wiegant, J. C. A. G., Dirks, R. W., Khan, S. M., Janse, C. J., and Waters, A. P. 2007. Translational Repression is essential for Plasmodium sexual development and mediated by a DDX6-type helicase. *Science*, 313(5787):667–669.

- Mashanov, G. I. and Molloy, J. E. 2007. Automatic detection of single fluorophores in live cells. *Biophysical Journal*, 92(6):2199–2211.
- Mata-Cantero, L., Lafuente, M. J., Sanz, L., and Rodriguez, M. S. 2014. Magnetic isolation of Plasmodium falciparum schizonts iRBCs to generate a high parasitaemia and synchronized in vitro culture. *Malaria Journal*, 13(1):1–9.
- McRobert, L., Taylor, C. J., Deng, W., Fivelman, Q. L., Cummings, R. M., Polley, S. D., Billker, O., and Baker, D. A. 2008. Gametogenesis in Malaria Parasites Is Mediated by the cGMP-Dependent Protein Kinase. *PLoS Biology*, 6(6):e139.
- Meissner, M., Schluter, D., and Soldatov, D. 2002. Role of Toxoplasma gondii Myosin A in Powering Parasite Gliding and Host Cell Invasion. *Science*, 298(5594):837–840.
- Miller, B. Y. L. H., Aikawa, M., Johnson, J. G., and Shiroishi, T. 1979. Interaction Between Cytochalasin B-Treated Malarial Parasites and Erythrocytes Attachment and Junction Formation. *The Journal of Experimental Medicine*, 149(1517):172–184.
- Mizuno, Y., Makioka, A., Kawazu, S. I., Kano, S., Kawai, S., Akaki, M., Aikawa, M., and Ohtomo, H. 2002. Effect of jasplakinolide on the growth, invasion, and actin cytoskeleton of Plasmodium falciparum. *Parasitology Research*, 88(9):844–848.
- Mogollon, C. M., van Pul, F. J. A., Imai, T., Ramesar, J., Chevalley-Maurel, S., de Roo, G. M., Veld, S. A. J., Kroeze, H., Frakne-Fayard, B. M. D., Janse, C. J., and Khan, S. M. 2016. Rapid Generation of Marker-Free P. falciparum Fluorescent Reporter Lines Using Modified CRISPR/Cas9 Constructs and Selection Protocol. *PLoS ONE*, 11(December):22.
- Montagna, G. N., Buscaglia, C. A., Münter, S., Goosmann, C., Frischknecht, F., Brinkmann, V., and Matuschewski, K. 2012. Critical role for heat shock protein 20 (HSP20) in migration of malarial sporozoites. *Journal of Biological Chemistry*, 287(4):2410–2422.
- Montigny, C., Lyons, J., Champeil, P., Nissen, P., and Lenoir, G. 2015. On the molecular mechanism of flippase- and scramblase-mediated phospholipid transport. *Biochimica et Biophysica Acta - Molecular and Cell Biology of Lipids*, 1861(8):767–783.
- Moon, R. W., Hall, J., Rangkuti, F., Ho, Y. S., Almond, N., Mitchell, G. H., Pain, A., Holder, A. a., and Blackman, M. J. 2013. Adaptation of the genetically tractable malaria patho-

- gen *Plasmodium knowlesi* to continuous culture in human erythrocytes. *Proceedings of the National Academy of Sciences of the United States of America*, 110(2):531–6.
- Moon, R. W., Taylor, C. J., Bex, C., Schepers, R., Goulding, D., Janse, C. J., Waters, A. P., Baker, D. A., and Billker, O. 2009. A cyclic GMP signalling module that regulates gliding motility in a malaria parasite. *PLoS Pathogens*, 5(9).
- Moreno, S. N. J., Ayong, L., and Pace, D. A. 2011. Calcium storage and function in apicomplexan parasites. *Essays in Biochemistry*, 51(1):97–110.
- Mueller, C., Klages, N., Jacot, D., Santos, J. M., Cabrera, A., Gilberger, T. W., Dubremetz, J. F., and Soldati-Favre, D. 2013. The toxoplasma protein ARO mediates the apical positioning of rhoptry organelles, a prerequisite for host cell invasion. *Cell Host and Microbe*, 13(3):289–301.
- Muhia, D. K., Swales, C. A., Deng, W., Kelly, J. M., and Baker, D. A. 2001. The gametocyte-activating factor xanthurenic acid stimulates an increase in membrane-associated guanylyl cyclase activity in the human malaria parasite *Plasmodium falciparum*. *Molecular Microbiology*, 42(2):553–560.
- Muhia, D. K., Swales, C. A., Eckstein-Ludwig, U., Saran, S., Polley, S. D., Kelly, J. M., Schaap, P., Krishna, S., and Baker, D. A. 2003. Multiple splice variants encode a novel adenylyl cyclase of possible plastid origin expressed in the sexual stage of the malaria parasite *Plasmodium falciparum*. *Journal of Biological Chemistry*, 278(24):22014–22022.
- Nacher, M., Singhasivanon, P., Silachamroon, U., Nacher, M., Singhasivanont, P., Silachamroont, U., Treeprasertsukt, S., Vannaphant, S., Gay, F., Mazier, D., and Looareesuwa, S. 2002. Decreased Hemoglobin Concentrations , Hyperparasitemia , and Severe Malaria Are Associated with Increased *Plasmodium falciparum* Gametocyte Carriage Treeprasertsuk , Thanawat Tosukhowong , Suparp Vannaphan , Frédérick Gay , Dominique Mazier and Sornchai Lo. *The Journal of Parasitology*, 88(1):97–101.
- Nasamu, A. S., Glushakova, S., Russo, I., Vaupel, B., Kim, A. S., Fremont, D. H., Tolia, N., Beck, J. R., Marvin, J., Niles, J. C., Zimmerberg, J., and Goldberg, D. E. 2017. Plasmeepsins IX and X are essential and druggable mediators of malaria parasite egress and invasion. *Science*, 358:518–522.

- Noedl, H., Se, Y., Schaecher, K., Smith, B. L., Socheat, D., and Fukuda, M. M. 2008. Evidence of Artemisinin-Resistant Malaria in Western Cambodia. *New England Journal of Medicine*, 359(24):2619–2620.
- Nofal, S. D., Peto, T. J., Adhikari, B., Tripura, R., Callery, J., Bui, T. M., von Seidlein, L., and Pell, C. 2019. How can interventions that target forest-goers be tailored to accelerate malaria elimination in the Greater Mekong Subregion? A systematic review of the qualitative literature. *Malaria Journal*, 18(1):1–10.
- O'Donnell, R. A., Hackett, F., Howell, S. A., Treeck, M., Struck, N., Krnajski, Z., Withers-Martinez, C., Gilberger, T. W., and Blackman, M. J. 2006. Intramembrane proteolysis mediates shedding of a key adhesin during erythrocyte invasion by the malaria parasite. *Journal of Cell Biology*, 174(7):1023–1033.
- Olivieri, A., Collins, C. R., Hackett, F., Withers-Martinez, C., Marshall, J., Flynn, H. R., Skehel, J. M., and Blackman, M. J. 2011. Juxtamembrane shedding of plasmodium falciparum AMA1 is sequence independent and essential, and helps evade invasion-inhibitory antibodies. *PLoS Pathogens*, 7(12).
- Ono, T., Cabrita-Santos, L., Leitao, R., Bettiol, E., Purcell, L. A., Diaz-Pulido, O., Andrews, L. B., Tadakuma, T., Bhanot, P., Mota, M. M., and Rodriguez, A. 2008. Adenylyl cyclase α and cAMP signaling mediate Plasmodium sporozoite apical regulated exocytosis and hepatocyte infection. *PLoS Pathogens*, 4(2).
- Otto, T. D., Wilinski, D., Assefa, S., Keane, T. M., Sarry, L. R., Böhme, U., Lemieux, J., Barrell, B., Pain, A., Berriman, M., Newbold, C., and Llinás, M. 2010. New insights into the blood-stage transcriptome of Plasmodium falciparum using RNA-Seq. *Molecular Microbiology*, 76(1):12–24.
- Parikh, S. and Rosenthal, P. J. 2009. Intermittent preventive therapy for malaria in pregnancy: Is sulfadoxine-pyrimethamine the right drug? *Clinical Pharmacology and Therapeutics*, 87(2):160–162.
- Parkyn Schneider, M., Liu, B., Glock, P., Suttie, A., McHugh, E., Andrew, D., Batinovic, S., Williamson, N., Hanssen, E., McMillan, P., Hliscs, M., Tilley, L., and Dixon, M. W. 2017. Disrupting assembly of the inner membrane complex blocks Plasmodium falciparum sexual stage development. *PLoS Pathogens*, 13(10):1–30.

- Pasloske, B. L. and Howard, R. J. 1994. Malaria, the red cell, and the endothelium. *Annual Review of Medicine*, 45(February):283–295.
- Passos, A. P. and Garcia, C. R. 1998. Inositol 1,4,5-trisphosphate induced Ca²⁺ release from chloroquine-sensitive and -insensitive intracellular stores in the intraerythrocytic stage of the malaria parasite *P. chabaudi*. *Biochemical and Biophysical Research Communications*, 245(1):155–160.
- Patel, A., Perrin, A. J., Flynn, H. R., Bisson, C., Withers-Martinez, C., Treeck, M., Flueck, C., Nicastro, G., Martin, S. R., Ramos, A., Gilberger, T. W., Snijders, A. P., Blackman, M. J., and Baker, D. A. 2019. *Cyclic AMP signalling controls key components of malaria parasite host cell invasion machinery*, volume 17.
- Paul, A. S., Saha, S., Engelberg, K., Jiang, R. H., Coleman, B. I., Kosber, A. L., Chen, C.-T., Ganter, M., Espy, N., Gilberger, T. W., Marc-Jan, G., and Duraisingh, M. T. 2015. Parasite calcineurin regulates host cell recognition and attachment by apicomplexans. *Cell Host & Microbe*, 18(1):49–60.
- Paulitschke, M. and Nash, G. B. 1993. Membrane rigidity of red blood cells parasitized by different strains of *Plasmodium falciparum*. *The Journal of Laboratory and Clinical Medicine*, 122(5):581–589.
- Payne, R. O., Silk, S. E., Elias, S. C., Miura, K., Diouf, A., Galaway, F., de Graaf, H., Brendish, N. J., Poulton, I. D., Griffiths, O. J., Edwards, N. J., Jin, J., Labbé, G. M., Alanine, D. G., Siani, L., Di Marco, S., Roberts, R., Green, N., Berrie, E., Ishizuka, A. S., Nielsen, C. M., Bardelli, M., Partey, F. D., Ofori, M. F., Barfod, L., Wambua, J., Murungi, L. M., Osier, F. H., Biswas, S., McCarthy, J. S., Minassian, A. M., Ashfield, R., Viebig, N. K., Nugent, F. L., Douglas, A. D., Vekemans, J., Wright, G. J., Faust, S. N., Hill, A. V., Long, C. A., Lawrie, A. M., and Draper, S. J. 2017. Human vaccination against RH5 induces neutralizing antimalarial antibodies that inhibit RH5 invasion complex interactions. *JCI Insight*, 2(21):1–19.
- Pease, B. N., Huttlin, E. L., Jedrychowski, M. P., Talevich, E., Harmon, J., Dillman, T., Kannan, N., Doerig, C., Chakrabarti, R., Gygi, S. P., and Chakrabarti, D. 2013. Global Analysis of Protein Expression and Phosphorylation of Three Stages of *Plasmodium falciparum* Intraerythrocytic Development. *Journal of Proteome Research*, 12(9):4028–4045.

- Pehrson, C., Salanti, A., Theander, T. G., and Nielsen, M. A. 2017. Pre-clinical and clinical development of the first placental malaria vaccine. *Expert Review of Vaccines*, 16(6):613–624.
- Pell, C., Straus, L., Andrew, E. V. W., Meñ Aca, A., and Pool, R. 2011. Social and Cultural Factors Affecting Uptake of Interventions for Malaria in Pregnancy in Africa: A Systematic Review of the Qualitative Research. *PLoS Neglected Tropical Diseases*, 6(7).
- Penzo, M., de las Heras-Dueña, L., Mata-Cantero, L., Diaz-Hernandez, B., Vazquez-Muñiz, M. J., Ghidelli-Disse, S., Drewes, G., Fernandez-Alvaro, E., and Baker, D. A. 2019. High-throughput screening of the Plasmodium falciparum cGMP-dependent protein kinase identified a thiazole scaffold which kills erythrocytic and sexual stage parasites. *Scientific Reports*, 9(1):1–13.
- Perrin, A. J., Collins, C. R., Russell, M. R. G., Collinson, L. M., Baker, D. A., and Blackman, M. J. 2018. The Actinomyosin Motor Drives Malaria Parasite Red Blood Cell Invasion but Not Egress. *mBio*, 9(4):1–17.
- Pinder, J. C., Fowler, R. E., Dluzewski, a. R., Bannister, L. H., Lavin, F. M., Mitchell, G. H., Wilson, R. J., and Gratzer, W. B. 1998. Actomyosin motor in the merozoite of the malaria parasite, Plasmodium falciparum: implications for red cell invasion. *Journal of cell science*, 111 (Pt 1:1831–9.
- Pino, P., Caldelari, R., Mukherjee, B., Vahokoski, J., Klages, N., Maco, B., Collins, C. R., Blackman, M. J., Kursula, I., Heussler, V., Brochet, M., and Soldati-favre, D. 2017. A multistage antimalarial targets the plasmepsins IX and X essential for Invasion and Egress. *Science*, 358(October):522–528.
- Prommana, P., Uthaiyibull, C., Wongsombat, C., Kamchonwongpaisan, S., Yuthavong, Y., Knuepfer, E., Holder, A. A., and Shaw, P. J. 2013. Inducible Knockdown of Plasmodium Gene Expression Using the glmS Ribozyme. *PLoS ONE*, 8(8):1–10.
- Read, L. K. and Mikkelsen, R. B. 1991. Comparison of Adenylate Cyclase and cAMP-Dependent Protein Kinase in Gametocytogenic and Nongametocytogenic Clones of Plasmodium falciparum. *The Journal of Parasitology*, 77(3):346.
- Recht, J., Ashley, E. A., and White, N. J. 2018. Use of primaquine and glucose-6-

- phosphate dehydrogenase deficiency testing: Divergent policies and practices in malaria endemic countries. *PLoS Neglected Tropical Diseases*, 12(4):1–27.
- Reddy, K. S., Amlabu, E., Pandey, A. K., Mitra, P., Chauhan, V. S., and Gaur, D. 2015. Multiprotein complex between the GPI-anchored CyRPA with PfRH5 and PfRipr is crucial for *Plasmodium falciparum* erythrocyte invasion. *Proceedings of the National Academy of Sciences*, 112(4):1179–1184.
- Rees-Channer, R. R., Martin, S. R., Green, J. L., Bowyer, P. W., Grainger, M., Molloy, J. E., and Holder, A. A. 2006. Dual acylation of the 45 kDa gliding-associated protein (GAP45) in *Plasmodium falciparum* merozoites. *Molecular and Biochemical Parasitology*, 149(1):113–116.
- Ridley, R. G. 2002. Medical need, scientific opportunity and the drive for antimalarial drugs. *Nature*, 415(1):686–693.
- Ridzuan, M. A. M., Moon, R. W., Knuepfer, E., Black, S., Holder, A. A., and Green, J. L. 2012. Subcellular location, phosphorylation and assembly into the motor complex of GAP45 during *Plasmodium falciparum* schizont development. *PLoS ONE*, 7(3).
- Robert-Paganin, J., Robblee, J. P., Auguin, D., Blake, T. C. A., Bookwalter, C. S., Kremntsova, E. B., Moussaoui, D., Previs, M. J., Jousset, G., Baum, J., Trybus, K. M., and Houdusse, A. 2019. *Plasmodium* myosin A drives parasite invasion by an atypical force generating mechanism. *Nature Communications*.
- Rosenberg, R. and Rungsiwongse, J. 1991. The Number of Sporozoites Produced by Individual Malaria Oocysts. *The American Journal of Tropical Medicine and Hygiene*, 45(5):574–577.
- Rosenthal, P. 2003. Antimalarial drug discovery: Old and new approaches. *Journal of Experimental Biology*, 206(21):3735–3744.
- RTS, S. 2015. Efficacy and safety of RTS,S/AS01 malaria vaccine with or without a booster dose in infants and children in Africa: final results of a phase 3, individually randomised, controlled trial. *The Lancet*, 386(9988):31–45.
- Ruecker, A., Shea, M., Hackett, F., Suarez, C., Hirst, E. M., Milutinovic, K., Withers-Martinez, C., and Blackman, M. J. 2012. Proteolytic activation of the essential para-

- sitophorous vacuole cysteine protease SERA6 accompanies malaria parasite egress from its host erythrocyte. *Journal of Biological Chemistry*, 287(45):37949–37963.
- Salazar, E., Bank, E. M., Ramsey, N., Hess, K. C., Deitsch, K. W., Levin, L. R., and Buck, J. 2012. Characterization of Plasmodium falciparum Adenylyl Cyclase- β and its role in Erythrocytic stage parasites. *PLoS ONE*, 7(6):1–8.
- Santos, J. M., Egarter, S., Zuzarte-Luís, V., Kumar, H., Moreau, C. A., Kehrer, J., Pinto, A., da Costa, M., Franke-Fayard, B., Janse, C. J., Frischknecht, F., and Mair, G. R. 2017. Malaria parasite LIMP protein regulates sporozoite gliding motility and infectivity in mosquito and mammalian hosts. *eLife*, 6:1–26.
- Schultz, J. E., Klumpp, S., Benz, R., Schurhoff-Goeters, W. J., and Schmid, A. 1992. Regulation of adenylyl cyclase from Paramecium by an intrinsic potassium conductance. *Science*, 255(5044):600–603.
- Seder, R. A., Chang, L.-J., Enama, M. E., Zephir, K. L., Sarwar, U. N., Gordon, I. J., Holman, L. A., James, E. R., Billingsley, P. F., Gunasekera, A., Richman, A., Chakravarty, S., Manoj, A., Velmurugan, S., Li, M., Ruben, A. J., Li, T., Eappen, A. G., Stafford, R. E., Plummer, S. H., Hendel, C. S., Novik, L., Costner, P. J. M., Mendoza, F. H., Saunders, J. G., Nason, M. C., Richardson, J. H., Murphy, J., Davidson, S. A., Richie, T. L., Sedegah, M., Sutamihardja, A., Fahle, G. A., Lyke, K. E., Laurens, M. B., Roederer, M., Tewari, K., Epstein, J. E., Sim, B. K. L., Ledgerwood, J. E., Graham, B. S., Hoffman, S. L., DiGiovanni, C., Williams, P., Luongo, N., Mitchell, J., Florez, M. B., Larkin, B., Berkowitz, N., Wilson, B., Clarke, T., Vasilenko, O., Yamshchikov, G., Sitar, S., Stanford, L., Pittman, I., Bailer, R. T., Casazza, J., Decederfelt, H., Starling, J., Williams, E. C., Lau, A., Antonara, S., Brocious, J., Kemp, M., Inglese, J., Dranchak, P., Abot, E. N., Reyes, S., Ganeshan, H., Belmonte, M., Huang, J., Belmonte, A., Komisar, J., Abebe, Y., Getachew, Y., Patil, A., Matheny, S., Nelson, K., Overby, J., Pich, V., Wen, Y., Fan, R., Fomumbod, E., Awe, A., Chakiath, C., King, M., Orozco, M. S., Murshedkar, T., Padilla, D., Jiang, B., Gao, L., KC, N., Xu, R., Adams, M., Plowe, C., Loblein, H., Renehan, P. Z., Kunchai, M., and Diep, L. 2013. Protection Against Malaria by Intravenous Immunization with a Nonreplicating Sporozoite Vaccine. *Science*, 341(6152):1359–1365.
- Sellers, J. R. 2000. Myosins: A diverse superfamily. *Biochimica et Biophysica Acta - Molecular Cell Research*, 1496(1):3–22.

- Serganov, A. and Nudler, E. 2013. A decade of riboswitches. *Cell*, 152(1-2):17–24.
- Shapiro, L. L., Whitehead, S. A., and Thomas, M. B. 2017. Quantifying the effects of temperature on mosquito and parasite traits that determine the transmission potential of human malaria. *PLoS Biology*, 15(10):1–21.
- Shaw, W. R., Marcenac, P., Childs, L. M., Buckee, C. O., Baldini, F., Diabate, A., Catteruccia, F., Sawadogo, S. P., and Dabire, R. K. 2016. Wolbachia infections in natural Anopheles populations affect egg laying and negatively. *Nature Communications*, (May).
- Sherling, E. S. and van Ooij, C. 2016. Host cell remodeling by pathogens: the exomembrane system in *Plasmodium*-infected erythrocytes. *FEMS Microbiology Reviews*, 40(5):701–721.
- Sidjanski, S. and Vanderberg, J. P. 1997. Delayed migration of Plasmodium sporozoites from the mosquito bite site to the blood. *American Journal of Tropical Medicine and Hygiene*, 57(4):426–429.
- Sinden, R. E. 1982. Gametocytogenesis of Plasmodium falciparum in vitro: An electron microscopic study. *Parasitology*, 84(1):1–11.
- Singh, S., Alam, M. M., Pal-Bhowmick, I., Brzostowski, J. A., and Chitnis, C. E. 2010. Distinct external signals trigger sequential release of apical organelles during erythrocyte invasion by malaria parasites. *PLoS Pathogens*, 6(2).
- Sinha, A., Hughes, K. R., Modrzynska, K. K., Otto, T. D., Dickens, N. J., Religa, A. A., Bushell, E., Graham, A. L., Cameron, R., Kafsack, B. F. C., Williams, A. E., Llinas, M., Billker, O., and Waters, A. P. 2014. A cascade of DNA binding proteins for sexual commitment and development in Plasmodium. *Nature*, 507(7491):253–257.
- Sissoko, M. S., Healy, S. A., Katile, A., Omaswa, F., Zaidi, I., Gabriel, E. E., Kamate, B., Samake, Y., Guindo, M. A., Dolo, A., Niangaly, A., Niaré, K., Zeguime, A., Sissoko, K., Diallo, H., Thera, I., Ding, K., Fay, M. P., O’Connell, E. M., Nutman, T. B., Wong-Madden, S., Murshedkar, T., Ruben, A. J., Li, M., Abebe, Y., Manoj, A., Gunasekera, A., Chakravarty, S., Sim, B. K. L., Billingsley, P. F., James, E. R., Walther, M., Richie, T. L., Hoffman, S. L., Doumbo, O., and Duffy, P. E. 2017. Safety and efficacy of Pf-SPZ Vaccine against Plasmodium falciparum via direct venous inoculation in healthy

- malaria-exposed adults in Mali: a randomised, double-blind phase 1 trial. *The Lancet Infectious Diseases*, 17(5):498–509.
- Smilkstein, M., Sriwilaijaroen, N., Kelly, J. X., Wilairat, P., and Riscoe, M. 2004. Simple and Inexpensive Fluorescence-Based Technique for High-Throughput Antimalarial Drug Screening. *Antimicrobial Agents and Chemotherapy*, 48(5):1803–1806.
- Smit, M. R., Ochomo, E. O., Aljanyoussi, G., Kwambai, T. K., Abong, B. O., Samuels, M., Desai, M. R., Howard, P. A. P., Kariuki, S. K., Wang, D., and Steve, A. 2018. Safety and mosquitocidal efficacy of high-dose ivermectin when co-administered with dihydroartemisinin-piperaquine in Kenyan adults with uncomplicated malaria (IVERMAL): a randomised, double-blind, placebo-controlled trial. *Lancet Infectious Diseases*, 18(6):615–626.
- Solyakov, L., Halbert, J., Alam, M. M., Semblat, J. P., Dorin-Semblat, D., Reiningger, L., Bottrill, A. R., Mistry, S., Abdi, A., Fennell, C., Holland, Z., Demarta, C., Bouza, Y., Sicard, A., Nivez, M. P., Eschenlauer, S., Lama, T., Thomas, D. C., Sharma, P., Agarwal, S., Kern, S., Pradel, G., Graciotti, M., Tobin, A. B., and Doerig, C. 2011. Global kinomic and phospho-proteomic analyses of the human malaria parasite *Plasmodium falciparum*. *Nature Communications*, 2(1).
- Srinivasan, P., Beatty, W. L., Diouf, A., Herrera, R., Ambroggio, X., Moch, J. K., Tyler, J. S., Narum, D. L., Pierce, S. K., Boothroyd, J. C., Haynese, J. D., and Millera, L. H. 2011. Binding of *Plasmodium* merozoite proteins RON2 and AMA1 triggers commitment to invasion. *Proceedings of the National Academy of Sciences of the United States of America*, 108(32):13275–13280.
- Stallmach, R., Kavishwar, M., Withers-Martinez, C., Hackett, F., Collins, C. R., Howell, S. A., Yeoh, S., Knuepfer, E., Atid, A. J., Holder, A. A., and Blackman, M. J. 2015. *Plasmodium falciparum* SERA5 plays a non-enzymatic role in the malarial asexual blood-stage lifecycle. *Molecular Microbiology*, 96(2):368–387.
- Steinhardt, L. C., Jean, Y. S., Impoinvil, D., Mace, K. E., Wiegand, R., Huber, C. S., Alexandre, J. S. F., Frederick, J., Nkurunziza, E., Jean, S., Wheeler, B., Dotson, E., Slutsker, L., Kachur, S. P., Barnwell, J. W., Lemoine, J. F., and Chang, M. A. 2017. Effectiveness of insecticide-treated bednets in malaria prevention in Haiti: a case-control study. *The Lancet Global Health*, 5(1):e96–e103.

- Sturm, A., Amino, R., Sand, C. V. D., Regen, T., Retzlaff, S., Rennenberg, A., Krueger, A., Menard, R., and Heussler, V. T. 2006. Manipulation of Host Hepatocytes by the Malaria Parasite for Delivery into Liver Sinusoids. *Science*, 313(September):1287–1291.
- Swank, D. M., Knowles, A. F., Suggs, J. A., Sarsoza, F., Lee, A., Maughan, D. W., and Bernstein, S. I. 2002. The myosin converter domain modulates muscle performance. *Nature Cell Biology*, 4(4):312–316.
- Swearingen, K. E., Lindner, S. E., Flannery, E. L., Vaughan, A. M., Morrison, R. D., Patrapuvich, R., Koepfli, C., Muller, I., Jex, A., Moritz, R. L., Kappe, S. H., Sattabongkot, J., and Mikolajczak, S. A. 2017. *Proteogenomic analysis of the total and surface-exposed proteomes of Plasmodium vivax salivary gland sporozoites*, volume 11.
- Swoboda, M., Cheng, H.-m., Brugger, D., Haltrich, D., Plumere, N., and Schlierf, M. 2012. Enzymatic Oxygen Scavenging for Photostability without pH Drop in Single-Molecule Experiments. *ACS Nano*, 6(7):6364–6369.
- Tang, Q., Andenmatten, N., Hortua Triana, M. A., Deng, B., Meissner, M., Moreno, S. N., Ballif, B. A., and Ward, G. E. 2014. Calcium-dependent phosphorylation alters class XIVa myosin function in the protozoan parasite *Toxoplasma gondii*. *Molecular Biology of the Cell*, 25(17):2579–2591.
- Tangpukdee, N., Duangdee, C., Wilairatana, P., and Krudsood, S. 2009. Malaria diagnosis: A brief review. *Korean Journal of Parasitology*, 47(2):93–102.
- Tanizaki, R., Kato, Y., Iwagami, M., Kutsuna, S., Ujiie, M., Takeshita, N., Hayakawa, K., Kanagawa, S., Kano, S., and Ohmagari, N. 2014. Performance of Rapid Diagnostic Tests for *Plasmodium ovale* Malaria in Japanese Travellers. *Tropical Medicine and Health*, 42(4):149–153.
- Taylor, C. J., McRobert, L., and Baker, D. A. 2008. Disruption of a *Plasmodium falciparum* cyclic nucleotide phosphodiesterase gene causes aberrant gametogenesis. *Molecular Microbiology*, 69(1):110–118.
- Thomas, J. A., Collins, C. R., Das, S., Hackett, F., Graindorge, A., Bell, D., Deu, E., and Blackman, M. J. 2016. Development and application of a simple plaque assay for the human malaria parasite *Plasmodium falciparum*. *PLoS ONE*, 11(6):1–14.

- Thomas, J. A., Tan, M. S., Bisson, C., Borg, A., Umrekar, T. R., Hackett, F., Hale, V. L., Vizcay-Barrena, G., Fleck, R. A., Snijders, A. P., Saibil, H. R., and Blackman, M. J. 2018. A protease cascade regulates release of the human malaria parasite *Plasmodium falciparum* from host red blood cells. *Nature Microbiology*, 3(4):447–455.
- Trager, W. and Jensen, J. B. 1976. Human Malaria Parasites in Continuous Culture. *Science*, 193:673–675.
- Treeck, M., Sanders, J. L., Elias, J. E., and Boothroyd, J. C. 2011. The phosphoproteomes of *Plasmodium falciparum* and *Toxoplasma gondii* reveal unusual adaptations within and beyond the parasites' boundaries. *Cell Host and Microbe*, 10(4):410–419.
- Tyska, M. J. and Warshaw, D. M. 2002. The Myosin Power Stroke. *Cell Motility and the Cytoskeleton*, 51:1–15.
- Uings, I. J. and Farrow, S. N. 2000. Cell receptors and cell signalling. *Journal of Clinical Pathology - Molecular Pathology*, 53(6):295–299.
- van den Berg, M., Ogutu, B., Sewankambo, N. K., Biller-Andorno, N., and Tanner, M. 2019. RTS,S malaria vaccine pilot studies: Addressing the human realities in large-scale clinical trials. *Trials*, 20(1):1–4.
- Vanderberg, J. P. and Frevert, U. 2004. Intravital microscopy demonstrating antibody-mediated immobilisation of *Plasmodium berghei* sporozoites injected into skin by mosquitoes. *International Journal for Parasitology*, 34(9):991–996.
- Verma, A. K., Bharti, P. K., and Das, A. 2018. HRP-2 deletion: a hole in the ship of malaria elimination. *The Lancet Infectious Diseases*, 18(8):826–827.
- Volz, J., Yap, A., Sisquella, X., Thompson, J., Lim, N., Whitehead, L., Chen, L., Lampe, M., Tham, W.-H., Wilson, D., Nebl, T., Marapana, D., Triglia, T., Wong, W., Rogers, K., and Cowman, A. 2016. Essential Role of the PfRh5/PfRipr/CyRPA Complex during *Plasmodium falciparum* Invasion of Erythrocytes. *Cell Host & Microbe*, pages 1–12.
- Wall, R. J., Zeeshan, M., Katris, N. J., Limenitakis, R., Rea, E., Stock, J., Brady, D., Waller, R. F., Holder, A. A., and Tewari, R. 2019. Systematic analysis of *Plasmodium* myosins reveals differential expression, localisation, and function in invasive and proliferative parasite stages. *Cellular Microbiology*, (March):1–12.

- Watson, P. Y. and Fedor, M. J. 2011. The glmS riboswitch integrates signals from activating and inhibitory metabolites in vivo. *Nature Structural and Molecular Biology*, 18(3):359–363.
- Weber, J. H., Vishnyakov, A., Hambach, K., Schultz, A., Schultz, J. E., and Linder, J. U. 2004. Adenylyl cyclases from Plasmodium, Paramecium and Tetrahymena are novel ion channel/enzyme fusion proteins. *Cellular Signalling*, 16(1):115–125.
- Weiss, G. E., Gilson, P. R., Taechalertpaisarn, T., Tham, W. H., de Jong, N. W., Harvey, K. L., Fowkes, F. J., Barlow, P. N., Rayner, J. C., Wright, G. J., Cowman, A. F., and Crabb, B. S. 2015. Revealing the Sequence and Resulting Cellular Morphology of Receptor-Ligand Interactions during Plasmodium falciparum Invasion of Erythrocytes. *PLoS Pathogens*, 11(2):1–25.
- Wentzinger, L., Bopp, S., Tenor, H., Klar, J., Brun, R., Beck, H. P., and Seebeck, T. 2008. Cyclic nucleotide-specific phosphodiesterases of Plasmodium falciparum: PfPDE α , a non-essential cGMP-specific PDE that is an integral membrane protein. *International Journal for Parasitology*, 38(14):1625–1637.
- WHO 2007. Technical Expert Group meeting on intermittent preventive treatment in pregnancy (IPTp). *World Health*, (July):11–13.
- WHO 2018. *World Malaria Report 2018*. 4.
- Yang, L., Uboldi, A. D., Seizova, S., Wilde, M. L., Coffey, M. J., Katris, N. J., Yamarlyo-Botté, Y., Kocan, M., Bathgate, R. A., Stewart, R. J., McConville, M. J., Thompson, P. E., Botté, C. Y., and Tonkin, C. J. 2019. An apically located hybrid guanylate cyclase-ATPase is critical for the initiation of Ca²⁺ signaling and motility in Toxoplasma gondii. *Journal of Biological Chemistry*, 294(22):8959–8972.
- Yeoh, S., O'Donnell, R. A., Koussis, K., Dluzewski, A. R., Ansell, K. H., Osborne, S. A., Hackett, F., Withers-Martinez, C., Mitchell, G. H., Bannister, L. H., Bryans, J. S., Kettleborough, C. A., and Blackman, M. J. 2007. Subcellular Discharge of a Serine Protease Mediates Release of Invasive Malaria Parasites from Host Erythrocytes. *Cell*, 131(6):1072–1083.
- Zanghì, G., Vembar, S. S., Baumgarten, S., Ding, S., Guizetti, J., Bryant, J. M., Mattei, D., Jensen, A. T., Rénia, L., Goh, Y. S., Sauerwein, R., Hermsen, C. C., Franetich, J. F.,

- Bordessoulles, M., Silvie, O., Soulard, V., Scatton, O., Chen, P., Mecheri, S., Mazier, D., and Scherf, A. 2018. A Specific PfEMP1 Is Expressed in *P. falciparum* Sporozoites and Plays a Role in Hepatocyte Infection. *Cell Reports*, 22(11):2951–2963.
- Zhang, M., Wang, C., Otto, T. D., Oberstaller, J., Liao, X., Adapa, S. R., Udenze, K., Bronner, I. F., Casandra, D., Mayho, M., Brown, J., Li, S., Swanson, J., Rayner, J. C., Jiang, R. H., and Adams, J. H. 2018. Uncovering the essential genes of the human malaria parasite *Plasmodium falciparum* by saturation mutagenesis. *Science*, 360(6388).
- Zhang, X. and Cote, R. H. 2005. cGMP Signalling in Vertebrate Retinal Photoreceptor Cells. *Frontiers in Bioscience*, 10:1191–1204.